Polymer solubilisation and lipid characterisation of bacterial and fungal membranes

Constanze Cavalier

Green Templeton College

University of Oxford

A thesis submitted for the degree of

MSc by Research

Michaelmas 2022

Acknowledgements

First of all I would like to thank Prof Anthony Watts and Associate Prof Maike Bublitz for accepting me to this research program and for introducing me to the work of their groups at the Biochemistry Department. I would like to thank all members of both groups for providing material and expertise.
Especially I thank Dr Sabine Heit, for supervising my project in the laboratory environment on a every day basis and for providing me with expertise and information and Dr Joanne Parker for her guidance and feedback through out my final year.
I want to also thank all current and former members of the Watts group for their advice and support throughout the years. Dr Henry Sawczyc, Dr Juan Francisco Bada Juarez, Dr Javier Vinals Camallonga, Dr Peter Judge, Dr Steven Lavington and Dr Natalia Fontana thank you for sharing your knowledge in developing this project as well in helping in all technical questions. Furthermore I want to thank all current and former members of the Bublitz group for their valuable support and contributions that made this project possible. Matthew Hankins, Dr Margaret Young, Maxwell Guerts and Samuel Bannon, thank you for providing support and kind words in the lab, during analysis and write up phase.
I would like to thank the all the Oxford academics and college personnel who have helped me develop my ideas, were there for questions and kept me to stay on, every step of the way. A particular thanks to Dr Gulsah Albayrak for support, particularly during the pandemic.
I would like to thank Dr Ben Jenkins at the IHR Core Metabolomics and Lipidomics Laboratory at Cambridge University for collaboration and provision of the lipidomics data presented in this work.
I would like to thank the Studienstiftung des deutschen Volkes and Deutscher Akademischer Austauschdienst for providing me with scholarships that made it possible for me to study in the UK.
I would like to thank my parents and grandparents for their encouragement and support as they who grew up in a country where it was unimaginable for them to study this freely abroad in the UK.
I want to thank all my friend and family for helping me through and supporting me through that the past years. Thank you for Matthias, Felix, Elisa, Sonja, Daniel, Alexander, Luise, José, Joe and Dominik for your encouragement and help to finalise this thesis.

Thank you to all new friends for sharing time and wisdom on how to navigate Oxford's environment and thank you to all old friends who always gave me a feeling of home, wherever I was.

Abstract

Fungal infections are a major threat to immunocompromised patients. A potential target for treating such invasive infections is Pma1, a P-Type ATPase that pumps protons across the plasma membrane of fungi to create an electrochemical gradient essential for the secondary transport of nutrients. As yet, efforts to study Pma1 in vitro have been focused on detergent solubilisation and purification, which does not necessarily preserve the native lipid environment and can potentially alter the native hexameric assembly and ATPase activity of Pma1. This study had two main aims: (i) to develop a protocol for purifying *Neurospora crassa* Pma1 from its native source using polymer-lipid-protein particles, with the aim of maintaining a native lipid environment, and (ii) to characterise the native lipidome of the host organism *N. crassa*, and identify those lipid species that co-purify with Pma1. The effectiveness of several commercially available polymers in solubilising fungal membranes under various conditions were evaluated and compared to bacterial membranes. The well-characterised polymer, styrene maleic acid (SMA 3:1), was identified as a potential candidate for solubilising Pma1 from *N. crassa*, and limitations of this polymer for assessing protein purity and activity for fungal membranes were investigated. Using LC/MS to analyse the full *N. crassa* lipidome, 420 different lipid species were identified. By analysing lipids present in different purification steps of Pma1 in detergent, it was observed that purified *N. crassa* Pma1 hexamers are characterised by an enrichment of inositol-containing ceramides. Knowing these tightly associated lipid species will aid with future efforts to preserve Pma1's native lipid environment during purification.

Covid Statement

Due to Covid pandemic and resulting loss of access to the lab, several experiments were prepared but not further executed. This effected particularly experimental repeats in Chapter 3 - 5. The focus of the presented thesis was therefore to evaluate the initial results in this context. Because of the disruptions additional prepared samples could not be sent for LC/MS analysis therefore an analysis of the lipid specificity of polymer solubilised membranes could not be executed within this thesis.

Contents

List of Figures

List of Tables

List of Abbreviations

$A_{860\,nm}$ . . . . . absorption at 860 nm

ABC . . . . . ATP-binding cassette

AB . . . . . Antibody

AEX . . . . . Anion-exchange chromatography

BCA . . . . . Bicinchoninic acid assay

BSA . . . . . Bovine serum albumin

Cer . . . . . Ceramides

ConA . . . . . Concavalin A

CPD . . . . . cysteine protease domain

cryo-EM . . . . cryo electron microscopy

CardioL, CL . . Cardiolipin

ddH_2O . . . . . Double distilled water

DDM . . . . . n-β-dodecyl-maltopyranoside

DG . . . . . diglyceride

DGPL . . . . . Diacylglycerophosphatidyl lipids

DH . . . . . hydrodynamic diameter

DIBMA . . . . Diisobutylene-maleic acid acid polymer

DLS . . . . . Dynamic light scattering

DMPC 1,2-dimyristoyl-sn-glycero-3-phosphocholine

DOC . . . . . Deoxycholic acid sodium salt

DTT . . . . . Dithiothreitol

ECL . . . . . Enhanced chemiluminescence

E. coli . . . . . *Escherichia coli*

EDTA . . . . . Ethylenediaminetetraacetic acid

EM . . . . . Electron microscopy

E_{rel} . . . . . Relative protein solubilisation efficiency

Erg . . . . . Ergosterol

FGSC . . . . . Fungal Genetics Stock Center

Gang . . . . . Gangliosides

GC . . . . . Gas chromatography

GFR . . . . . Green flourescent protein

GPCR . . . . . G protein-coupled receptors

HEPES . . . . . 4-(2-hydroxyethyl)-1-piperazineethanesulfonic acid

IMAC . . . . . Ion metal affinity chromatograpy

IP-Cer . . . . . Inositol phosphorylceramid

IPTG Isopropyl-D-1-thiogalactopyanoside

LC/MS . . . . Liquid chromatography mass spectrometry

LDS . . . . . Lithium dodecylsulphate

LPC . . . . . lysophosphatidylcholine

LPE . . . . . lysophosphatidylethanolamine

LPI . . . . . lysophosphatidylinositol

LPS . . . . . lysophosphatidylserine

LysoPL . . . . . Lysophospholipids

M . . . . . Molar

MD . . . . . Molecular dynamics

MIP-Cer . . . . Mannosyl-phosphatidylinositol-ceramides

MDIP-Cer . . . Mannosyl-di-phosphatidylinositol-ceramides

MS . . . . . Mass spectrometry

MCC . . . . . membrane compartment containing Can1

MCP . . . . . membrane compartment containing Pma1

MCT . . . . . membrane compartment containing TORC2

MembrL . . . . Membrane forming lipids

MG . . . . . monoglyceride

MM . . . . . Minimal medium

MprF . . . . . Multiple peptide resistance factor

M_r . . . . . Molecular mass

MS . . . . . Mass spectrometry

MW . . . . . Molecular weight

M/Z . . . . . Mass-to-charge ratio

N. crassa . . . *Neurospora crassa*

NcPma1 . . . . *Neurospora crassa* Pma1

PA . . . . . Phosphatidic acid

PC . . . . . phosphatidylcholine

PCA . . . . . perchloric acid

PE . . . . . phosphatidylethanolamine

PG . . . . . phosphatidylglycerol

PI . . . . . phosphatidylinositol

Pi . . . . . free inorganic phosphate

PLD . . . . . Phospholipase D

PM . . . . . Plasma membrane

PMA . . . . . Polymethacrylate copolymer

Pma1 . . . . . Plasma membrane P-Type ATPase 1

PS . . . . . phosphatidylserine

RT . . . . . Room temperature

S . . . . . Sulfatides

SDS . . . . . Sodium dodecyl sulfate

SDS-PAGE . . Sodium dodecyl sulfate polyacrylamide gel electrophoresis

S. cerevisiae . . *Saccharomyces cerevisiae*

ScPma1 . . . . *Saccharomyces cerevisiae* Pma1

SEC . . . . . Size-exclusion chromatography

SF . . . . . Glycerides (Storage Fats)

SL . . . . . Sphingolipids

SM . . . . . Sphingomyelin

SMA . . . . . Styrene-maleic acid copolymer

SMALP . . . . Styrene maleic acid lipid particle

SMAnh . . . . Styrene maleic anhydride polymer

SOP . . . . . Standard order of practice

TCA . . . . . trichloroacetic acid

TEM . . . . . Transmission electron microscopy

TG . . . . . Triacylglycerols

TLC . . . . . Thin layer chromatography

TM . . . . . Transmembrane

Tm . . . . . Transition temperature

UV . . . . . Ultraviolet

UV-Vis . . . . . Ultraviolet-Visible spectroscopy

v/v . . . . . Volume to volume ratio

w/v . . . . . Weight to volume ratio

WC . . . . . Whole cells

WT . . . . . Wild type

w/w . . . . . Weight to weight ratio

Chapter 1

Introduction

1.1 Biological membranes

All organisms have membranes, which define their cells and separate the cytoplasm from the external environment. These membranes perform many vital roles including cell-cell communication, energy transduction and cell division. Biological membranes are made of a lipid bilayer in which proteins are embedded, typically making up about 50 % of the dry weight of the membrane [1]. A bilayer of (phospho-)lipid molecules gives the structural base of a biological membrane with integrated membrane proteins that are functional units of the membrane and maintain cell function.

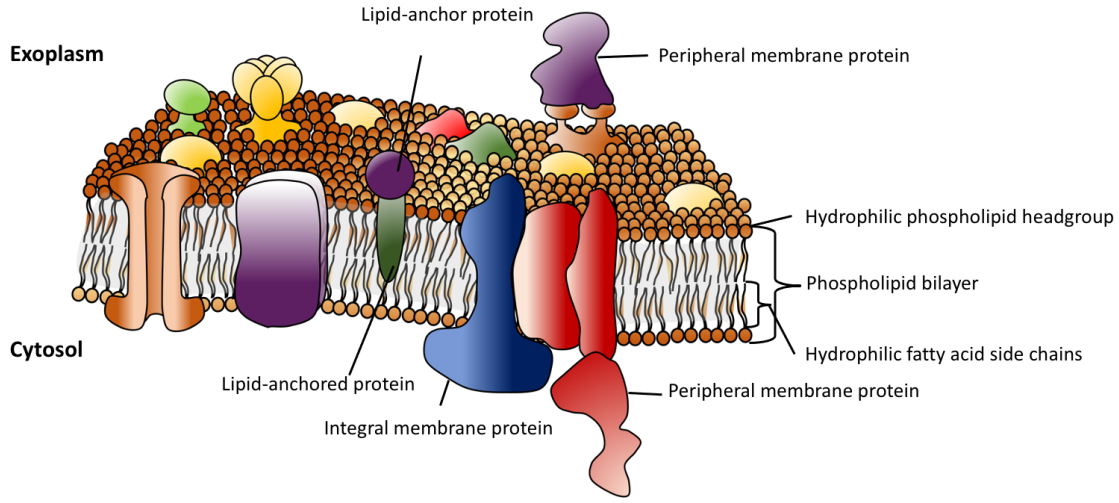

Figure 1.1: Schematic representation of a typical biological membrane, which consists of a lipid bilayer in which membrane proteins are inserted.
The fluid mosaic model: Lipids form a bilayer where different modes of insertion of membrane protein are illustrated. Reproduced from [2].

The lipid and protein composition varies between species [3–5], cell type [4, 6, 7], cell organelles [8, 9], location within the membrane [10], and lipid leaflet (referred to as lipid asymmetry) [8], further reviewed in [11]. Sugar molecules, lipid- and protein-bound, are found on the extracellular membrane leaflet, giving a unique surface fingerprint to the cell and providing recognition sites for other cellular receptors [2, 12]. The selectively permeable property of the membrane makes it possible to separate environments and build up a concentration and an electrical gradient (electrochemical gradient) across the membrane.

1.2 Membrane lipids

The main lipid components of biological membranes are glycerophospholipids, sphingolipids and sterols [11]. Glycerophospholipids and sphingolipids are amphiphilic molecules with hydrophobic and hydrophilic properties and particularly glycerophospholipids comprise the main component of all biological lipids.

In glycerophospholipids (particularly diacyl glycerophospholipids (DGPL)), two fatty acids form the hydrophobic tail and are linked by an ester bond to a glycerol backbone. Acyl (fatty) acids are hydrocarbon chains which can be saturated or unsaturated (containing double bonds between carbons), most commonly in *cis*-conformation. For example, DGPLs usually contain one saturated or monounsaturated fatty acid (R1) and one mono- or polyunsaturated fatty acid (R2) [4]). The glycerol is further linked via a phosphoester to various types of polar groups, forming the hydrophilic head group [11] as outlined in Fig 1.2 B. The complexity of lipids comes from differences in their head groups and the variation of chain length and carbon saturation level of the fatty acyl tails. The polar head group defines the overall charge of the phospholipid, and the membrane fluidity, thickness and lateral pressure within the membrane are mitigated by the lipid tails or, in case of membrane curvature, a combination of both [10, 13, 14]. In eukaryotic cells, the glycerophospholipid head groups are phosphatidylcholine (PC), phosphatidylethanolamine (PE), phosphatidylinositol (PI), phosphatidylserine (PS), phosphatidylglycerol (PG) and phosphatidic acid (PA) as shown in Fig 1.2 C. PC and PE both have positively charged head groups and with the negative phosphate group create

an overall neutral zwitterionic lipid. On the other hand, neutral head groups result in anionic (negatively charged) phospholipids, such as PG, PA, PS and PI. Lysolipids are derivatives of lipids in which one or both acyl chains have been hydrolytically removed, examples are lysophosphatidylcholine (LPC), lysophosphatidylethanolamine (LPE), lysophosphatidylinositol (LPI), lysophosphatidylserine (LPS).

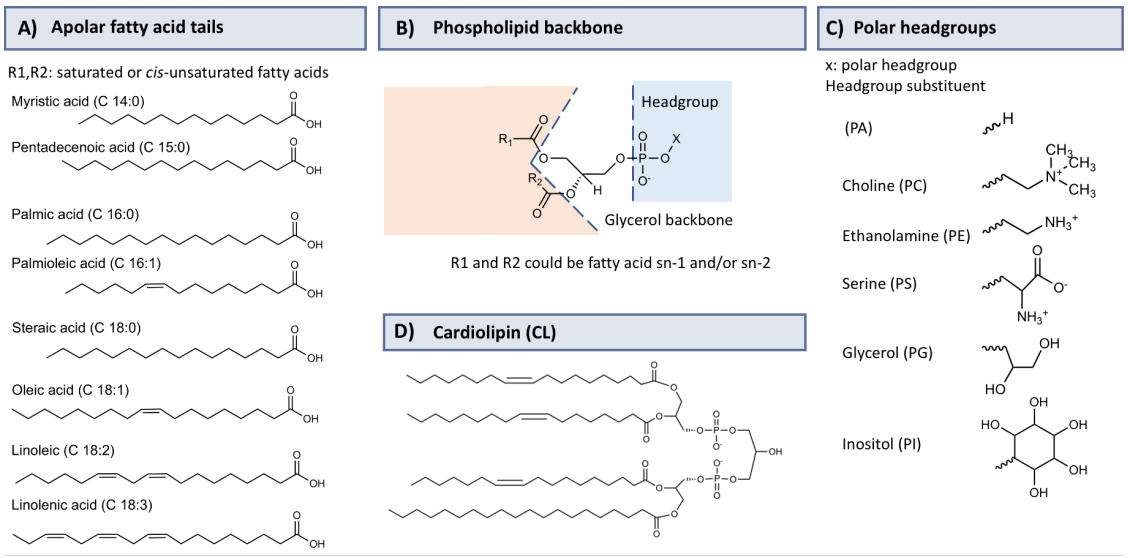

Figure 1.2: Structural components of glycerophospholipids
A) Apolar fatty acid chains (Cx:y; no of carbons (x); degree of unsaturation (y); Chain can be x: 10-24 (or more); y: 0-6) , B) The glycerophospholipid backbone, with its polar headgroup (blue) and apolar lipid tails (orange), C) The polar head groups of different phospholipid classes are shown protonated at physiological pH, D) Representative structure of a cardiolipin.

Depending on their headgroup to acyl chain relationship, naturally occurring PC and PS lipids predominantly show over all cylindrical shape, leading to a flat membrane, whereas PE and PA contain small headgroups and form conical lipids leading to a negative curvature [11, 15]. On the other hand lysophospholipids and PI have an overall inverted conical shape leading to a positive curvature of the membrane [11].

Additionally to the geometrical influences on the membrane curvature [16], specific phospholipids play crucial roles in cellular mechanisms, also mediated by their overall charge (electrostatics of the overall lipid). For example, PS lipids are a highly abundant component of the plasma membrane, with up to 34 % of the diacyl phospholipids of *S. cerevisiae* plasma membranes [17] and are mainly found in the cytosolic leaflet

of mammalian cells and serve there as a signalling molecule for apoptosis, inducing macrophagic response and degradation of cells when exposed to the extracellular side of the lipid bilayer [18, 19]. Furthermore, PI, which makes up around 28 % in diacyl phospholipids of *S. cerevisiae* plasma membranes [17], is also highly prevalent in the cytosolic leaflet in the plasma membrane [20]. PI lipids contain an inositol group that can be phosphorylated and this serves as an important signalling mechanism within the cell [21]. PA is a precursor for DGPL synthesis and is a signalling molecule which has been implicated in the maintenance of lipid homeostasis in yeast [22].

Cardiolipins (Fig 1.2 D) are phosphoryl glycerides with four long fatty acids, made from phosphatidylglycerol and phosphatidyl acid and are mostly found in the membranes of prokaryotic cells and the inner membrane of mitochondria in eukaryotic organisms [17, 23]. This uniquely conical lipid shape enables cardiolipins to play key roles in stabilising the cristae structure of mitochondria [24]. In addition, cardiolipin has been implicated in a number of key mitochondrial processes for example the organisation of large protein supercomplexes [25, 26]; these roles are reviewed in detail in [27].

Sterols (Fig 1.3) like cholesterol (in mammalian membranes) and ergosterol (in fungal membranes) plays a role in membrane organisation, by inserting into the membrane they maintains lipid homogeneity and fluidity at lower temperatures [28]) and have been suggested to be important in lipid raft formation in mammalian cells through interaction with sphingolipids via hydrogen-bonds [10, 29].

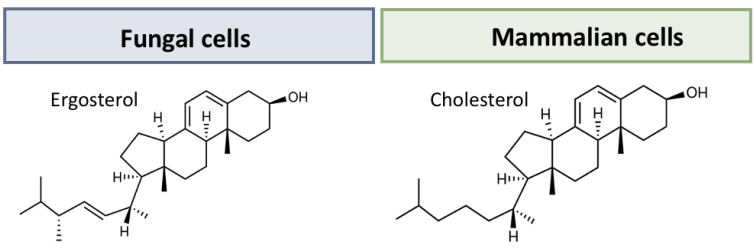

Figure 1.3: Chemical structure of fungal and mammalian sterols

An important component, particularly of the plasma membrane of complex organisms [30] are sphingolipids (Fig 1.4) and have been identified to be involved in cellular processes such as trafficking of transporters to the plasma membrane and influence of their functionality (reviewed in [31]). The precursor for the sphingolipid synthesis is dihydrosphingosine or phytosphingosine (typically C18 or C20) sphingosine (C18) in fungal and mammalian cells, respectively [32]. This long-chain base is linked via an amide bond to a fatty acid and forms ceramide (Cer) which is the backbone for other sphingolipids. The length of the long chain base and the fatty acid can vary, and both chains can be hydroxylated and contain double bonds. The sphingoid base or ceramide can be phosphorylated at the C-1 hydroxyl group making phosphosphingolipids [33], and their main representatives in fungi have a phosorylinositol (inositolphosphoryl-ceramide, IP-Cer), a mannosylated phosphorylinositol (mannosyl-inositolphosphoryl-ceramide, MIP-Cer) or two linked phosphorylinositol molecules of which one is mannosylated (mannosyl-di-(inositol-phosphoryl)-ceramide, $M(IP)_2Cer$ or MDIP-Cer) bound to a ceramide. Sphingomyelin (SM) is a common example of a glycerophosphosphingolipid, where a phosphatidylcholine molecule is bound to a ceramide, this can be found in animal cells where it has been described as source of bioactive sphingolipids, like ceramides or Sphingosine-1-phosphate (S1P) [34]. In previous studies of fungal membrane composition SM has not been reported [34, 35]. Other types of sphingolipids are cerebrosides where a mono hexose (mainly galactose) is glycosidic bound to a ceramide, a special case of these are sulfatides (S) where a sulphate is bound to the glycosyl moiety, and ganglioside (Gang), which are complex di-oligosaccharides with one to four silica acids. Because of their backbone and headgroups, sphingolipids are able to act both as a hydrogen bond donor and acceptor and are able to form large hydrogen bond networks leading to tight membrane structures [36] and higher melting temperature [37]). Most importantly, sphingolipids are structural components of the plasma membrane and part of the compartmentalisation of membranes into specific lipid domains (known as lipid rafts), components of sphingolipids, such as ceramides or their phosphorylated inositol headgroups [38]) have signalling effects during their metabolism, and influence cellular processes of eukaryotes. Their functions are reviewed in more detail in [32, 39, 40].

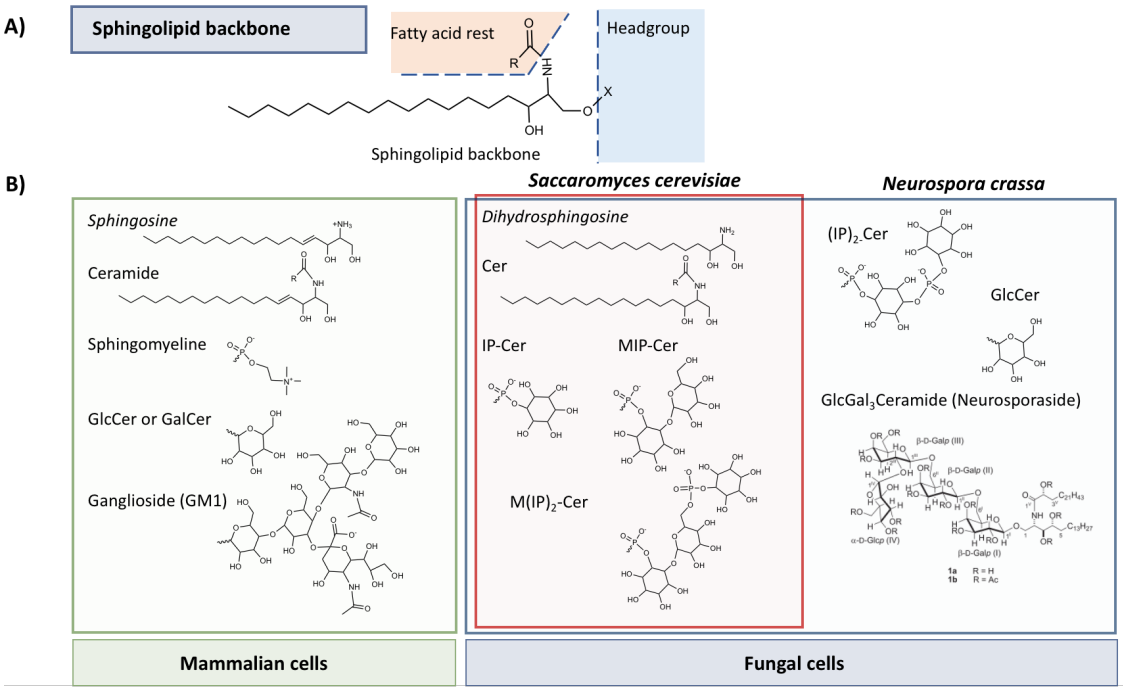

Figure 1.4: Structures of complex sphingolipids found in the plasma membrane of fungi and mammals
A) The sphingolipid backbone, with its polar headgroup (blue) and apolar lipid tails (orange) B) representative structures of sphingolipid found in the plasma membrane of complex organisms: mammalian cells (left, green) and fungal cells (blue, right) particularly *Neurospora crassa* (filamentous and slime [41–43]), highlighted in red is the subset of sphingolipids present in the budding yeast *Saccharomyces cerevisiae*. (Overview adapted from [32])
IP-Cer, inositolphosphorylceramide; MIP-Cer, mannosylinositolphosphorylceramide; $M(IP)_2$-Cer, mannosyldiinositolphosphorylceramide; $(IP)_2$-Cer, diinositolphosphorylceramide; GlcCer, glucosylceramide; GM1, ganglioside GM1; SM, sphingomyelin and GalCer, galactosylceramide.

To study the lipid composition of samples, lipids are commonly extracted with organic solvents (e.g. Folch extraction [44]) and analysed with methods such as thin layer chromatography (TLC) [45], phosphorus determination [46], gas chromatography [47] and mass spectrometry such as shotgun mass spectrometry [48–50], liquid chromatography - mass spectrometry (LC/MS) [51] or native mass spectrometry [52]. Analysis methods for determining the lipid content of a sample have advanced significantly in recent years, and mass spectrometry has developed into a valuable tool.

The lipid composition of different organisms and even between individual cell organelles varies and is outlined in Table 1.1. Certain lipids are characteristic for specific cell

organelles, e.g. mitochondria are characterised by having a high cardiolipin content and the plasma membrane by a high PS and a high sphingolipid content (e.g. in *S. cerevisiae* [17, 53, 54]). Furthermore, in eukaryotic cells the sterol and sphingolipid composition shows an asymmetry between the plasma membrane and membranes earlier in the secretory pathway [55] influencing the maturation of membrane proteins during membrane trafficking [3] for example ceramides are required for the the surface delivery of the *S. cerevisiae* plasma membrane ATPase [56–58].

Table 1.1: (Phospho-) Lipid composition of different model organisms and cellular organelles
PC-phosphatidylcholine, PE-phosphatidylethanolamine, PI-phosphatidylinositol, PS-phosphatidylserine, CL-cardiolipin, PA-phosphatidic acid, PG-phosphatidylglycerol, values are rounded, others are such as lyso-phospholipids or unknown substances; nd – non detectable; nr – not reported; WC – whole cell

	Overall Lipid Composition	**Phospholipid content** (mol% of total phospholipids)	**Ref**
Prokaryotic organisms			
E. coli		70–80 % PE, 20–25 % PG and <5 % CL	[59]
Eukaryotic organisms			
Fungi		35–50 % PC, 14–35 % PE, <25 % PS and PI	[60]
S. cerevisiae WC		51 % PC, 25 % PE, nr PG, 11 % PI, 5 % PS, 4 % CL, 1 % PA, 3 % others	[61]
Plasma membrane (PM)	0.23 mg/mg protein per phospholipid, 0.4 mg/mg protein Ergosterol, [17] 0.27 mg/mg protein Sphingolipids [54], [62]	17 % PC, 20 % PE, nr PG, 4 % PA, 18 % PI, 34 % PS, <1 % CL, 7 % others	[17]
Endoplasmatic reticulum (ER)	0.22 mg/mg protein per phospholipid, 0.05 mg/mg protein Ergosterol, [17] 0.14 mg/mg protein Sphingolipids [54, 62]	45 % PC, 22 % PE, nr PG, 4 % PA, 11 % PI, 8 % PS, 1 % CL	[62]
Vacuoles	0.51 mg Phospholipid, 0.05 mg/mg Ergosterol protein [17] 0.2 mg/mg protein Sphingolipids [54, 62]	47 % PC, 19 % PE, nr PG, 2 % PA, 18 % PI, 4 % PS, 2 % CL, 8 % others	[17]
Mitochondria	0.09 mg/mg protein Phospholipid, 0.01 mg/mg protein Ergosterol, [17] 0.02 mg/mg protein Sphingolipids [54, 62]	40 % PC, 27 % PE, nr PG, 2 % PA, 15 % PI, 3 % PS, 13 % CL, and others	[17]
N. crassa WT WC		37 % PC, 34 % PE, 6 % PI, 3 % PS, 4 % PA, <1 % PG, 5 % CL, 12 % others	[63]
Mitochondria		34 % PC, 40 % PE, 7 % PI, 3 % PS, 1 % PA, 1 % PG, 5 % CL, 10 % others	[63]
N. crassa (slime) WC		45 % PC, 36 % PE, 11 % PI/PS, 4 % PA, 4 % CL (31 °C)	[64]
Plasma membrane (PM)	53 mol% Phospholipid, 42 mol% free sterols, 6 mol% Sphingolipids (37 °C [65])	29 % PC, 28 % PE, 19 % PI/PS, 20 % PA, 4 % CL (31 °C)	[64]
Insect cell			
Sf9 insect cells	11 % SM, 0.03 mol/mol Sterol [15]	16 % PC, 38 % PE, 3 % PG, 18 % PS, 13 % PI, nr CL	[15]
mammalian cell			
Human embryonic kidney (HEK)	11% SM, 0.24 mol/mol Sterol [15]	36 % PC, 16 % PE, 3 % PG, 23 % PS, 7 % PI, nr CL	[15]

Both the head group composition and acyl chain length, along with the number of double bonds per chain may vary between organisms. In eukaryotic cells carbon chains

contain fatty acids with mostly 16 and 18 but up to 24 carbon atoms [66, 67].

Even within the membranes lipids are differently distributed and lipids and proteins in the membrane influence each other [68, 69]. Lipids in the membrane can be differentiated into three main subclasses (bulk lipids, annular lipids and non annular lipids), and these are defined by the strength of their interaction with membrane proteins [29]. Furthermore lipids can also be direct substrates for proteins, e.g. during lipid transport [70]. Bulk lipids are not in direct proximity with the proteins, and do not interact with them directly, but they play a role in membrane heterogeneity as specific affinity between certain lipids can create distinct membrane environments and can sort proteins into distinct membrane compartment [71]. Annular lipids are in the direct environment of the protein, forming a ring (annulus) around the protein transmembrane domains (TMDs) and non-specifically interact with the protein [29]. In contrast, specific interaction between non-annular lipids and some proteins can modulate protein conformation and function [72, 73] directly through lipid-binding motifs [74, 75] or electrostatic interactions between protein and lipids of the membrane [76, 77]. Specific lipids can influence membrane protein function as cofactors to carry out function and activity or as "co-structures" to maintain correct folding and stability [69]. By influencing the membrane protein's geometry and through electrostatic interactions and hydrogen bonds between certain lipids [29], these bulk lipid environments can influence the protein dynamics and diffusion rate [78] and function like signalling [79–81], transport [82, 83], and motility [84, 85]. Specific lipid-protein interactions can influence enzyme/receptor activity [86], structural properties e.g. conformational state of the protein [87, 88] or the oligomeric state [89] as reviewed in [29].

1.3 Membrane proteins — with an emphasis on transporters

Membrane proteins are an essential component of the biological membrane performing a wide variety of crucial functions for the cell. Membrane proteins can have different modes of attachment to the membrane either integral or peripheral (Fig 1.1) [2]. Integral membrane proteins are embedded in the bilayer with a transmembrane component

spanning both layers of the membrane. Peripheral proteins can be associated with the membrane either by an electrostatic interaction, anchoring to lipid components or transient insertion of part of their sequence into the membrane [2]. Membrane proteins play key roles in signal transduction, have enzymatic activity, facilitate membrane adhesion and transport of material across the membrane [90].

Movement of biological components across membranes is required for many important cellular processes either by providing substrates for cellular activities or by producing electrochemical gradients to power other processes (Fig 1.5) [91]. The movement of chemical species across the membrane can either be passive or active. Passive processes achieve transport through a favourable concentration gradient whereas active transport processes require an external energy source to move chemical species against their concentration gradient [91].

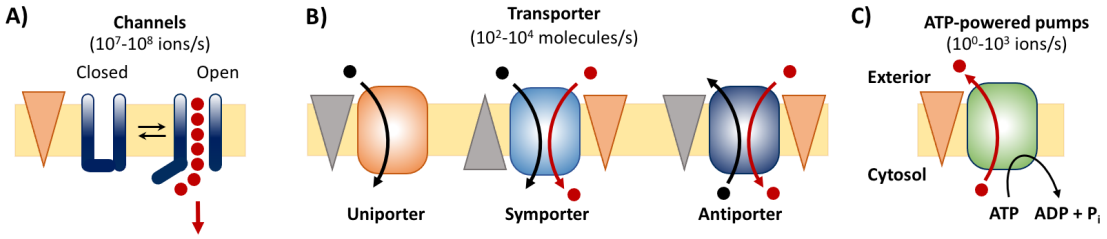

Figure 1.5: Schematic of protein types vital for the molecular movement through biological membrane
The triangles indicate the (electro-)chemical gradient; Channel A), transporters B), which in case to the symporter and antiporter utilise a concentration gradient that was built up by ATP driven pumps C). Reproduced from [91].

Some small uncharged polar molecules such as gases (as CO_2, O_2) follow their concentration gradient and diffuse across the membrane [92]. However, charged components can not move across the hydrophobic tightly packed bilayer and require membrane proteins to facilitate their diffusion or transport across the membrane. Ion channels (Fig 1.5 A) provide a hydrophilic route for smaller charged and polar compounds e.g. potassium (K^+) moving down their concentration gradient and when open can conduct high rates of transport as the movement of a single ion does not require the protein undergoing a catalytic cycle [93]. For ions that need to be transported

against their concentration gradient and for larger compounds such as amino acids and sugars, movement across the membrane is carried out by transporters, which need to cycle between multiple structural states in order to transport a single molecule of compound [91]. The transition between structural states requires an energy source. For facilitated diffusion the energy source comes from the binding energy of the compound being transported (uniporter, Fig 1.5 B) whereas for active transport against the gradient this energy source is either ATP (primary active transporter, Fig 1.5 C), e.g. P-Type ATPases [94], ABC transports [95], or another favourable ion gradient such as protons (H^+) or sodium (Na^+)(secondary active transporter, Fig 1.5 B), e.g. many members of the solute carrier (SLC) family [96]. Secondary active transporters are important to drive the uphill transport of one substrate utilising the downhill gradient of the co-substrate; and this co-substrate can flow in the same directions as the substrate being transported (symporter) or in the opposite direction (antiporter) [91] (Fig 1.5 B). Transporters are important for nutrient and metabolite uptake into the cell (e.g. [96]) and play other important roles in cell function as regulation of their ionic balance and pH [97].

Membrane proteins represent around 30 % of the human genome [90] and make up about 60 % of drug targets [98]. Some membrane proteins take up certain drugs and transport them into the cell [99, 100], others are pathogen specific and perform crucial cellular mechanisms that can be specifically targeted [101]. Both are examples for membrane proteins of great interest for pharmaceutical studies and (structure driven) drug design.

1.4 Plasma membrane ATPase 1 (Pma1)

The fungal P-Type ATPase Pma1 (Plasma membrane ATPase 1) transports protons across the plasma membrane in an ATP-dependent manner and is a necessary protein for fungi including *Saccharomyces cerevisiae* and *Neurospora crassa* [102]. It generates the electrochemical gradient that is used by secondary transporters to import essential nutrients. Pma1 does not have a mammalian homologue and therefore is a potential drug target for the treatment of fungal infections which are often lethal in immunosuppressed

patients [101, 103].

The Pma1 monomer has a molecular weight of ∼100 kDa (920 amino acids, UniProt, accession number: P07038, sequence in Appendix A.4) and 10 trans membrane spanning α-helices, which form hexamers in the plasma membrane [94]. Pma1 belongs to the P-Type ATPase family of cation transporters which can be found in all organisms and like other P-type ATPases, Pma1 is phosphorylated during ion transport cycle via hydrolysis of ATP. During the course of this thesis, the cryo-EM structures of *N. crassa* Pma1 hexamer (at 3.3 Å resolution [104]) and *S. cerevisiae* Pma1 hexamer [105] were published. The structure of *N. crassa* Pma1 is shown in Fig 1.6 highlighting its five domains membrane or transport domain (M, grey), phosphorylation domain (P, dark blue), where phosphate becomes covalently bound to a conserved Asp residue, nucleotide binding domain (N, red), which forms the ATP binding pocket, actuator domain (A-yellow), which removes phosphate at the end of transport cycle, the COOH-terminal regulatory domain (R, light blue) as well as the NH_2-terminal extension (orange), furthermore two Glu residues form the binding site for K^+.

Pma1 is highly abundant in the plasma membrane up to 10 % in *N. crassa* and up to 50 % in *S. cerevisiae* [106], and highly regulated. Unique features of Pma1 are that it forms a hexamer, which is unusual within P-type ATPases [104] and might aid cooperative activation [105]. Furthermore, its R-domain auto inhibits its function in a starving environment but it is activated by glucose signalling through phosphorylation of the R-domain. Particularly the hexamer formation and autoinhibition can be informative for structure-based drug development [104].
The lipid interactions of Pma1 have been primarily studied in *S. cerevisiae* [107] and it has been shown that Pma1 resides within detergent-insoluble glycolipid enriched complexes (DIGs) [108], which are required for the delivery to the plasma membrane [109]. In addition, sphingolipids with very long chain fatty acids (C26) have also been shown to be particularly important for the transport of the Pma1 to the surface [57, 58]. Pma1 defines the membrane compartment containing Pma1 (MCP), one of the three

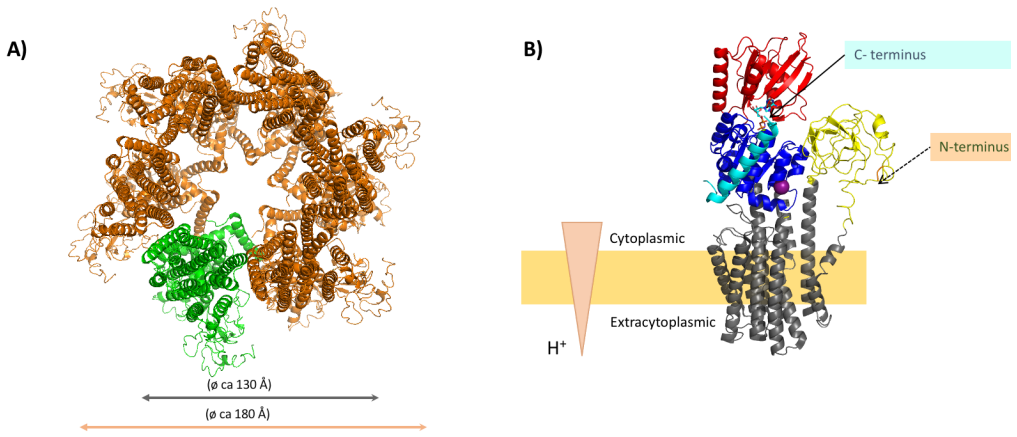

Figure 1.6: *N. crassa* Plasma membrane P-type ATPase Pma1
N. crassa Pma1 structure (monomer 7NXF.pdb and hexamer 7NY1.pdb) solved via cryo EM, published in [104]. A) view of the hexameric state of Pma1 from the extra cytoplasmic side, one monomer is highlighted in green. B) Functional description of the H^+-ATPase Pma1, which hydrolyses ATP into ADP and inorganic phosphate ($ATP \longrightarrow ADP + P_i$). Highlighted are the COOH-terminal **R**egulatory (Light blue), **P**hosphorylation (dark blue), **N**ucleotide binding (red), **A**ctuator (yellow) and **M**embrane (grey) domains as well as the NH_2-terminal extension (orange), including potassium ion (purple sphere) and ADP. The residues 1-65 in the NH_2-terminal extension (dashed line) and 881-891 in the R-domain could not be modelled and are not shown.

main lipid domains characterised in *S. cerevisiae* [110, 111]. The other domains are MCC/eisosomes (membrane compartment containing Can1) and MCT (membrane compartment containing TORC2); each domain differs in proteins and lipid composition [112–114]. *S. cerevisiae* MCP mainly contains the sphingolipids, IP-Cer, MIP-Cer, and MDIP-Cer) [110, 111, 113, 115].

N. crassa is a different fungal model organism for the study of Pma1. *N. crassa* is a filamentous fungus and has been used as a model organism for over 80 years and exists in a variety of strains [116–119]. Mutant strains of *Neurospora crassa* which lack a cell wall and therefore have an exposed plasma membrane to the environment are known as *N. crassa* slime [120–122]. *N. crassa* slime mutants mimic artificially produced protoplasts that are stable and referred to as spheroplasts [123] and are particularly experimentally useful as it is not necessary to remove a cell wall in order to access plasma membrane proteins.

The lipid composition of *N. crassa* slime mutants and their plasma membrane have

been studied in the past primarily with thin layer chromatography (TLC) [64, 124], differential scanning calorimetry (DSC) [64] and gas chromatography (GC) [124], [65] and has been published on different *N. crassa* slime strains (FGSC #1118 published by [125], further used by [120], lipid analysis by [64, 124], FGSC #326 [65]). The phospholipid distribution differs between the publications but shows that *N. crassa* expresses poly-unsaturated fatty acids [64] which *S. cerevisiae* lacks [50, 60, 126], and has additional and more complex sphingolipids [32, 41],Fig 1.4.

The network-like microdomain structure of *N. crassa* plasma membrane has not been studied as widely as *S. cerevisiae* but lipid ordered domains have been found in the plasma membrane of *N. crassa* WT as well as *N. crassa* slime [127]. Specific lipids have also been implicated for the function of Pma1, in particular ceramides are necessary for the oligomeric state of Pma1 in yeast [56] and anionic lipids for ATPase activity [128]. The recent structural analysis of the Pma1 hexamer revealed lipid interactions of a central lipid plug in the *S. cerevisiae* Pma1 hexamer [105] and potential lipid mediated monomer interactions and a proton attracting funnel in the *N. crassa* Pma1 hexamer [104].

This thesis uses *N. crassa* slime mutant FGSC #4761 (*fz;eg;os-1*) [121], the lipid composition of which has not previously been analysed with mass spectrometry. Furthermore the lipid analysis of any *N. crassa* Pma1 has not been reported beforehand. Given the recent interest and technical advances in lipidomics analysis, a more updated approach to the analysis is needed and will highlight differences and give insights into the nature of co-purified lipids with Pma1 hexamer. If not otherwise specifically stated, the following analysis is focused on whole cells, plasma membrane and purified Pma1 from this *N. crassa* slime mutant and will further be referred to as *N. crassa*.

1.5 Membrane mimetics for the purification of membrane proteins

Due to their wide range and different components, biological membranes are complex and the membrane proteins of interest are often only present in very small numbers. Experimental methods for structural biology and biophysics generally require homogenous samples with high protein concentration. Unless at a very high abundance in native

membrane (e.g. bacteriorhodopsin [129]), proteins must be extracted from the membrane and purified before experimental characterisation. Furthermore membrane proteins are difficult to study, because they rely on solubilisation and purification systems that should not interfere with their stability and activity. For this different systems have been developed that either replace the lipid environment of proteins by detergents or amphipols and allow for a reconstitution of detergent-solubilised membrane protein in a lipid environment using scaffolding platforms (liposomes, bicelles, Picodisc and (Peptide-Nanodisc) or directly extract membrane proteins with their natural membrane environment using polymers (outlined in Fig 1.7 and reviewed in [130]).

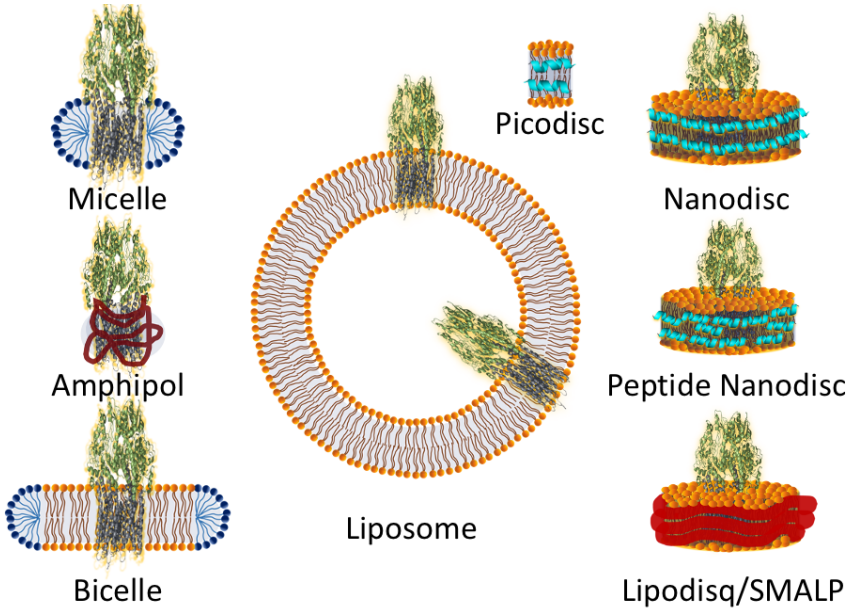

Figure 1.7: Membrane mimetics for biophysical studies of membrane proteins
Detergents and amphipols replace the native lipids and mimic a lipid environment. After detergent solubilisation, membrane proteins can be reconstituted into a lipid environment using scaffolding platforms like liposomes, bicelles, Picodisc and (Peptide-) Nanodisc. Polymer-based methods like Lipodisq/SMALPs allow the extraction of membrane proteins directly from the host membrane in which they are expressed. Colour-coded are membrane lipids (orange), detergents (dark blue), amphipholes (dark red), protein-based stabilising scaffolds (light blue), and polymer-based scaffolds forming polymer-lipid nanoparticles (red). Reproduced from [130]

Detergents are amphipathic molecules with a polar head group and a nonpolar tail, which are able to form spherical micellar structures above the critical micellar concentration (CMC). Detergents can be distinguished according to their charge as ionic (anionic, cationic, zwitterionic) or non-ionic, and by their hydrophilic and hydrophobic components,

such as carboxylates or sugar molecules and hydrocarbon open chains (aliphatic chains) or non aromatic rings (alicyclic structures) respectively (Fig 1.8, reviewed in [131]).

Non-ionic detergent like DM (n-decyl-β-maltoside) and DDM (n-dodecyl-β-D-maltoside) are relatively mild and non denaturating and usually do not break protein-protein interactions. However DM and DMM have short chains that can have a deactivating effect on the protein's function [132] (Fig 1.8 B). Ionic detergents like SDS (sodium-dodecyl-sulphate) solubilise membrane proteins efficiently but often with a denaturating effect. Whereas bile acid salts such as DOC (Sodium deoxycholate) are also charged but are milder and do not generally deactivate the protein's function [132] (Fig 1.8 A).

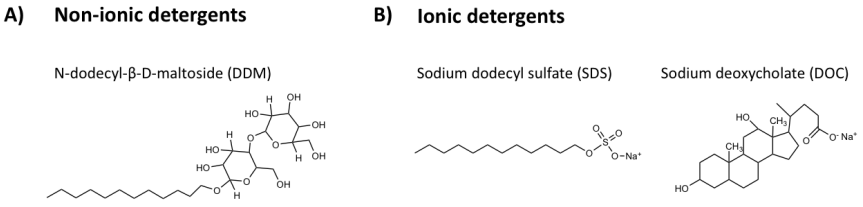

Figure 1.8: Types of detergent used in membrane protein studies
Detergent used in the study of membrane protein with examples that were used in this thesis.

After solubilisation and purification of membrane proteins, excess of detergent can be removed e.g. by dilution or dialysis, hydrophobic adsorption to biobeads or size exclusion chromatography [133]. Detergents are widely used as the primary step for reconstitution of the membrane proteins into other membrane-mimicking systems as described below. Detergents are capable, while interacting with membranes, to isolate membrane proteins forming micellar structures around them and allowing for their solubility in an aqueous environment and are widely used in membrane protein research [132] but provide disadvantages. The solubilisation and consecutive purification of the membrane proteins is disrupting interactions between protein and native lipids which may be accompanied by a loss of activity and/or stability of the protein [134]. Occlusion of binding sites for ligands/substrates in the membrane protein [135] and the limited ability of detergent micelle to mimic the lateral pressure profile of a native membrane may also lead to an

inability of the protein to function [136].

There are other methods to study membrane proteins, such as discoidal lipid-based nanoparticles. These nanoparticles provide a lipid environment for membrane proteins, which is encapsulated by either peptides or polymers. In peptide-based discs or Nanodiscs [137,138] peptides such as the membrane scaffold protein (MSP) saposin [139] are used. Polymers such as SMA are used to form SMA-lipid-nanoparticles known as Lipodisq (LQ) [140] or SMALPs [141]. Both these techniques can provide more monodisperse particles and better mimic the membrane allowing access to both sides of the protein within the same aqueous environment.

After purification with detergent, membrane proteins can be reconstituted into the nanodiscs particles which are made of a lipid bilayer with controlled lipid composition. These coin-shaped particles are monodisperse and can mimic membranes better due to their controlled lipid composition and lateral tension; they still depend on detergents during preparation [137,138].

Hydrolysed copolymer of styrene and maleic anhydride (SMA) (Fig 1.9 A) can be used to solubilise membranes and form SMA-lipid-nanoparticles [140,141], in the literature referred to as Lipodisq (LQ) [140] or SMALP (SMA-lipid particles) [142]. When added to a lipid mixture and at a controlled pH SMA forms approximate 10 nm disc shaped lipid particles, where the polymer wraps around the lipids and encloses membrane proteins [143] which can be further purified as outlined in 1.9 E. With this method it is possible to solubilise membrane proteins directly from their native membrane as described in [144–146] without the use of additional detergents.

Since the initial solubilisation of native *E. coli* PagP as well as Bacteriorhodopsin [141] the field has massively expanded and has demonstrated the utility of SMALPs in a variety of biophysical techniques both in better understanding protein structure and interaction (reviewed in [147]). To this date SMA solubilisation has been effectively used

for a range of membrane proteins, such as ABC transporters [148], G protein-coupled receptors [149] (reviewed in [150]) and ion channels [151, 152].

Additionally to SMA several alternative polymers of have become available such as poly(diisobutylene-*alt*-maleic acid) (DIBMA) [153] (Fig 1.9 C), in which the aromatic groups of SMA were replaced by aliphatic hydrophobic group, and poly(methacrylate) PMA [154] (Fig 1.9 D) which contains no styrene or maleic group. Furthermore SMA based derivatives have been developed such as SMA-ED [155], SMA-SH [156], SMA-EA [157, 158]), SMI [159], SMA-QA [157, 160] (as outlined in Fig 1.9 B), the styrene based (poly-acrylic-acid-co-styrene) AASTY [161] and others (reviewed in [162]) but most of these alternative polymers are not yet commercially available [163].

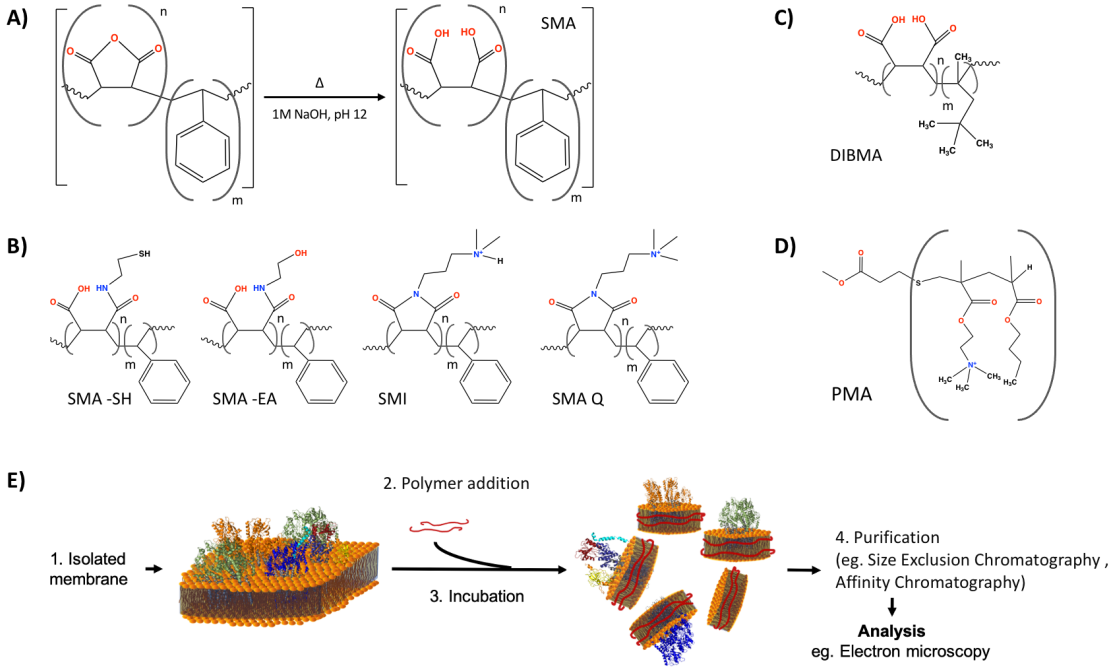

Figure 1.9: Polymer solubilisation of membrane proteins
A-D) Structural formulae of commercially available polymers. A) structural formulae of styrene-maleic anhydride (SMA) (shown are non-hydrolysed and hydrolysed versions, the ratio of styrene (m) to maleic acid (n) can vary between 2:1 to 4:1 (reviewed in [164]), B) different modified types of SMA: SMA-SH, SMA-EA, SMI, SMA Q, (adapted from [157, 165], reviewed in [162]) and C) maleic based polymer DIBMA and D) PMA. E) Cartoon of membrane protein purification using SMA, a polymer (e.g. copolymer of styrene-maleic anhydride (SMA) can be used to solubilise and purify membrane proteins for structural analysis directly from their host membrane [141]. Addition of polymers to the membrane forms polymer-nanoparticles encapsulating the membrane protein, adapted from [166].

The development of alternative polymers has been necessary since SMA has been shown to be limited by incompatibility with low pH (<6.5) and sensitivity to divalent cations (>5 mM) and heterogeneity of formed disc size [145, 167, 168]. The alternative DIBMA also precipitates at acidic pH but is less affected by cations hence an increased potential compatibility with ATPase activity [153]. The characterisation of PMA is more limited up to this date, but it has been successfully used for functional solubilisation of a GPCR expressed in Sf9 cells (NTSR1) [169].

Despite these limitations, polymer lipid-nanoparticles have been shown in successful cases of polymer solubilised membrane proteins to be compatible with a wide range of biophysical techniques which include microscale thermophoresis (MST) [170, 171], circular dichroism (CD) spectroscopy (e.g. [148, 171, 172]) , fluorescence spectroscopy (e.g. [173]), electron paramagnetic resonance (EPR) [174, 175], nuclear magnetic resonance (NMR) [141], liquid chromatography mass spectrometry (LC/MS) [115], hydrogen deuterium exchange (HDX) mass spectrometry [176], native mass spectrometry [177], tandem mass spectrometry (MS/MS) (e.g. [172, 178]), X-Ray crystallography [167] and electron microscopy (EM) (e.g. [179]). Additionally to structural membrane protein research, SMA is also used in drug delivery studies [180].

The ability to solubilise membrane proteins directly from membranes, without additional detergents, makes these polymers advantageous over other reconstitutions, allowing for the retention of native lipids that are potentially important for protein structure and function. Cryo EM structures of transmembrane proteins using SMA (AcrB expressed in *E. coli* [181], ACII expressed in *F. johnsoniae* [179]) or DIBMA (YnaI expressed in *E. coli* [182]) to solubilise bacterial membranes revealing co purified lipids such as PE or PE/PC respectively. Furthermore, the cryo EM structure of SMA solubilised SLAC1 ion channel from fungal membrane (*S. pombe*) revealed sphingolipids [178].

1.6 Aim of the thesis

Studying membrane proteins in isolation represents a major challenge, as using detergents for extraction can alter protein stability, activity, and oligomeric assemblies. In this thesis the *N. crassa* P-Type ATPase Pma1 is studied. Several membrane mimetic polymers are explored for solubilisation and purification of *N. crassa* Pma1 as an alternative to detergent solubilisation. The aim is to enhance the protein yield from *N. crassa* membranes while preserving the native lipid and environment.

In **Chapter 3**, the ability of commercially available polymers to solubilise *N. crassa* membranes is investigated. A small scale strategy to best study solubilisation efficiency and to identify suitable parameters for solubilisation is devised and tested for comparison of initial membrane solubilisation by polymers on *E. coli* and *S. cerevisiae* membranes. With this method suitable conditions for the polymer solubilisation of *N. crassa* membrane are identified.

In **Chapter 4**, the purification and characterisation of polymer-solubilised native Pma1 from *N. crassa* is explored.

In **Chapter 5**, the lipid composition of *N. crassa* Pma1 hexamer is analysed with LC/MS. As a starting point the initial lipid composition of whole cell *N. crassa* slime is re-evaluated in comparison to *S. cerevisiae* using this contemporary methodology. Furthermore the lipid composition changes during the purification process of detergent-solubilised Pma1 hexamer is analysed.

Chapter 2

Material and Methods

2.1 Cell cultivation and membrane preparation

2.1.1 *N. crassa* plasma membrane preparation

Native Pma1 was obtained from *N. crassa* slime Fungal Genetics Stock Center (FGSC, Kansas, U.S.A.) #4761 in the Bublitz group and prepared with assistance from Dr Sabine Heit, as described previously [104]. The preparation protocol is schematically outlined in Fig 2.1 and buffers used in Table 2.1.

Table 2.1: *N. crassa* plasma membrane preparation buffer list

N. crassa growth medium	Vogel's medium [183], 2 %(w/v) mannitol, 0.75 %(w/v) yeast extract (Difco), 0.75 %(w/v) nutrient broth (Difco)
Buffer A	50 mM Tris pH 7.5, 10 mM $MgSO_4$, 250 mM mannitol
Lysis buffer	10 mM Tris pH 7.5, 1 mM $MgCl_2$, 1 mM $CaCl_2$, 1.5 µg/ml chymostatin, 1 µg/ml DNase I, 1.2 % sodium deoxycholate (DOC)
Buffer B	10 mM Tris pH 7.5, 1.5 µg/ml chymostatin

Briefly, cell wall-less *N. crassa* strain [Fungal Genetics Stock Center (FGSC), strain #4761] was grown (at 30 °C or 35 °C in *N. crassa* growth medium) to an $OD_{600\,nm}$ of 1, harvested by centrifugation (700g, 15 min, 4 °C) and resuspended in ice-cold Buffer A. The membranes were washed and were agglutinated with 0.5 mg/ml Concanavalin A (ConA) in Buffer A (10 min, RT and 10 min on ice). Agglutinated cells were pelleted by centrifugation (200g, 6 min, 4 °C) and washed once with ice-cold buffer A. Cells were

lysed in ice-cold Lysis Buffer using a glass homogeniser. The membranes were pelleted by centrifugation (14 000g, 30 min , 4 °C), resuspended in Buffer B containing 0.6 % DOC, and centrifuged again (14 000g, 30 min , 4 °C) and resuspended in DOC-free Buffer B. After centrifugation (14 000g, 30 min, 4 °C), the pellet was resuspended in Buffer B containing 0.5 M α-methyl mannoside and incubated for 5 min at 30 °C to dissociate ConA from the plasma membrane. The dissociated membranes were diluted with ice-cold Buffer B, pelleted by centrifugation (14 000g, 30 min , 4 °C) and washed once with ice-cold Buffer B. After resuspension in ice-cold Buffer B, membranes were aliquoted and flash frozen in liquid nitrogen and stored at −80 °C until further use. Additionally an alternative plasma membrane preparation protocol was tested (in collaboration with Dr Sabine Heit) analogously to described above but where the DOC wash was replaced by a high molar NaCl wash (step wise washes with 20 mM HEPES with 2 M, 1 M, 0.5 M and 0 M NaCl), these membranes are further referred to as noDOC or PM-NaCl.

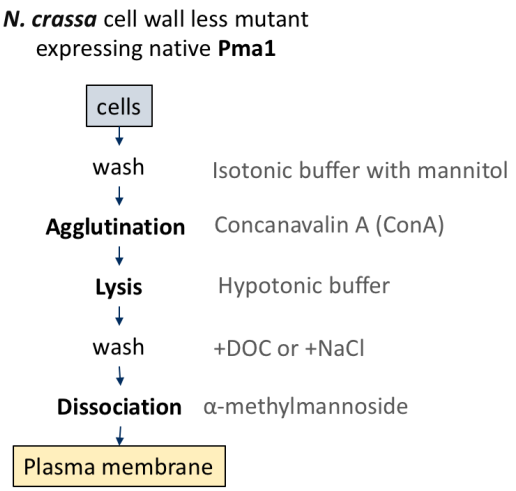

Figure 2.1: Schematic of *N. crassa* plasma membrane preparation following [104]

2.1.2 *E. coli* membrane preparation

MprF-His_6 and $MprF^{1-545}$-GFP-Strep expressed in *E. coli* were kindly provided by Matthew Hankins (Bublitz group). Briefly, MprF-His_6 and $MprF^{1-545}$-GFP-Strep plasmids were expressed in C-41 *E. coli* cells and grown in Terrific Broth (TB, Table 2.2). Expression was induced with 0.5 mM Isopropyl β-D-1-thiogalactopyanoside (IPTG) and

grown for 15 h at 20 °C. Cells were harvested by centrifugation (4500g, 20 min, 4 °C). The cell pellets were resuspended in 20 mM HEPES buffer pH 7.5, and cells were lysed using a cell disruptor (Constant Systems, Northants, UK) operated at 30 kpsi. Membranes were isolated by ultracentrifugation (100 000g, 1 h, 4 °C) and resuspended in 20 mM HEPES buffer. Membranes were aliquoted and flash frozen in liquid nitrogen and stored at −80 °C until further use.

Table 2.2: *E. coli* membrane preparation buffer list

Terrific Broth (TB)	0.017 M KH_2PO_4, 0.72 M K_2PO_4, 12 g/l tryptone, 24 g/l yeast extract, 0.4 %(v/v) glycerol

2.1.3 *S. cerevisiae* membrane preparation

The *S. cerevisiae* membrane preparations containing N. crassa Pma1-Strep (NcPma1-Strep) were kindly provided by Maxwell Guerts (Bublitz group). Briefly, galactose induced overexpression of *N. crassa*-Pma1 was carried out in *S. cerevisiae* W303.1b gal4-Δpep4 strain (ATCC 201238, provided by the Bublitz group) (contains an additional lac operon inducer - gal4 - and deletion of vacuolar protease A - Δpep4) grown according to a published protocol [184], used media and buffers are outlined in Table 2.3.

Table 2.3: *S. cerevisiae* membrane preparation buffer list

Minimal Medium-Ura selection media (MM)	22 g/l yeast nitrogen base (without amino acids, with ammonium sulphate), 64 g/l (D^+)-glucose, 1.9 g/l yeast drop out media without uracil
S. cerevisiae lysis buffer	50 mM Tris pH 7.6, 20 %(v/v) glycerol, 3 mM $MgCl_2$, 5 mM BME, 50 µM ATP protease inhibitor 1 tab/100 ml, 100 mM KCl

Firstly, the strains were grown in 10 ml Minimal Medium-Ura (MM) selection media overnight at 30 °C shaking at 120 rpm. For scaling up, the cells were diluted in 500 ml MM and grown for two more days at 30 °C. This culture was used to inoculate 500 ml of MM + 0.5 % glucose at a starting $OD_{600\,nm}$ of 0.1 and grown at 30 °C shaking

to an $OD_{600\,nm}$ of 1. *N. crassa* Pma1-Strep expression was induced by adding 2 % galactose and grown for 48 h before harvesting by centrifugation (40 000g, 1 h, 4 °C). Cells were resuspended in *S. cerevisiae* lysis buffer and lysed using a cell disruptor (Constant Systems, Northants, UK) operated at 40 kpsi. Membranes were isolated by centrifugation (40 000g, 1 h, 4 °C). The pellet was washed with 20 mM HEPES pH 8 or 7, by centrifugation (40 000g, 1 h, 4 °C) (3 times) and resuspended at a final concentration of 60 mg/ml (wet weight) in 20 mM HEPES pH 8 or 7, flash frozen and stored at −80 °C until further use.

2.2 Detergent and Polymer solubilisation

2.2.1 Membrane preparation for polymer solubilisation

Membranes from *N. crassa*, *S. cerevisiae* or *E. coli* were thoroughly washed (3 times) in 20 mM HEPES buffer at pH 7 or 8 and centrifuged (40 000g, 30 min, 4 °C). The wet weight of the membranes was estimated by measuring the weight of the pellet after removal of the supernatant. The membranes were resuspended at a final concentration of 60 mg/ml wet weight membrane in 20 mM HEPES at pH 7 or 8 and kept on ice or flash frozen and stored at −80 °C until further use.

2.2.2 Polymer preparation

SMA 2:1 and SMA 3:1 were kindly provided by Malvern Cosmeceutics (Malvern, UK) and hydrolysed from their anhydrous form following the protocol described by [148]. DIBMA was kindly provided by Prof. Sandro Keller (University Gratz, Austria). SMA and DIBMA polymers were washed with ddH_2O and dialysed overnight to remove excess salt and to adjust the pH before lyophilisation. 20 mM HEPES buffer was added to the resulting powder to achieve a final polymer concentration of 100 mg/ml (10 % w/w) and pH adjusted. Polymers were prepared with assistance from Dr Henry Sawczyc and Dr Juan Bada. PMA was kindly provided by Avanti (Alabaster, AL, U.S.A.) and diluted to a polymer concentration of 100 mg/ml (10 % w/w). Polymer solutions were sealed and stored at RT or −20 °C in the case of PMA until further

use. Details on the average molecular mass and expected ratio of components of the polymers used are given in Table 2.4.

Table 2.4: Details on used polymers in this thesis

Polymer	expected ratio of components	av. molar mass (kDa)	Ref	Gifted from
SMA 2:1	2:1 styrene:maleic acid	∼9.5	[185]	Malvern Cosmeceutics (Malvern, UK)
SMA 3:1	3:1 styrene:maleic acid	∼9.5	[185]	Malvern Cosmeceutics (Malvern, UK)
DIBMA	1:1 diisobutylene:maleic acid	∼12	[153]	Prof. Sandro Keller (University Gratz, Austria) Trade name Sokalan CP9 (BASF, Germany)
PMA	0.4:0.6 methacroylcholine: butyl methacrylate	∼4.7	[154]	Avanti (Alabaster, AL, U.S.A.) Polymer: N−C4−40−4.7 Lot: 880134P-500MG-A-010

20 mM HEPES buffer with 1M NaCl was prepared in the desired pH and used as a stock solution for adjustment to the right salt concentration.

2.2.3 Small scale solubilisation assay of *N. crassa* membrane by light scattering measurements

For light scattering measurements, eight *N. crassa* membrane dilutions were prepared for final membrane concentration from 1 mg/ml to 60 mg/ml total membrane concentration (after adding polymer) (Table 2.5). For additional homogenisation, *N. crassa* membrane samples underwent three freeze-thaw cycles before use. 27.8 mg 1,2-dimyristoyl-sn-glycero-3-phosphocholine (DMPC) lipid (powder) was dissolved in 600 µl 20 mM HEPES pH 8 buffer. From this stock solution, 12 dilutions were made from 0.46 mg/ml to 46 mg/ml final lipid concentration (after adding polymer) (Table 2.6).

Table 2.5: Dilution series of *N. crassa*
N. crassa membrane dissolved at a final concentration of 2.65 vol% SMA 3:1

membrane weight mg/ml	60	40	30	20	15	10	5	1

Table 2.6: Dilution series of DMPC
DMPC dissolved at a final concentration of 2.13 vol% SMA 3:1

Lipid mg/ml	46	41.4	36.8	32.2	27.6	23	18.4	13.8	9.2	4.6	2.3	0.46

Both dilution series were prepared directly in a 96-well plate. Absorbance was measured at 350 nm using a BMG LABTECH CLARIOstar plate reader at 30 °C. SMA 3:1 was added after 5 min for a final concentration of 2.67 vol% or 2.13 vol% for *N. crassa* and DMPC, respectively, and incubated at 30 °C for 10 min before measurement. Afterwards, the temperature was increased to 37 °C and measured at ∼35 min. $A_{350\,nm}$ was measured every 10–15 min, and to aid mixing before each measurement the well plate was shaken for 3 min at 300 rpm the final measurement was taken at ∼75 min.

2.2.4 Small scale membrane solubilisation assay by total protein quantification

Fig 2.2 describes the workflow of the sample preparation for the small scale solubilisation assay.

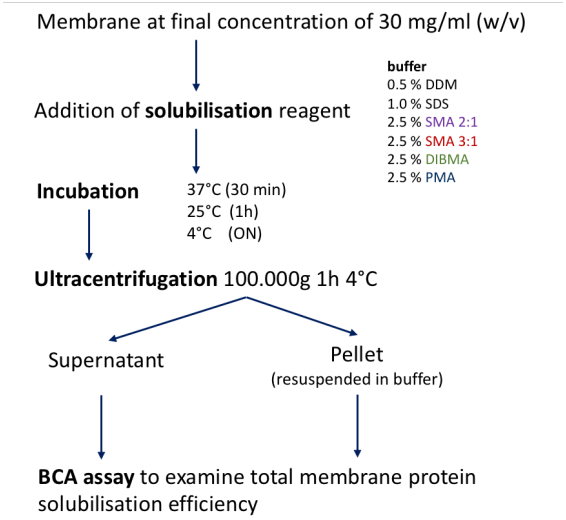

Figure 2.2: Schematic workflow of the small scale solubilisation assay using total protein quantification

2.2.4.1 Sample preparation

For the initial solubilisation screening, 0.25 ml aliquots of membrane (*E. coli*, *S. cerevisiae* or *N. crassa*, at 60 mg/ml wet weight concentration) were thawed on ice. A final concentration of 20 nM HEPES pH 7 or 8 and 0.1 or 0.5 M NaCl were added from 1 M stocks. The final membrane concentration for solubilisation was 30 mg/ml wet weight. The solubilisation agent was added at a final concentration (w/v) of 2.5 %

for polymers, 1 % for SDS, 0.5 % for DDM and as a negative control, 20 nM HEPES buffer. The samples were individually homogenised using homogenising pestles (Thomas Scientific). Afterwards, each sample was split into aliquots of 160 µl and separately incubated for different durations at different temperatures: 4 °C overnight, 25 °C for 1 h or 37 °C for 30 min, leading to 12 different conditions tested for each solubilisation agent. To stop solubilisation and to separate the solubilised fraction, the samples were centrifuged (100 000g, 1 h, 4 °C). The supernatant was carefully collected, and the remaining pellet was resuspended in 160 µl 20 nM HEPES buffer. The protein concentration of each sample was measured using the BCA assay (Section 2.2.4.2). The remaining sample was flash frozen and kept at −80 °C in preparation for lipid analysis, SDS PAGE, immunoblotting or activity assays.

2.2.4.2 Protein concentration determination via BCA Assay

To determine the protein content of the samples, the Pierce™BCA Protein Assay Kit was used in a microplate procedure. 10 µl of the sample (supernatant or re-solubilised pellet) were pipetted in triplicate into wells on the 96-well plate. Mixtures of the respective buffer with solubilisation agents were used as negative control and all samples were compared against a protein standard curve of BSA as per the manufacturer's procedure. The typical 96-well plate layout is given in Fig 2.3. 200 µl assay reagent was added to each well. The incubation temperature of the BCA assay and time were modified according to the manufacturer's instructions for the "enhanced protocol". The 96-well-plate was incubated for 30 min at 60 °C. $A_{562\,nm}$ was measured on a CLARIOstar plate reader (BMG Labtech).

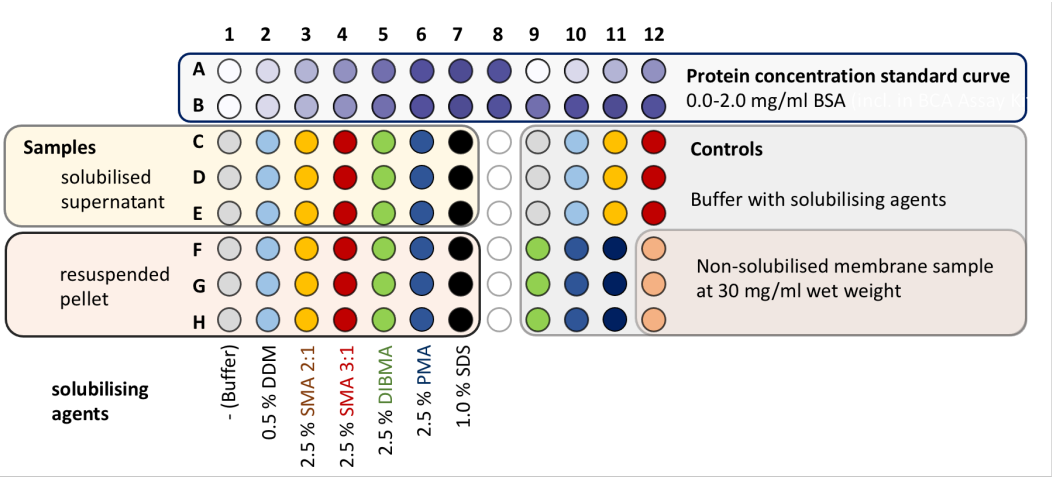

Figure 2.3: The pipetting scheme for a typical 96-well plate
Wells in A and B: Protein standard curve (included in BCA Assay) ranging from 0.0–2.0 mg/ml; C-H 1-7: solubilised samples (solubilised supernatant and resuspended pellet), C-H 9-12 buffer with solubilisation agent as negative controls, F, G, H 12:membrane sample (30 mg/ml wet weight).

2.2.4.3 Calculation of relative protein solubilisation efficiency

The absorption values of supernatant and pellet samples were measured in triplicates (on one 96-well plate) and averaged. The standard deviation was calculated for each sample. The relative protein solubilisation efficiency (E_{rel}), defined as the percentage of solubilised membrane protein as compared to total membrane protein, was calculated based on the $A_{562\,\mathrm{nm}}$ values of the supernatant (A_{super}) and pellet (A_{pellet}), corrected for the background absorption (A_{buffer}).

$$E_{\mathrm{rel}} = \frac{A_{\mathrm{super}} - A_{\mathrm{buffer}}}{A_{\mathrm{super}} + A_{\mathrm{pellet}} - 2A_{\mathrm{buffer}}} \tag{2.1}$$

Details on the development of the formula are given in the appendix (Appendix A.1, equation A.6). The total standard deviation is given by derivation of the relative solubilisation using the standard deviation of each sample(see Appendix A.1).
Comparison of the results from all 12 solubilisation conditions and all solubilisation agents were performed in Microsoft Excel and Python.

2.2.5 Polymer solubilisation of membranes

For further experiments, the polymer solubilisation of membranes was achieved in 20 mM HEPES, 100 mM NaCl, pH 8 at a final membrane concentration of 30 mg/ml (wet weight) with 2.5 % total polymer concentration, incubated at 37 °C for 30 min and unless otherwise stated. The solubilised fraction was then separated by centrifugation (100 000g, 1 h, 4 °C). The supernatant was collected carefully, and in case it was not immediately used, stored on ice or flash frozen and kept at −80 °C.

2.3 Protein purification

2.3.1 Detergent purification of *N. crassa* Pma1

Detergent-purified Pma1 was kindly provided by Dr Sabine Heit (Bublitz group). A detailed purification protocol was recently published [104], the used buffers are outlined in Table 2.7. Briefly, solubilisation of *N. crassa* membranes was achieved by incubation for 1 h at 12–19 °C with 0.225 % (25x CMC) β-dodecyl-maltopyranoside (DDM) in Pma1 detergent solubilisation buffer at a total membrane protein concentration of 2 mg/ml, determined by BCA assay. To separate the solubilised fraction the sample was ultracentrifuged (100 000g, 1 h, 4 °C). The sample was further purified with a glycerol or sucrose density gradient from 20–40 % (w/v) (5 % steps) and a Q-HP anion exchange (AEX) column (GE Healthcare). For final purification, the sample was subjected to size-exclusion chromatography (SEC) on a Superose 6 Increase 10/300 (GE Healthcare) column. Desired fractions were collected and concentrated, flash frozen and stored at −80 °C until further analysis.

Table 2.7: List of buffers for detergent solubilisation of Pma1 from *N. crassa* plasma membrane

Pma1 detergent solubilisation buffer	10 mM Tris pH 7.5, 150 mM NaCl, 1 mM Na_2–ATP, 5 mM $MgSO_4$, 0.1 mM Na_3VO_4, 2 µg/ml chymostatin
Pma1 detergent SEC buffer	50 mM MES/Tris pH 6.5, 200 g/l glycerol, 50 mM KCl, 5 mM $MgSO_4$, 2 mM EDTA, 1 mM DTT, 2 µg/mL chymostatin, 0.15 mg/mL DDM

The following detergent-solubilised and purified *N. crassa* Pma1 samples (Table 2.8) were prepared and provided by Dr Sabine Heit for lipidomic analysis (Section 2.5). Pma1 was purified from plasma membranes of *N. crassa* slime grown at 30 °C or 35 °C. Furthermore, in some samples the anion exchange (AEX) step was omitted. For the AEX purified samples, different fractions of the consecutive SEC were collected. Pma1 identity was confirmed by immunoblotting and oligomeric status was determined by native PAGE (Dr Sabine Heit).

Table 2.8: Detergent solubilised and purified Pma1 samples analysed further by lipidomics analysis

Sample name	*N. crassa* growth temp.	AEX	Density gradient	SEC pool	sample volume	protein concentration
Pma1 hexamer, (30 °C, glycerol)	30 °C	omitted	glycerol	Pool 1 (hexamer)	20 µl	1.3 mg/ml
Pma1 hexamer, (30 °C, sucrose)	30 °C	omitted	sucrose	Pool 1 (hexamer)	10–12 µl	4 mg/ml
Pma1 hexamer, (35 °C, glycerol, AEX)	35 °C	yes	glycerol	Pool 1 (hexamer)	20 µl	1.9 mg/ml
Pma1 lower oligomer, (35 °C, glycerol, AEX)	35 °C	yes	glycerol	Pool 3 (lower oligomer)	20 µl	6.0 mg/ml

2.3.2 Polymer purification of *N. crassa* Pma1

N. crassa plasma membrane (in 20 mM HEPES, 100 mM NaCl, pH 8) were solubilised at a final concentration of 40 mg/ml wet weight membrane with 2.5 % SMA 3:1 (final concentration) for 30 min at 37 °C under gentle rotation. The small volume of 500 µl contained about 20 mg wet weight membrane and ∼2 mg total membrane protein determined by BCA Assay. After separating insoluble material with ultracentrifugation

(100 000g, 1 h, 4 °C), the supernatant was subjected to a size exclusion chromatography (SEC) using a Superose 6 increase 16/60 column, 20 mM HEPES, 100 mM NaCl, pH 8. For further purification, selected fractions were pooled, concentrated, and subjected to a second SEC (Superose 6 increase 10/300). Comparative SEC traces of detergent-purified Pma1 were provided by Dr Sabine Heit.

2.4 Protein detection and quantification methods

2.4.1 SDS Gel Electrophoresis PAGE

Samples for SDS PAGE were prepared by mixing 15 µl sample with 5 µl lithium dodecyl sulphate (LDS) and were run on NuPAGE™ 10 % or 12 % Bis-Tris gels (Life Technologies) in NuPAGE™ MES SDS running buffer (Life Technologies). Self-cast gels were used with 25 mM Tris base (Sigma), 0.25 M glycine and 0.1 % SDS. Gels were run at 180 V, 40 mA for 40 min and were either stained in Coomassie or by silver staining. As Ladder SeeBlue™ Plus 2 (Thermo Fisher) Pre-stained Protein Standard or PageRuler™ Prestained Protein Ladder were used.

2.4.2 Coomassie staining

Gels were stained with Coomassie blue dye using InstantBlue (C.B.S Scientific Company, San Diego, USA) protein stain. The gel was stained at room temperature (RT, 25 °C) for a minimum of 30 min under gentle agitation and further destaining in ddH_2O.

2.4.3 Silver staining

To detect smaller quantities of protein that were otherwise not detected by Coomassie, gels were stained with more sensitive silver staining using a Bio-Rad Silver Stain Plus kit (Bio-Rad Laboratories, Hercules, USA). To avoid background staining, the silver staining protocol was modified so that the washing step with water was extended to 1 h and gels were left in acetic acid for up to 1 h.

2.4.4 Immunostaining /Immunodetection assays

Table 2.9 outlines the buffers used in the following immunodetection assays.

Table 2.9: Buffer list, blot development and immunostaining

Phosphate-buffered saline (PBS)	137 mM NaCl 2.7 mM KCl 10 mM Na_2HPO_4 1.8 mM KH_2PO_4
PBST	PBS + Tween 20 (0.1 % by volume) (Sigma)
Western Blot transfer buffer	25 mM Tris pH 8.3, 192 mM glycine
"standard" blocking solution	PBST with 5 % skim milk powder

For immunostaining the following antibodies and protein conjugates (further collectively referred to as antibodies, Table 2.10) were used in "standard" blocking solution (PBST with 5 % milk powder), if not otherwise stated.

Table 2.10: Antibodies (AB) used for immunostaining

Anti-Pma1 antibodies		
Primary Anti Pma1 AB	poly clonal anti Pma1 from rabbit, (MELON Gel purified, gift from Kenneth Allen, Yale, USA)	used at a dilution of 1:3.000
Secondary Pma1 AB	goat anti-rabbit-HRP (Sigma Aldrich)	used at a dilution of 1:2.000
Anti-His antibodies		
Primary AB	H1029 mouse anti-His (Sigma Aldrich)	used at a dilution of 1:3000
Secondary AB	anti-mouse-HRP (Sigma Aldrich)	used at a dilution of 1:2500
Strep-Tag binding protein conjugate (Anti-Strep)		
Anti-Strep	Strep-Tactin® HRP Conjugate (IBA Lifesciences)	used at a dilution of 1:4000

2.4.5 Western Blot

Proteins were separated by SDS-PAGE and transferred to a PVDF membrane (GE Healthcare) by semi-dry transfer (Trans-Blot, BioRad) following the manufacturer's protocol at 100 mA for 1.5 h, using Western Blot transfer buffer. The membrane was subsequently immunostained and visualised as described in Section 2.4.7.

2.4.6 Dot blot

After activating the PVDF membrane with methanol, triplets of 3 drops of the sample were added to the membrane and allowed to dry. The membrane was subsequently immunostained and visualised as described in Section 2.4.7.

2.4.7 Blot development and Immunostaining

After blotting, the membranes were immunostained. The membranes were incubated in various blocking solutions (see Table 2.11) for 1 h at 4 °C with shaking, before incubation with the primary antibody overnight at 4 °C with shaking. The membranes were washed three times with each 10 ml PBST for 10 min shaking at 25 °C. Afterwards, the membranes were incubated with the secondary antibody solution, shaking for 2 h at 25 °C. The membranes were washed three times with 10 ml PBST for 10 min shaking at 25 °C. Antibodies were visualised using the enhanced chemiluminescence (ECL) method (Pierce™ ECL Western Blotting Substrate, Thermo Science) following the manufacturer's protocol. Three different blocking solutions were tested for anti-Pma1 immunostaining. The blocking solutions and the antibodies were prepared in one of the following blocking buffers in Table 2.11.

Table 2.11: Tested blocking buffers for anti-Pma1 immunoblotting

"Standard"	PBST with 5 % milk powder
"Enhancer"	Immobilon® signal enhancer (Millipore, WBSH0500)
"Optimised"	PBST with 5 % milk powder and 25 mM L-Arginine, to mask unspecific binding, following suggestions from [146]

To overcome the immunostaining issues with the anti-Pma1 antibody, other protocols were tried, as detailed in the Appendix Section A.5(Table A.3).

2.4.8 ATPase activity assay (Baginski assay)

To explore the activity of Pma1, the Baginski Assay [186] was used. ATPases hydrolyse ATP in a Mg^{2+} dependent manner [186] ATP $\longrightarrow$ ADP + P_i) (Fig 2.4 A). The Baginski assay measures the released free phosphate (P_i). To exclude the measurement

of other ATPases, several specific inhibitors are added to inhibit their activity [187]: Azide (NaN_3) as the inhibitor of mitochondrial ATPase [188], nitrate (KNO_3) as the inhibitor of vacuolar ATPases and molybdate ($(NH_4)_2MO_4$) as the inhibitor of nonspecific phosphatases [188]. The concentration of free Pi in the sample can be colourimetrically determined using a molybdenum reaction, where a blue complex is formed between Molybdenum and free orthophosphate after reduction with ascorbic acid (Fig 2.4 B). The colour formation can be quantified by absorption measurements at 860 nm against a phosphate standard and is proportional to the activity of the ATPase.

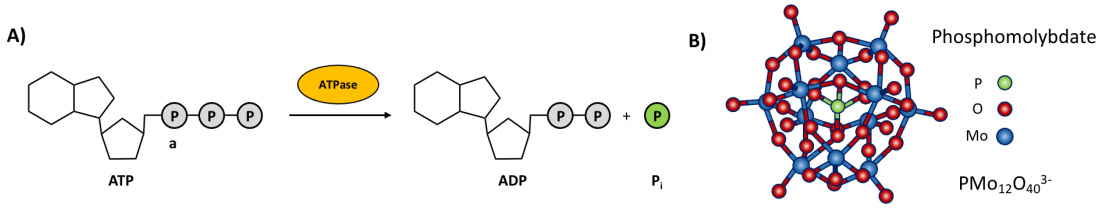

Figure 2.4: Colorimetric reaction, ATPase activity measurement of P-Type ATPase with the Bagsinki assay (Adapted from [186])
A) ATPases hydrolyse ATP which releases free phosphate (Pi). In the Baginski assay [186] Molybdenum ($Mo\,VI^{+}$) in an acidic environment forms with Pi a complex of phosphomolybdate ion ($PMo_{12}O_{40}{}^{3-}$, adapted from [189], B) which is reduced by ascorbic acid to form a blue-colored $PMo_{12}O_{40}{}^{7-}$ ion, is further stabilised by the addition of arsenic. The colour formation can then be quantified by absorbance at 860 nm on a spectrophotometer.

The Baginski assay is prepared in a 96-well plate, following the originally published protocol [186], slightly modified by Dr Sabine Heit, used buffers are outlined in Table 2.12. For the assay preparation, 15 µl ddH_2O are pipetted in all sample wells and 15 µl 10 % SDS per well for negative controls. 5 µl sample are added in triplicate or 5 µl phosphate standards in duplicates or triplicates to the plate, followed by 40 µl reaction buffer per well. The 96-well plate is incubated for 60 min at RT (25 °C) before the colourimetric reaction is initiated. For this, 23.3 µl Baginski solution B per well are added. Afterwards, 41.7 µl Baginski solution A per well are added and incubated for 10 min at RT. To end the colourimetric reaction, 75 µl arsenic solution per well are added and incubated at RT for 30 min. The absorption of $A_{860\,nm}$ is measured on a CLARIOstar plate reader (BMG Labtech).

Table 2.12: Buffer list for Baginski Assay

Baginski buffer (containing specific ATPase inhibitors)	50 mM MES/Tris pH 6.8, 3 mM Na_2-ATP, 1 mM $MgCl_2$, 5 mM NaN_3, 50 mM $NaNO_3$, 0.25 mM Na_2MoO_4, for non membrane samples: additionally 0.2 mg/ml Folch Fraction I in 50 mM MES/Tris pH 6.8
phosphate standard	0 – 0.9138 – 1.875 – 3.75 – 7.5 – 15 mM KH_2PO_4 in ddH_2O
Baginski solution A	0.15 g Ascorbic acid in 5 ml 0.5 M HCl; (freshly prepared, place on ice)
Baginski solution B	0.035 g Ammonium heptamolybdate in 1 ml ddH_2O (place on ice until use), when used additionally 1.8 ml 10 % SDS (then kept at RT)
Arsenic solution	20 g metal arsenic, 20 g $Na_3-citrate \cdot H_2O$, 400 ml ddH_2O 20 ml acetic acid, additional ddH_2O for total 1 l;(stored at RT)

2.4.9 Negative Stain Electron Microscopy

Samples of SMA 3:1 lipid polymer nanoparticles from *N. crassa* membrane were analysed by negative stain electron microscopy (EM). EM grids were prepared and imaged with assistance from Dr Sabine Heit. EM samples of polymer solubilised *N. crassa* membrane were prepared by pipetting 3 µl of sample (containing protein-polymer particles with an absorption of $A_{260\,nm} = 0.0017$ determined on a Nanodrop™ spectrophotometer) onto a glow discharged carbon grid (carbon support film 400 mesh copper, uncoated) and incubated for 30 s before blotting in a 45 °C angle with filter paper. 3 µl ddH_2O were added and blotted; this washing step was repeated four times. 3 µl of 2 % uranyl acetate stain were added to the grid and blotted after 15 s incubation. This staining step was repeated twice, and the grid was let dry at room temperature. Imaging was performed at a FEI Tecnai 12 TEM at the COSMIC facility in the Dunn School of Pathology, Oxford. Collected Micrographs were analysed using EMAN2 software. Recording of EM micrographs, particle picking and creation of preliminary 2D class averages were performed by Dr Sabine Heit.

2.5 Lipid Analysis

Exploratory lipid extraction from *N. crassa* cells with Bligh and Dyer extraction [190] has been performed and evaluated with Thin Layer Chromatography (TLC), (see Appendix, Section B.2, Fig B.1). However, a more detailed and specific lipid analysis a collaboration with the NIHR Core Metabolomics and Lipidomics Laboratory at Cambridge University was set up, using LC-MS Liquid Chromatography Mass Spectrometry (LC/MS) [191]. The outline of the lipid analysis workflow is depicted in Fig 2.5.

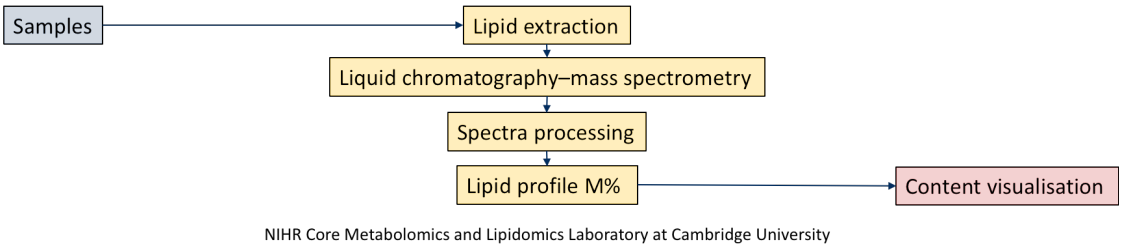

Figure 2.5: Lipid analysis of biological samples with LC-MS

2.5.1 Samples sent for lipid analysis

The following samples have been sent for lipid analysis with LC/MS:

- *N. crassa* whole cells grown at 30°C (n=6) or 35°C (n=2)
- *N. crassa* plasma membrane preparation, washed with DOC (as described in Section 2.1.1); from cells grown at 30°C (DOC A n=2, DOC B n=1) or 35°C (n=2)
- *N. crassa* plasma membrane from cells grown at 30°C, in which the DOC wash was replaced by a high molar NaCl wash (step wise washes with 20 mM HEPES with 2 M, 1 M, 0.5 M and 0 M NaCl) (PM-NaCl n=1), provided by Dr Sabine Heit.
- DDM-solubilised fraction (0.5 % DDM) of *N. crassa* plasma membrane from cells grown at 30°C (n=1) as an intermediate step to purified Pma1
- Four detergent-solubilised Pma1 protein samples, as outlined in Section 2.3.1, were sent for analysis. The identity and oligomeric state had been verified by immunoblotting and native page (Bublitz lab, unpublished data):
  - a. *N. crassa* Pma1 hexamer, grown at 30°C, glycerol gradient, SEC

  - b. *N. crassa* Pma1 hexamer, grown at 30°C, sucrose gradient, SEC
  - c. *N. crassa* Pma1, hexamer, grown at 35°C, glycerol gradient, AEX, SEC
  - d. *N. crassa* Pma1 lower oligomer, grown at 35°C, glycerol gradient, AEX, SEC
- *S. cerevisiae* whole cells grown at 30°C (n=1)
- *S. cerevisiae* plasma membrane, prepared as outlined in Section 2.1.3 (n=1)

2.5.2 Lipid Extraction and LC/MS

Samples were provided in an aqueous buffer, flash-frozen and sent for Lipidomic analysis. Lipid extraction and lipid analysis was performed in the collaborating laboratory IHR Core Metabolomics and Lipidomics Laboratory at Cambridge University by Dr Ben Jenkins. The lipid extraction and LC/MS method has been published [191]. The samples were analysed using a Shimadzu HPLC system with a Thermo Exactive Orbitrap. The data was processed through the vendor's software, looking for the accurate mass at the corresponding retention time. The data were normalised to the internal standards and the sample amount [191] and results were provided in Mol% and µM where applicable.

2.5.3 Lipidomics data visualisation

The acquisition of LC/MS spectra of the samples described in Section 2.5.1 allowed for the relative quantification of a total of about 420 individual lipid species belonging to 20 lipid classes. The nomenclature of these lipid species is defined by their molecular composition: lipid class (defined by the headgroup), sum of carbon atoms in the fatty acids and sum of double bonds in the fatty acids (e.g. PC 34:0). In case hydroxyl groups were measured in sphingolipids species, additionally the sum of hydroxyl groups in the long chain base and the fatty acid moiety is given (e.g. Cer 44:0;3) (see lipid maps e.g. [50, 192]). Analysis of the lipidomic dataset was performed using Microsoft Excel and Python. Details on the analysis are given in the appropriate sections in Chapter 5.

Chapter 3

Results and Discussion 1 — Comparison of commercially available polymers for the solubilisation of eukaryotic and bacterial membranes

This chapter looks to determine and compare the ability of commercially available polymers to solubilise *N. crassa* membranes.

The aims of this chapter are:

- To develop a small scale strategy to study solubilisation efficiency and identify suitable parameters for solubilisation of membranes. For this, different methods for membrane solubilisation analysis directly with light scattering measurements and indirectly via protein content analysis are evaluated. This is used to devise and test a standard order of practice (SOP) to compare initial membrane solubilisation by polymers on *E. coli* and *S. cerevisiae* membranes to gain further insights into the polymer's behaviour.
- To determine and compare the ability of commercially available polymers to solubilise *N. crassa* membranes.

3.1 Solubilisation of *N. crassa* membrane by light scattering measurement

The initial solubilisation efficiency of SMA 3:1 polymer was investigated by light scattering through absorption measurements at 350 nm (A_{350nm}) (similar to [193]), which exploits the ability of particles to scatter light which results in reduced light transmission in the pathway. For this direct measurement of SMA 3:1 solubilisation, *N. crassa* plasma membrane (Fig 3.1 A) and a model lipid suspension, further referred to as model membrane made of neutral DMPC lipids (Fig 3.1 B) of known concentrations were compared.

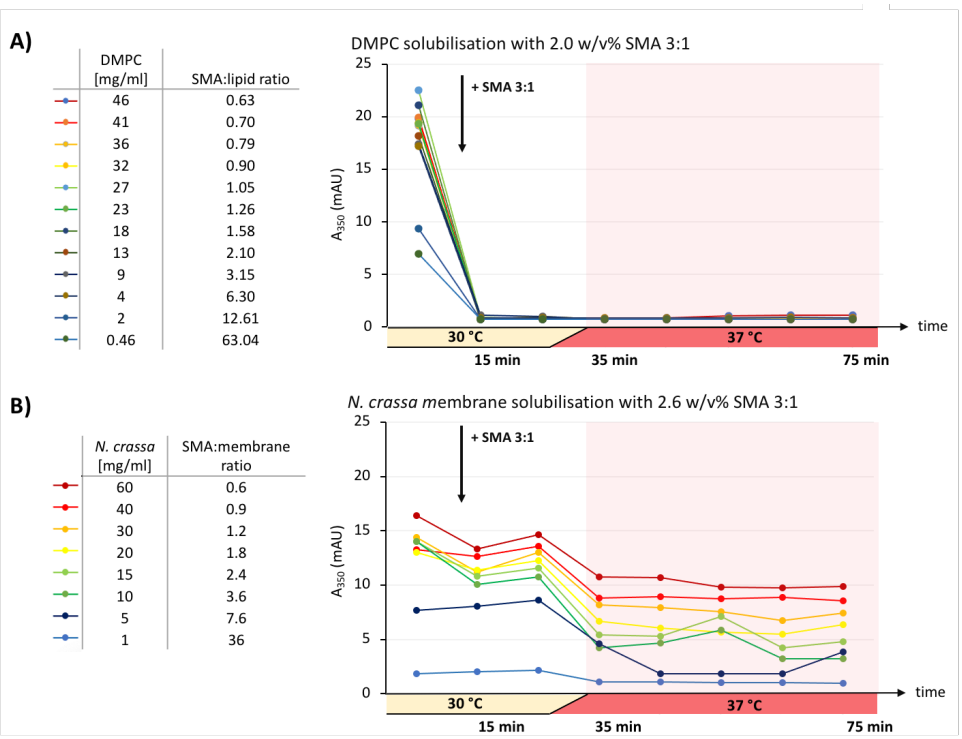

Figure 3.1: Results from light scattering measurements to evaluate membrane solubilisation with SMA 3:1
Solubilisation of a simple model membrane made of DMPC lipids A) in comparison with *N. crassa* membranes B) Absorption at 350 nm measured over time (intervals ca 10-15 min) after the addition of SMA 3:1 (black arrow) and the increase of temperature from 30°C to 37°C (red area). Each plotted line and colour represent the absorption measurements for one membrane dilution, detailed in the corresponding table.

After the addition of SMA 3:1, the A_{350nm} of DMPC membranes (Fig 3.1 A) decreases rapidly and indicates fast and complete solubilisation of liposomes, independent of

the lipid concentration or temperature. The *N. crassa* membrane preparation on the other hand shows less clear solubilisation (Fig 3.1 B). Only slight differences are measured when comparing the initial A_{350nm} value and after adding the solubilisation agent and increasing temperature. The first decrease in A_{350nm} measurement of the *N. crassa* membrane is probably due to a dilution effect of the added SMA 3:1; this decreases slightly after shaking, leading to a more equal particle distribution. However, solubilisation using SMA 3:1 seems to be aided slightly by incubating the *N. crassa* membrane at 37°C, with a drop in absorption observed when the sample was incubated at this temperature. However, overall the A_{350nm} measurements measure only a tiny shift in turbidity throughout the experiment.

These results suggest that SMA 3:1 might be less effective in its solubilisation of the complex biological membrane of *N. crassa*. However, from these results alone, it is unclear whether the solubilisation is limited or whether light scattering measurement as an indicator for solubilisation has its limitations. For example, *N. crassa* membranes have a fast pelleting behaviour and might not stay in even distribution within the plate reader well for long enough and collect in the bottom of the well, disturbing the light path. Furthermore, the *N. crassa* membranes are full of proteins, which might precipitate during the procedure and add to the turbidity. Light scattering measurements depend on a homogenous sample within the cuvette and might be a better choice for simple model membrane compositions like DMPC, which are more homogeneous.

3.2 Indirect measurement: Development of solubilisation assay by total protein quantification

Given the potential artefacts caused by light scattering as a measure of solubilisation, a second method was chosen, where the solubilisation of membranes is determined by the release of membrane protein. Membrane samples were treated with different polymers and solubilised fractions were collected via ultracentrifugation. The pellet was resuspended in the same buffer volume. The total protein content in the supernatant and pellet was determined by BCA assay. To be able to compare simultaneously many

different conditions and polymers, the proposed method allowed for small sample size and high throughput analysis using a 96 well plate format and measurement and analysis via Excel or alternatively a Python script. For the initial evaluation of this method, more conventional and abundant membranes (*S. cerevisiae* and *E. coli*) were tested to reveal the limitations of this method. *E. coli* was chosen as a commonly used model organism, and compared to the eukaryotic fungal organisms *S. cerevisiae* and *N. crassa*.

3.2.1 Polymer solubilisation of *E. coli* and *S. cerevisiae* membranes

The relative protein solubilisation efficiency (E_{rel}) of *E. coli* and *S. cerevisiae* membranes was measured for 12 different conditions and by four commercially available lipid-nanoparticle forming polymers: SMA 2:1, SMA 3:1, DIBMA and PMA compared with the commonly used detergents DDM and SDS. The conditions tested included different pH values (pH 7 and 8) and salt concentrations furthermore, different incubation temperatures and times as outlined in Fig 3.2. Due to the Covid Pandemic the presented experiments could not be executed several times and the lack of repeats should be taken into account when interpreting the following results.

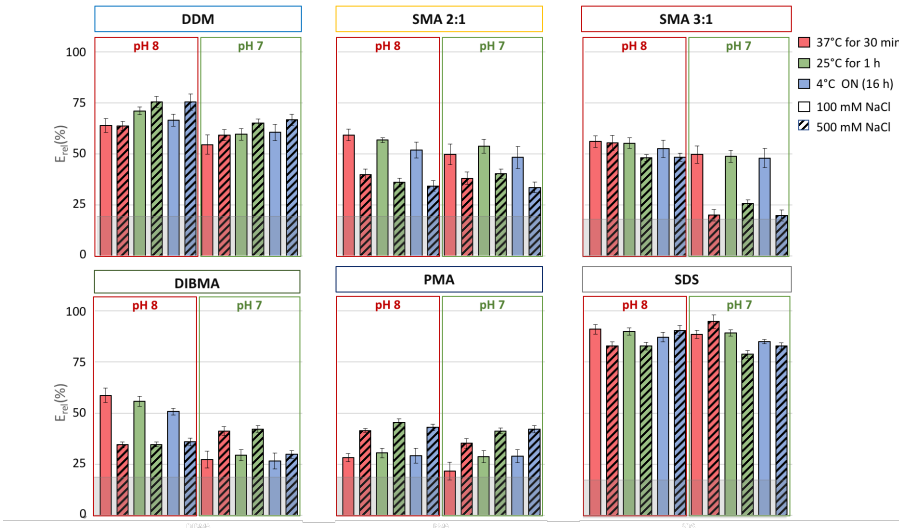

Figure 3.2: *E. coli* membrane solubilisation with different solubilisation agents
The relative protein solubilisation efficiency (E_{rel}) is shown in *E. coli* membranes. The error bars result from multiple technical measurements via BCA Assay. The control is protein content after the addition of buffer only (highlighted in light grey). N=1 Error bars are based on the internal variation of the measurements in triplicates.

Surprisingly high solubilisation readouts without solubilising agent in the *E. coli* membrane solubilisation (Fig 3.2 grey area) are seen compared to the *S. cerevisiae* membrane (Fig 3.3 grey area). This may be due to the presence of lightly solubilising proteins that are not membrane proteins but potentially remaining cytosolic proteins from the *E. coli* membrane preparation. To overcome any potential influence of these proteins on the solubilisation efficiency readout it could be beneficial to separate the membrane from them with ultra-centrifugation before solubilisation as a higher g-force may be necessary to pellet the *E. coli* membrane compared to *S. cerevisiae* membranes. It is also worth mentioning, that for future experiments it would be advisable to work with membrane diluted enough to contain less than 2 mg/ml total protein to be well in the linear range of the assay.

For *E. coli* membranes, the initial measurements (Fig 3.2, Appendix Table A.1) indicate that detergent solubilisation efficiency (E_{rel}) with DDM is ~60 %, but less than SDS solubilisation with ~90 % and independent of salt concentration. However, the relative solubilisation of *E. coli* membrane with polymers seems to be generally lower than these detergents tested with up to 30 % reduced solubilisation for some conditions.

For the different polymers, the solubilisation efficiency appears to be more influenced by the salt concentration than for the chosen detergents. SMA 2:1 solubilised more efficiently in a lower salt environment independently of the pH, because at 0.1 M NaCl it generally solubilised 10–20 % more than with 0.5 M NaCl. For SMA 3:1 and pH 8 the salt concentration appears not to make a clear difference and solubilised about 50 % of membrane proteins but for pH 7 a lower salt concentration is observed to aid solubilisation, as E_{rel} decreased to 25 % at 0.5 M NaCl compared to 50 % at 0.1 M NaCl. For DIBMA at pH 8 a lower salt concentration seems to aid solubilisation (E_{rel} ~55 % at 0.1 M NaCl compared to ~35 % at 0.5 M NaCl). In contrast, at pH 7 a different trend is seen where higher salt appears to be preferential (compare E_{rel} ~30 % at 0.1 M NaCl and ~40 % at 0.5 M NaCl for RT and above). The overall trend that higher incubation temperature (e.g. 37°C) aids solubilisation would need to be

evaluated further for SMA and DIBMA, but has been shown previously for example for SMA [194]. PMA seems to be solubilising *E. coli* membranes more effectively in a higher salt environment, independent of temperature and pH shown by 10–15 % increased solubilisation at 0.5 M than 0.1 M NaCl.

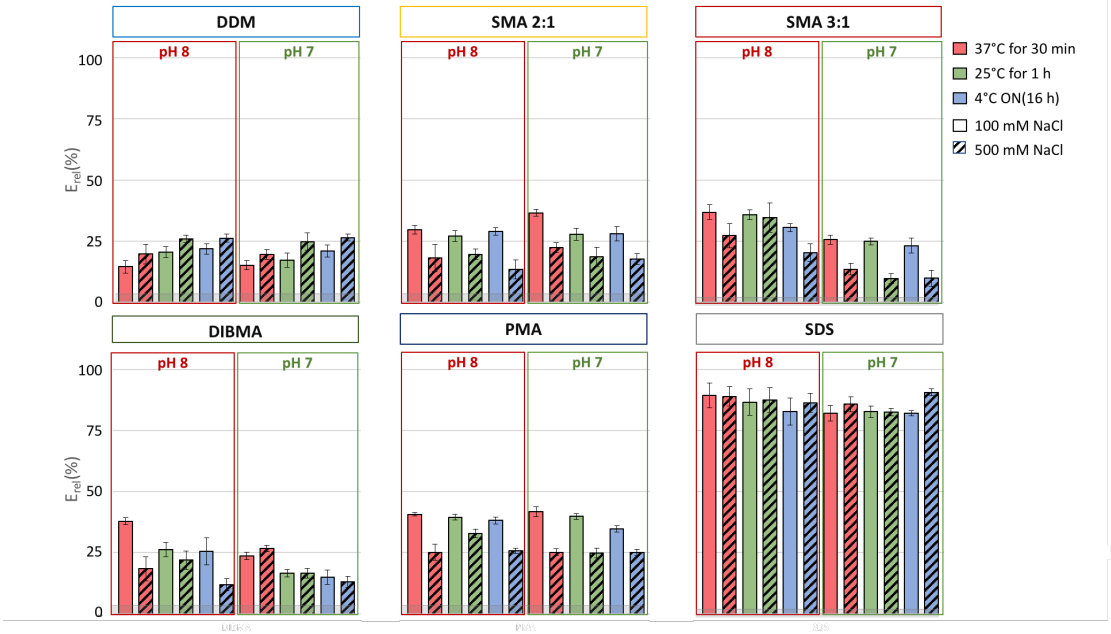

Figure 3.3: *S. cerevisiae* membrane solubilisation with different solubilisation agents The relative protein solubilisation efficiency (E_{rel}) is shown in *S. cerevisiae* membranes. The error bars result from multiple technical measurements via BCA Assay. The control is protein content after the addition of buffer only (highlighted in light grey). N=1 Error bars are based on the internal variation of the measurements in triplicates.

For *S. cerevisiae* membranes the initial measurements (Fig 3.3, Appendix Table A.1) indicate overall lower solubilisation with all polymers and DDM than for *E. coli* membranes (Fig 3.2). However, the control anionic detergent SDS is able to solubilise both membranes at a similar level. For the detergent solubilisation of *S. cerevisiae* DDM seems to perform less well (E_{rel} ~20 %) compared to the SDS (E_{rel} ~80 %). DDM solubilisation seems to be slightly more efficient with higher salt concentration, which seems independent of the pH. Its apparent higher solubilisation at lower incubation temperatures (both seen in *E. coli* and *S. cerevisiae*) might be an effect of the longer incubation time, and would need to be explored further in future experiments.

For all polymers tested there was a optimum solubilisation condition of *S. cerevisiae* membrane that gave a higher E_{rel} value (up to ∼40 %) than all those measured for DDM (up to ∼25 %) indicating that there were specific instances where polymers outperformed conventional detergent solubilisation. SMA 2:1 solubilises slightly more efficiently with lower salt concentrations (0.1 M NaCl E_{rel} ∼30 % versus 0.5 M NaCl ∼20 %). For SMA 3:1 a solubilisation at pH 8 seems slightly more efficient (E_{rel} ∼30 %) than at pH 7 (E_{rel} ∼20 %), and also within each pH range, a lower salt may be more beneficial, as the data showed a 10 % increase in E_{rel} at 0.1 M versus 0.5 M NaCl. For solubilisation with DIBMA the trends in salt and pH dependency as seen in *E. coli* solubilisation are not seen in *S. cerevisiae*. For the SMA and DIBMA polymers, a higher incubation temperature may be beneficial, but this would need further exploration. For PMA a lower salt concentration seems to be beneficial as at 0.1 M NaCl it showed a ∼10 % increase in E_{rel} compared to 0.5 M NaCl, which is independent of the pH and the temperature. This is an opposite trend to *E. coli* membrane solubilisation with PMA, where a higher salt concentration was beneficial, and may be due to the overall lipid and protein compositions of the two membranes [194].

The harsher anionic detergent SDS solubilises both membranes similarly efficiently. However, the milder detergent DDM performance depends on the membrane type and, in the case of *S. cerevisiae*, similar to the polymers. DDM solubilisation of *S. cerevisiae* membrane is generally quite low (E_{rel} ∼20 %) and similar to the polymers containing maleic acids (E_{rel} ∼25 %), notably PMA shows about 12 % higher E_{rel} compared to DDM. The low solubilisation efficiency of DDM might either be due to the low concentration (0.5 %) used or because it is not an optimal detergent for *S. cerevisiae* membrane solubilisation. A more efficient detergent for *S. cerevisiae* seems to be lysophosphatidylcholine-16 (LPC16) (unpublished results, Bublitz group). However, DDM solubilised *E. coli* membranes better than polymers (with ∼25 % higher E_{rel} for DDM compared to polymers). This is in line with published solubilisation results using DIBMA [182], where the solubilisation efficiency of DIBMA from *E. coli* is only a third of the solubilisation of the target protein with DDM, but giving improved stability of

the solubilised protein for cryo-EM.

Based on the data shown the polymer solubilisation of the biological membranes appears to be influenced by pH. The overall charge distribution of polymers changes due to the pH, DIBMA polymers have more charges distributed over their length and are therefore less influenced by ionic strength [195] than SMA. The opposite trends in the solubilisation of *E. coli*, with lower salt aiding solubilisation at pH 8 and decreasing solubilisation at pH 7 cannot be explained solely by the pH differences (Fig 3.2). Whether this apparent effect is genuine should be investigated further.

Ionic strength seems to influence overall membrane solubilisation with polymers more than detergent DDM and SDS solubilisation (Fig 3.2 and 3.3). Most lipids and proteins contribute to the overall surface charge of the biological membrane. Detergents are small molecules that integrate with the hydrophobic core of the lipid bilayer and replace lipids [133, 196]. Polymers are large molecules that are bulky and charged, which as a whole need to interact with the membrane surface before their hydrophobic part can integrate and disrupt the lipid bilayer [197]; the pH and ionic strength likely mediates this interaction [193]. Furthermore it has been reported that the addition of divalent cations can increase the membrane solubilisation efficiency of DIBMA [198] which also be indicative of such a complex interaction between charge distribution of polymer, membrane and aqueous environment. The incubation temperature for membrane solubilisation to extract functional membrane proteins with polymer has been reported in a wide range from 4°C for 20 min [199] to 37°C for 3h [200] for DIBMA and SMA. The membrane fluidity can influence polymer solubilisation [194]. To ensure higher membrane fluidity an extraction at growth temperature or slightly higher could be suggested. Based on the previous results for *S. cerevisiae* (Fig 3.3) a good starting point for the solubilisation of a fungal membrane like *N. crassa* with SMA 3:1 would be at pH 8 with a 100 mM salt concentration at higher solubilisation temperature e.g. 37°C for half an hour, where approximately a third of total membrane protein would be

expected to be extracted.

The presented results show an overall higher polymer solubilisation efficiency of the prokaryotic *E. coli* membrane compared to the fungal *S. cerevisiae* membrane. It has been reported in the literature that polymer solubilisation of mammalian and insect cells appears to be more efficient than that of prokaryotes or fungi. In fact, the solubilisation efficiency of mammalian cells using polymers like DIBMA and SMA has been reported to be higher for human Jurkat cells (∼90 %) compared to the prokaryotic *E. coli* cells (50–60 %) [201]. Furthermore [202] achieved better polymer solubilisation of their target protein in the prokaryotic *E. coli* and insect Sf9 cells than in yeast *S. pastoris*. The efficiency of polymer solubilisation of membranes is thought to be mediated by the bulk membrane properties [194], which likely involves a complex interplay between membrane proteins and lipids. Differences in lipid composition between mammalian cells and fungi, particularly in terms of their complex sphingolipids and sterols, which have the ability to form hydrogen bonds, may influence the membrane bulk properties and fluidity. Single-cell organisms such as fungi and prokaryotes may have evolved to adapt their bulk plasma membrane properties, as well as cell wall-like structures, to withstand environmental influences. In contrast, insect and mammalian cells exist in a more complex network/tissue-like arrangement, which may also contribute to the observed differences in polymer solubilisation efficiency.

3.3 Polymer solubilisation of *N. crassa* membrane

The indirect measurement of solubilisation by evaluation of protein content, as described in Section 3.2, was used to analyse the polymer solubilisation of *N. crassa* membranes at pH 8 and 37°C for 30 min and compared with the results for *E. coli* and *S. cerevisiae* membranes.

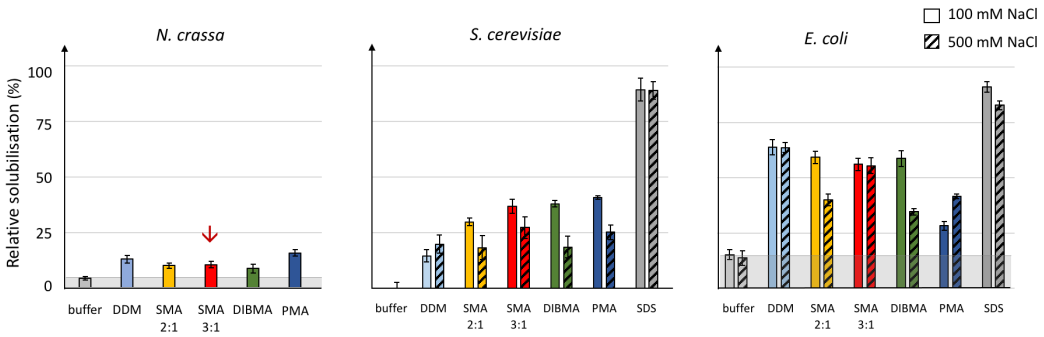

Figure 3.4: Results from solubilisation with different solubilisation agents for different membranes
Relative solubilisation of membranes from different organisms using different solubilisation agents N=1 Error bars are based on the internal variation of the measurements in triplicates. The red arrow indicates the chosen condition for further evaluation of Pma1 solubilisation in Chapter 4.

The solubilisation results for *E. coli* and *S. cerevisiae* in Fig 3.4 are selected results from the previous Section 3.2 (Fig 3.2 and Fig 3.3 respectively) and are presented to compare to *N. crassa* membranes. The results show the highest polymer solubilisation efficiency for *E. coli* (E_{rel} 30–65 %), followed by *S. cerevisiae* (E_{rel} 15–40 %) and *N. crassa* membranes (E_{rel} 10–15 %) at pH 8 and incubation . The solubilisation results in Fig 3.4 reveal a generally low solubilisation efficiency of *N. crassa* membranes, similar to the previous direct measurement via light scattering measurement, as described in Section 3.1. A low solubility of *N. crassa* membranes (judged by SDS PAGE) has also been observed in previous solubilisation attempts with a 1.25x excess of SMA : membrane (2.5 % (w/v) SMA 3:1: 20 mg/ml membrane). To work in a scalable range similar to detergent solubilisation, with 4mg/ml total protein in 30 mg/ml wet weight membrane, 2.5 % SMA 3:1: 30 mg/ml wet weight membrane was used, leading to an 0.8x excess of SMA 3:1: membrane.

To further examine the protein content of solubilised *N. crassa* membranes, supernatants of selected solubilised samples were applied to a SDS PAGE and silver stained (Fig 3.5). The pattern of the protein content of polymer solubilised *N. crassa* membranes vary widely between the three polymers seen in Fig 3.5. Due to the low amount of solubilised protein, silver staining was necessary for *N. crassa* samples. Even with an

initial protein concentration of over 4 mg/ml total protein the protein content in the supernatant was only visible with the sensitive silver staining protocol, supporting the general low solubility results in the BCA assay.

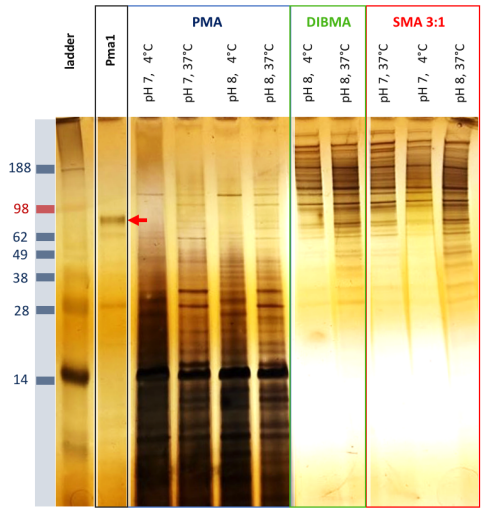

Figure 3.5: SDS PAGE of polymer solubilisation of *N. crassa* membrane
SDS PAGE of solubilised *N. crassa* membranes using three polymers and under different incubation conditions with 100 mM NaCl. A sample of detergent purified Pma1 is highlighted with the red arrow. The visible artefacts (white blur) are discussed in the text.

PMA seems to preferentially solubilise smaller proteins, as intense protein bands are seen below 38 kDa (Fig 3.5). For this polymer, the solubilisation temperature seems to play a role, as different protein patterns are visible for 37°C compared to 4°C, particularly around 28 kDa and between 188 kDa and 98 kDa. This effect seems independent of the pH. High-density bands above 62 kDa indicate that the polymers DIBMA and SMA 3:1 solubilise higher molecular weight proteins than PMA. This might be due to the size of the polymers particles which can then include higher molecular weight proteins. The lack of protein bands below 28 kDa shows the limitations with silver staining (Fig 3.5). The artefacts in the white area are due to two reasons: frequency and over exposure of the light source when imaging the gel and a shielding effect caused by DIBMA and SMA 3:1 in combination with lipids, not stained by silver. The possibility that lower molecular weight proteins that are just not stained can therefore not be excluded. For DIBMA and SMA, the most efficient condition for overall membrane protein solubilisation seems

to be pH 8 and an incubation temperature of 37°C.

Generally, the individual bulk membrane properties play a role in the polymer solubilisation of the individual membrane [194]. Several factors can contribute to the generally low solubilisation of *N. crassa* membranes. Firstly, *N. crassa* and *S. cerevisiae* are fungi with more complex membrane compositions than the prokaryote *E. coli*. Both fungi membranes contain ergosterol and other complex lipids, possibly decreasing the solubility compared to *E. coli*. Secondly, The tested *N. crassa* plasma membranes originate from a cell wall-less mutant (*N. crassa* slime). Even though a cell wall would be considered a hindering factor in solubilisation, the cell wall-less mutant might have adapted to the harsh conditions by adjusting its membrane composition to create a more rigid and mechanically strong environment. Altered protein compositions and a particular lipid environment in the cell wall less this *N. crassa* slime mutant might lead to a rigid membrane as a protective mechanism due to the lack of cell walls. The general lipid composition of *N. crassa* might be influencing the solubility of its plasma membranes through saturated chain lipids and sphingolipid packing and the presence of ergosterol (cholesterol-like molecules, which are not present in *E. coli*) making the membrane sturdier and limiting the polymer to interact with the hydrophobic core of the lipid bilayer. This tighter packing is supported by previous reporting that high amounts gel-like domains were found in *N. crassa* whole cells (measured with fluorescence microscopy) and that the melting of these domains in WT occured at 30°C and at higher temperatures in the *N. crassa* slime mutant [127]. Thirdly, the membrane preparation of *N. crassa* is particularly focused on the enrichment of the plasma membrane, whereas the *S. cerevisiae* membrane preparation might still contain high levels of other membrane types. The described effect of a sturdy plasma membrane leading to a lower solubilisation might particularly play a role in the *N. crassa* samples compared to the *S. cerevisiae* membrane sample, which has a mix of various cell membranes including the plasma membrane and might also explain the discrepancy in solubilisation between the samples from both organisms (Fig 3.4). Fourthly, during the plasma membrane preparation a detergent wash is used. This detergent (desoxycholate) DOC might change the protein [122]

and potentially lipid environment in a way that might not be beneficial for polymer solubilisation. The washing step might influence the lipid composition by depleting easy soluble lipids (and some proteins) and therefore enrich the protein content in the membrane. This dense packing of proteins and lipids could be overcome by adding PC lipids (e.g. POPC) to dilute the membrane with lipids. Unpublished results from the Watts lab support that adding PC lipids at the solubilisation state aids polymer solubilisation of the *N. crassa* membrane. Unfortunately, adding PC lipids would defeat the purpose of analysing the lipid content of the native membrane, but this is already difficult due to the DOC wash during membrane preparation.

The primary objective of the polymer solubilisation trial was to identify solubilisation conditions to prepare for the polymer solubilisation of Pma1 from *N. crassa*. When comparing the polymer solubilisation samples for the target protein Pma1 (Fig 3.5, red arrow), just below the 98 kDa band (Uniprot ~100 kDa as outlined in section 1.4, in DIBMA and SMA 3:1 are more prominent bands seen at this apparent protein size. This indication and in comparison of a good solubilisation condition for another complex membrane *S. cerevisiae*, as established previously, 20 mM HEPES 100 mM NaCl pH 8 was identified as the starting condition for further solubilisation of Pma1, which is explored in Chapter 4.

3.4 Summary and Conclusion

The solubilisation of *N. crassa* plasma membrane with polymers has not been established previously. This chapter compared the ability of commercially available polymers to solubilise *N. crassa* membranes. Because of the limited availability of both membranes and polymers, it was necessary to develop a small-scale strategy to best study solubilisation efficiency and identify suitable parameters for the solubilisation of *N. crassa* with polymers. Polymer solubilisation conditions of the prokaryote *E. coli* have been established previously, and initially quantified with light scattering measurements [194]. However the light scattering measurements of SMA 3:1 solubilisation for *N. crassa* (Section 3.1), were inconclusive, therefore a different approach was developed: measuring the release of membrane protein (Section 3.2) similar to [201]. Additionally to *E. coli* membrane the eukaryotic membrane, *S. cerevisiae*, was used to test this approach as a large amount of starting material was available and to give insights into the polymers behaviour. Table 3.1 outlines suitable solubilisation conditions for the different membranes based on the presented initial measurements, and further studies may be needed to confirm and optimise these conditions for specific applications.

Table 3.1: Summary of solubilisation conditions for different membranes

Solubilising agent	**Best solubilisation condition**		**Notes for solubilisation**
	E_{rel}	condition	
organism: *E. coli*			
DDM	∼70 %	500 mM NaCl with longer incubation time, independent of pH	slightly beneficial is a higher salt concentration and longer incubation temp (e.g. >1h)
SMA 2:1	∼60 %	pH 8, 100 mM NaCl, 37°C	generally lower salt concentration (100 mM NaCl)
SMA 3:1	∼50 %	pH 8, 100 −500 mM NaCl	slightly basic pH (pH 8), for pH 7 lower salt (100 mM NaCl)
DIBMA	∼60 %	pH 8, 100 mM NaCl, 37°C	pH 8 with lower salt (100 mM NaCl), pH 7 with higher salt (500 mM NaCl), tendency to higher incubation temp (RT or above)
PMA	∼40 %	500 mM NaCl independent of pH but longer incubation time	higher salt concentration (500 mM NaCl) with potentially longer incubation time (e.g. >1h)
SDS	∼85 %	no clear pattern	no clear pattern
organism: *S. cerevisiae*			
DDM	∼20 %	500 mM NaCl independent of pH and temperature	Slightly beneficial is a higher salt concentration and longer incubation temp (e.g. >1h)
SMA 2:1	∼35 %	pH 7, 100 mM NaCl, 37°C	generally lower salt concentration (100 mM NaCl)
SMA 3:1	∼35 %	pH 8, 100 −500 mM NaCl	tendency to slightly basic pH (pH 8), generally lower salt concentration (100 mM NaCl) particularly at pH 7
DIBMA	∼40 %	pH 8, 100 mM NaCl, 37°C	generally pH 8 and tendency to higher incubation temp (37°), in terms of salt concentration at pH 8 lower salt (100 mM NaCl) at pH 7 higher salt (500 mM NaCl) seems beneficial
PMA	∼40 %	100 mM NaCl independent of pH and temperature	low salt (100 mM NaCl)
SDS	∼85 %	no clear pattern	no clear pattern

From the initial results for *S. cerevisiae* (Section 3.2.1), lower salt concentrations (100 mM NaCl), as well as pH 8 (results for SMA 3:1, DIBMA and PMA) were chosen for the polymer solubilisation of *N. crassa* slime membranes. An increase in incubation temperature (37°C over 30°C) was observed to aid the solubilisation of *N. crassa* membrane with polymers in preliminary solubilisation tests (Section 3.1) as well as in solubilised protein observed via SDS PAGE (Section 3.3). Based on these results, a higher incubation time was chosen for further solubilisation of *N. crassa* membranes. Based on the presented small-scale solubilisation tests, pH 8 and 100 mM NaCl was identified as a starting condition for solubilisation optimisation and subsequent purification of *N. crassa* Pma1 from its endogenous membranes, as discussed in Chapter 4.

Chapter 4

Results and Discussion 2 — Establish a polymer purification protocol to purify *N. crassa* Pma1 from native source

Historically, native sources have provided the primary source of membrane proteins (MP) for characterisation and functional work (e.g. SERCA from rabbit membranes [203]), although obtaining sufficient material is often challenging. Heterologous expression and purification of *N. crassa* Pma1 have proven challenging; however, as Pma1 shows high abundance within the plasma membrane of *N. crassa*, purification from its native organism is still the most promising approach to date. This approach has the added benefit of preserving native lipids, especially using polymers as a solubilisation reagent, rather than the more traditional detergents that can lead to delipidation of the MPs. Importantly, current purification protocols of native Pma1 in detergent suffer from poor solubilisation efficiency, overall heterogeneity and poor reproducibility. For these reasons, the project sets out to establish an alternative purification protocol using amphipathic polymers.

The aims of this chapter are:

- To develop a purification protocol using SMA 3:1 of *N. crassa* Pma1 from its native source.
- To determine the compatibility of polymers with various methods for the characterisation of Pma1, such as ATPase activity assays.
- To evaluate the compatibility of different polymers (SMA 3:1, 2:1, DIBMA and PMA) with immunoblotting (anti-Pma1) to verify the presence of Pma1 in the sample.
- To evaluate the usability of the polymers with different antibodies (anti-His and anti-Strep) for potential recombinantly expressed *N. crassa* Pma1 using a bacterial protein (heterologously expressed MprF in *E. coli*).

4.1 Polymer solubilisation and purification of Pma1 from *N. crassa*

4.1.1 Solubilisation and characterisation of Pma1 in SMA lipid nanoparticles

N. crassa membranes display a very low solubilisation efficiency with detergent and polymers, as described in Section 3.3. For the subsequent purification attempts, 2.5 % SMA 3:1, in 20 mM HEPES, 100 mM NaCl, pH 8 and incubation (37°C, 30 min), was chosen as this had been determined as one of the most suitable conditions for solubilisation of *N. crassa* membrane (Section 3.3). After solubilisation, insoluble material was removed by centrifugation, and the supernatant was analysed by SDS PAGE and Western blot - a DDM solubilised sample was added as a positive control (Fig 4.1).

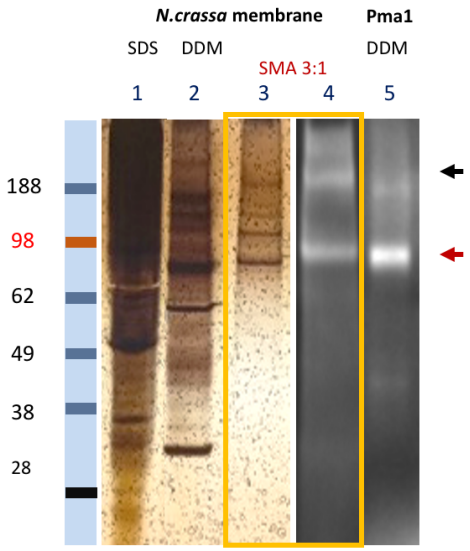

Figure 4.1: Solubilisation and characterisation of Pma1 in polymer-lipid nanoparticles Solubilisation of Pma1 with 2.5 % SMA 3:1 in 20 mM HEPES, 100 mM NaCl, pH8 for 30 min at 37°C. Lanes: 1-3. SDS PAGE, silver stained, 4-5. Western blot (signal enhancer), anti Pma1. *N. crassa* membrane solubilised with (1) SDS, (2) DDM or (3) and (4) SMA 3:1; DDM solubilised and purified Pma1 (5). Highlighted are the Pma1 monomer (red arrow) and a potential Pma1 oligomer (black arrow).

In Fig 4.1, supernatants of SDS (lane 1), DDM (lane 2) and SMA 3:1 (lane 3) solubilised *N. crassa* membrane are compared. Furthermore, Western blot analysis using an anti-Pma1 antibody is shown for the polymer solubilised supernatant in comparision to DDM

solubilised and purified Pma1 (lanes 4 and 5, respectively).

In the presence of SMA polymers silver and Coomassie staining of SDS PAGE gels produce artefacts as mentioned before(as visible in Fig A.3 in the Appendix, personal observation). Silver staining is more sensitive and can detect low protein concentrations and contaminations. Notably, the SDS-PAGE of the DDM solubilised sample (Fig 4.1 lane 2) generally shows more discernible protein bands, below 70 kDa, than in the SMA solubilised samples (Fig 4.1 lane 3). In the presence of polymers, in comparison to membrane samples, bands below 70 kDa might not be individually stained, indicating that the polymers might mask these smaller proteins.

The Pma1 monomer is ∼100 kDa in size, but due to the increased hydrophobic properties of the transmembrane region membrane proteins tend to run at a lower apparent molecular weight (Mw) on SDS PAGE [204]. Therefore, the Pma1 monomer typically runs below the 98 kDa marker. Furthermore, the additional band seen at around 188 kDa likely represents an oligomeric state not fully denatured by SDS incubation. The corresponding Western blot of the positive control (DDM solubilised) shows both these signals, with the monomer presenting a stronger signal. The initial solubilisation trial of Pma1 from *N. crassa* with SMA 3:1 shows the same anti-Pma1 immunoblotting signals and a band at the expected height in SDS PAGE. Therefore, the SMA 3:1 solubilised sample was further purified by size-exclusion chromatography (Section 4.1.2).

4.1.2 Size exclusion chromatography (SEC) of SMA 3:1 solubilised Pma1

As described above, SMA 3:1 shows the potential to solubilise Pma1 from its native source *N. crassa*; consequently, a purification strategy was established to enrich the Pma1 content of the sample. There are several methods to purify membrane proteins, including affinity chromatography (with the presence of tags), ion exchange chromatography, size-exclusion chromatography, and density gradient centrifugation [205]. However, only size-based methods are feasible for purifying the polymer-solubilised Pma1 from native *N. crassa*. As a native protein without tags, the targeted Pma1 is not feasible for affinity

chromatography. Immunoprecipitation to selectively enrich Pma1 was not feasible due to the limited quantity of the selective antibody used for immunoblotting. Using a density gradient centrifugation, as in the established purification protocol for detergent solubilised Pma1 [104], would have required a downscaling of the gradient due to the limited availability of polymer solubilised sample. Also, the polymer SMA 3:1 is not expected to be compatible with an anion exchanger due to its negative charge [164]; therefore, only size-exclusion chromatography was available as a feasible purification protocol. Consequently, size exclusion chromatography (SEC) was selected for further purification of the SMA-solubilised particles from *N. crassa*.

A Superose 6 HR 16/60 column was chosen due to its capacity for high-resolution purification in a broad molecular weight range (M_r ca. 5 kDa to ca. 5 MDa for globular proteins), which would suit the Pma1 hexamer with 660 kDa.

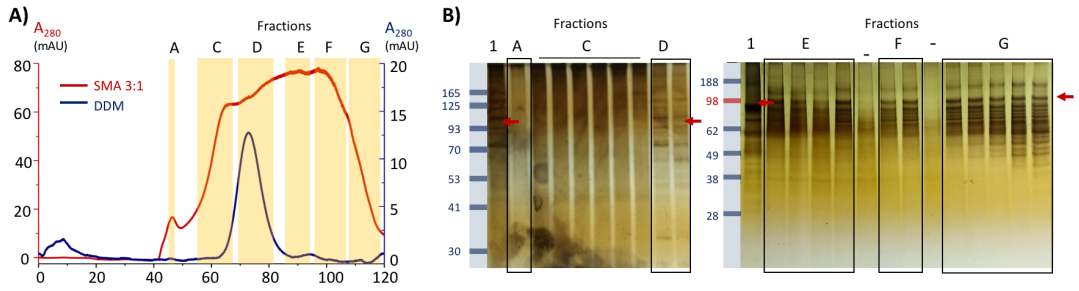

Figure 4.2: Two step purification by size exclusion chromatography of Pma1 in SMA 3:1-lipid nanoparticles
A) Chromatogram of SMA 3:1 solubilised Pma1 (red) in comparison with DDM solubilised and glycerol gradient-purified Pma1 (blue). B) Silver stained SDS-PAGE of various SMA 3:1 SEC fractions, Lane 1- SEC load, A-G refer to the SEC elution fractions as indicated in A), silver stained. Highlighted is the position of the expected Pma1 monomer (red arrow).

The absorption profile at 280 nm of SMA 3:1 solubilised *N. crassa* membrane shows a polydisperse trace (Fig 4.2 A, red trace), with proteins spread almost over the whole elution volume. The pre-peak at 45 ml (Fraction A) could be aggregated protein, as the void volume of this column is 40 ml. Due to the polydisperse trace observed, the elution trace of a DDM solubilised Pma1 sample was compared (Fig 4.2 A, blue trace). The first shoulder at 60 ml of the elution (fractions C) did not show any Pma1 signal

in SDS-PAGE and could be empty lipid polymer particles which can absorb at 280 nm. The fractions D are particularly interesting since the DDM purified Pma1 hexamer is eluted at this volume (blue trace). The denaturing SDS-PAGE (Fig 4.2 B) shows a protein band at the expected height of the Pma1 monomer within these fractions (red arrow). The later SEC fractions E, F and G also show protein at the expected position of the Pma1 monomer in the SDS-PAGE, hence they might contain smaller Pma1 oligomers, in addition to other membrane proteins. Based on the SDS PAGE analysis, SMA 3:1-solubilised Pma1 appears to elute from 70 ml onwards (fractions D). The physiologically relevant hexameric state is desired for further analysis; hence the earliest elution fractions containing a protein at the expected molecular weight (MW) were chosen to be used further. For this step, the fractions C and D were concentrated separately (Fig 4.3 A), and a protein at the expected size of Pma1 monomer was observed in fractions D. The concentrated fractions D were then subjected to a second size exclusion chromatography for further separation (Fig 4.3 B and C).

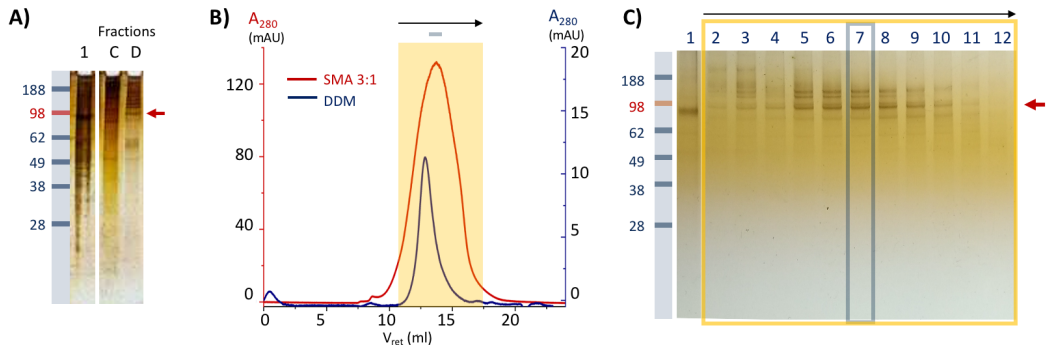

Figure 4.3: Second size exclusion chromatography of Pma1 solubilised in SMA 3:1-lipid nanoparticles
A) SDS-PAGE, lane 1, detergent solubilised Pma1, and concentrated fractions C and D from the primary SEC (Fig 4.2). B) Elution profile of 2nd SEC where fractions D (71 −83 ml) of the first SECwere loaded (Superose 6 increase 10/300) SMA 3:1 (red) or DDM (blue) solubilised Pma1. C) SDS-Page: lane 1- Pma1 in DDM; Lanes 2-12, 2nd SEC elution fractions (11.5 −17.75 ml), silver stainedHighlighted is the peak fraction (lane 7) and the expected band position of Pma1 (red arrow).

The protein absorption at 280 nm in the size exclusion chromatogram (Fig 4.3 B) shows a narrow elution profile for the detergent solubilised Pma1 hexamer (Fig 4.3 B, blue trace) eluting at 13-14 ml. The SMA 3:1 solubilised sample has a similar

elution profile (Fig 4.3 B, red trace) with a peak at 14 ml. When analysing the corresponding elution fractions (Fig 4.3 B orange area) with SDS-PAGE (Fig 4.3 C) they show a protein band at the expected height of the Pma1 monomer, at a slightly higher position compared to the detergent purified Pma1 sample (Fig 4.3 C, lane 1) as seen in SDS-PAGE before. Based on the results from this SDS-PAGE and that the sample had a similar elution volume to detergent-purified Pma1, the SMA 3:1 particles have potential to contain Pma1, but its presence needs to be confirmed further. Therefore, the purified sample was subjected to further evaluation by immunoblotting, ATPase activity assay and negative stain electron microscopy.

4.2 Identification and characterisation of Pma1 in polymer solubilised samples

In the following section, the polymer-solubilised *N. crassa* membrane particles are further characterised. A common way to identify the presence of Pma1 in a sample is immunoblotting with a Pma1-specific antibody. Here, the compatibility of polymers with the anti-Pma1 antibody and an ATPase activity assay is evaluated, and methods for structural analysis are explored.

4.2.1 Immunoblotting of polymer solubilised Pma1

A Western blot analysis for the presence of Pma1 is shown in Fig 4.4 using an anti-Pma1 antibody with the eluted fractions from Section 4.1 (Fig 4.2).

The Western blot (Fig 4.4 A) shows a prominent band below 98 kDa in the detergent-purified Pma1 sample (Fig 4.4 A, lane 2). In contrast, no clear Pma1-specific signal is visible in the SEC fractions of the SMA 3:1 solubilised sample (Fig 4.4 A lanes 3-8). The anti-Pma1 Western blot remains challenging because even though the size exclusion samples of the D fractions (Fig 4.4 A, orange area) showed a signal at the expected height for Pma1, lower molecular weight regions were non-specifically stained (Fig 4.4 A, green arrows). Due to these ambiguous results, immunoblotting of anti-Pma1 in the presence of polymers requires optimisation since verification of the presence of Pma1 is crucial before larger polymer solubilisation and purification of Pma1 can be conducted.

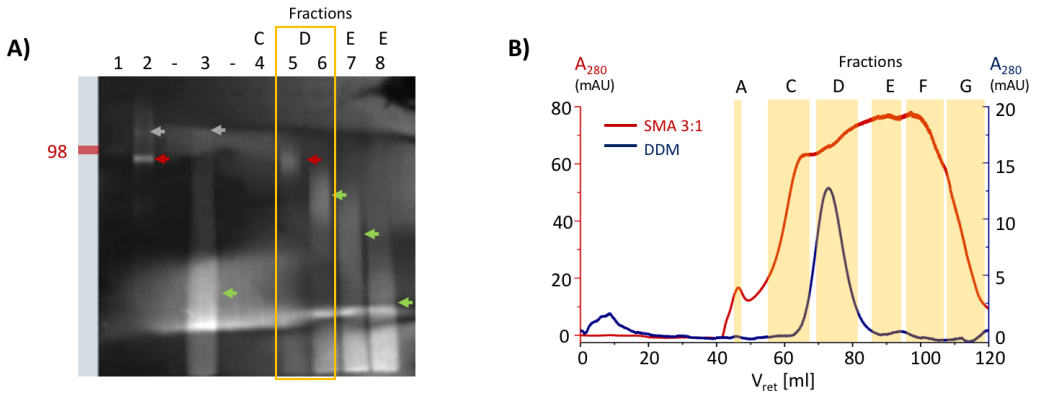

Figure 4.4: Western Blot of fractions from the initial SEC of Pma1 in SMA 3:1-lipid nanoparticles
A) Westernblot Anti-Pma1, signal enhancer, lane 1, Ladder , lane 2 DDM- solubilised Pma1, lane 3 SMA 3:1 solubilised *N. crassa* membrane, supernatant before loading onto SEC, lane 4-8 selected SEC elution fractions C-F (as in B) from SMA 3:1 solubilisation. B) reproduction of Fig 4.2 A), 1st SEC of SMA 3:1 solubilised Pma1 (red), DDM solubilised and purified Pma1 (blue). Highlighted are the sizes of the expected Pma1 monomer (red arrow), a potential oligomer (grey arrow) and non-specific immunoblotting signal (green arrows).

4.2.2 Optimisation of anti-Pma1 immunoblotting via Dot blots

In previous Western blots (Fig 4.1 and 4.4), an anti-Pma1 signal of SMA 3:1-solubilised *N. crassa* membranes was only obtained using a commercial signal enhancer for immunostaining. The regular immunostaining condition (PBST with 5 % milk powder) used for detergent-solubilised Pma1 did not show any signal. Following this, dot blots with different blocking conditions were tested to improve the immunoblotting of anti-Pma1 in the presence of polymers. Several samples containing the polymers SMA 3:1, SMA 2:1 or DIBMA were evaluated on dot blots (Fig 4.5) with different immunoblotting conditions, namely *N. crassa* plasma membrane, detergent solubilised and purified Pma1, DMPC lipids at a final concentration of 34 mg/ml, HEPES buffer with polymers, and SEC fractions from purification of SMA 3:1 solubilised Pma1 (Section 4.1). To evaluate whether the negative charge of the polymer could cause an artefact, L-Arginine was added to the regular immunostaining protocol to exploit its shielding properties [146] in the presence of polymers (referred to as "improved condition").

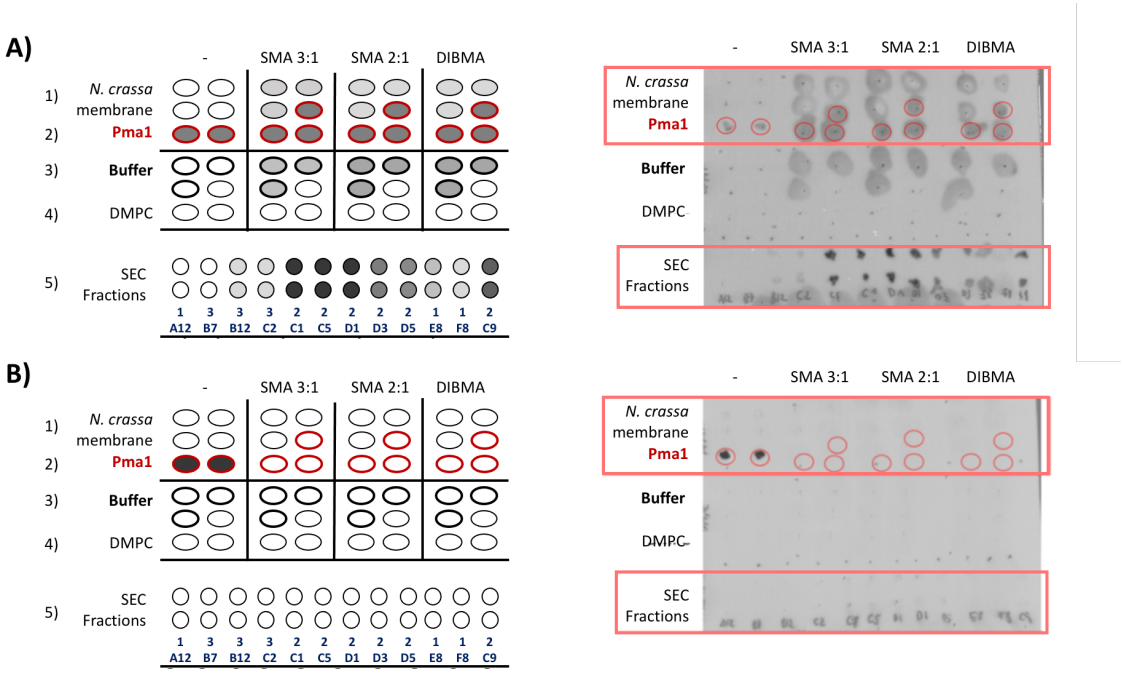

Figure 4.5: Dotblot of Pma1 in the presence of polymers
Immunoblotting of Pma1 using an anti Pma1 antibody, developed in A) Immobilon Signal Enhancer (Merck) or B) skim milk powder and L-Arginine (to shield negatively charged polymer), with schematic sample arrangement on the left and dot blot results on the right. Samples were added in 3 replicates with or without one of the polymers SMA 3:1, SMA 2:1 or DIBMA: *N. crassa* membrane samples (1), DDM purified Pma1 protein (circled in red) (2), buffer (20 mM Hepes pH 8) (3), DMPC lipid in 20 mM Hepes pH 8 (4) and fraction samples from size exclusion of SMA 3:1 solubilised *N. crassa* membrane from Section 4.1 (5)

The anti-Pma1 antibody, in combination with the signal enhancer, stains non-specifically all polymer-containing samples but not DMPC lipid samples (Fig 4.5 A) could be that this nonspecific binding reaction is due to free polymer. While the same amount of total polymer solubilised different membrane types to different extents (Section 3.2), it is possible that the polymers did not solubilise the *N. crassa* membranes properly, and as a result, the sample contains a lot of free polymers. In the case of the DMPC lipid samples, the amount of free polymer might be less, as most polymers formed particles with the lipids since polymer solubilisation of DMPC lipids works very well (Section 3.1).

Furthermore, SEC samples from SMA 3:1 solubilised *N. crassa* membranes (see Section 4.1, Fig 4.3, and Section 4.2 Fig 4.4) were added to the dot blot. In the presence of signal enhancer (Fig 4.5 A), the SEC samples display an intensity increase in the

same elution fractions where detergent purified Pma1 was expected (Fractions C and D, compare Fig 4.4 B, blue line). Based on these SEC elution profiles (Fig 4.4 B) and SDS-PAGE of detergent-purified Pma1 and SMA solubilised samples in (Fig 4.3 C), this anti-Pma1 signal increase might indicate that Pma1 is present in these samples. It is worth noting that in the SEC fractions analysed by dot blots (Fig 4.5 block 5) the concentration of free SMA is expected to be significantly lower than in the initial solubilisation conditions. Therefore, the immunostaining of the SEC fractions might not be as affected by free SMA as in the control samples. However, due to the nonspecific staining in the presence of signal enhancer in the polymer-only samples, this is still not enough information to verify if the SEC samples contain Pma1.

In the optimised staining conditions using the L-Arginine "shielding conditions", there is a clear signal in the detergent-purified Pma1 sample but a suppressed signal in the presence of polymers. One reason could be that adding the polymers had diluted the sample so much that not enough Pma1 was subjected to the dot blot membrane, which was tried overcome by increasing the drops per dot. Another possibility is that the polymers obstruct the binding site of the polyclonal anti-Pma1 antibody. Unexpectedly, no signal for Pma1 in the *N. crassa* membrane samples was detected (Fig 4.5 B). These samples still contain membrane lipids, other proteins and further residual material that might shield the antibody binding site on Pma1 and interfere with immunodetection. These samples would probably need to be prepared with an SDS-containing sample buffer to expose the antibody binding site of Pma1.

In conclusion, the SMA 3:1 showed potential to solubilise Pma1 from its native source *N. crassa* membrane, and size-exclusion chromatography was chosen for further purification. Pma1 solubilisation and purification via SEC seemed promising based on SDS-PAGE and SEC profile. However, Western blots and further optimised immunostaining were incompatible with the available anti-Pma1 antibody. The anti-Pma1 immunoblotting (Fig 4.5) shows ambiguous results: i) polymers (SMA 3:1, SMA 2:1 and DIBMA) suppress the anti-Pma1 signal; ii) blot development with an enhancer to overcome low protein content of the samples, leads to a false positive signal. The anti-Pma1 antibody

seems to cross-react with the polymers in the presence of a signal enhancer. In other immunoblotting conditions, the polymers seem to shield the anti-Pma1 binding site, interfering with assessing polymer solubilisation and purification of Pma1 in SMA 3:1. Ways to overcome similar issues with antibody binding in the presence of polymers in Western blots have been reported in the literature, e.g. [146], indicating that challenges with immunoblotting of target proteins in the presence of polymers are not unique to this project. Several further polymer removal methods were explored as outlined in the Appendix, Section A.5, Table A.3, but did not show the desired results and would need further optimisation.

It appears that the anti-Pma1 antibody reliably detects Pma1 in detergent-solubilised samples but is not suitable for use in the presence of polymers like SMA. Therefore, verifying the presence of Pma1 in polymer particles requires a different approach, e.g. mass spectrometry or a robust activity assay. In particular, the clear bands at the expected MW for the Pma1 monomer in Fig 4.3 C, could be extracted and sent for identification of protein with mass spectrometry.

4.2.3 ATPase activity assay (Baginski assay)

In the previous sections, the polymer solubilisation of *N. crassa* membranes was evaluated to purify Pma1. The traceability of Pma1 during this process was challenging due to ambiguous immunoblotting results in the presence of polymers. The Bagsinki assay [186], an ATP hydrolysis assay, was used to evaluate the presence of active Pma1 in polymer-solubilised membrane samples. During the purification trials with SMA 3:1 (Section 4.1), various samples were tested with the Baginski assay. However, in none of the SMA 3:1 solubilised samples and fractions from the consecutive SEC runs, colour development was seen when tested with the assay. As this colour development results from free inorganic phosphate (P_i) released by Pma1, no Pma1 activity was measured in these samples. To understand whether solubilisation with SMA 3:1 is compatible with the activity assay, the activity of *N. crassa* membranes incubated in the presence or absence

of SMA 3:1 polymer was determined against a membrane control at RT (25°C).

The ATPase activity of the *N. crassa* plasma membrane decreased to 10 % when incubated with SMA 3:1 compared to the membrane control (Fig 4.6). Therefore the lack of ATPase activity observed in the SEC fractions could be due to the presence of SMA 3:1. It appears that the SMA 3:1 polymer is either inhibiting Pma1 activity or is not compatible with the Baginski assay.

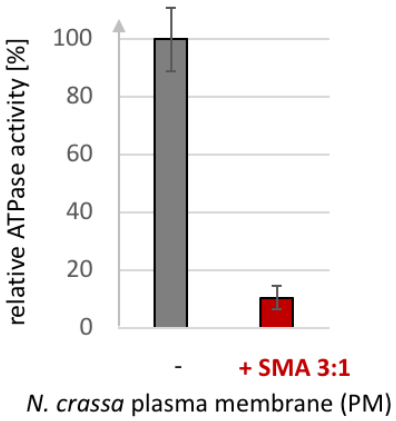

Figure 4.6: Polymer compatibility with ATPase activity assay
Relative ATPase activity of *N. crassa* plasma membrane, after incubation with polymer (2.5% SMA 3:1 (final concentration), in 20 mM HEPES, 100 mM NaCl, pH 8 at 25°C), Baginski assay measurement performed in triplicates at pH 6.8.

Pma1's ATPase activity is magnesium dependent, but SMA forms insoluble complexes with these divalent cations [168]. The therefore reduced amount of free Mg^{2+} might have caused the ATPase activity to decrease, or the complexes could have destabilised the ATPase. ATP titrated with Mg^{2+} before addition to the assay could prevent complex formation with SMA 3:1 if Mg^{2+} has a higher affinity for ATP than SMA. Due to the use of size exclusion chromatography, the SEC fractions analysed with this assay are anticipated to have lower concentrations of free SMA than the membrane-polymer sample in 4.6. As a result, the observed lack of measurable activity in the presence of Mg^{2+} cannot be attributed solely to a possible precipitation of free SMA with free Mg^{2+}. If Mg^{2+} is the influencing factor it would need to have also had an effect on the particle-bound polymer instead of being solely reduced in its concentration. Furthermore, Pma1

might be conformationally restricted when residing in polymer particles. The choice of polymer used to solubilize a membrane protein can dictate changes in conformation, as reported in the literature [206]. In particular, [206] demonstrated that different polymers (e.g. SMA, SMI and DIBMA) can induce different conformational states in membrane protein rhodopsin. This conformational restriction can be used as an advantage and provide researchers with a toolkit for studying different conformational states and expanding the range of downstream applications, including generating specific intermediate states and variations in thermostability [206]. A restriction in polymer particles could be explained as it seems that SMA 3:1 does not solubilise intact Pma1 hexamers (following Section 4.2.4). Therefore, if SMA solubilised other Pma1 oligomers, it might not preserve their structural integrity, or possess an increased lateral pressure that may affect activity. Removing SMA for functional characterisation would be challenging, as a commonly used polymer removal protocol use precipitation of protein with $CH_3OH/CHCl_3/H_2O$ [153], which could denature Pma1. Resolubilisation of the SMA-lipid particles with detergent could be a way to overcome the restriction [207], but SMA would need to be fully removed because if it was still present in the sample it might precipitate with Mg^{2+}. The compatibility of other commercially available polymers (e.g. DIBMA or PMA) with the ATPase activity assay should be tested. These experiments had been prepared but not executed due to the Covid pandemic

4.2.4 Electron microscopy of SMA 3:1-solubilised *N. crassa* plasma membrane

Structural characterisation by electron microscopy (EM) was planned once Pma1 was successfully purified in polymer particles. For this, the initial setup to visualise the purified samples from Section 4.1 with negative stain electron microscopy was tested. For this, SMA 3:1 solubilised particles from *N. crassa* membranes, eluted from a secondary SEC (corresponding peak fraction in Fig. 4.3 C and fraction D1 in Fig 4.5 A), were subjected to negative stain electron microscopy (see Fig 4.7 A).

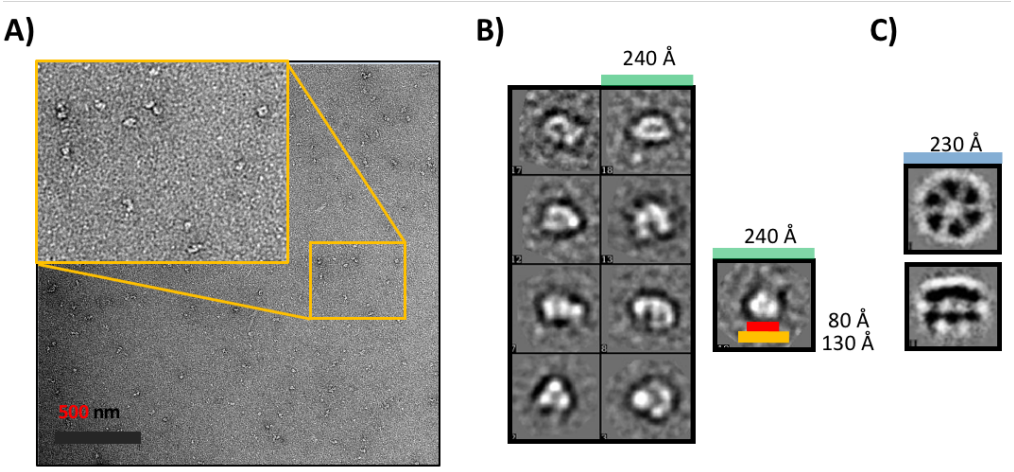

Figure 4.7: Negative stain EM of SMA 3:1 solubilised *N. crassa* membrane after SEC purification
A) EM micrograph of SMA 3:1 solubilised particles from the secondary SEC (corresponding peak fraction in Fig. 4.3 , and fraction D1 in Fig 4.5 A); B) selected 2D class averages of 511 particles, processed with Eman2; C) Reproduced Fig 3 from [208]: cryo EM Pma1 (detergent solubilised).

The TEM micrograph (Fig 4.7 A) of SMA 3:1 solubilised *N. crassa* membranes purified in two consecutive SEC reveals heterogeneous particles. 511 particles were picked and processed to give preliminary 2D class averages, with an estimated 12 −13 nm diameter corresponding to the expected size of empty SMA 3:1 particles of 10 −12 nm [164, 185]. However, when comparing these class averages with the expected Pma1 hexamer, which shows a characteristic ring-shaped particle with a diameter of about 23 nm (Fig 4.7 C) , measured particles are smaller and more heterogeneous. The lack of definable features to distinguish between different orientations makes it difficult to characterise them to build a structure model.

The Pma1 hexamer is expected to have a diameter of about 160 Å containing 60 transmembrane α-helices. The presented polymer particles eluted in a similar volume in the size exclusion chromatography as the DDM detergent purified Pma1 (Fig 4.3 B) but differed in appearance from the expected Pma1 hexamer. The hexameric state of Pma1 is vital for insertion into the plasma membrane, as the monomer is degraded if the hexamer integration fails in the Golgi [56]. It remains unclear if the hexameric state is mandatory after integration in the plasma membrane. Recent structural analysis

suggests that the hexamer stays intact [104]. Even though the SMA 3:1-solubilised particles elute at a similar volume as the detergent-solubilised hexamer (Fig 4.2 and Fig 4.3), the particles shown in Fig 4.7 B are smaller than and lack the 6 fold symmetry of hexameric Pma1. This suggests that a lower oligomeric state of Pma1 is captured by SMA solubilisation or that a different protein species is purified.

Particles formed by SMA 3:1 may be too small to accommodate the whole Pma1 hexamer with its 60 transmembrane α-helices. Albeit the Alternative Complex III (MW of 464 kDa) is the largest protein successfully solubilised with SMA to this date and is larger than previously thought possible with SMA [179], its 48 transmembrane α-helices are still less than the 60 transmembrane α-helices of the whole Pma1 hexamer. If the imaged particles do contain Pma1, SMA 3:1 might have disrupted the hexameric integrity of Pma1 during solubilisation. This disruption could artificially lead to lower oligomers, resulting in the presented diverse shapes (Fig 4.5 B), especially since various orientations of these particles would be imaged. Co-solubilised lipids and the polymer belt could increase the apparent particle size and let encapsulated proteins run differently from the detergent-solubilised protein on the size exclusion chromatogram. Following the suggestion that the imaged particles may be a mix between lower Pma1 oligomers, they could be trimers or tetramers. Whether these would be native oligomers or artificially formed oligomers would need to be evaluated further, e.g. by native PAGE optimised for polymer encapsulated MPs [146].

In conclusion, the initial EM data collected of SMA 3:1-solubilised SEC fractions showed heterogeneous particles smaller than the expected Pma1 hexamer. These observations and preliminary dynamic light scattering (DLS) measurements (in the Appendix, Table A.4) of the prepared particles suggest that SMA 3:1 forms smaller particles than necessary to preserve the hexameric integrity of Pma1. Since the apparent size of SMA particles is too small to contain intact Pma1 hexamers and due to previously described reasons, the presence of Pma1 cannot be verified (Section 4.2.2 and 4.2.3). Other polymers should be evaluated for Pma1 solubilisation. Native mass spectrometry could further give information about the identity of the proteins in polymer particles.

4.2.5 Exploring DIBMA and PMA as an alternative to SMA for polymer solubilisation

Diisobutylene-maleic acid (DIBMA) [153] was evaluated as an alternative to SMA to solubilise Pma1 hexamer from *N. crassa* membrane. DIBMA particles are estimated to have a larger diameter, of ∼25 nm [168], compared to ∼8.2 ±4.4 nm for SMA 3:1 particles (Table 3.1 in [185]). Hence, they might be able to solubilise and incorporate the whole Pma1 hexamer. However, as seen in Section 4.2.2, DIBMA showed similar cross-reactions to SMA in the immunoblotting of Pma1 when using a signal enhancer and seemed to suppress the anti-Pma1 signal in all other evaluated blotting methods.

Recently, a promising new polymethacrylate polymer (PMA) was developed [154] as an alternative to the maleic acid-based polymers SMA and DIBMA. PMA is shown to be less sensitive to divalent cations due to its lack of chelating groups [154]. Therefore, PMA was explored as an alternative polymer for the solubilisation of Pma1 with the potential to be compatible with the ATPase activity assay (Baginski assay). The compatibility of PMA with the anti-Pma1 antibody was first evaluated via a dot blot analysis with different immunostaining conditions (similar to Section 4.2.2). The samples were added to a membrane and immunostained with anti-Pma1 antibody in "improved conditions" with L-Arginine to shield negatively charged polymers.

From the dot blot image (Fig 4.8 A, B), the PMA polymer suppresses the anti-Pma1 signal less than SMA or DIBMA when added to detergent-purified Pma1. Since this shows the potential compatibility of PMA with the anti-Pma1 antibody, an initial solubilisation attempt of Pma1 with PMA was performed analogously to SMA 3:1 solubilisation (Section 4.1) and evaluated by SDS PAGE (Fig 4.8 C). Unfortunately, PMA appears to preferentially solubilise smaller proteins than the target protein Pma1 (110 kDa), which is supported by the SEC elution profile at 280 nm (Fig 4.8 D). PMA solubilised samples show a single peak at 100 ml elution volume (black line), compared to the polydisperse trace spreading between 60 and 110 ml of SMA 3:1 solubilised membrane (red line), and particles do not elute at the expected retention volume of Pma1 hexamer (orange area). The PMA - model lipid particle is estimated to have a size of about ∼9.3(±3.4) nm

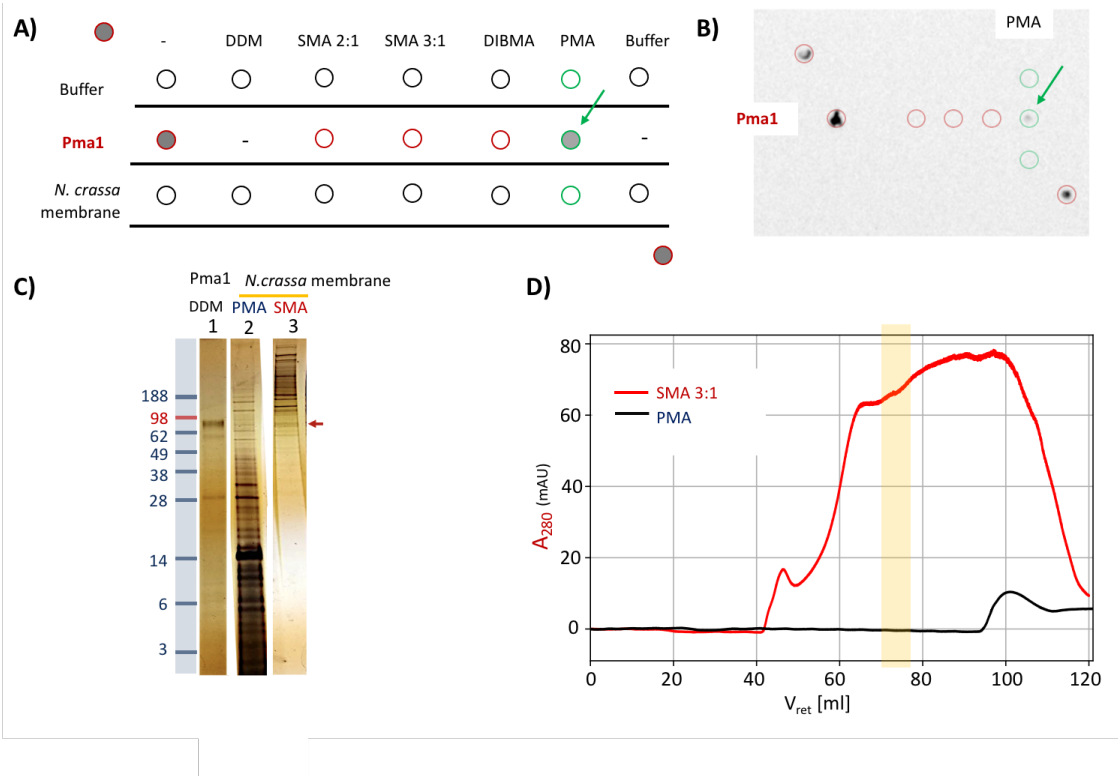

Figure 4.8: Evaluation of PMA to solubilise and purify Pma1
A) and B) Anti-Pma1 dot blot developed in "improved conditions" milk powder and L-Arginine (to shield negatively charged polymer), schematic sample arrangement of the dot blot A) and dot blot B). The following samples were added: 20 mM HEPES pH 8 (Buffer), DDM purified Pma1 protein (Pma1) (circled in red) and *N. crassa* membrane samples with either nothing (-), DDM, one of the polymers SMA 3:1, SMA 2:1, DIMBA, PMA (green circles) or buffer, the green arrow highlights the Pma1 sample with added PMA. C) SDS-PAGE , lane 1 Detergent solubilised Pma1, Supernatant of solubilised Pma1 containing *N. crassa* membranes with 2.5 % PMA (lane 2) or SMA 3:1 (lane 3) pH 8, the red arrow depicts the size of the expected Pma1 monomer. D) Size Exclusion Chromatography (SEC) of solubilised Pma1 containing *N. crassa* membranes with PMA (black) and SMA 3:1 (red) in 20 mM HEPES, 100 mM NaCl, the orange area highlights the expected elution volume of detergent solubilised Pma1 hexamer.

determined via DLS [185], and it might have been too small to accommodate the whole Pma1 hexamer. The largest (and only) membrane protein successful solubilised with PMA to this date has been the GPCR NTSR1 with about ~46 kDa MW [169].

In conclusion, DIBMA and PMA seem to not be feasible for the solubilisation and full biochemical characterisation of native Pma1 from *N. crassa*. Evaluation of other alternative polymers for solubilisation of Pma1 was discontinued due to the Covid-19 pandemic.

4.3 Assessing the use of polymers to solubilise and purify proteins from less complex, bacterial membranes

The polymer solubilisation of *N. crassa* membranes has proven challenging and especially the confirmation of Pma1 presence with the provided anti-Pma1 antibody has been unfeasible. To examine whether the handling of polymers was insufficient, or the Western blots in general, polymer solubilisation on a less complex membrane was explored. In addition, polymer compatibility with an anti-Strep and anti-His antibody was also analysed to inform future heterologous expression of Pma1 with affinity tags.

4.3.1 A bacterial integral membrane protein expressed in *E. coli* as an alternative model for polymer solubilisation

E. coli membranes have been used in several polymer solubilisation studies (e.g. [167, 209, 210]). In order to have a direct comparison between fungal and bacterial membranes and to assess the compatibility of several polymers (SMA 2:1, SMA 3:1, DIBMA, PMA) for immunoblotting with commercially available antibodies (anti-His and anti-Strep), the bacterial integral membrane protein MprF from *Pseudomonas aeruginosa*, overexpressed in *E. coli* membranes as either His- or Strep-tag fusion, was used as a model system. Prokaryotic Multiple peptide resistance Factor (MprF) is a class of lipid-biosynthetic enzymes with two separable functional domains. One modifies PG by adding an aminoacyl to Lys-PG or Ala-PG, and one acts as a lipid flippase to translocate the resulting lipid over the membrane [211]. MprF from *Pseudomonas aeruginosa* (881 amino acids, UniProt accession number: Q9I537) modifies PG with alanine and translocates the Ala-PG over the bacterial membrane (unpublished results, Bublitz group). MprF is involved in resistance to cationic antimicrobial agents such as daptomycin [211] and, therefore, a target for drug development. Some of the transmembrane domains of MprF seem to be related to the protonmotive force-dependent major facilitator protein superfamily [212], and it has been recently proposed that MprF is a whole class of general prokaryotic lipid flippases through a unique domain called prokaryotic phospholipid translocator (PplT) [213].

4.3.2 Polymer solubilisation of MprF-His$_6$

Initial polymer solubilisation of *E. coli* membrane containing an MprF construct with a C-terminal cysteine protease domain (CPD) and a His$_6$ tag was tested using commercially available polymers to assess their solubilisation of MprF-CPD-His$_6$ and their compatibility with the anti-His antibody. Crude *E. coli* membranes were incubated with polymers (SMA 2:1, SMA 3:1, DIBMA and PMA) at different temperatures (4 °C overnight (∼16 h) or 37 °C for 30 min) and different pH (7, 7.5 and 8). Solubilised proteins were separated by SDS-PAGE and visualised by Western blot (Fig 4.9). The estimated molecular weight for the whole MprF-CPD-His$_6$ construct is about 120 kDa, with 95 kDa for the MprF and 24 kDa for the C-terminal cysteine protease domain. Current data suggest that MprF can form homodimers [214], and different oligomeric states of MprF, namely monomers, dimers and tetramers, had been detected in detergent (Bubliz group, unpublished work).

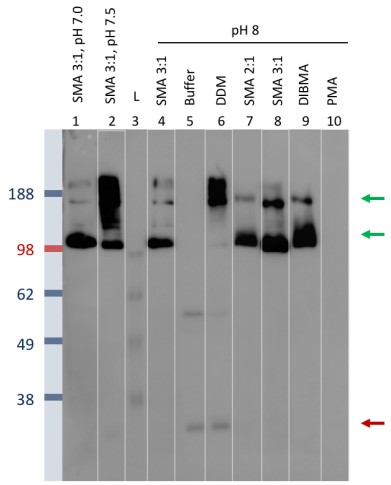

Figure 4.9: Solubilisation of MprF-CPD-His$_6$ with different commercially available polymers
Western blot (Anti His), self casted gel (10 %), SMA 3:1 solubilised MprF-CPD-His$_6$ at 4°C overnight at pH 7.0 (lane 1), Crude *E. coli* membrane containing MprF-CPD-His$_6$ (lane 2), Ladder-L (lane 3), SMA 3:1 solubilised MprF-CPD-His$_6$ at 37°C for 30 min at pH 7.5 (lane 4), (lanes 5-11) solubilised MprF-CPD-His$_6$ in 20 mM HEPES, 100 mM NaCl, pH 8 for 37°C 30 min with different solubilisation agents: buffer as a negative control (lane 5), DDM (lane 6), SMA 2:1 (lane 7), SMA 3:1 (lane 8), DIBMA (lane 9), PMA (lane 10), the green arrow depicts the monomeric (lower) and dimeric (higher) state of MprF-CPD-His$_6$, the red arrow at 28 kDa the -CPD-His6 tag alone.

The anti-His Western blot (Fig 4.9) reveals a monomeric (lower, 100 kDa) and dimeric

(higher, 180 kDa) state of MprF-CPD-His$_6$ (green arrows). The self-cleaving cysteine protease domain alone appears in the DDM solubilised sample (Fig 4.9 lane 6) below 38kDa (compare red arrows on gels Fig 4.10). High-intensity bands in the polymer samples (Fig 4.9 lane 7-9) show that most polymers tested, except PMA (Fig 4.9 lane 10), solubilise MprF-CPD-His$_6$. A prominent dimeric state is seen in the detergent solubilised sample (DDM, Fig 4.9 lane 6), whereas the monomeric form prevails in the polymer samples. SMA 3:1 and DIBMA seemed to preserve the dimer better than SMA 2:1.

Since SMA 3:1 was, at this point, one of the most used and well-characterised polymers, it was used for further solubilisation assessments. *E. coli* membrane was solubilised with SMA 3:1, incubated at different temperatures (4°C overnight (16 h) or 37°C for 30 min) and different pH (7 or 7.5) and separated by ultracentrifugation. Solubilised proteins were separated by SDS-PAGE gel and visualised by silver staining and Western blot (Fig 4.10).

4.10

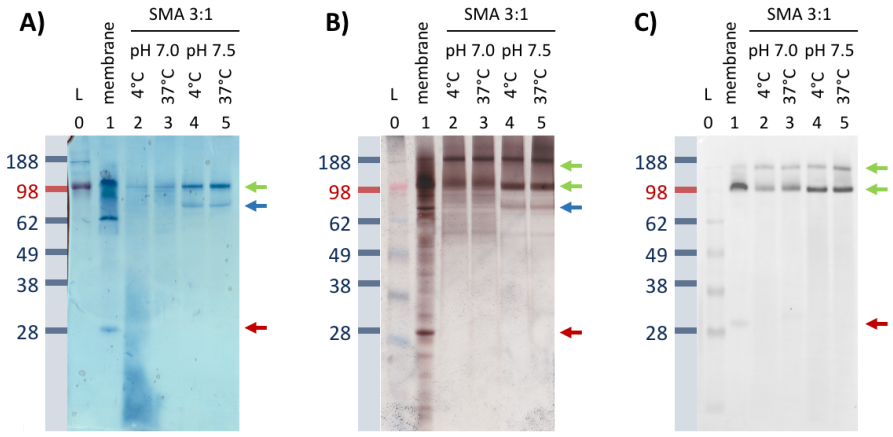

Figure 4.10: Solubilisation of MprF-CPD-His$_6$ with SMA 3:1,
SDS Page, stained with A) coomassie and B) silver C) Western blot (Anti-His). Lanes in all panels are as follows: (0) Ladder-L, (1) Crude *E. coli* membrane containing MprF-CPD-His$_6$, (2) SMA 3:1 solubilised MprF-CPD-His$_6$ at 4°C overnight at pH 7.0, (3) at 37°C 30 min at pH 7.0, (4) at 4°C overnight at pH 7.5, (5) at 37°C 30 min at pH 7.5 (5).The green arrows depicts the monomeric (lower) and dimeric (higher) states of MprF-CPD-His$_6$, the blue arrow the MprF protein after autocleavage of the C-terminally fused cysteine protease domain, the red arrow at 28 kDa marks the cysteine protease domain with His$_6$-Tag.

The Western blot (Fig 4.10 C) shows an anti-His antibody signal, also in the presence of polymers (Fig 4.10 lane 2-5). The anti-His antibody shows that the MprF-CPD-His_6 monomers run to an apparent weight of about 100 kDa with possible incompletely dissociated dimers running at ~188 kDa (Fig 4.10 C, green arrow). This dimer is not as prominent in the membrane sample but visible in the polymer solubilised samples, particularly in a more sensitive silver stain (Fig 4.10 B) rather than a Coomassie stain (Fig 4.10 A). LDS might be the reason for its amount reduction leading to dissociation or denaturation of the dimer. The apparent size of the oligomers is not unexpected since membrane proteins tend to run slightly lower than similar soluble proteins due to their hydrophobic properties [204]. Furthermore, there are several possible reasons for the absence of signal in the SMA 3:1 samples below 60 kDa, it could be that there is no protein sample present, but it is more likely that the presence of polymers and lipids is masking the area from being silver stained (discussed in Section 3.3).

Based on the intensity of the band at 100 kDa in the Western Blot, a pH of 7.5 (Fig 4.10 C lanes 4-5) seems to be slightly beneficial over pH 7 (Fig 4.10 C lane 2-3) for solubilisation of MprF-CPD-His_6 with SMA 3:1, and this seems to be independent of temperature (4°C vs 37°C). In the Coomassie-stained gel (Fig 4.10 A), a protein band at 70 kDa (blue arrow) can be observed, this band has been shown in the lab to belong to cleaved MprF as incubation with LDS initiates auto cleavage of the fused CPD domain. Since this MprF protein remains without the cysteine-protease-His-tag, it would not be visible in the Western Blot compared to the remaining cysteine protease-His visible at 28 kDa (Fig 4.10 C lane 1, red arrow). In previous detergent solubilisation studies (Bublitz group, unpublished data), DDM solubilisation was achieved with 1.2 % DDM in 50 mM Tris, 200 KCl, 20 % glycerol, pH 7.6, at 4°C for 1h. Thermal stability evaluation with CD spectroscopy suggested that MprF has a melting point in detergent at about 56°C. Here the solubilisation of MprF with polymers was achieved at 37°C for 30 min, this higher temperature might aid solubilisation similar to [194].

As seen in Fig 4.10, SMA 3:1 and DIBMA seemed to preserve the dimer better than SMA 2:1 and were therefore chosen as promising. Initial purification attempts with affinity chromatography purification were conducted but require further optimisation.

4.3.3 SMA 3:1 solubilisation of MprF$^{1-545}$-GFP-Strep

As a second construct, a GFP-Strep-tagged truncated version of MprF heterologously expressed in *E. coli* was solubilised with SMA 3:1 at different incubation temperatures (and times) as well as pH (7, 7.5 and 8) (Fig 4.11). The MprF$^{1-545}$-GFP-Strep construct comprises the transmembrane domain (14 transmembrane α-helices) of MprF with a C-terminal GFP-Strep-tag with a total estimated molecular weight of 85 kDa.

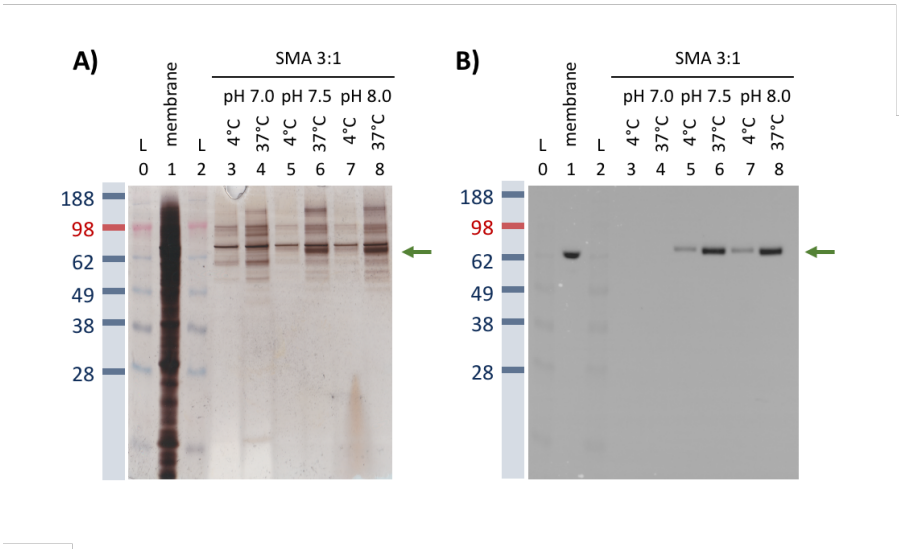

Figure 4.11: Solubilisation of MprF$^{1-545}$-GFP-Strep with SMA 3:1
A) SDS PAGE silver stained, B) Western blot (Anti Strep). Lanes in all panels are as follows: (0) Ladder, (1) Crude *E. coli* membrane containing MprF1-545-GFP-Strep, (2) Ladder, (3) SMA 3:1 solubilised MprF1-545-GFP-Strep at 4°C overnight at pH 7.0, (4) at 37°C 30 min at pH 7.0, (5) at 4°C overnight at pH 7.5, (6) at 37°C 30 min at pH 7.5, (7)at 4°C overnight at pH 8.0, (8) at 37°C 30 min at pH 8.0.The green arrow depicts the monomeric states of MprF$^{1-545}$-GFP-Strep.

In the Western blot (Fig 4.11 B) of the MprF$^{1-545}$-GFP-Strep construct in the crude membrane (Fig 4.11 B lane 1) as well as in the SMA 3:1 solubilised samples (Fig 4.11 B lane 3-8) Anti-Strep shows a signal at ~62 kDa (green arrow). This truncated

construct appears to not display the same dimer species as the complete construct (Fig 4.9, 4.10), suggesting that the lack of the cytosolic domain or the added GPF could prevent dimerisation.

From these solubilisation trials, a higher pH of 7.5-8 (Fig 4.11 lanes 5-8) and a higher incubation temperature of 37°C (Fig 4.11 lanes 6 and 8) seemed beneficial for polymer solubilisation of this truncated protein. This is consistent with the polymer solubilisation of the full length protein and shows similar beneficial trends through higher temperature (37°C) and higher pH. In previous detergent solubilisation trials of this protein, the gels showed degradation (Bublitz group, unpublished data). In contrast, single bands throughout the SMA 3:1 solubilisation trial indicate that this sample underwent no degradation, and that the SMA 3:1 solubilisation does not destabilise the protein (Fig 4.11 B, lanes 3-8).

SMA 2:1, SMA 3:1 and DIBMA have shown their potential to solubilise MprF from *E. coli*. This could lead to further studies of MprF in polymer particles for example to investigate its lipid environment.

4.3.4 Compatibility of polymers with common fusion tag antibodies

Since the available anti-Pma1 is not compatible with polymers, the compatibility of polymers with more commonly used antibodies was evaluated. MprF from Pseudomonas aeruginosa recombinantly expressed in *E. coli* was examined as a different model protein for polymer solubilisation. These results confirmed that SMA 2:1, SMA 3:1 and DIBMA are compatible with anti-His (Section 4.3.2) and SMA 3:1 with anti-Strep (Section 4.3.3) antibodies. The compatibility of SMA 3:1 with the anti-Strep antibody, as described in this section shows the potential of applying polymer solubilisation to Strep-tagged Pma1 expressed recombinantly. The polymer solubilisation efficiency of *S. cerevisiae* membranes shows promise, as described in Section 3.2.1.

Recombinant expression of *N. crassa* Pma1 is challenging due to the protein's complex structure and essential role in cell function. Successful expression of NcPma1 requires that the protein is active, can oligomerize into its hexameric state, and can be regulated through autoinhibition in the presence of high glucose levels (activation).

In filamentous *N. crassa*, NcPma1-C-terminal fused GFP has been expressed via a plasmid for locational studies, but not structural studies [106]. Yeast-like organisms such as (cell wall-less) *N. crassa* slime or *S. cerevisiae* are preferred for structural studies of membrane proteins due to their ability to provide high cell mass and protein density for purification. However, due to the limited molecular tools available for this fungus, the recombinant expression of *N. crassa* slime Pma1 is challenging. Previous studies have recombinantly expressed ScPma1 in *S. cerevisiae* via plasmid transformation of ScPma1-C-terminal-YPet-His_{10}-tag [115] and PCR-based genomic epitope-tagging of endogenous ScPma1 with a C-terminal triple-FLAG [105]. Still, they have not accounted for the oligomeric state and activity or phosphorylation state (activation), respectively. To date, recombinant expression of active hexameric NcPma1 has yet to be achieved due to several challenges associated with tagging the protein (Bublitz lab, unpublished data). Structural analysis of native NcPma1 has revealed complex interactions of the terminal ends with critical domains which can be disrupted by terminal tags. N-terminal tagging presents difficulties as the N-terminal region of NcPma1 is close to the hexamer contact interface in the A domain. Disruption at the interface could lead to interference with hexamerization and movement restriction. Moreover, the A domain interacts with the membrane, particularly through a triple Arginine motif that is believed to pull lipids from the membrane [215] and a tag close to this motif could disrupt the protein-membrane lipid interaction. C-terminal tagging is also challenging as the C-terminal helix is located near critical functional structures in the protein, such as the phosphorylation domain. A tag in this region could interfere with autoinhibition and restrict access of kinases to critical amino acids for phosphorylation. To circumvent these issues, successful recombinant expression of *N. crassa* Pma1 could be achieved by using a very long

C-terminal linker that is cleavable (Bublitz lab, unpublished data).

Additionally, since Pma1 is essential for fungal homeostasis, its expression and activation are tightly regulated. In previous studies, overexpression might have been only possible through the expression of partially inactive Pma1 to avoid competition with functional Pma1. Furthermore, in the successful expression of recombinant ScPma1 hexamer [105] it was not verified that the tag did not interfere with activation (phosphorylation state) beyond a basal levels of H^+-electrochemical gradient. To overcome these challenges with overexpression, recombinant expression of NcPma1 can be induced in *S. cerevisiae* by using a plasmid containing a glucose-dependent promoter, while regular ScPma1 is expressed under a galactose-dependent promoter [216]. This way, the strain normally expresses ScPma1 when provided with galactose, but when provided with glucose, it would express NcPma1. This way, basal levels of H^+-electrochemical gradient could be maintained with regular ScPma1, and glucose activation could also act on the recombinant NcPma1, given the *S. cerevisiae* proteins for glucose-induced phosphorylation would act on NcPma1, which would need to be investigated.
Even though establishing the expression of *N. crassa* Pma1 with a Strep-tag in a heterologous expression system like *S. cerevisiae* is challenging (as described above), it would allow a robust antibody detection to evaluate polymer solubilisation of Pma1 and offers the use of affinity chromatography for purification.

4.4 Summary and Conclusions

The aim of this chapter was to establish a polymer purification protocol to purify *N. crassa* Pma1 from its native source.

- SMA 3:1 showed potential to solubilise Pma1 from *N. crassa*, and size-exclusion chromatography was chosen for further purification (Section 4.1). Pma1 solubilisation and purification via SEC seemed promising based on SDS-PAGE and SEC profile.

- However, Western blots and further optimised immunostaining were incompatible with the available anti-Pma1 antibody (Section 4.2.1, 4.2.2), where it seems to cross-react with the polymers in the presence of a signal enhancer. Otherwise, the polymers seem to shield the anti-Pma1 binding site, interfering with assessing polymer solubilisation and purification of Pma1 in SMA 3:1.
- Similarly, the commonly used ATPase activity assay (Baginski assay) was incompatible with SMA 3:1 due to its sensitivity to divalent cations, forming insoluble aggregates with Mg^{2+}, a mandatory cofactor for Pma1 (Section 4.2.3).
- The initial EM data of SEC fractions of SMA 3:1 solubilised *N. crassa* membrane showed heterogeneous particles smaller than the expected Pma1 hexamer. This suggests that SMA 3:1 forms smaller particles than necessary to preserve the hexameric integrity of Pma1 (Section 4.2.4).
- DIBMA and PMA were explored as alternative polymers to solubilise Pma1 from the *N. crassa* membrane (Section 4.2.5). However, in SDS-PAGE analysis, the PMA solubilised fractions did not show protein bands at the expected MW of Pma1. DIBMA showed similar cross-reactions in the immunoblotting of Pma1 when using a signal enhancer and seemed to suppress the anti-Pma1 signal in all other evaluated blotting methods.
- SMA 3:1 is incompatible for the solubilisation of native Pma1 from *N. crassa* due to its low solubilisation efficiency and therefore not yielding enough protein for conclusive characterisation but based on the presented results it is potentially not in the right oligomeric state either. To overcome the issues with low yield recombinantly (over-) expressed Pma1, could yield higher amounts of Pma1. The presented work shows that potentially recombinant Pma1-Strep could lead to more successful purification as the anti-Strep antibody can be used to follow the polymer solubilisation (Section 4.3.3, 4.3.4).

Chapter 5

Results and Discussion 3 - Lipid analysis of *N. crassa* Pma1 purification from native source

Lipids play a vital role for the transport of the Pma1 hexamer to the plasma membrane Pma1 [57, 58, 109] as outlined in the introduction. To identify co-purified lipids when solubilising and purifying Pma1 from the *N. crassa* slime plasma membrane, a lipid analysis using LC/MS of various *N. crassa* slime samples was performed and is presented in the following chapter. The aims of this chapter are:

- To compare the lipid composition of *N. crassa* slime whole cells grown at different temperatures and *S. cerevisiae* (W303.1b gal4-Δpep4) whole cells, both expressing Pma1.
- To analyse the lipid composition of the *N. crassa* plasma membrane and the influence of the preparation on its lipid composition.
- To analyse lipids purifying with detergent solubilised NcPma1.
- To identify lipid candidates that may play a role in stabilising the hexameric state of NcPma1.

If not otherwise specifically stated the following analysis is focused on whole cells, plasma membrane and purified NcPma1 from the *N. crassa* slime mutant and will further be referred to as *N. crassa* and Pma1 and the *S. cerevisiae* mutant W303.1b gal4-Δpep4 as *S. cerevisiae*.

5.1 Samples sent for lipids analysis

For a comprehensive lipid analysis of a diverse set of *N. crassa* slime samples, it was necessary to identify a method and establish a collaboration to analyse its lipid content. For this analysis, a collaboration with the NIHR Core Metabolomics and Lipidomics Laboratory at Cambridge University was set up, which is specialised in lipid analysis using Liquid Chromatography Mass Spectrometry (LC/MS) [191] and can perform lipid extraction in-house. Samples to analyse the purification pipeline of *N. crassa* Pma1 from whole cell and plasma membrane preparation via DDM solubilisation to purified Pma1 in different oligomeric states were sent as aqueous samples and analysed by the collaboration. Various samples were sent for lipid analysis with LC/MS, as outlined in Fig 5.1 and Section 2.5.1,

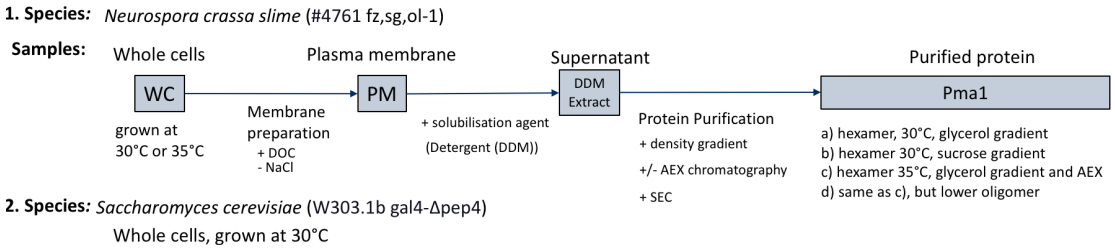

Figure 5.1: Schematics of samples sent for lipidomics analysis

Whole cells of *N. crassa* were compared to *S. cerevisiae*, which acts as a technical and biological control because it is a well-studied organism, such as its lipid composition with mass spectrometry (MS) (e.g. [48]). Previous analysis of *N. crassa* has been using TLC (e.g. [64]) and gas chromatography [65]. Using *S. cerevisiae* as a control aims to ensure the reliability and accuracy of the results obtained from the LC/MS analysis of *N. crassa*, as it provides a reference point for comparison when using a new technique and helps to guide the data analysis. Additionally, both *N. crassa* and *S. cerevisiae* express Pma1, the protein of interest, and *S. cerevisiae* is explored as a heterologous expression system for NcPma1 (Bublitz lab, unpublished data), therefore comparing the two can provide insight into the similarities and differences between the two organisms potentially relevant for the Pma1 expression and function.

5.2 Overview on measured lipids with LC/MS

The lipid analysis with LC/MS of the total 21 samples resulted in a total of 420 identified lipid species. The 420 lipid species were classified into the lipid classes and categories outlined in Fig 5.2. The results in this chapter are presented in Mol% normalised to their respective categories. Sterol content of the samples was not analysed in this experimental set up.

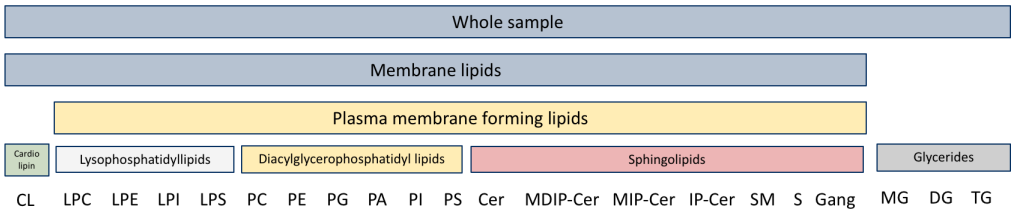

Figure 5.2: Identified lipid classes and their classification provided through lipid analysis with LC/MS
Sterols (e.g. ergosterol) have not been analysed during the presented lipid analysis.

The details of frequency and specifics of the reported lipid classes are outlined in Table B.7 in the appendix. The whole lipid profile of all samples was categorised into the main lipid categories and compared, detailed values can be found in the Appendix (Table B.9).

When comparing the total number of detected lipid species (Table 5.1) for each lipid category, a larger number of distinct lipid species were reported for *N. crassa* samples than for *S. cerevisiae* samples (20–60 % more, depending on the sample). The number of individual detected lipid species decreased during the purification steps from *N. crassa* whole cells to purified Pma1 protein but remains higher for most *N. crassa* samples compared to the *S. cerevisiae* samples, except for lysophospholipids and glycerides. This difference of average total number of detected lipid species between the two organisms, particularly in the average total number of membrane forming lipids (40 % i.e. 167 vs 273 species respectively) suggests an increased complexity in the lipid distribution and lipid synthesis of *N. crassa* compared to *S. cerevisiae*. Since both organisms express Pma1 differences in their lipid composition are further analysed in Section 5.3.

Table 5.1: Number of individual lipid species measured per sample type
Reported lipid species were only counted if Mol%>0

	Lysophospho-lipids	Diacylglycero-phospholipids	Sphingolipids	Cardiolipin	Glycerides	plasma membrane forming lipids	Total
N. crassa							
WC	**40**	**104**	**89**	**40**	**53**	**273**	**326**
PM	24	98	82	40	54	243	297
DDM	13	90	78	41	27	222	249
Pma1 Protein	15	84	67	38	31	204	236
S. cerevisiae	**33**	**73**	**36**	**25**	**43**	**167**	**213**

5.3 Whole cell lipid analysis comparing the slime mutant *N. crassa* with a *S. cerevisiae* mutant

To analyse the differences of the lipid composition of the two fungal species the whole cell lipid profile of *S. cerevisiae* (grown at 30°C, n=1) and *N. crassa* (grown at 30°C, n=6 and 35°C, n=2) were compared. Due to the lack of multiple samples for *S. cerevisiae*, the following comparison can mainly give indications for a preliminary qualitative analysis and highlight trends.

5.3.1 Whole cell lipid analysis slime mutant *N. crassa* vs *S. cerevisiae*

Lipids were categorised into distinct types and categories and compared for the two organisms (Fig 5.3, for detailed values please refer to Appendix Table B.9). This data shows a large difference between glycerides (or storage fat; SF) and cardiolipin content between both organisms, with a higher glyceride content observed in *S. cerevisiae* (58 %) compared to *N. crassa* (14–18 %) (Fig 5.3 A). Furthermore the overall glyceride content in whole cell *N. crassa* may be slightly raised by higher growth temperature (14($\pm$1) % at 30°C and 18($\pm$1)% at 35°C). Excluding glycerides gives the subset of lipids capable of forming membranes within the cell (Fig 5.3 B). Furthermore, exclusion of cardiolipin, which are found predominantly in mitochondria [17, 23], allows for a refined analysis of only plasma membrane forming lipids (Fig 5.3 C). This shows that the relative amount of diacylglycerophospholipids is similarly high in *N. crassa* and *S. cerevisiae*, and under these conditions no clear difference was measured between the organisms.

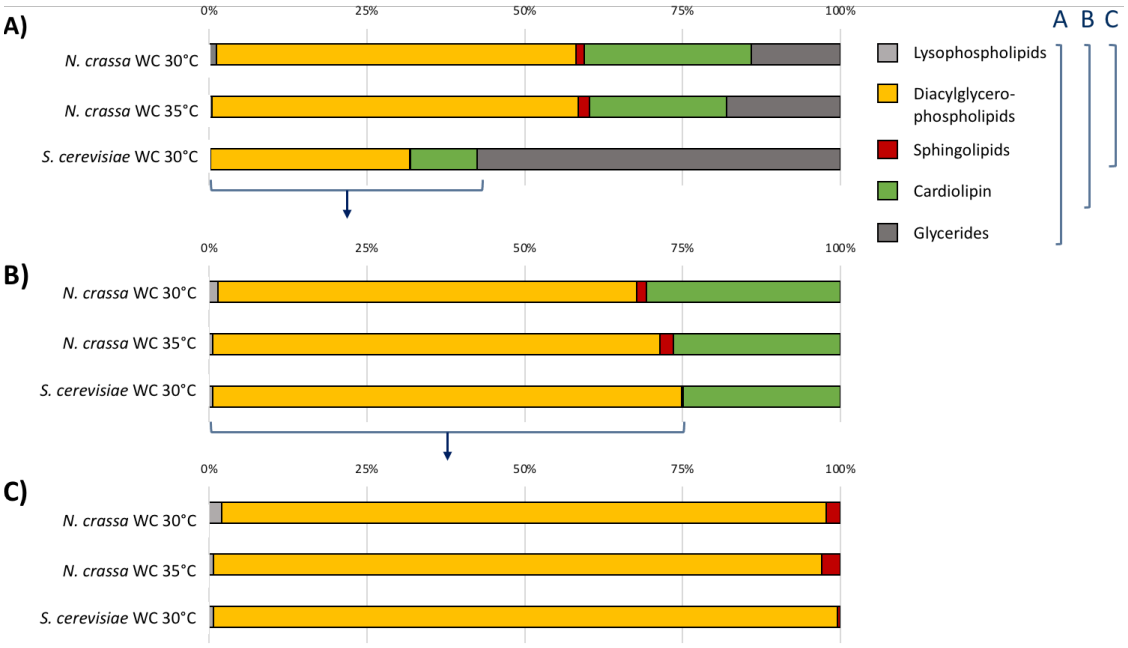

Figure 5.3: Analysis of lipid categories of *N. crassa* and *S. cerevisiae* from whole cell samples
LC/MS lipid analysis of whole cell (WC) samples, of *N. crassa* grown at 30°C (n=6) and 35°C (n=2) and *S. cerevisiae* (n=1), comparing the distribution of lipid categories for all lipids A), for membrane forming lipids B) and for membrane lipids excluding cardiolipin C).

The variations of lipid types were further analysed for each lipid category and the relative content of each lipid class was normalised accordingly.

5.3.2 Diacylgylcerophospholipids (DGPL) in *N. crassa* and *S. cerevisiae*

To identify potential differences in lipid distribution between the two fungi *N. crassa* and *S. cerevisiae* diacylglycerophospholipids were analysed (Fig 5.4). The diacylglycerophospholipids distribution of *S. cerevisiae* is characterised by a high amount of PC, PA and PE, followed by PI and PS, and only trace amounts of PG (Fig 5.4 A). *N. crassa* shows an overall similar lipid profile, compared to *S. cerevisiae*, albeit with less PC and more PE than *S. cerevisiae* (Fig 5.4 A). In the whole cell of *N. crassa*, a temperature change might slightly increase PA and decrease PC and PE, but the high variation within the samples does not permit changes in PA and PC to be conclusive. Due to the lack of multiple samples for *S. cerevisiae*, this comparison should be re-evaluated.

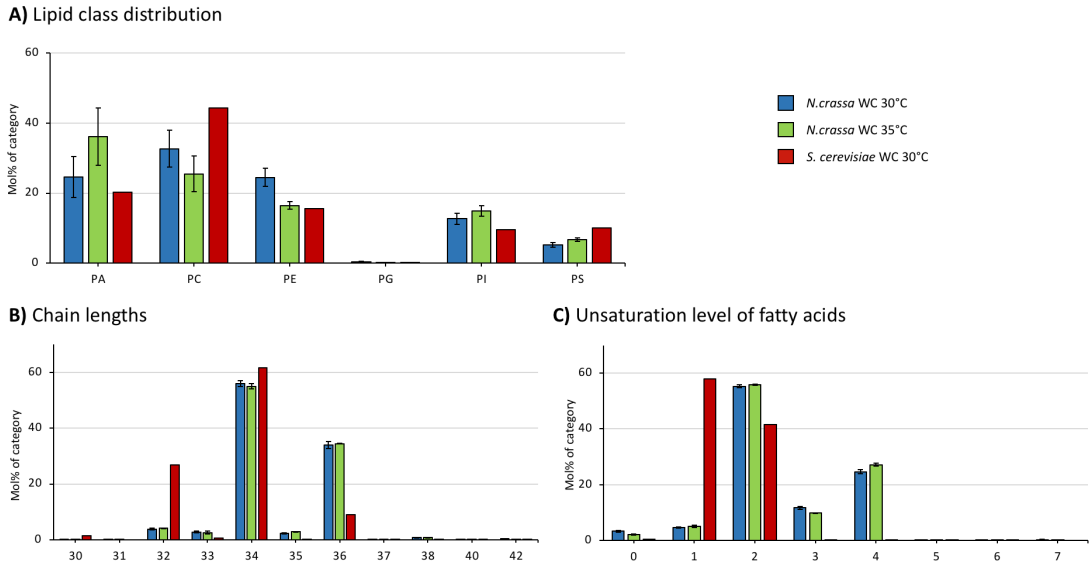

Figure 5.4: Diacylglycerophospholipids distribution of whole cell samples of *N. crassa* and *S. cerevisiae*
LC/MS lipid analysis of whole cell (WC) samples of *N. crassa* grown at 30°C (n=6, light blue) and 35°C (n=2, green) and *S. cerevisiae* grown at 30°C (n=1, red), comparing the distribution of lipid classes A), total chain lengths B), and total unsaturation level of both fatty acids, (x-axis: Number of double bonds) C) of diacylglycerophospholipids.

The fatty acid chain content of diacylglycerophospholipids was further analysed (Fig 5.4 B). LC-MS measurements report the total chain length of the lipid species and give the sum of carbon atoms of the two fatty acid chains of each lipid. Both organisms' most abundant diacylglycerophospholipids species have a total chain length of 34 carbon atoms (∼60 %). The next most abundant species in *S. cerevisiae* have 32 carbon atoms (∼30 %), in comparison to 36 in *N. crassa* (∼35 %). More odd numbered total chain lengths were measured in *N. crassa* than in *S. cerevisiae*, where almost only even numbers were measured.

A further difference between *N. crassa* and *S. cerevisiae* was observed when comparing the total unsaturation level of the fatty acid side chains in diacylglycerophospholipids (Fig 5.4 C). For *S. cerevisiae* diacylglycerophospholipids, predominantly 1 or 2 double bonds were measured, with only trace levels of lipids having higher levels of unsaturation. In contrast, *N. crassa* diacylglycerophospholipids showed higher degrees of unsaturation,

ranging from 0-4 double bonds with highest unsaturation levels being 2 and 4.

It has been previously reported that *N. crassa* slime mutant and wild type does synthesise polyunsaturated fatty acids [64, 124] (overview in Appendix, Table B.5), such as C18:2 (∼54 % of whole cell lipid composition) and C18:3 (∼13 %) [64], which would explain the higher total level of unsaturation seen compared to *S. cerevisiae*. Furthermore, monounsaturated and fully saturated fatty acids have been measured, such as C18:1 (∼4 %), C16:1 (∼3 %), C16:0 (∼23 %), C18:0 (∼2 %), C15:0 (∼1 %) and C14:0 (∼1 %) [64]. The most prevalent fatty acids of *N. crassa* slime grown at about 30°C have 18 carbon atoms and make up 75–80 % of all fatty acids compared to fatty acids with 16 carbon atoms which comprise 20 % [64].

These reported fatty acid species are in agreement with total lipid chain length in Fig 5.4 B, with the most abundant species of C34 and C36 likely comprising combinations of C16 and C18 fatty acid chains. The low level of C33 lipid observed could comprise of C15 and C18 fatty acids, however the observed C35 fraction would require C20, C19 or C17 fatty acids, which had not been previously reported in literature of *N. crassa*. Further lipidomic analysis of individual fatty acids using for example LC/MS-MS, would be required to validate their presence.

Except for the changes in diacylglycerophospholipid headgroup distribution, no clear difference in the overall chain length or number of double bonds can be seen for *N. crassa* between the two growth temperatures at a whole cell level from this measurement.

5.3.3 Lysophospholipids in *N. crassa* and *S. cerevisiae*

The analysis of lysophospholipids showed that the total lysophospholipid pool of all *N. crassa* slime samples contain is on average comprised of 70 % LPC (60–90 %), 23 % LPE (5–30 %), 3 % LPI (0–7 %) and 1 % LPS (0–3 %), with no clear changes in distribution during any of the purification steps. Whereas, the lysophospholipid distribution of *S. cerevisiae* consists of about 80 % LPC, 2 % LPE, 16 % LPI and 3 %

LPS. In both fungal species the overall lysophospholipid content was relatively low (∼2 % in *N. crassa* whole cells and ∼0.7 % in *S. cerevisiae* whole cells) and the average distribution of the lysophospholipid species differs between the fungal organism with a higher LPE and lower LPI content in *N. crassa* compared to *S. cerevisiae*.

5.3.4 Cardiolipin types differs between the two fungal organisms

Cardiolipins are essential eukaryotic lipids primarily localities to mitochondria [17, 23]. The high cardiolipin content in *N. crassa* whole cells (Fig 5.3) could indicate an increase in mitochondria in the cell due to increased energy demand to adapt to a less favourable environment with its lack of a protective cell wall. Previous findings in [65] support this.

More distinct cardiolipin species were measured in *N. crassa* compared to *S. cerevisiae* (40 vs 25 species, respectively) whole cells. In Fig 5.5 the cardiolipin profile of both organisms grown at 30°C are qualitatively compared regarding their total chain length and saturation level. The quality of cardiolipin differs between the two organisms. When omitting the glycerides content, the fraction of cardiolipin in the membrane forming lipids is ∼31 % for *N. crassa* and 25 %for *S. cerevisiae*.

The fatty acid moieties (Fig 5.5 A) of the measured cardiolipins vary in their total length. In *N. crassa* they are between 66-74 carbon atoms with ∼80 % having 70 or more carbon atoms compared to only ∼25 % having 70 or more carbon atoms in *S. cerevisiae* with a similar range. The saturation level of cardiolipins vary between the two organisms (Fig 5.5 B); in *S. cerevisiae* they have mostly 2-4 double bonds with the most common being 3 double bonds whereas the number of double bonds in *N. crassa* cardiolipins are distributed between 2-10 double bonds.

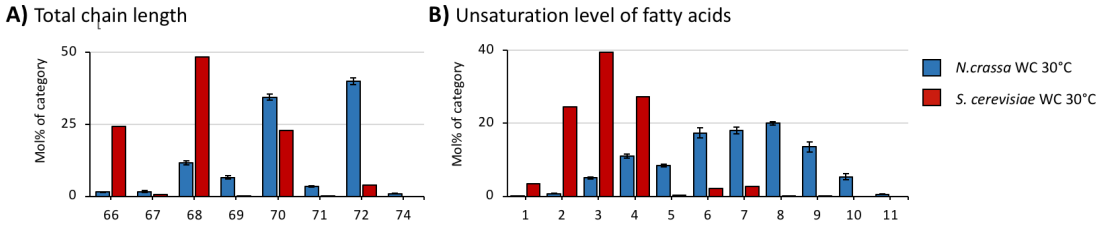

Figure 5.5: Analysis of cardiolipin of *N. crassa* and *S. cerevisiae*
LC/MS lipid analysis of whole cell (WC) samples, grown at 30°C of *N. crassa* (n=6, light blue) and *S. cerevisiae* (n=1, red), comparing the distribution of total chain lengths A) and unsaturation level of the sum of all fatty acids, (x axis: Number of double bonds) B) of cardiolipins.

The cardiolipin of *S. cerevisiae* has been reported to contain mainly fatty acids of 16:1 and 18:1 [217], therefore total unsaturation levels of up to 4 would be in agreement with this. Furthermore cardiolipin up to 72 carbon atoms would be expected, the highest amount presented with 68 carbon atoms could be a 1:1 mix of these 16:1 and 18:1 fatty acids. The higher diversity of cardiolipin, with its four fatty acids, would be in alignment with the diverse and higher number of double bonds as previously described in Section 5.3.2.

The difference of cardiolipin types between the two fungi can be indicative of the variation in lipid metabolism of the organism, particularly of the fatty acid synthesis with longer fatty acid chains with larger number of double bonds. Furthermore it has been reported that in a different *N. crassa* slime mutant than used in this study (type #1118) mitochondria also change their appearance with longer growth [123]. This may also be the case for the type #4761 mutant. Longer fatty acid chains and a higher number of double bonds might be a sign of the morphologically changed mitochondria.

5.3.5 Sphingolipid types differ between the fungal organisms *N. crassa* and *S. cerevisiae*

Sphingolipids, being an integral part of the plasma membrane lipid bilayer, were further analysed. 96 distinct sphingolipid species were reported in the data set, which were further subdivided into different classes; ceramides (Cer), sphingomyelin (SM) and

inositol containing ceramides, such as phosphatidylinositol-ceramides (IP-Cer), mannosyl-phosphatidylinositol-ceramides (MIP-Cer), and mannosyl-di-phosphatidylinositol-ceramides (MDIP-Cer). Furthermore, only minor traces of gangliosides (Gang) and sulfatides (S) were measured and are not specifically discussed here (data in the appendix, Table B.17). Generally a low total sphingolipid content is measured in the whole cells samples with 0.15 %of all lipid types in *S. cerevisiae*, and 1.3 ($\pm$0.2) % and 1.8 ($\pm$0.3) % in *N. crassa* slime grown at 30°C and 35°C respectively (Appendix, Table B.9). Surprisingly, *N. crassa* contained a far higher number of distinct individual lipids of sphingolipids, with 89 being identified in total, compared to only 36 for *S. cerevisiae*.

The relative distribution of sphingolipid classes differs between both fungal species (Fig 5.6 A, Table Appendix B.17). In *S. cerevisiae*, the majority of sphingolipids are IP-Cer and MIP-Cer with smaller contributions from Cer. In contrast in *N. crassa*, SM is the dominant sphingolipid (55–80 %), which is measured at less than 1 % in *S. cerevisiae*, followed by Cer (15–35 %) and IP-Cer (5–10 %) and only minor amounts of MIP-Cer. MDIP-Cer and sulfatides (S) were measured present in both species at less than 1 % .

The total sphingolipid content of *S. cerevisiae* consists to 95 % of 4 lipid species: IP-Cer 44:0 (40 %), IP-Cer 46:0 (16 %), MIP-Cer 44:0 (21 %) and MIP-Cer 46:0 (18 %). In *N. crassa* 89 different sphingolipid species were measured. 17 sphingolipid species that were measured at a relative distribution of more than 1 % made up about 89 % of the total sphingolipid content of *N. crassa* whole cells and the 4 most common species were SM 34:2 ($\sim$18 %), SM 34:1 ($\sim$13 %), Cer 42:0 ($\sim$9 %), IP-Cer 42:0 ($\sim$9 %).

The largest variety between the number of sphingolipid species measured in *N. crassa* and *S. cerevisiae* whole cells were Cer (32 and 10 different lipid species respectively) and SM (22 and 3 different lipid species, respectively) and S (21 and 4 different lipid species respectively). Total chain length of the sphingolipid fatty acid moiety (Fig 5.6 B) ranged in *N. crassa* from 32-48 carbon atoms with a majority of 34 and 42 carbon atoms, and

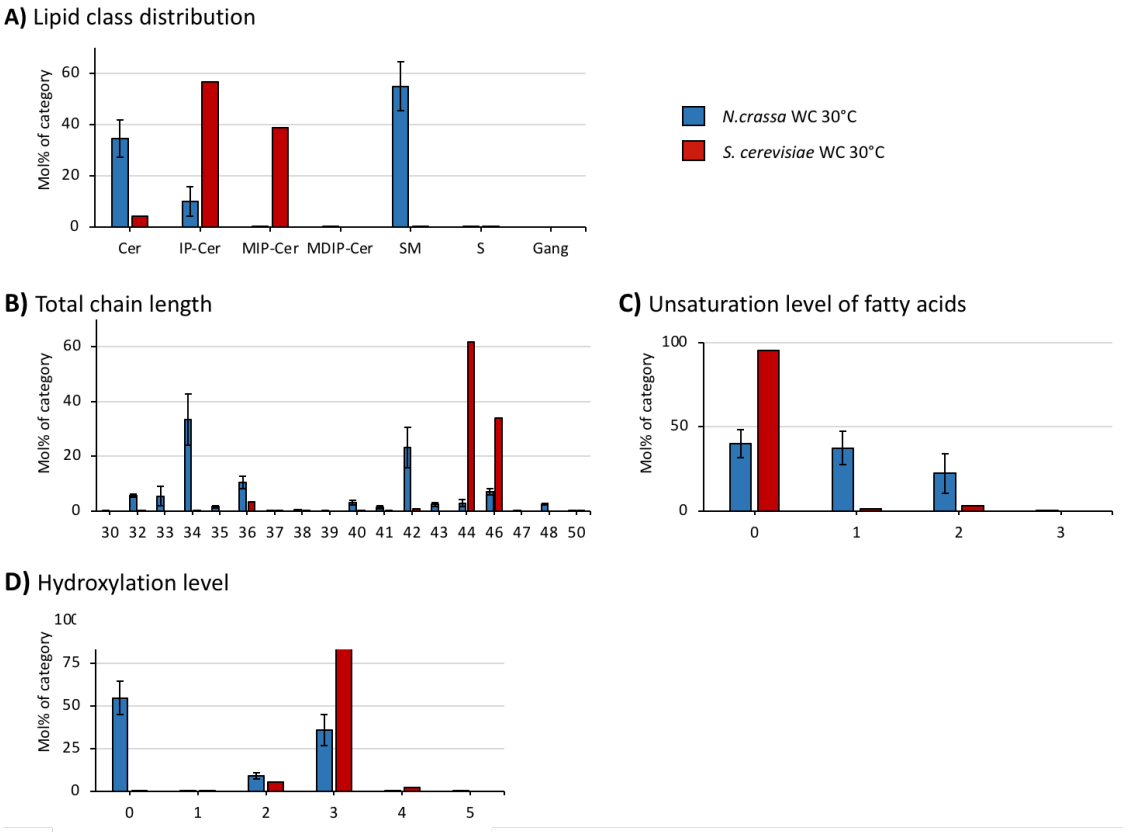

Figure 5.6: Analysis of sphingolipid distribution of whole cell samples of *N. crassa* and *S. cerevisiae*
LC/MS lipid analysis of whole cell (WC) samples, grown at 30°C of *N. crassa* (n=6, light blue) and *S. cerevisiae* (n=1, red), comparing the distribution of lipid classes A), total chain lengths B), Saturation level of fatty acids, (x-axis: number of double bonds) C) and hydroxyl groups D).

in *S. cerevisiae* ranging at C36 and C42-46 with a majority of C44 and C46 side chain moieties. *S. cerevisiae* has more lipids with even total number of carbon atoms in the fatty acid moiety than *N. crassa*. The relative content of odd number of carbon atoms in the sphingolipids of *S. cerevisiae* is ∼0.01 % and in *N. crassa* at ∼11 %, a similar trend to the overall membrane forming lipids with odd numbered side chain moieties of ∼0.8 % in *S. cerevisiae* is and ∼5 % in *N. crassa*. The number of double bonds (Fig 5.6 C) in sphingolipids of *S. cerevisiae* is predominantly 0, whereas for *N. crassa* lipids more equal distribution 0, 1 and 2 double bonds can be found. The hydroxylation levels were measured for ceramides and inositol containing ceramides, which then contribute to the overall hydroxylation level reported (Fig 5.6 D). In *S. cerevisiae* whole cells a higher number of hydroxylated sphingolipids were measured compared to *N. crassa* whole cells

(Fig 5.6 D).

N. crassa whole cells were compared to *S. cerevisiae* to evaluate the results of the LC/MS lipidomic methods and to put them in context with other recent lipid analysis methods. Albeit the quantity for each lipid species in the presented lipid analysis of *S. cerevisiae* differs from the previously reported lipidomic analysis of *S. cerevisiae* [50], the same overall lipid classes were identified. Particularly the presence of inositol-containing sphingolipid classes (e.g. IP-Cer, MIP-Cer) was confirmed in *S. cerevisiae*, and sphingomyelin-like lipids were only measured in *N. crassa* (Fig 5.6). This is in line with the literature, so that the spingolipid classes differ between both fungi as outlined in the introduction (Fig 1.4). Even though the measurement results for *S. cerevisiae* differ from published results [50], it is possible to use them to understand the *N. crassa* result and to evaluate further results for NcPma1. The presence of Sphingomyelin-like lipids are further discussed in Section 5.4.6.

5.4 Lipid content during the purification process of *N. crassa* Pma1

To identify potentially important lipids for the hexameric state of *N. crassa* Pma1, changes in lipid composition were analysed during the purification from whole cells via plasma membrane to DDM solubilised and purified protein. Pma1 is targeted to the plasma membrane [56, 109], therefore the analysis focused on plasma membrane forming lipids. A complete sample pipeline was analysed for a glycerol gradient purified Pma1 hexamer sample that originated from *N. crassa* whole cells grown at 30°C, and compared to alternative samples when appropriate. Any lipids enriched during the protein purification focusing on Pma1 would be assumed to be a combination of tightly bound, non-annular lipids with potential structural and functional relevance for the protein, as well as remaining generally highly present lipids in the plasma membrane.

5.4.1 Plasma membrane forming lipids during purification process of *N. crassa* Pma1

The plasma membrane lipid composition of each sample along the purification pipeline was normalised for comparison (Fig 5.7). The plasma membrane samples and all consecutive Pma1 purification steps contain higher sphingolipid content and relatively reduced diacylglycerophospholipid levels compared to the whole cell fractions (respectively sphingolipids ∼15 % vs ∼2.5 % and diacylglycerophospholipids ∼80 % vs ∼95 % of all plasma membrane lipids). This is supported by previous studies which have shown that sphingolipids are most abundant in the eukaryotic plasma membrane, and typically contain about (∼10–20 %) sphingolipids [8]. In previous publications 4–9 % Sphingolipids have been reported in the *N. crassa* plasma membrane [65].

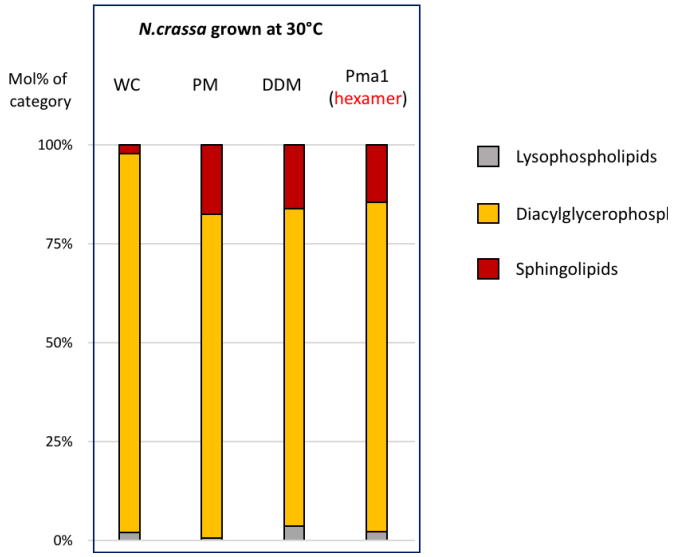

Figure 5.7: Ratio of plasma membrane forming lipids during DDM solubilisation and purification of Pma1
Distribution of lysophospholipids (grey), diaclyglycerophopholipids (DGPL, orange) and sphingolipids (SL, red) for *N. crassa* grown at 30°C. Pma1 hexamer was purified with glycerol gradient.

There seems to be a small relative increase in lysophospholipids with DDM solubilisation of the plasma membrane (Fig 5.7). Even though the overall lysophospholipid content increased slightly with the purification of *N. crassa* Pma1 no clear difference of lysophospholipid species distribution was measured in the various Pma1 samples compared to

the whole cells or plasma membranes, suggesting no enrichment of a particular species in the purification of Pma1.

The variations of lipid types were further analysed for each lipid category and the relative content of each lipid class was normalised accordingly.

5.4.2 Lipid analysis of *N. crassa* plasma membrane preparation

To evaluate the effect of the plasma membrane preparation on the diacylglycerophospholipid content of the plasma membrane sample, two plasma membrane samples from *N. crassa* cells grown at 30°C are compared in Fig 5.8 (samples washed with desoxycholate (DOC) A and B). Due to the complexity of the protocol [104, 122] the *N. crassa* slime plasma membrane preparations vary in their purity. Particularly the agglutination of the samples with Concanavalin A worked variably well, potentially retaining different amounts of contamination in the plasma membrane sample compared to other residual organelle membranes. More cardiolipin was measured in the membrane forming lipids of DOC A ($\sim$45 %) sample compared to the DOC B ($\sim$35 %) sample (see appendix Table B.10). Cardiolipin can be considered an indicator for mitochondrial contamination of plasma membrane samples, suggesting that the DOC B is of higher purity. Indeed the Pma1 purified from DOC A contained a high amount of co-purification of mitochondrial Complex I (Bublitz group, unpublished data), whereas DOC B is a clean plasma membrane sample, judged by SDS PAGE (Bublitz group, unpublished data). As such, the diacylglycerophospholipid composition of the analysed DOC A plasma membrane is overall similar to that of whole cells (Fig 5.8 A). To be able to normalise and evaluate the effect of mitochondrial lipids on the measured lipid composition, purified mitochondria from *N. crassa* slime should be analysed in the future as there is currently no reported MS data in the literature for this strain.

In contrast, DOC B is characterised by a high PS content (35 %) (Fig 5.8), that is in line with published data for plasma membranes of *N. crassa* [64] and *S. cerevisiae* [17].

Therefore, a low cardiolipin and a high PS content might be a good indicator for successful plasma membrane preparation. The next largest variation between the two plasma membrane preparations is seen in the PA and PC content, whereas both show less PI and PE content in the plasma membrane compared to the whole cells.

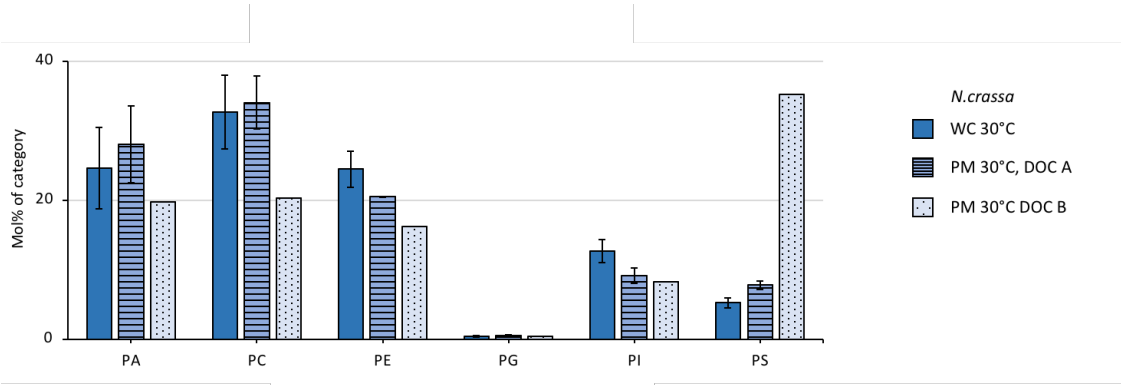

Figure 5.8: Diacyl glycerophospholipid classes during the purification of Pma1
LC/MS lipid analysis of plasma membrane preparation from *N. crassa* grown at 30°C comparing the distribution of lipid classes of diacyl glycerophospholipids. Whole cells (WC, n=6, blue), plasma membrane (DOC A blue hashed, 30°C n=2), compared to an additional plasma membrane sample (DOC B, blue dotted, 30°C n=1) with lower levels of impurities as discussed in the text.

A high baseline PA content was measured in all samples during the Pma1 purification process, ranging from 11–39 % of all diacylglycerophospholipids (Table 5.2). In samples from each purification step about 10 % higher relative PA content within diacylglycerophospholipids is measured in samples from *N. crassa* grown at 35°C compared to 30°C (Table 5.2). Even though this increased PA content in *N. crassa* between the growth temperatures might be physiological, a general dominant PA content in whole cells has not been reported in the literature (compare ∼4 % PA for whole cells measured with TLC in [64]). The discrepancy between the presented measurement and published results could also be due to their difference in resolution or be an artefact in one of the used measurement techniques (TLC and LC/MS) and should be evaluated further.

Table 5.2: Relative PA content within diacyl glycerophospholipids

Temperature	PA content (%) in Diacylglycerophospholipids		
	Whole cell	plasma membrane	glycerol gradient purified Pma1 hexamer
30°C	~25	~25 with DOC wash ~53 w/o DOC wash	~11
35°C	~36	~39	~23

Previous studies have reported an increased PA content during *N. crassa* membrane preparation compared to whole cells [65] (following the protocol published in [120]). The higher PA content might be more characteristic of the whole cell rather than plasma membrane as seen in Fig 5.8 and the measured high PA content in the membrane might be an artefact due to the preparation method [65]. The activity of the most abundant phospholipase, phospholipase D (PLD) which hydrolyses PC to PA, could increase the relative PA content. PLD is membrane-associated and may remain in the sample even after several purification steps. This is supported by the increased PA content in the high molar NaCl wash (step wise washed with 2 M,1 M, 0.5 M and 0 M NaCl) (~53 % PA of the diacylglycerophospholipid content) compared to samples prepared with a DOC wash (~25 %) (Table 5.2). The DOC wash was reported by [122] to improve the purification of Pma1 by removing proteins from the membrane, probably including smaller peripherally bound membrane proteins. The NaCl wash may not remove these proteins and a remaining high load of active PLD could explain the high PA content in the sample. Even the DOC washes may not remove all of the PLD, so future membrane preparations should be prepared with EDTA present; chelation of its metallic cofactors (as suggested by [65]) could reduce PLD activity and so could then be analysed to see whether PA content remains high.

Furthermore, the NaCl washed membrane samples had an overall similar lipid composition to the whole cell, but no enriched relative cardiolipin content (~20 % of membrane lipids). Whilst it is well documented that washing the plasma membrane with DOC reduces the level of contaminating protein [122], it also appears, in comparison to an

NaCl washed membrane, to reduce the total lipid content; for the same mass of sample ∼90 µM total lipids/mg total protein were measured in the DOC samples compared to ∼500 µM total lipids /mg total protein in the NaCl sample. Furthermore DOC washed membranes contain a higher proportion of glycerides (50–80 % of whole lipids Appendix B.9) compared to NaCl washed membranes (25 %) suggesting that DOC wash removes a higher proportion of membrane lipids. This may produce a membrane with more densely packed protein and which may be reminiscent of detergent induced lipid rafts [218], which could explain the resistance of these membranes to solubilisation by polymers (Section 3.3). As such, the NaCl wash should be explored further in the plasma membrane preparation protocol, particularly to allow for a detergent-free purification in future polymer solubility studies.

In addition to individual diacylglycerophospholipid classes the chain lengths and saturations of diacylglycerophospholipid fatty acid moieties from whole cell and plasma membrane were analysed (Fig 5.9). The overall chain length of diacylglycerophospholipids seems to increase between whole cells and plasma membrane, with an increase in the fraction of C36 total chain length (Fig 5.9 B). This is supported by the DOC B sample (Fig 5.9 A) where a higher level of lipids with more carbon atoms are measured (∼45 % C34 and ∼45 % C36) compared to the whole cells (∼55 % C34 and ∼35 % C36). This increase in longer diacylglycerophospholipids within the plasma membrane samples is supported by the observation that the plasma membrane is known to be thicker in comparison to internal organelles [219].

Additionally, the overall diacylglycerophospholipid unsaturation level decreases from the whole cell to the plasma membrane, indicated by an increase of lipid species with one or fewer double bonds of ∼10 % to ∼12–40 %, respectively (Fig 5.9 B). An increase in fully saturated fatty acids in the plasma membrane was predominantly seen in the more pure plasma membrane (DOC B) sample (Fig 5.9 B). This is in line with published results which measured more fully saturated fatty acids in the plasma

membrane compared to the whole cells ([64], Appendix Table B.5), which would likely reduce fluidity of the membrane.

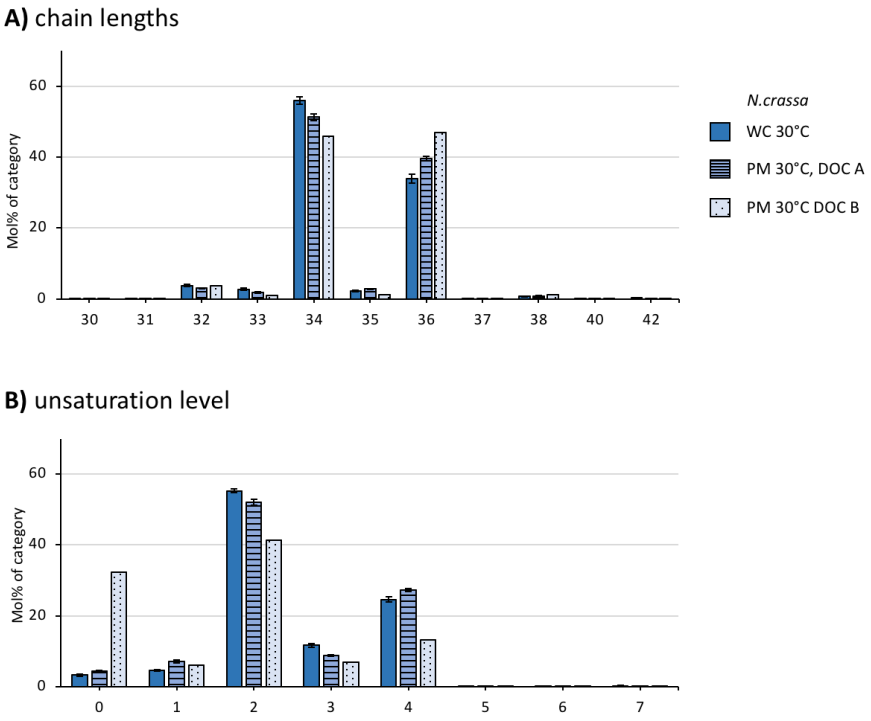

Figure 5.9: Chain length and unsaturation levels of diacyl glycerophospholipids *N. crassa* plasma membrane preparation
LC/MS lipid analysis of Plasma membrane preparation from *N. crassa* grown at 30°C comparing the distribution of total chain lengths A) and total unsaturation level of both fatty acids, (x-axis: Number of double bonds) B) of Diacyl Glycerophospholipids. With whole cells (WC, n=6, blue), plasma membrane (PM,DOC A blue hashed, 30°C n=2), compared to an additional plasma membrane sample (PM, DOC B, blue dotted, 30°C n=1) with lower levels of impurities as discussed in the text.

Due to the mentioned impurities of the plasma membrane, the effect of temperature on the diacylglycerophospholipid lipid distribution, particularly in their saturation level in the plasma membrane, can only be inferred from literature. Previous studies reported [65] (mutant #326) that the most common fatty acid in *N. crassa* slime plasma membrane grown at 37°C is C18:2, and when the growth temperature is lowered (down to 15°C) most of the 18:1 and 18:2 decreases (by $\sim$23 % and $\sim$10 % respectively) and 18:3 increases (by $\sim$12 %) (Appendix, Table B.5). A similar change in fatty acids composition has also been measured in *N. crassa* slime whole cells grown at 30°C compared to

15 % [124] (mutant #1118), with most of the 18:1 and 18:2 decreases (by ∼24 % and ∼4 % respectively) and 18:3 increases (by ∼27 %) (Appendix,Table B.5).

The differences in the fatty acid composition within the cell should be further studied on a defined subcellular level, as the presented results show an average over a mix of membranes because of impurities.

5.4.3 Diacylglycerophospholipids (DGPL) during purification process of *N. crassa* Pma1

The original membrane (DOC A) of the following analysed Pma1 protein (Fig 5.10 and Fig 5.11) can be considered having high impurities of mitochondria and potentially other types of membrane, as discussed before (Section 5.4.2). DDM solubilisation of the plasma membrane seems to retain a similar diacylglycerophospholipid composition (Fig 5.10) with a slight decrease of PA and increase in PE. The main difference between the DDM-supernatant and the Pma1 hexamer is a further decrease in PA, and an increase in PE.

Because DDM solubilisation seems to retain a similar lipid profile to the original membrane, enriched or depleted lipids in the Pma1 sample can still be interpreted in the context of the impure plasma membrane it originates from. Even though for a more conclusive analysis it would be best to analyse Pma1 samples directly from very clean plasma membrane samples, still any enrichment of lipids in the Pma1 samples can be interpreted in the context of the impure plasma membrane it originates from.

The PA amount is decreased with Pma1 hexamer purification even further (Fig 5.10). PG is enriched during the purification of Pma1. However only minor traces of PG in *N. crassa* slime plasma membrane were measured (Fig 5.8) and PG is not an abundant component of the plasma membrane of fungi [17, 64]. This sample was purified by glycerol gradient and a separate sample purified by sucrose gradient, did not show this enrichment of PG (Appendix Table B.12). Therefore the high PG signal could be an

artefact due to glycerol remaining from the purification.

When comparing diacylglycerophospholipid classes between glycerol and sucrose purified samples, a higher level of PC content was observed in the sucrose purified sample (Appendix Table B.12). However the original plasma membrane of this sample might be rich in lipids of other cell organelles, indicated by a high cardiolipin content of 70% within membrane lipids (Appendix Table B.10) indicating a suboptimal purification of Pma1, which is supported by reported protein impurities in the sucrose gradient purified Pma1 sample (Bublitz group, unpublished data). In addition, the sucrose gradient seems to have retained high levels of glycerides compared to glycerol (97% vs ∼40% of all lipids (Appendix Table B.9) and based on this the glycerol gradient seems to be a better choice for Pma1 purification.

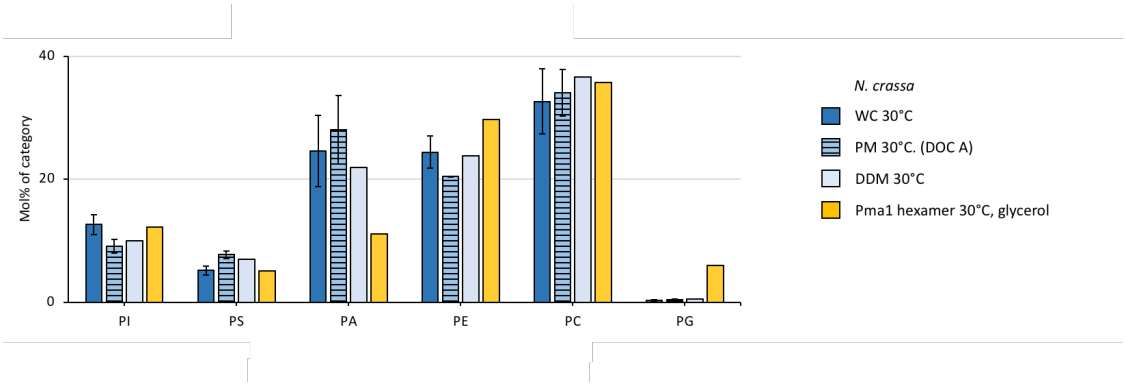

Figure 5.10: Diacyl glycerophospholipid classes during the purification of Pma1
LC/MS lipid analysis of Pma1 purification from *N. crassa* grown at 30°C comparing the distribution of lipid classes of Diacyl glycerophospholipids. Follows the purification of Pma1 hexamer from whole cells (WC, n=6, blue), plasma membrane (PM, DOC A blue hashed, 30°C n=2), supernatant of DDM solubilised membrane (light blue, n=1) and glycerol gradient purified Pma1 hexamer (orange, n=1).

Similar to previously discussed, the DDM solubilised samples of plasma membranes exhibit a similar fatty acid chain length and saturations to total plasma membrane content (Fig 5.11), indicating that DDM does not preferentially solubilise particular lipid species. When looking specifically at lipids copurified with Pma1 , there seems to be enrichment of shorter chained diacylglycerophospholipids compared to those in the whole plasma membrane (Fig 5.11 A). There is a strong increase in diacylglycerophospholipids

with a total number of single double bonds instead of fully saturated lipids seen in the pure plasma membrane sample (DOC B Fig 5.11 B). This suggests that the lipids around Pma1 are characterised by shorter diacylglycerophospholipids with a total chain length of C32 and C34 (Fig 5.11 A) and more single unsaturated fatty acids (Fig 5.11 B) compared to the plasma membrane.

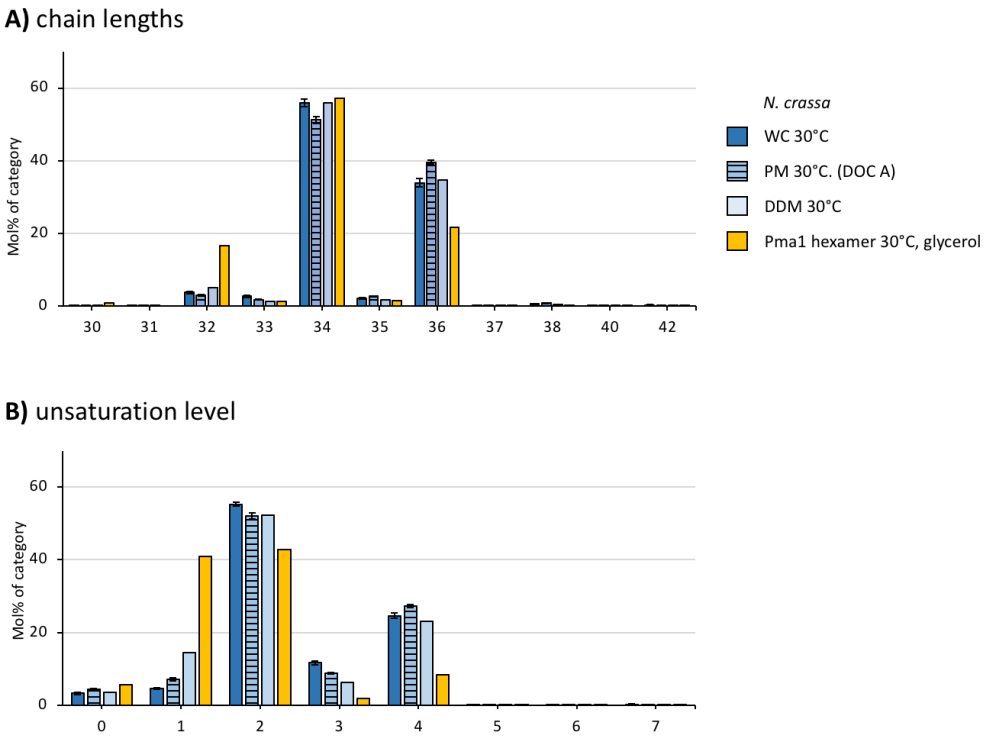

Figure 5.11: Chain length and unsaturation levels of diacyl glycerophospholipids during the purification of Pma1
LC/MS lipid analysis of Pma1 purification from *N. crassa* grown at 30°C comparing the distribution of total chain lengths A) and total unsaturation level of both fatty acids, (x-axis: Number of double bonds) B) of diacyl glycerophospholipids. Follows the purification of Pma1 hexamer from whole cells (WC, n=6, blue), plasma membrane (PM, DOC A, blue hashed, 30°C n=2), supernatant of DDM solubilised membrane (light blue, n=1) and glycerol gradient purified Pma1 hexamer (orange, n=1).

5.4.4 Diacylgylcerophospholipids (DGPL) in purified *N. crassa* Pma1 samples

To evaluate further details of the diacylglycerophospholipid composition of the DDM-solubilised and purified Pma1 hexamer, it is analysed in comparison with Pma1 samples

which differ in the temperature of expression and the addition of an AEX chromatography purification step. In addition, Pma1 hexamer is compared with a lower oligomer separated after the AEX.

The measured DDM-solubilised and purified Pma1 samples vary in their diacylglycerophospholipid content (Fig 5.10 A, B Appendix Table B.12).

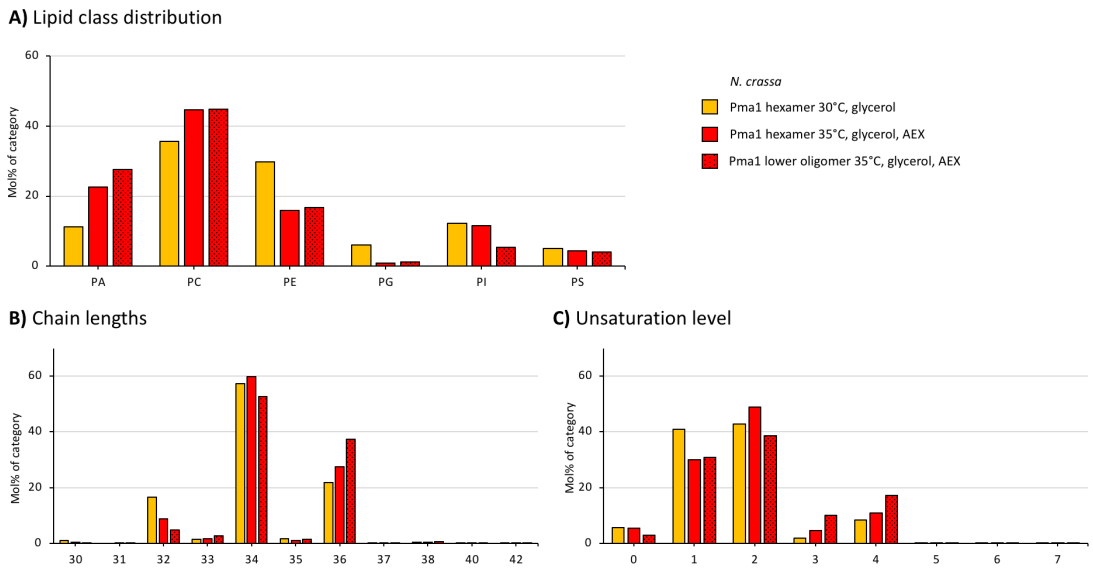

Figure 5.12: Diacyl glycerophospholipids comparison of DDM purified N.crassa Pma1 LC/MS lipid analysis of Pma1 hexamers from different plasma membranes grown at 30°C (orange) and 35°C (red). After DDM solubilisation the protein samples have been purified with a glycerol density gradient. Pma1 hexamer, with expression temperature of 35°C samples and purified with an additional AEX chromatography is compared to a lower oligomer Pma1 from the same purification (dotted). Comparison of the distribution of lipid classes A), total chain lengths B) and total unsaturation level of both fatty acids (x-axis: total number of double bonds) C) of diacyl glycerophospholipids.

The difference between both glycerol purified Pma1 hexamers from membranes grown at 30°C or 35°C (Fig 5.12 A) are characterised by a higher PA and PC and lower PE with higher growth temperature. Even though the difference could be attributed to the difference in purification methods (with an additional AEX step in the 35°C sample), it is potentially due to an increased growth temperature, since a similar temperature-dependence was also observed in whole cells (Fig 5.4 Section 5.3.2).

Overall a PS content of about 10 % was measured in all samples, which is lower than in the plasma membrane (Fig 5.8 and Section 5.4.3). A polymer extraction study on *S. cerevisiae* published during the course of this thesis showed a higher PS content in membrane compartments containing Pma1 (MCP) compared to its bulk plasma membrane [115]. A possible explanation for this discrepancy would be that the entire membrane compartments (including MCP) extracted with polymers [115] are enriched in PS but that these lipids are less enriched in the direct environment of Pma1. This is supported by MD simulations of Pma1 [104] where PS is localised enriched in the interface between the Pma1 monomers but relatively depleted in the remaining direct environment of the Pma1 hexamer.The detergent solubilisation and further purification steps might strip away the bulk of loosely associating lipids like the majority of PS. Thus remaining lipid species might indicate stronger lipid interactions with the protein for example by being bound to Pma1 or in the center of the hexamer as seen in [105].

The lipid composition of the samples originating from the same purification pipeline (*N. crassa* grown at 35°C, glycerol gradient, AEX, SEC) containing different oligomeric states of Pma1 is overall similar (Fig 5.10 B). The variation between both samples can be attributed to the oligomeric state of the protein, with a main difference of higher PI and lower PA in the Pma1 hexamer compared to the lower oligomer. A possible hexamer stabilising effect of PI and destabilising effect of PA should be investigated further.

The hexamer sample seems to be surrounded by lipids with shorter fatty acid tails indicated by 10–20 % lower amounts of diacylglycerophospholipids with C36 chains (∼20–30 % C36) compared to in the plasma membrane samples (∼40–45 % C36) (Fig 5.10 C). An increase in C32 moieties is further measured consisting of PC 32, PE 32 and PG 32 moieties (Appendix Table B.15 or B.16) with the latter two predominantly found in the 30°C Pma1 glycerol sample and not the other, which might be due to contaminations, as PG is are reduced with the AEX chromatography step (Fig 5.12).

A tendency to more saturated lipids can be observed in purified Pma1 compared to its originating plasma membrane sample (Fig 5.11 B). Lipids with total double bonds of 1 make up about 30–40 % diacylglycerophospholipids in the purified sample (Fig 5.11 B), but no increase in fully saturated lipids, as was seen in the DOC B sample (Fig 5.9 B), can be observed. This data indicates an increase in saturated fatty acids in the plasma membrane but an environment of Pma1 containing lipids with a single monounsaturated fatty acid contributing to a level of fluidity due to the double bond.

5.4.5 Sphingolipids content during Pma1 purification

Sphingolipids, being an integral part of the plasma membrane lipid bilayer, were subsequently analysed for the Pma1 purification samples.

5.4.5.1 Sphingolipid classes during Pma1 purification

The data suggests that the plasma membrane is characterised by high ceramide levels and reduced relative sphingomyelin content compared to the whole cells (Fig 5.13 A). DDM solubilisation of the plasma membrane (DOC A) seems to yields a similar total relative sphingolipid content (∼16 % within plasma membrane forming lipids) (Fig 5.7) to its original plasma membrane (DOC A) but seems to preferentially solubilise IP-Ceramides while retaining a similar sphingomyelin content (Fig 5.13 A). The DDM solubilisation of the plasma membrane seems to preferentially solubilise membrane areas with a decreased ceramide content (42 % of sphingolipids) compared to the plasma membrane (60 %), with an increased IP-Cer content (48 % compared to 28 % in the plasma membrane). The DDM solubilised supernatant has a 10x increased MIP-Cer content (∼0.1 %) compared to 0.09 % in the originating plasma membrane (Fig 5.11 A).

The Pma1 hexamer samples from membranes grown at 30°C contain about 15 % sphingolipids (within plasma membrane forming lipids), similar to the plasma membrane and DDM solubilised fraction (Fig 5.7, Appendix Table B.11). The Pma1 hexamer from membranes grown at 35°C, which underwent additional AEX chromatography,

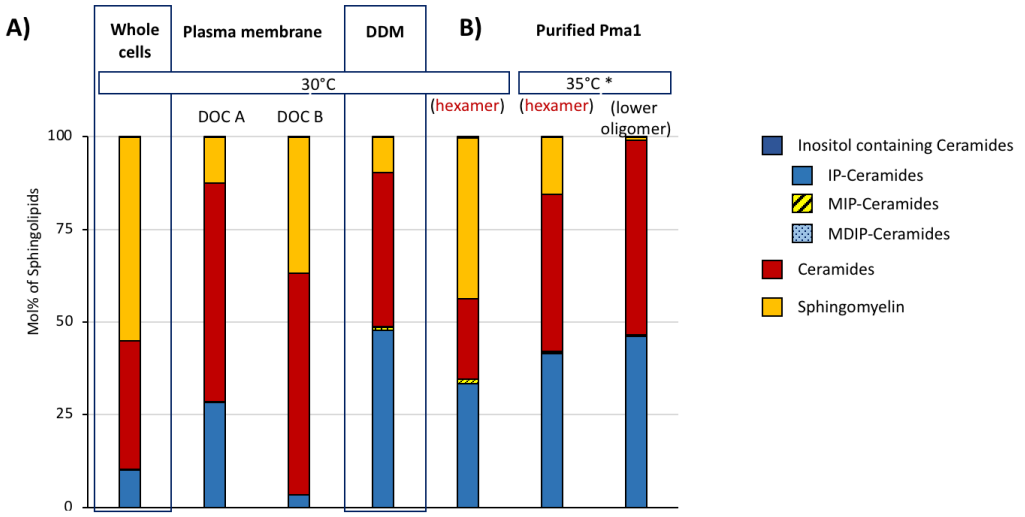

Figure 5.13: Relative distribution of sphingolipid classes during DDM solubilisation and purification of Pma1
The relative distribution of ceramides (red), inositol containing ceramides (IP-Cer,MIP-Cer(hashed) and MDIP-Cer(dotted), (blue) and sphingomyelin (orange) are compared along the the purification of Pma1 from *N. crassa* grown at 30°C A) and for purified Pma1 samples B). The purification steps are outlined as whole cells (WC), plasma membrane (PM), supernatant of solubilisation with DDM (DDM) and Pma1 glycerol gradient purified. The Pma1 protein at 35°C has further been subjected to an AEX chromatography (indicated by the star). Detailed values can be found in the Appendix Table B.17.

contains 26 % sphingolipids, more than double compared to the lower Pma1 oligomer (11 %) (Appendix Table B.11). This might indicate stronger association of sphingolipids with Pma1 in its hexameric form than with lower order oligomers. Whether the higher sphingolipid content in the 35°C Pma1 hexamer compared to the 30°C sample is due to the AEX chromatography or the higher growth temperature should be evaluated further.

The purified Pma1 samples contain high amounts of inositol-containing ceramides (30–45 %), predominantly IP-Cer but vary in their sphingomyelin and ceramide content (Fig 5.13 A and B). The sphingomyelin content is higher in Pma1 hexamers from *N. crassa* grown at 30°C (Fig 5.13 A) compared to 35°C (Fig 5.13 B). Sphingomyelin is almost absent in the lower Pma1 oligomer (Fig 5.13 B).

An enrichment of MIP-Cer content can be seen in the Pma1 hexamer samples compared

to the plasma membrane, with a relative MIP-Cer content of 0.09 % (within Sphingolipids) in plasma membrane up to 1.2–1.3 % in Pma1 30°C growth temperature (Fig 5.13 B) and 0.45 % in Pma1 35°C growth temperature (Fig 5.13 B), similarly to the DDM solubilised fraction as discussed before. MIP-Cer is potentially co-purified with the Pma1 hexamer, which is indicated by an increase in the relative MIP-Cer of the Pma1 hexamer (0.45 %) and lower oligomer (0.21 %) (Pma1 35°C Fig 5.13 B). Which effect the additional AEX chromatography has on the lipid environment of Pma1 and which role increased growth temperature plays should be evaluated further.

5.4.5.2 Sphingolipid chain lengths during Pma1 purification

The *N. crassa* plasma membrane samples contain long sphingolipids, which is indicated by an increase of long side chain moieties with C40-50 from up to ∼40 % in whole cells to ∼70 % in plasma membrane samples (Fig 5.14 A). The DDM solubilisation and consecutive purification of Pma1 retain these high levels of long sphingolipids (Fig 5.14 A). When comparing the Pma1 hexamer samples with its lower oligomer counterpart (Pma1 35°C, Fig 5.14 B and C) the hexamer samples generally have more sphingolipids with very long fatty acids (sum of carbon atoms of C46 and more) than the lower oligomer. Particularly high C48 moieties are present in all Pma1 hexameric samples but not measured in the lower Pma1 oligomer (Fig 5.14 C) .
Pma1 hexamer from *S. cerevisiae* has been reported to be accompanied by sphingolipids containing C26 fatty acid side chains on its propagation to the plasma membrane [108]. A similar trend of very long chained sphingolipids (total C46 and more) in the Pma1 hexamer sample can be seen in the presented *N. crassa* data (Fig 5.12 A), where the lower oligomer contains less of these lipids compared to the hexameric form (Pma1 35°C).

The long chain base composition of glycosphingolipids of *N. crassa* slime has been reported [65] with 70–80 % C18, and 20–30 % C19 and C20 (see appendix Table B.3). Combining these sphingolipid bases with fatty acids to the observed sphingolipids with long (C40-44) and very long (C46-50) side chain moieties, would require the presence of fatty acids with 20-28 carbon atoms, to be in line with the measures lipid species in

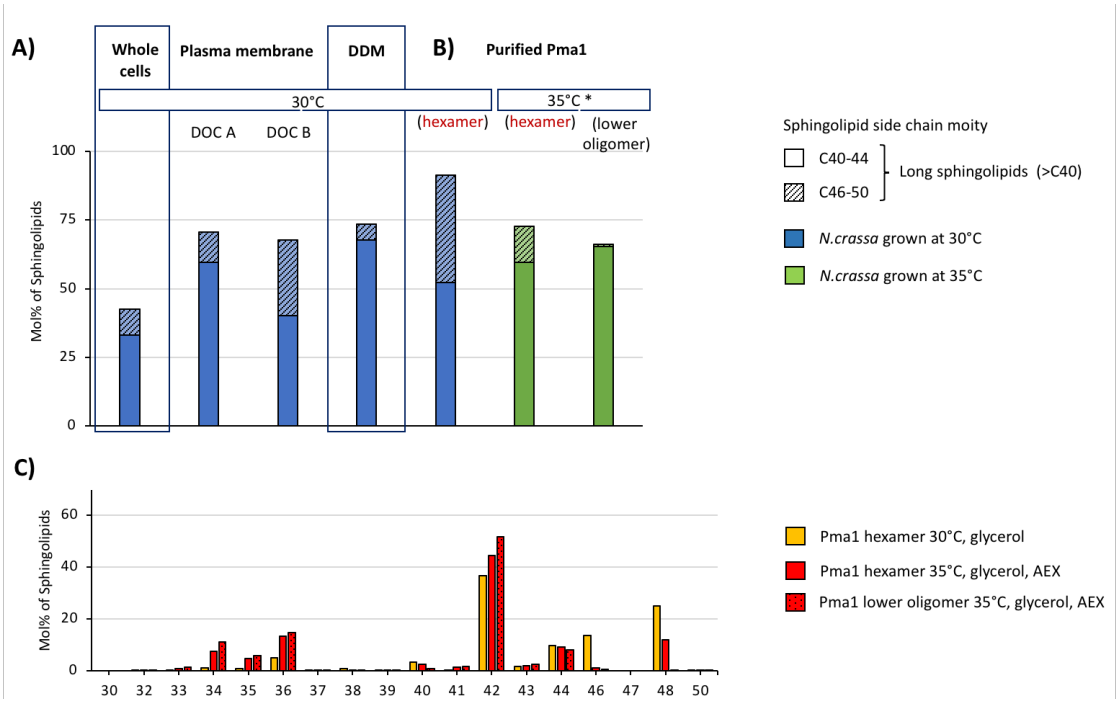

Figure 5.14: Relative distribution of sphingolipid chain lengths during DDM purification of Pma1
Distribution of long sphingolipids (total carbon atoms of C40-51) in *N. crassa* samples, compared to shorter sphingolipids (C32-39), which contribute to 100 %. Following the purification of Pma1 from whole cells, via plasma membrane to purified Pma1 A). C) detailed sphingolipid total chain length distribution of purified Pma1 hexamers from different plasma membranes grown at 30°C (orange) and 35°C (red). After DDM solubilisation the protein samples have been purified with a glycerol density gradient. Pma1 hexamer, with expression temperature of 35°C samples and purified with an additional AEX chromatography is compared to a lower oligomer Pma1 from the same purification (dotted).

Fig 5.14 C. This highlights the importance to re-evaluate the fatty acid composition of *N. crassa* particularly long chain base composition of sphingolipids, to be able to explain the presence of sphingolipids with C40-51 side chain moieties, which seem to be the most prevalent in the plasma membrane and Pma1 hexamer (Fig 5.14 B).

5.4.5.3 Unsaturation levels of sphingolipids during Pma1 purification

The sphingolipid unsaturation level in the plasma membrane differs from the whole cell (Fig 5.15 A). There seems to be a shift towards higher levels of fully saturated fatty acids in the plasma membrane preparation, supported by more than 50 % of measured sphingolipids having no double bonds in the plasma membrane (Fig 5.15 A) and Pma1 samples (Fig 5.15 B). Complex sphingolipids possessing saturated fatty acids are highly

abundant in the membrane compartment containing Pma1 [220], which is in line with the finding of Pma1 samples containing high levels of saturated chain lengths (Fig 5.15 B).

The long chained sphingomyelin SM 48:2, is increased in the plasma membrane compared to the whole cells and particularly increased in all Pma1 hexamer samples, making up 9–15 % of all sphingolipids in in Pma1 hexamers, compared to about ∼2 % in plasma membrane and whole cells, but is not observed in the lower Pma1 oligomer (Appendix Table B.22, B.21).

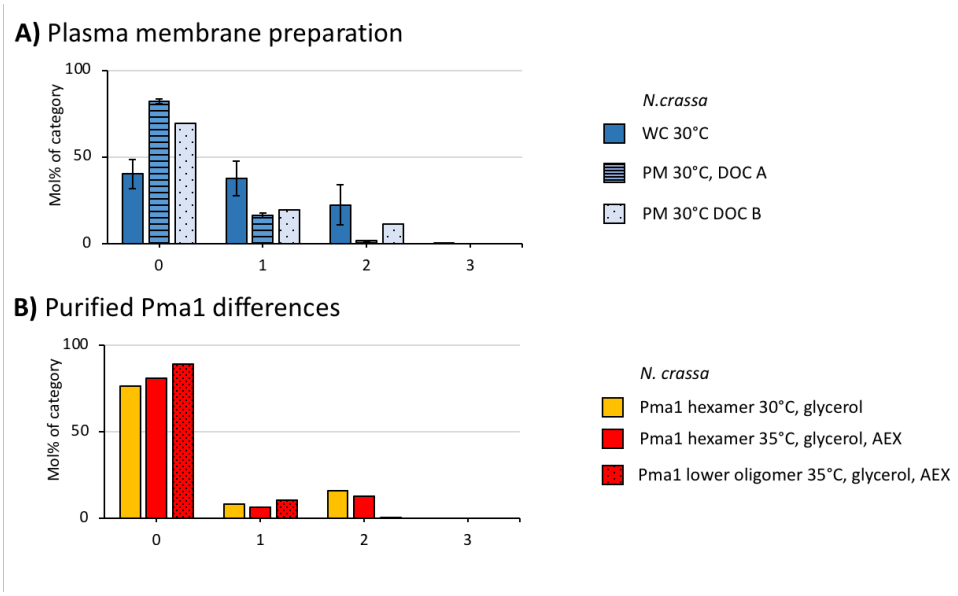

Figure 5.15: Relative distribution of sphingolipid unsaturation distribution during DDM purification of Pma1
LC/MS lipid analysis of sphingolipid unsaturation level (x-axis: Number of double bonds) comparing A) *N. crassa* whole cells (WC) at 30°C (n=6, light blue) and 35°C (n=2, green) with their consecutive plasma membrane preparation (hashed, 30°C n=3, 35°C n=2), B) comparing DDM purified *N. crassa* Pma1 hexamers from different plasma membranes grown at 30°C (orange) and 35°C (red). After DDM solubilisation the protein samples have been purified with a glycerol density gradient. Pma1 hexamer, with expression temperature of 35°C samples and purified with an additional AEX chromatography is compared to a lower oligomer Pma1 from the same purification (dotted).

5.4.5.4 Sphingolipid hydroxyl groups during Pma1 purification

The fatty acid side chains of sphingolipids, particularly ceramide and inositol containing ceramides, can contain hydroxyl groups and their overall occurrence seems to decrease

in whole cells and plasma membrane with higher growth temperature (Fig 5.16 A). The relative amount of sphingolipids with one or more hydroxyl groups is higher in 30°C grown samples compared to 35°C (whole cells ∼45 % vs ∼17 % respectively and plasma membrane ∼80 % vs ∼47 % respectively).

Generally there seems to be a high level of hydroxyl groups in the purified Pma1 samples (Fig 5.16 B) but a reverse trend in terms of growth temperature (Pma1 30°C 47–58 % and 35°C 85–99 % of all sphingolipids containing 1 or more hydroxyl groups). The main contributors to this change of hydroxyl groups during the purification steps of Pma1 are seen in IP-Ceramides. The inositol ceramide IP-Cer 42:0;3 which is an abundant components in *N. crassa* whole cells (4–9 % of sphingolipids) in the plasma membrane (11–15 % of sphingolipids), retained with DDM solubilisation (36 % of sphingolipids) and constitutes ∼25 % of sphingolipids in all Pma1 oligomers, whereas the lipid species IP-Cer 42:0;2 (dihydroxy) is additionally enriched in Pma1-35°C -AEX samples contributing to 10 % of all sphingolipids but only 1 % in the Pma1 hexamer from cells grown at 30°C (Appendix Table B.21)

The loss of hydroxyl groups from the ceramide moiety can influence the lateral diffusion of membrane proteins in *S. cerevisiae* [220]. The lateral diffusion can probably be maintained through an interaction of membrane proteins with the hydroxyl group (C2-OH or particularly C4-OH). The slight decrease of hydroxyl groups with higher growth temperature could be to maintain a more rigid lipid environment. The Pma1 containing membrane compartment (MCP) which is most likely purified in the presented samples might contain a high number of sphingolipids with high numbers of hydroxyl groups to overcome the low fluidity caused by saturated lipids; this hypothesis should be investigated further.

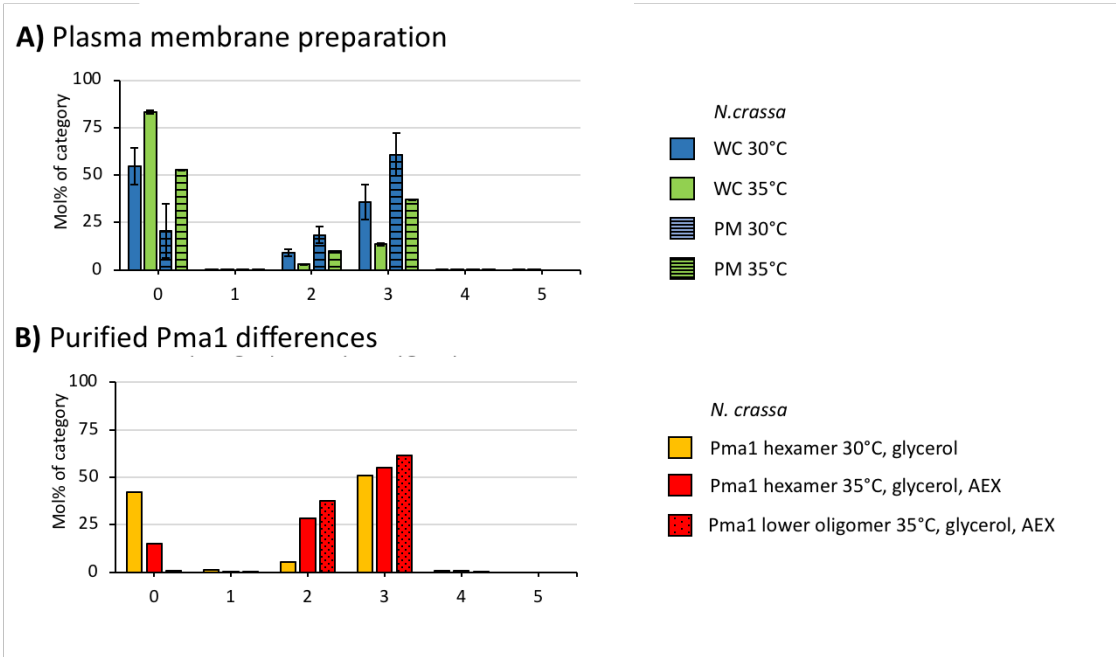

Figure 5.16: Relative distribution of sphingolipid hydroxy group distribution during DDM purification of Pma1
LC/MS lipid analysis of sphingolipid hydroxyl group distribution comparing A) *N. crassa* whole cells (WC) at 30°C (n=6, light blue) and 35°C (n=2, green) with their consecutive plasma membrane preparation (hashed, 30°C n=3, 35°C n=2), B) comparing DDM purified *N. crassa* Pma1 hexamers from different plasma membranes grown at 30°C (orange) and 35°C (red). After DDM solubilisation the protein samples have been purified with a glycerol density gradient. Pma1 hexamer, with expression temperature of 35°C samples and purified with an additional AEX chromatography is compared to a lower oligomer Pma1 from the same purification (dotted).

5.4.5.5 Discussion on sphingolipids during Pma1 purification

Sphingolipids were measured in the *N. crassa* slime increased with the enrichment of plasma membrane and purification of Pma1 compared to whole cells. Notably the types of sphingolipids differ between the two fungi *S. cerevisiae* and *N. crassa* and unexpectedly, sphingomyelin is measured in *N. crassa* slime. In *S. cerevisiae* inositol ceramides and ceramides dominate, sphingomyelin is only measured at 0.4 % of all sphingolipids. Sphingomyelin is expected to only be found in mammalian cells and not in fungi (no report of sphingomyelin except in old literature where it was used as a synonym for sphingolipids (compare [65]). Currently the presence of sphingomyelin in *N. crassa* can not be explained, and many previous studies on *S. cerevisiae* and *N. crassa* have not detected it. Instead of sphingomyelin rather IP_2-Cer and other

glycosylceramides similar to previously detected in *N. crassa* [41] are expected. It might be worth exploring the biological meaning of this previously unreported sphingomyelin species in *N. crassa* slime, particularly due to its high abundance in all *N. crassa* samples and its apparent enrichment for the Pma1 hexamer, particularly of SM 48:2. Details on alternative and expected fungal sphinoglipids in *N. crassa* are outlined in Section 5.4.6.

A technical explanation for a potential miss-identification of fungal sphingolipids as spingomyelin could be an error in M/Z peak interpretation and for example for SM 48:2 (SM d20:2(4E,8E)/28:0) according to LIPID-MAPS the [M+H]+ ion could have a peak at about 897.7783 m/z and potentially another glycosphingolipid species show the same peak. Another hypothesis could be that a combination of lipolytic enzymatic activity and m/z peak interpretation could be the reason, with a misinterpretation of free choline, from Phospholipase D activity (as outlined in Section 5.4.2) with a high ceramide content could lead to misidentification of sphingomyelin like lipids in *N. crassa*. This explanation might, however, be unlikely because of added lipid controls (as outlined in [191]) and since in the LC/MS workflow lipid isomers are first isolated through phase separation on the LC column (by hydrophobicity and polarity in headgroups) and the retention time of sphingomyelin was controlled. Afterwards the lipids are ionised and measured with mass spectrometry which has a wide detection range: 100-1800 m/z. The error would need to be systematic and an error in the interpretation software, because various different sphingomyelin species were detected and are represented in all *N. crassa* samples.

In mammalian plasma membranes, lipid microdomains (or rafts) are formed by sphingolipids and cholesterol and are important for signal transduction [220, 221]. In *S. cerevisiae* plasma membrane, lateral domains are assumed [220] which are characterised by their most abundant membrane protein: The membrane compartment containing Pma1 (MCP), containing Can1 (MCC) and containing target of rapamycin kinase complex 2 (MCT) [112–114]. The membrane compartment containing Pma1 is reported to be composed of the three complex sphingolipids, IP-Cer, MIP-Cer, MDIP-Cer [56, 58, 108, 110]. Therefore, an enrichment in inositol containing lipids would be

assumed in the proximity of Pma1, which was possible to see by an enrichment in the samples with purified Pma1 hexamer (Fig 5.13). Based on the presented results, the Pma1 hexamer containing lipid environment contains long, fully saturated sphingolipids, which are in yeast mainly IP-Cer [110] and in the case of *N. crassa* Pma1 potentially also SM 48:2. In molecular dynamics simulations (Bublitz group, unpublished results and [104]) inositol containing lipids seem to aggregate in close proximity to Pma1, which is supported by the measured enrichment of inositol containing ceramides during the purification of Pma1. A higher hydroxylation level of lipids in the Pma1 proximity (Fig 5.16) might aid interaction between the membrane protein and its otherwise rigid complex sphingolipid environment [220].

Sphingolipids with longer total chain lengths (number of carbon atoms 40 and more) are enriched with plasma membrane preparation and similarly found in the DDM soluble fraction as well as the purified Pma1 samples. This trend of longer acyl chains in the plasma membrane is not visible in diacyl glycerophospholipids and not clear in Lysophospholipids either, which is probably due to the fact, that other residual membranes contribute to the diacylglycerophospholipid and lysophospholipid content, whereas the sphingolipids are most prevalent in the plasma membrane and therefore are indicative of the plasma membrane. A better analysis of cleaner plasma membrane or with polymer solubilisation of particular membrane proteins [115] can be of interest.

A low lateral diffusion was reported of the Pma1 hexamer in the plasma membrane of *S. cerevisiae* [220] and *N. crassa* slime and WT [127]. The sphingolipid enriched environment around Pma1 contains a high number of long chained lipids with a generally lower saturation level, which might contribute to tighter packing. A low ergosterol content has been reported for the equivalent membrane compartment containing Pma1 in *S. cerevisiae* plasma membrane [115]. The difference of sterol environment of the Pma1 samples compared to the plasma membrane would be very interesting to investigate further as the MCP in *S. cerevisiae* is considered to be mainly sphingolipids rather

than sterol-rich like MCC [56, 58, 108, 110]. The measured sphingomyelin-like lipids in *N. crassa*, with their high enrichment in the Pma1 hexamer should be further analysed.

5.4.6 Details on the sphingolipid synthesis in *N. crassa*

Sphingomyelin-like sphingolipids have been identified in *N. crassa* in the presented lipid analysis with LC/MS. In the following section the possible homologues of proteins in the known sphingomyelin synthesis pathway were analysed with respect to *N. crassa* (Section 5.4.6.1). Furthermore the known synthesis pathways of complex sphingolipids in fungi are described with a focus on *N. crassa* sphingolipids (Section 5.4.6.2).

5.4.6.1 Synthesis of sphingomyelin

Sphingomyelin is a key sphingolipid in mammalian cells [222] and its synthesis is catalysed by sphingomyelin synthases which adds a choline headgroup to a ceramide. In mammalian cells three main types of sphingomyelin synthases (SMS) can be found namely SMS1 and SMS2 and SMSr. The sphingomyelin content of the biological membranes is highly regulated and reduced by sphingomyelinases (SMases). Fig 5.17 outlines the pathway of sphingomyelin synthesis and coordinated breakdown.

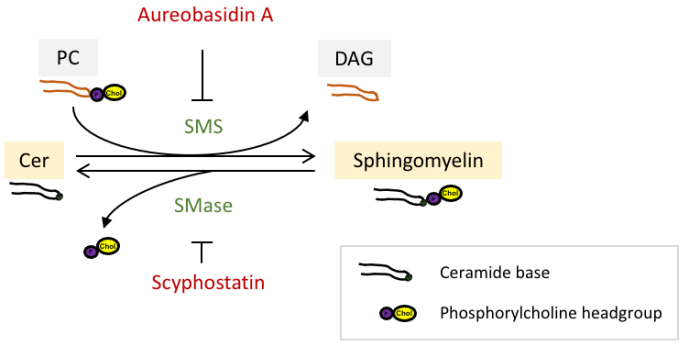

Figure 5.17: Sphingomyelin synthesis pathway in mammalian organisms
Adapted from [223]. Highlighted are the enzymes involved in this pathway Sphingomyelin Synthases (SMS) and Sphingomyelinases (SMase) (green) and their inhibitors (red) [223, 224]. Abbreviations are: Cer - ceramide, PC - phosphatidylcholine, DAG - diacylglycerol

Under the assumption that sphingomyelin is indeed a native lipid in *N. crassa*, homologues of genes and proteins involved in the known sphingomyelin pathway may be found in *N. crassa*. The *N. crassa* genome has been published for the filamentous wild type

OR74A [225]. Homology searches were conducted at https://www.ncbi.nlm.nih.gov/homologene and their results are given in Table 5.3 and detailed below.

Table 5.3: Genes involved in the sphingmyelin synthesis pathwayreviewed in [222], Homology searches were conducted at https://www.ncbi.nlm.nih.gov/homologene

Gene name	HomoloGene ID	Protein name		Conserved in
Sphingomyelin Synthesis				
SGMS1	27040	SMS1	sphingomyelinsynthase 1	Bilateria
SGMS2	32705	SMS2	sphingomyelinsynthase 2	Eutelestomi
SAMD8	41670	SMSr	sterile α-motif domain containing 8 TM	Bilateria
Sphingomyelinases				
SMPD1	457	ASMase	sphingomyelin phosphodiesterase 1, acid lysosomal	Opistokonia
SMPD2	31129	(lyso PAF-phospholipase C)	sphonodiesterase 2, neutral membrane	Bilateria
SMPD3	10260	NSMase 2	sphingomyelin diesterase 3, neutral membrane	Eutelestomi
SMPD4	9813	NSMase 3	sphingomyelin phosphodesterase 4, neutral membrane	Bilateria

As reviewed in [222] sphingomyelin synthases SMS1 (encoded by SGMS1) and SMS2 (encoded by SGMS2) were identified in human HelaCells and at least two members of spingomylelinsythases can be found in most mammalian species as well as a possible third family SMSr (encoded by SAMD8). SMS are similar to lipid phosphate phosphatase family 6 transmembrane domains and their catalytic side is facing the Golgi-lumen or extracellular space. In mammalian cells SMS1 and 2 can both be found in the trans-Golgi whereas SMS2 can also be found in the plasma membrane, which is there regulating additional spingomyelin content in the membrane [222]. The conducted homology search for these genes has not given any results for fungi (Table 5.3).

The sphingomyelin content is regulated by coordinated breakdown through Sphingomyelinases which cleave the choline headgroup. Acid sphingomyelinase (encoded by SMPD1) can be found in lysosomal, endosomal membranes and is also secreted to extracellular space, where this secretory SMAse is Zn^{+} dependent [222, 226]. Genes encoding neutral sphingomyelinases (NSMase) are SMPD3 (resulting in NSMase2) and SMPD4 (resulting in NSMase3) [226]. The gene SMPD2 encodes the lyso-PAF-phospholipase C, which is not a sphingomyelinase [226]. The homology search of SMPD1 (HomoloGene ID: 457, Table 5.3) reveals that there is a homologue in *N. crassa* (NCU06697), with a BLAST ident percentage of 30.15%, that encodes a Ser/Thr protein phosphatase (Accession Number: XP_961012.1). All of the other genes appear to have no homologues in fungi

(Table 5.3).

In summary, except for a single 30.15% percent identical homologue (BLAST) of SMPD1, no homologues of the known proteins involved in the sphingomyelin pathway have been found in *N. crassa*. The 30.15% percent identical homologue of SMPD1 found in *N. crassa* (gene NCU06697) has been assigned to be a Ser/Thr protein phosphatase, which is a different function than sphingomyelinases in mammalian cells. The lack of homologues of proteins in the sphingomyelin synthesis or breakdown pathways is consistent with published statements that the sphingomyelin synthesis pathway is unique to mammalian cells and the inositol phosphoceramide synthesis pathway unique to fungi [224].

5.4.6.2 Synthesis of complex fungal sphingolipids

In the literature several complex fungal glycosphingolipids have been reported in *N. crassa* which would provide an alternative explanation to the unique sphingomyelin-like lipid class found predominantly in *N. crassa* compared to *S. cerevisiae* (Section 5.3.5). Fig 5.18 summarises these potential candidates and the current knowledge on their headgroup synthesis pathway. Fig 1.4 in the introduction outlines the the chemical structures of these sphigolipids. The fungal sphingolipids (glycosphingolipids) can be distinguished in glycosylceramides and inositolphosphorylceramides [43, 223, 224]. Particularly the inositolphosphorylceramide pathway is unique to fungi and not found in mammalian organisms and is, therefore a target of antifungal drug development [224].

Neutral glycosylsphingolipids (Fig 5.18 A) are ceramides with head groups containing one or more sugar residues, most commonly glucose (GlcCer) or galactose (GalCer). GlcCers have been identified in *N. crassa* [230], and the proteins and genes involved in their pathway have also been studied in this fungi [43]. The synthesis of GlcCer involves a glycosylceramide synthase (GSC, encoded by gsc-1), which is present in *N. crassa* (NCU01116, [227]) but not in *S. cerevisiae* [228] (Fig 5.18 4). GlcCer are mainly found in fungal cell walls, and disruption of their synthesis pathway can lead to apoptosis

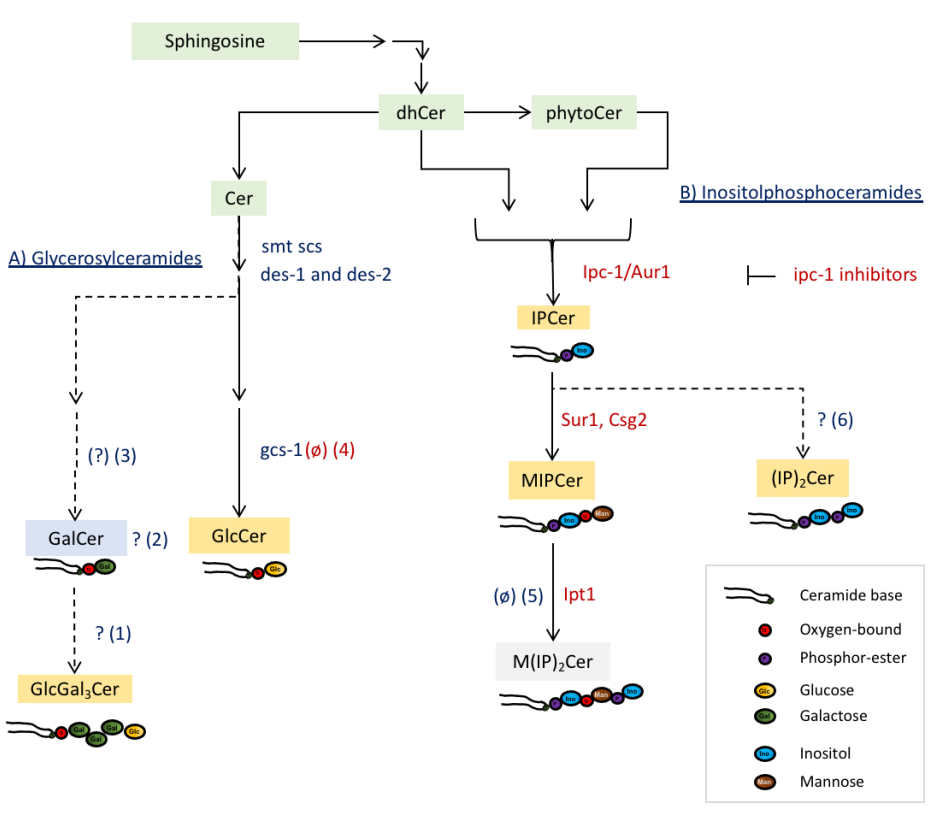

Figure 5.18: Excerpt of fungal glycosphingolipids pathway with highlights on head-group synthesis
Identified glycosphingolipids in *N. crassa* are highlighted in orange, compounds not expected in grey and not assumed in blue. Precursors for glycosphingolipids are highlighted in green. Genes studied in *S. cerevisiae* are highlighted in red (reviewed in [32]), and those studied in *N. crassa* in blue [43]. Genes and compounds that have not been identified in *N. crassa* are marked with a question mark and discussed in the text (1-3,6).(4) The presence of gcs has been confirmed in *N. crassa* [227] but not in *S. cerevisiae* [228]. (5) Although ipt1 has been studied in *S. cerevisiae*, no homologue has been identified with BLAST search in *N. crassa* [229]. Abbreviations used: dhCer - dihydroceramide, phytoCer - phytoceramide, Cer - ceramide, GalCer - galactosylceramide, GlcCer - glucosylceramide, $GlcGal_3Cer$ - tetraglycosylated ceramide/Neurosporaside [41, 42], IPCer - inositolphosphoceramide, MIPCer - mannosylinositolphosphoceramide, $M(IP)_2Cer$ - mannosyldiinositolphosphoceramide, and $(IP)_2Cer$ - diinositolphosphoceramide [41]. Examples for ipc-1 inhibitors: Aurebasidin (ipc1), Khadrefungin (ScAur1), Rustimicin, Pleofungins [224] Pathway excerpt based on [43, 223, 224] with further information from [41, 42]

in fungal cells due to the accumulation of ceramides [231]. Furthermore, ceramides containing multiple sugar moieties have also been characterised in *N. crassa*, such as a tetraglycosylated ceramide with three galactose and one glucose moiety [41], that has further been structurally determined by mass spectrometry as a galactosylceramide with further two galactose and one glucose moiety ($GlcGal_3Cer$ or Neurosporaside) [42]. To

synthesise this tetra glycosylated ceramide (Fig 5.18 1), a pathway for the precursor GalCer (Fig 5.18 2) could be assumed, which would require the presence of ceramide galactosyltransferase (CGT) (Fig 5.18 3). However, the presence of GalCer has only been confirmed in a few fungal species, such as *M. grisea* [232] or *A. fumigatus* [233], and summarised in [234]. Information on the potential function of GalCer in most fungi or on the proteins involved in their synthesis is sparse. The presence of GalCer (Fig 5.18 2) as a precursor for $GlcGal_3Cer$ [42] in *N. crassa* should be further verified using methods such as mass spectrometry.

Inositolphosphorylceramide (IPC) (Fig 5.18 B) synthesis is considered unique to fungal organisms and is a target for antifungal drugs [223, 224]. In fungal cells, inositolphosphorylceramides (IP-Cer) are key sphingolipids that serve as precursors for more complex sphingolipids. IP-Cer synthesis occurs through the catalytic addition of inositol to a dihydroceramide (dCer) or phytoceramide (phytoCer) by the Inositol-phosphoryl ceramide synthase 1 (Ipc1). Ipc1 is encoded by the ipc-1 gene (also known as aur1 (aureobasidin resistance protein)) in *S. cerevisiae* (YKL004W) and *N. crassa* (NCU02282.2, HomoGene ID 6380 and [229]). Through the addition of mannose to IP-Cer MIP-Cer is synthesised through a mannosyltransferase. This mannosyltransferase is encoded by csg-2 in *S. cerevisiae* (YBR036C) and *N. crassa* (NCU07247.2 [229]) or csg-1/sur1 in *S. cerevisiae* [235]. A misregulation of IP-Cer levels e.g. through disrupted MIP-Cer biosynthesis causes hypersensitivity to a growth environment with low pH in *S. cerevisiae* [236]. MIP-Cer is further mannosylated to $M(IP)_2$-Cer by a Inositolphosphoryltransferase which is encoded by ipt-1 in *S. cerevisiae* (YDR072C [237]) for which no homologue could be found in the *N. crassa* genome through BLAST search in [229] (Fig 5.18 5). In the presented lipid analysis of *N. crassa* and *S. cerevisiae* (Section 5.3.5) low levels of $M(IP)_2$-Cer (less than 1% of sphingolipids) were detected in both organisms and should be evaluated further. An additional inositolphosphorylceramide IP_2Cer has been reported in *N. crassa* [41], but its synthesis pathway has yet to be studied (Fig 5.18 6).

In summary, alternative sphingolipid classes to the reported sphingomyelin-like lipids measured in this analysis have been reported in fungi and particularly *N. crassa*. It might be worth reevaluating the lipid content of *N. crassa* and Pma1, focusing on the previously measured glycosphingolipids. As outlined above, one potential lipid class group is glycosylceramides such as mono glycosylated ceramides such as GlcCer [43] or potentially GalCer and more complex glycosylated lipids like the tetra glycosylated ceramide (or Neuroporaside) as reported in [42]. An in-depth analysis of alternative inositol species such as IP_2Cer (as reported in [41]) could reveal important species for the *N. crassa* plasma membrane and Pma1. Inostitol containing ceramides might be particularly interesting, since glycosylceramides such as GlcCer have been reported as an essential lipid in the fungal cell wall [231]. Furthermore, whether the sphingomyelin-like lipid is a potential inositolphosphoylceramide is particularly interesting as ceramide precursors containing C24 and C26 fatty acids bound to phytosphinganine (C18) are predominantly targeted for the inositolphosphoylceramide synthesis [238]. The measured sphingomyelin-like lipids with total chain lengths of up to C50 would require the presence of very long side chains with C24 or C26, and ceramides with these chains have also been implicated in the hexamerisation and trafficking Pma1 to the plasma membrane [58].

5.5 Summary and Outlook

The fungal species *N. crassa* slime and *S. cerevisiae* both express the plasma membrane P-type ATPase Pma1 and were therefore compared. Both species differ in their lipid composition and particularly in the number of distinct lipid species (Section 5.2, 5.3.1) and the types of sphingolipids (Section 5.3.5) and cardiolipin (Section 5.3.4) they synthesise, suggesting an increased complexity in the present lipid types and lipid synthesis of *N. crassa* compared to *S. cerevisiae*.

The sphingolipid composition of both organisms is characterised by ceramides (Cer) and inositol containing ceramides (IP-Cer, and MIP-Cer). IP-Cer can be found in abundance in both organisms and in the case of *N. crassa* only minor traces of MIP-Cer (Section 5.3.5). Surprisingly high amounts of particular sphingolipid species, which were

identified as sphingomyelin, were measured in *N. crassa* (Section 5.3.5). Differences in the sphingolipid composition of both organisms are particularly important since sphingomyelin-like lipids are not reported for either organism, as discussed in Section 5.4.6. Both organisms also differ in their fatty acid composition, indicating differences in their fatty acid synthesis, as *N. crassa* in comparison to *S. cerevisiae* expresses polyunsaturated fatty acids, which is confirmed in the differences of their cardiolipin types (Section 5.3.4).

For the purification of Pma1, plasma membranes are prepared from whole cells following an established protocol [104, 122], exploiting the agglutination of the plasma membrane with Concanavalin A, which changes their sedimentation behaviour and allows for the separation from other subcellular fractions. In a further purification step a DOC wash removes further (loosely bound) membrane proteins [122]. The lipid analysis reveals difficulty in separating the subcellular fractions during this purification step and confirms, based on high cardiolipin content, high contamination with mitochondrial membranes and potential other organelles, which have an impact on interpretation of diacylglycerophospholid composition (Section 5.4.2).

In all samples high PA content was measured (Section 5.3.2 and 5.4.2), which might have biological reasons for *N. crassa* as it seems to be increased with higher growth temperature (Section 5.3.2 and 5.4.2). To exclude enzymatic reasons for the increased PA content, EDTA could be used to suppress the activity of Phospholipase D. Well performed plasma membrane preparation is indicated by an enrichment of PS and sphingolipids compared to the whole cell (Section 5.4.2).

The particular lipids environment of the Pma1 hexamer, seems to be is characterised by higher amounts of inositol-containing lipids, particularly inositol-containing ceramides (Section 5.4.5) and PI compared to the lower oligomer which has a slight increased PA content (Section 5.4.3). These initial findings give further indications for lipids that

might stabilise the hexameric ensemble of Pma1 and should be investigated further.

Sphingolipids are physiologically enriched in the plasma membrane [30] and consist of longer and more saturated sphingolipids (Section 5.4.5) compared to the whole cell samples. Pma1 has been reported to reside in membrane compartments within the plasma membrane which are enriched in inositol containing ceramides [110, 111, 113, 115]. Enrichment of inositol containing ceramides, particularly in the highly abundant IP-Cer as well as the minor component MIP-Cer, can be seen in the presented *N. crassa* slime results following the DDM solubilisation and consecutive purification of Pma1 hexamers (Section 5.4.5). The sphingolipids surrounding Pma1, particularly IP-Cer and MIP-Cer seem to be enriched in their hydroxylation level (Section 5.4.5). A surprising find was the sphingolipid sphingomyelin SM 48:2 which was enriched in Pma1 hexamer samples and not found in the lower Pma1 oligomer sample (Section 5.4.5). The identity and actual presence of this lipid should be further investigated and which role it might play in the membrane fluidity of the Pma1 environment.

Overall conclusion:

- The fungal species *N. crassa* has more distinct lipid types compared to *S. cerevisiae* and differs in their lipid composition particularly in terms of sphingolipid types.
- Unexpectedly high amounts of sphingomyelin were found in the *N. crassa* samples particularly an enrichment of the species SM 48:2 in the Pma1 hexamer warrants further investigation into the identity of these species as well as their biological function in *N. crassa* and in relation to the protein.
- Furthermore the data suggests that the lipid environment of Pma1 hexamer is characterised by a high amount of inositol containing lipids particularly PI and IP-Cer and that the PI content is higher in the Pma1 hexamer compared to its lower oligomeric state and might therefore be important for the stabilisation of the oligomeric ensemble of Pma1.

Chapter 6

Future Work

While polymers can be used as an complementary method for the solubilisation of biological membranes, using polymers is a nuanced decision and depends on the chemical nature of polymers, as they might depend on the absence of divalent cations or a specific pH range or ionic strength as well as the chemical requirements of the target protein or the methods to assess protein activity and purity. Based on the presented results future work and experiments are proposed in the following sections.

6.1 Polymer solubilisation of Pma1 from *N. crassa* slime

Due to the presented limitations of the polymer solubilisation and detection of native Pma1 it may be worthwhile to explore the use of recombinantly expressed Pma1-Strep, as the compatibility of SMA 3:1 (Section 4.3.3, 4.3.4) with the anti-Strep antibody suggests potential for successful solubilisation and immunodetection of this form of Pma1. Further alternative polymers for the solubilisation of *N. crassa* like SMI [159] or others [163], could be evaluated to assess the feasibility of using polymers to solubilise this membrane using the in Chapter 3 devised small scale assay. The polymer solubilisation can then be tailored to purify Pma1 but particularly their compatibility with the ATPase activity assay should be evaluated. Initially, it might be worth exploring DIBMA solubilisation of Pma1 due to its larger size of up to 25 nm diameter [168], which could encapsulate the whole Pma1 hexamer. The use of DIBMA is under the provision that there is an alternative method to the existing anti-Pma1 antibody to verify the presence of NcPma1

in the sample, e.g. through mass spectrometry or immunodetection of recombinantly expressed NcPma1, containing, e.g. a Strep-Tag. DIBMA can be particularly interesting since adding Mg^{2+} might aid solubilisation similar to [198]. The ATPase Pma1 requires Mg^{2+}, and the compatibility of DIBMA with Mg^{2+} might aid compatibility with the ATPase Assay. Similarly, due to its resistance to Mg^{2+} and Ca^{2+} ions up to 100 mM in combination with a larger diameter than SMA [159, 239], it might be worth exploring cationic SMI as an alternative SMA-derived polymer. Furthermore, continuation of the prepared experiments for lipid analysis of the polymer lipid particles (similar to [201]) could give insights into the effects of the lipid composition on the polymer solubilisation efficiency of fungal membranes. Additionally expanding the range of solubilisation conditions tested could allow for better tailoring of polymer solubilisation of *N. crassa* membrane and other complex membranes.

6.2 Lipid analysis of Pma1 from *N. crassa*

As discussed in Chapter 5 *N. crassa* slime displays differences in its lipid composition, compared to *S. cerevisiae*. Notable high amounts of sphingomyelin were observed in *N. crassa* samples (Section 5.3.5) which were not reported previously in this fungus [41, 65] and discussed in Section 5.4.6. Therefore immediate future work should focus on repeating the lipidomics experiments but specifically looking at sphingolipids to confirm sphingomyelin was the actual lipid class, or if alternative glycosphingolipids previously detected in *N. crassa* can be confirmed as outlined in Section 5.4.6.2. Another way to verify the existence of sphingomyelin in *N. crassa* is to measure a potential enzymatic breakdown of sphingomyelin. A sphingomyelinase activity assay could be tested [226, 240], which uses sphingomyelin as its substrate and measures the resulting DAG content. If sphingomyelin is shown to be present in the repeats, its enrichment in Pma1 hexamer samples from *N. crassa*, particularly SM 48:2 (Section 5.3.5), should be investigated further as it has not been reported in the environment of Pma1 in *S. cerevisiae* [115]. This particularly warrants further investigation as both model organisms are used to study Pma1 and so significant variations in the sphingolipids types in plasma membrane should be taken into account when studying Pma1 from

both organisms.

Furthermore the lipid composition of the direct lipid environment surrounding the Pma1 hexamer in *N. crassa* plasma, could be analysed by trying to isolate specifically the membrane compartment containing Pma1 by gradient purification (eg OptiPrep Gradient [241]) or by polymer solubilisation and affinity purification of recombinantly expressed marker protein (similar to [115]). This can be used to verify the high amount of inositol containing lipids particularly PI and IP-Cer in the lipid environment surrounding the Pma1 hexamer in *N. crassa* (Section 5.4.3 and 5.4.5 respectively).

The presented findings suggest specific lipid species that may play a role in *N. crassa* Pma1 stability, activity, and oligomeric assemblies, however tightly bound lipids to the Pma1 hexamer could be further analysed with native mass spectrometry [52], and interactions in lipids could further be simulated with molecular dynamic simulations [104] with an adjusted lipid composition based on the presented results with contain more sphingolipids containing longer side chains and inositol headgroups outlined below (Section 6.2.1).

During this lipidomic analysis sterol content was not analysed and should be measured in any future analysis. In fungi the sterol component is ergosterol. In *S. cerevisiae* the sterol content of whole cells is considered to be about 12 % [50]. The general ergosterol content in *N. crassa* slime mutant was reported as ∼40 % of total lipids and a 4-10 fold increase of sterols/phospholipid ratio in the plasma membrane compared to the whole cell [65]. Furthermore they observed that the total sterol content of the plasma membrane appears to remain constant when the growth temperature is lowered from 37°C to 15°C, but the phospholipid content decreases from 50 % to 20 % and the glycosphingolipid content increases from 6 % to 37 % (see Appendix Table B.2), resulting in a change in the free sterol-to-phospholipid ratio from 0.8 (37°C) to nearly 2.0 (15°C). The impact of sterols on the plasma membrane microdomain organisation

and Pma1 should be investigated further.

Additionally to analysis of the outlined lipid classes and species, biological and technical repeats are needed which allow for appropriate statistical analysis of the presented lipid analysis results. Since inferences in enrichment of lipids in the Pma1 hexamer are made from changes in lipid composition of the purification pipeline of Pma1 the lipid composition of subcellular fractions of *N. crassa* slime, particularly its mitochondria, should be studied to be able to evaluate their influence on the diacylglycerophospholipid composition of the measured plasma membrane samples.

Furthermore, for the analysis of the effect of the growth temperature on the lipid composition of *N. crassa* whole cells, the growth status of the cells should be rigorously controlled and a larger temperature range (e.g. 15°C, 25°C, 30°C, 35°C) should be analysed. To exclude any potential effect of Phospholipase D sample treatment with 10 mM EDTA to avoid PA should be analysed (as outlined in Section 5.4.2). For the future, each sample sent for lipid analysis could be split into smaller aliquots, to account for any differences in sample handling. Furthermore to make better interpolations of lipid enrichment each purified Pma1 sample should be compared to its originating membrane. It might also be interesting to further analyse the effects of the detergent used in the membrane preparation on the plasma membrane and whether adding certain lipids would improve solubilisation of Pma1.

6.2.1 Suggestions for molecular dynamics (MD) simulation of the lipid environment of *N. crassa* Pma1

The results from the lipids analysis of Pma1 purification with LC/MS (Section 5.4) could not determine the specific identity of tightly bound lipids to the analysed Pma1 hexamer, but allow for the analysis of enrichment of lipids during the purification process of Pma1. The analysis allowed the identification of co-purified lipids that would be assumed to be in the close environment of Pma1, and therefore potentially important lipids for the stability or activity of Pma1 hexamer. One tool to assess interactions of lipids

with proteins is coarse grained molecular dynamic (MD) simulations using the Martini forcefield [242], which has been published for *N. crassa* Pma1 [104]. Unpublished work in the Bublitz group has identified inositol headgroups as a potential binding candidate for Pma1. Based on the presented results from lipid analysis (Section 5.4) and literature analysis a native-like the modification of the lipid composition for MD simulation can be proposed and is outlined in the Appendix (Section B.3 and Table B.23). Inositol-containing headgroup lipids with a C26 fatty acid are found in the Pma1-containing detergent resistant membrane area in *S. cerevisiae* [108]. The interaction with Pma1 could be supported by the inositol headgroup and the sphingosine backbone might not be the contributing factor (unpublished MD simulation from the Bublitz group). Based on the presented results the influences of very long C26 side chains as well as the inositol - ceramide headgroups on the Pma1 hexamer could be simulated. An increase of very long fatty acids (total carbon atoms C46 and longer) during the protein purification might be worth recreating *in silico*. Further molecular dynamics simulations have the potential to shine light on potential interactions between the suggested lipids and the Pma1 hexamer.

Bibliography

[1] Guido Guidotti. Membrane proteins. *Proteins*, 1972.

[2] Bruce Alberts. *Molecular Biology of the Cell.* Garland Science, New York, New York, sixth ed. edition, 2015.

[3] J. Thomas Hannich, Kyohei Umebayashi, and Howard Riezman. Distribution and functions of sterols and sphingolipids. *Cold Spring Harbor Perspectives in Biology*, 3(5):1–14, 2011.

[4] Atsushi Yamashita, Yasuhiro Hayashi, Yoko Nemoto-Sasaki, Makoto Ito, Saori Oka, Takashi Tanikawa, Keizo Waku, and Takayuki Sugiura. Acyltransferases and transacylases that determine the fatty acid composition of glycerolipids and the metabolism of bioactive lipid mediators in mammalian cells and model organisms. *Progress in Lipid Research*, 53(1):18–81, 2014.

[5] J. Thomas Hannich, Denia Mellal, Suihan Feng, Andreas Zumbuehl, and Howard Riezman. Structure and conserved function of iso-branched sphingoid bases from the nematode: Caenorhabditis elegans. *Chemical Science*, 8(5):3676–3686, 2017.

[6] Sabine Grösch, Susanne Schiffmann, and Gerd Geisslinger. Chain length-specific properties of ceramides. *Progress in Lipid Research*, 51(1):50–62, 1 2012.

[7] Takeshi Harayama, Miki Eto, Hideo Shindou, Yoshihiro Kita, Eiji Otsubo, Daisuke Hishikawa, Satoshi Ishii, Kenji Sakimura, Masayoshi Mishina, and Takao Shimizu. Lysophospholipid acyltransferases mediate phosphatidylcholine diversification to achieve the physical properties required in vivo. *Cell Metabolism*, 20(2):295–305, 8 2014.

[8] Gerrit van Meer. Membrane lipids, where they are and how they behave. *Nat Rev Mol Cell Biol.*, 9(2):112–124, 2008.

[9] Bruno Antonny, Stefano Vanni, Hideo Shindou, and Thierry Ferreira. From zero to six double bonds: Phospholipid unsaturation and organelle function. *Trends in Cell Biology*, 25(7):427–436, 7 2015.

[10] Erdinc Sezgin, Ilya Levental, Satyajit Mayor, and Christian Eggeling. The mystery of membrane organization: Composition, regulation and roles of lipid rafts. *Nature Reviews Molecular Cell Biology*, 18(6):361–374, 6 2017.

[11] Takeshi Harayama and Howard Riezman. Understanding the diversity of membrane lipid composition. *Nature Reviews Molecular Cell Biology*, 19(5):281–296, 5 2018.

[12] Leonhard Möckl. The Emerging Role of the Mammalian Glycocalyx in Functional Membrane Organization and Immune System Regulation. *Frontiers in Cell and Developmental Biology*, 8:253, 4 2020.

[13] Francesc Xabier Contreras, Andreas Max Ernst, Felix Wieland, and Britta Brügger. Specificity of intramembrane protein-lipid interactions. *Cold Spring Harbor Perspectives in Biology*, 3(6):1–18, 2011.

[14] Robert Ernst, Christer S. Ejsing, and Bruno Antonny. Homeoviscous Adaptation and the Regulation of Membrane Lipids. *Journal of Molecular Biology*, 428(24):4776–4791, 12 2016.

[15] Rosie Dawaliby, Cataldo Trubbia, Cédric Delporte, Caroline Noyon, Jean Marie Ruysschaert, Pierre Van Antwerpen, and Cédric Govaerts. Phosphatidylethanolamine is a key regulator of membrane fluidity in eukaryotic cells. *Journal of Biological Chemistry*, 291(7):3658–3667, 2 2016.

[16] Anthony G. Lee. How lipids affect the activities of integral membrane proteins, 11 2004.

[17] E. Zinser, C. D.M. Sperka-Gottlieb, E. V. Fasch, S. D. Kohlwein, F. Paltauf, and G. Daum. Phospholipid synthesis and lipid composition of subcellular membranes in the unicellular eukaryote Saccharomyces cerevisiae. *Journal of Bacteriology*, 173(6):2026–2034, 1991.

[18] Jun Suzuki, Masato Umeda, Peter J. Sims, and Shigekazu Nagata. Calcium-dependent phospholipid scrambling by TMEM16F. *Nature*, 468(7325):834–840, 12 2010.

[19] Jun Suzuki, Daniel P Denning, Eiichi Imanishi, H Robert Horvitz, and Shigekazu Nagata. Xk-Related Protein 8 and CED-8 Promote Phosphatidylserine Exposure in Apoptotic Cells. *Science*, 341(6144):403–406, 2013.

[20] Jorge Cerbón and Víctor Calderón. Changes of the compositional asymmetry of phospholipids associated to the increment in the membrane surface potential. *BBA - Biomembranes*, 1067(2):139–144, 8 1991.

[21] Johan Owen De Craene, Dimitri L. Bertazzi, Séverine Bär, and Sylvie Friant. Phosphoinositides, major actors in membrane trafficking and lipid signaling pathways. *International Journal of Molecular Sciences*, 18(3), 3 2017.

[22] Susan A. Henry, Sepp D. Kohlwein, and George M. Carman. Metabolism and regulation of glycerolipids in the yeast Saccharomyces cerevisiae. *Genetics*, 190(2):317–349, 2 2012.

[23] Edward Ross Pennington, Katsuhiko Funai, David A. Brown, and Saame Raza Shaikh. The role of cardiolipin concentration and acyl chain composition on mitochondrial inner membrane molecular organization and function. *Biochimica et Biophysica Acta - Molecular and Cell Biology of Lipids*, 1864(7):1039–1052, 7 2019.

[24] Nikita Ikon and Robert O. Ryan. Cardiolipin and mitochondrial cristae organization. *Biochimica et Biophysica Acta - Biomembranes*, 1859(6):1156–1163, 2017.

[25] Eugenia Mileykovskaya and William Dowhan. Cardiolipin-dependent formation of mitochondrial respiratory supercomplexes. *Chemistry and Physics of Lipids*, 179:42–48, 2014.

[26] James A. Letts and Leonid A. Sazanov. Clarifying the supercomplex: The higher-order organization of the mitochondrial electron transport chain. *Nature Structural and Molecular Biology*, 24(10):800–808, 10 2017.

[27] Giuseppe Paradies, Valeria Paradies, Francesca M. Ruggiero, and Giuseppe Petrosillo. Role of cardiolipin in mitochondrial function and dynamics in health and disease: Molecular and pharmacological aspects. *Cells*, 8(7), 7 2019.

[28] Erick J. Dufourc. Sterols and membrane dynamics. *Journal of Chemical Biology*, 1(1-4):63–77, 11 2008.

[29] Taras Sych, Kandice R Levental, and Erdinc Sezgin. Lipid-Protein Interactions in Plasma Membrane Organization and Function. *Annual Review of Biophysics*, 51:135–156, 2022.

[30] J. L. Patton and R. L. Lester. The phosphoinositol sphingolipids of Saccharomyces cerevisiae are highly localized in the plasma membrane. *Journal of Bacteriology*, 173(10):3101–3108, 1991.

[31] Robert C. Dickson. Roles for sphingolipids in saccharomyces cerevisiae. *Advances in Experimental Medicine and Biology*, 688:217–231, 2010.

[32] Filipa C. Santos, Joaquim T. Marquês, Andreia Bento-Oliveira, and Rodrigo F.M. de Almeida. Sphingolipid-enriched domains in fungi. *FEBS Letters*, 594(22):3698–3718, 2020.

[33] Gerald N. Rechberger. Phosphosphingolipids. In *Encyclopedia of Lipidomics*, pages 1–3. Springer Netherlands, 2015.

[34] Makoto Taniguchi and Toshiro Okazaki. The role of sphingomyelin and sphingomyelin synthases in cell death, proliferation and migration - From cell and animal models to human disorders, 2014.

[35] Joan M. Boggs. Lipid intermolecular hydrogen bonding: influence on structural organization and membrane function. *BBA - Reviews on Biomembranes*, 906(3):353–404, 1987.

[36] Bodil Ramstedt and J. Peter Slotte. Sphingolipids and the formation of sterol-enriched ordered membrane domains. *Biochimica et Biophysica Acta - Biomembranes*, 1758(12):1945–1956, 2006.

[37] Deborah A. Brown and Erwin London. Structure and function of sphingolipid- and cholesterol-rich membrane rafts. *Journal of Biological Chemistry*, 275(23):17221–17224, 2000.

[38] Domenico Russo, Seetharaman Parashuraman, and Giovanni D'Angelo. Glycosphingolipid–protein interaction in signal transduction. *International Journal of Molecular Sciences*, 17(10):1–21, 2016.

[39] Mary L. Kraft. Sphingolipid organization in the plasma membrane and the mechanisms that influence it, 1 2017.

[40] L. Ashley Cowart and Lina M. Obeid. Yeast sphingolipids: Recent developments in understanding biosynthesis, regulation, and function. *Biochimica et Biophysica Acta - Molecular and Cell Biology of Lipids*, 1771(3):421–431, 2007.

[41] R. L. Lester, S. W. Smith, G. B. Wells, D. C. Rees, and W. W. Angus. The isolation and partial characterization of two novel sphingolipids from Neurospora crassa: di(inositolphosphoryl)ceramide and [(gal) 3glu]ceramide. *Journal of Biological Chemistry*, 249(11):3388–3394, 1974.

[42] Valeria Costantino, Alfonso Mangoni, Roberta Teta, Galia Kra-Oz, and Oded Yarden. Neurosporaside, a tetraglycosylated sphingolipid from neurospora crassa. *Journal of Natural Products*, 74(4):554–558, 2011.

[43] Anna Huber, Gregor Oemer, Nermina Malanovic, Karl Lohner, Laura Kovács, Willi Salvenmoser, Johannes Zschocke, Markus A Keller, and Florentine Marx. Membrane Sphingolipids Regulate the Fitness and Antifungal Protein Susceptibility of Neurospora crassa. *Frontiers in Microbiology*, 10(APR):1–18, 2019.

[44] J. Folch, M. Lees, and G. H. Sloane Stanley. A simple method for the isolation and purification of total lipides from animal tissues. *The Journal of biological chemistry*, 226(1):497–509, 1957.

[45] A. Archana, B. and Khale Anubha. An Overview on Thin Layer Chromatography. *International Journal of Pharmaceutical Sciences and Research*, (March):256–267, 2011.

[46] J S Ellingson and W E Lands. Phospholipid reactivation of plasmalogen metabolism. *Lipids*, 3(2):111–120, 3 1968.

[47] Mathias Brands, Philipp Gutbrod, and Peter Dörmann. Lipid Analysis by Gas Chromatography and Gas Chromatography–Mass SpectrometrySpectrometry. In Dorothea Bartels and Peter Dörmann, editors, *Plant Lipids: Methods and Protocols*, pages 43–57. Springer US, New York, NY, 2021.

[48] Christer S. Ejsing, Julio L. Sampaio, Vineeth Surendranath, Eva Duchoslav, Kim Ekroos, Robin W. Klemm, Kai Simons, and Andrej Shevchenko. Global analysis of the yeast lipidome by quantitative shotgun mass spectrometry. *Proceedings of the National Academy of Sciences of the United States of America*, 106(7):2136–2141, 2009.

[49] Dominik Schwudke, Kai Schuhmann, Ronny Herzog, Stefan R. Bornstein, and Andrej Shevchenko. Shotgun lipidomics on high resolution mass spectrometers. *Cold Spring Harbor Perspectives in Biology*, 3(9):1–13, 2011.

[50] Christian Klose, Michal A. Surma, Mathias J. Gerl, Felix Meyenhofer, Andrej Shevchenko, and Kai Simons. Flexibility of a eukaryotic lipidome - insights from yeast lipidomics. *PLoS ONE*, 7(4), 2012.

[51] Tomas Cajka and Oliver Fiehn. Comprehensive analysis of lipids in biological systems by liquid chromatography-mass spectrometry. *TrAC - Trends in Analytical Chemistry*, 61:192–206, 2014.

[52] Joseph Gault, Idlir Liko, Michael Landreh, Denis Shutin, Jani Reddy Bolla, Damien Jefferies, Mark Agasid, Hsin Yung Yen, Marcus J.G.W. Ladds, David P. Lane, Syma Khalid, Christopher Mullen, Philip M. Remes, Romain Huguet, Graeme McAlister, Michael Goodwin, Rosa Viner, John E.P. Syka, and Carol V. Robinson. Combining native and 'omics' mass spectrometry to identify endogenous ligands bound to membrane proteins. *Nature Methods*, 17(5):505–508, 2020.

[53] Michel E. Van Der Rest, Anne H. Kamminga, Akihiko Nakano, Yasuhiro Anraku, Bert Poolman, and Wil N. Konings. The plasma membrane of Saccharomyces cerevisiae: Structure, function, and biogenesis. *Microbiological Reviews*, 59(2):304–322, 1995.

[54] Giinther Daum and Jean E Vancet. Import of Lipids into Mitochondria. *Lipid Res*, 36(3):103–130, 1997.

[55] Jorge Bernardino de la Serna, Gerhard J. Schütz, Christian Eggeling, and Marek Cebecauer. There is no simple model of the plasma membrane organization. *Frontiers in Cell and Developmental Biology*, 4(SEP), 9 2016.

[56] Marcus C.S. Lee, Susan Hamamoto, and Randy Schekman. Ceramide biosynthesis is required for the formation of the oligomeric H+-ATPase Pma1p in the yeast endoplasmic reticulum. *Journal of Biological Chemistry*, 277(25):22395–22401, 2002.

[57] Barbara Gaigg, Birgit Timischl, Linda Corbino, and Roger Schneiter. Synthesis of sphingolipids with very long chain fatty acids but not ergosterol is required for routing of newly synthesized plasma membrane ATPase to the cell surface of yeast. *Journal of Biological Chemistry*, 280(23):22515–22522, 2005.

[58] Barbara Gaigg, Alexandre Toulmay, and Roger Schneiter. Very long-chain fatty acid-containing lipids rather than sphingolipids per se are required for raft association and stable surface transport of newly synthesized plasma membrane ATPase in yeast. *Journal of Biological Chemistry*, 281(45):34135–34145, 2006.

[59] Krzysztof Murzyn, Tomasz Róg, and Marta Pasenkiewicz-Gierula. Phosphatidylethanolamine-phosphatidylglycerol bilayer as a model of the inner bacterial membrane. *Biophysical Journal*, 88(2):1091–1103, 2005.

[60] J.D. Weete. *Fungal Lipid Biochemistry*. Plenum Press, New York, 1974.

[61] Susanne E. Horvath, Andrea Wagner, Ernst Steyrer, and Günther Daum. Metabolic link between phosphatidylethanolamine and triacylglycerol metabolism in the yeast Saccharomyces cerevisiae. *Biochimica et Biophysica Acta - Molecular and Cell Biology of Lipids*, 1811(12):1030–1037, 12 2011.

[62] Susanne E. Horvath and Günther Daum. Lipids of mitochondria. *Progress in Lipid Research*, 52(4):590–614, 2013.

[63] Gerhard Hallermayer and Walter Neupert. Lipid Composition of Mitochondrial Outer and Inner Membranes of Neurospora Crassa. *Hoppe-Seyler's Zeitschrift fur Physiologische Chemie*, 355(1):279–288, 1974.

[64] Kenneth J Friedman and David Glick. Role of lipids in the Neurospora crassa membrane: III. Lipid composition and phase transition properties of the plasma membrane, and its components. *The Journal of Membrane Biology*, 54(3):183–190, 1980.

[65] Lawrence R. Aaronson and Charles E. Martin. Temperature-induced modifications of glycosphingolipids in plasma membranes of Neurospora crassa. *BBA - Biomembranes*, 735(2):252–258, 1983.

[66] T. W. Keenan, D. James Morré, Diane E. Olson, W. N. Yunghans, and Stuart Patton. Biochemical and morphological comparison of plasma membrane and milk fat globule membrane from bovine mammary gland. *Journal of Cell Biology*, 44(1):80–93, 1970.

[67] Tomáš Řezanka, Irena Kolouchová, and Karel Sigler. Lipidomic analysis of psychrophilic yeasts cultivated at different temperatures. *Biochimica et Biophysica Acta - Molecular and Cell Biology of Lipids*, 1861(11):1634–1642, 2016.

[68] Anthony Watts and Jan Joep HHM de Pont. *Progress in protein-lipid interactions*. Elsevier Science & Technology, 1986.

[69] M. Opekarová and W. Tanner. Specific lipid requirements of membrane proteins - A putative bottleneck in heterologous expression. *Biochimica et Biophysica Acta - Biomembranes*, 1610(1):11–22, 2 2003.

[70] Elina Ikonen and Xin Zhou. Cholesterol transport between cellular membranes: A balancing act between interconnected lipid fluxes. *Developmental Cell*, 56(10):1430–1436, 2021.

[71] Matti Javanainen, Giray Enkavi, Ramon Guixà-Gonzaléz, Waldemar Kulig, Hector Martinez-Seara, Ilya Levental, and Ilpo Vattulainen. Reduced level of docosahexaenoic acid shifts GPCR neuroreceptors to less ordered membrane regions. *PLoS Computational Biology*, 15(5):1–16, 2019.

[72] Matthieu Chavent, Dimple Karia, Antreas C. Kalli, Jan Domański, Anna L. Duncan, George Hedger, Phillip J. Stansfeld, Elena Seiradake, E. Yvonne Jones, and Mark S.P. Sansom. Interactions of the EphA2 Kinase Domain with PIPs in Membranes: Implications for Receptor Function. *Structure*, 26(7):1025–1034, 2018.

[73] Hsin Yung Yen, Kin Kuan Hoi, Idlir Liko, George Hedger, Michael R. Horrell, Wanling Song, Di Wu, Philipp Heine, Tony Warne, Yang Lee, Byron Carpenter, Andreas Plückthun, Christopher G. Tate, Mark S.P. Sansom, and Carol V. Robinson. PtdIns(4,5)P2 stabilizes active states of GPCRs and enhances selectivity of G-protein coupling. *Nature*, 559(7714):423–427, 2018.

[74] Cecilia Cannarozzo, Senem Merve Fred, Mykhailo Girych, Caroline Biojone, Giray Enkavi, Tomasz Róg, Ilpo Vattulainen, Plinio C. Casarotto, and Eero Castrén. Cholesterol-recognition motifs in the transmembrane domain of the tyrosine kinase receptor family: The case of TRKB. *European Journal of Neuroscience*, 53(10):3311–3322, 2021.

[75] Robert V. Stahelin. Lipid binding domains: More than simple lipid effectors. *Journal of Lipid Research*, 50(SUPPL.):S299–S304, 2009.

[76] Hanna Juhola, Pekka A. Postila, Sami Rissanen, Fabio Lolicato, Ilpo Vattulainen, and Tomasz Róg. Negatively Charged Gangliosides Promote Membrane Association of Amphipathic Neurotransmitters. *Neuroscience*, 384:214–223, 2018.

[77] Patrick W. Simcock, Maike Bublitz, Flaviu Cipcigan, Maxim G. Ryadnov, Jason Crain, Phillip J. Stansfeld, and Mark S.P. Sansom. Membrane Binding of Antimicrobial Peptides Is Modulated by Lipid Charge Modification. *Journal of Chemical Theory and Computation*, 17(2):1218–1228, 2021.

[78] Sivaramakrishnan Ramadurai, Andrea Holt, Victor Krasnikov, Geert Van Den Bogaart, J. Antoinette Killian, and Bert Poolman. Lateral diffusion of membrane proteins. *Journal of the American Chemical Society*, 131(35):12650–12656, 2009.

[79] Cédric M. Blouin, Yannick Hamon, Pauline Gonnord, Cédric Boularan, Jérémy Kagan, Christine Viaris de Lesegno, Richard Ruez, Sébastien Mailfert, Nicolas Bertaux, Damarys Loew, Christian Wunder, Ludger Johannes, Guillaume Vogt, Francesc Xabier Contreras, Didier Marguet, Jean Laurent Casanova, Céline Galès, Hai Tao He, and Christophe Lamaze. Glycosylation-Dependent IFN-γR Partitioning in Lipid and Actin Nanodomains Is Critical for JAK Activation. *Cell*, 166(4):920–934, 2016.

[80] Günes Özhan, Erdinc Sezgin, Daniel Wehner, Astrid S. Pfister, Susanne J. Kühl, Birgit Kagermeier-Schenk, Michael Kühl, Petra Schwille, and Gilbert Weidinger. Lypd6 enhances wnt/β-catenin signaling by promoting lrp6 phosphorylation in raft plasma Membrane Domains. *Developmental Cell*, 26(4):331–345, 2013.

[81] Erdinc Sezgin, Yagmur Azbazdar, Xue W. Ng, Cathleen Teh, Kai Simons, Gilbert Weidinger, Thorsten Wohland, Christian Eggeling, and Gunes Ozhan. Binding of canonical Wnt ligands to their receptor complexes occurs in ordered plasma membrane environments. *FEBS Journal*, 284(15):2513–2526, 2017.

[82] Deborah A. Brown and John K. Rose. Sorting of GPI-anchored proteins to glycolipid-enriched membrane subdomains during transport to the apical cell surface. *Cell*, 68(3):533–544, 1992.

[83] Patrick Lajoie and Ivan R. Nabi. Lipid rafts, caveolae, and their endocytosis. In *International Review of Cell and Molecular Biology*, volume 282, pages 135–163. Elsevier Inc., 1 edition, 2010.

[84] Bo Jian Lin, Shun Hao Tsao, Alex Chen, Shu Kai Hu, Ling Chao, and Pen Hsiu Grace Chao. Lipid rafts sense and direct electric field-induced migration. *Proceedings of the National Academy of Sciences of the United States of America*, 114(32):8568–8573, 2017.

[85] Michael J. Tisza, Weina Zhao, Jessie S.R. Fuentes, Sara Prijic, Xiaoling Chen, Ilya Levental, and Jeffrey T. Chang. Motility and stem cell properties induced by the epithelialmesenchymal transition require destabilization of lipid rafts. *Oncotarget*, 7(32):51553–51568, 2016.

[86] Heinrich Sandermann. Lipid-Dependent Membrane Enzymes: A Kinetic Model for Cooperative Activation in the Absence of Cooperativity in Lipid Binding. *European Journal of Biochemistry*, 127(1):123–128, 1982.

[87] Ünal Coskun, Michał Grzybek, David Drechsel, and Kai Simons. Regulation of human EGF receptor by lipids. *Proceedings of the National Academy of Sciences of the United States of America*, 108(22):9044–9048, 2011.

[88] Annie M. Westerlund, Oliver Fleetwood, Sergio Pérez-Conesa, and Lucie Delemotte. Network analysis reveals how lipids and other cofactors influence membrane protein allostery. *Journal of Chemical Physics*, 153(14), 2020.

[89] Andreas Anderluh, Tina Hofmaier, Enrico Klotzsch, Oliver Kudlacek, Thomas Stockner, Harald H. Sitte, and Gerhard J. Schütz. Direct PIP 2 binding mediates stable oligomer formation of the serotonin transporter. *Nature Communications*, 8(May 2016), 2017.

[90] Markus Sällman Almén, Karl J.V. Nordström, Robert Fredriksson, and Helgi B. Schiöth. Mapping the human membrane proteome: A majority of the human membrane proteins can be classified according to function and evolutionary origin. *BMC Biology*, 7:50, 2009.

[91] H. Lodish. *Molecular cell biology*. New York: W.H. Freeman, 6th edition, 2008.

[92] Narendra Tuteja, Mahesh Chandra, Renu Tuteja, and Mithilesh K. Misra. Nitric oxide as a unique bioactive signaling messenger in physiology and pathophysiology. *Journal of Biomedicine and Biotechnology*, 2004(4):227–237, 2004.

[93] Declan A Doyle, João Morais Cabral, Richard A Pfuetzner, Anling Kuo, Jacqueline M Gulbis, Steven L Cohen, Brian T Chait, Roderick Mackinnon, Declan A Doyle, Joao Morais Cabral, Richard A Pfuetzner, Anling Kuo, Jacqueline M Gulbis, Steven L Cohen, Brian T Chait, and Roderick Mackinnon. The Structure of the Potassium Channel : Molecular Basis of K + Conduction and Selectivity. 280(5360):69–77, 2016.

[94] M. Bublitz, J. P. Morth, and P. Nissen. P-type ATPases at a glance. *Journal of Cell Science*, 124(15):2515–2519, 2011.

[95] Douglas C. Rees, Eric Johnson, and Oded Lewinson. ABC transporters: The power to change. *Nature Reviews Molecular Cell Biology*, 10(3):218–227, 2009.

[96] Mattia D. Pizzagalli, Ariel Bensimon, and Giulio Superti-Furga. A guide to plasma membrane solute carrier proteins. *FEBS Journal*, 288(9):2784–2835, 2021.

[97] Elja Eskes, Marie Anne Deprez, Tobias Wilms, and Joris Winderickx. pH homeostasis in yeast; the phosphate perspective. *Current Genetics*, 64(1):155–161, 2018.

[98] John P. Overington, Bissan Al-Lazikani, and Andrew L. Hopkins. How many drug targets are there ? PubMed Commons. *Nature reviews. Drug discovery*, 5(12):10, 2006.

[99] Kathleen M Giacomini, Shiew Mei Huang, Donald J Tweedie, Leslie Z Benet, Kim L.R. Brouwer, Xiaoyan Chu, Amber Dahlin, Raymond Evers, Volker Fischer, Kathleen M Hillgren, Keith A Hoffmaster, Toshihisa Ishikawa, Dietrich Keppler, Richard B Kim, Caroline A Lee, Mikko Niemi, Joseph W Polli, Yuicchi Sugiyama, Peter W Swaan, Joseph A Ware, Stephen H Wright, Sook Wah Yee, Maciej J Zamek-Gliszczynski, and Lei Zhang. Membrane transporters in drug development. *Nature Reviews Drug Discovery*, 9(3):215–236, 3 2010.

[100] Simon Newstead. Recent advances in understanding proton coupled peptide transport via the POT family. *Current Opinion in Structural Biology*, 45:17–24, 2017.

[101] David S. Perlin, Donna Seto-Young, and Brian C. Monk. The plasma membrane H+-ATPase of fungi. A candidate drug target? *Annals of the New York Academy of Sciences*, 834:609–617, 1997.

[102] Werner Kühlbrandt. Biology, structure and mechanism of P-type ATPases. *Nature Reviews Molecular Cell Biology*, 5(4):282–295, 4 2004.

[103] Gordon D. Brown, David W. Denning, Neil A.R. Gow, Stuart M. Levitz, Mihai G. Netea, and Theodore C. White. Hidden killers: Human fungal infections. *Science Translational Medicine*, 4(165):1–10, 2012.

[104] Sabine Heit, Maxwell M.G. Geurts, Bonnie J. Murphy, Robin A. Corey, Deryck J. Mills, Werner Kühlbrandt, and Maike Bublitz. Structure of the hexameric fungal plasma membrane proton pump in its autoinhibited state. *Science Advances*, 7(46):1–13, 2021.

[105] Peng Zhao, Chaoran Zhao, Dandan Chen, Caihong Yun, Huilin Li, and Lin Bai. Structure and activation mechanism of the hexameric plasma membrane H+-ATPase. *Nature Communications*, 12(1):1–11, 2021.

[106] Rosa A. Fajardo-Somera, Barry Bowman, and Meritxell Riquelme. The plasma membrane proton pump PMA-1 is incorporated into distal parts of the hyphae independently of the spitzenkörper in Neurospora crassa. *Eukaryotic Cell*, 12(8):1097–1105, 2013.

[107] Anthony Ambesi, Manuel Miranda, Valery V Petrov, and Carolyn W Slayman. Structure and Function of the Yeast Plasma-Membrane H+-ATPase. *The Journal of Experimental Biology*, 203(203):155–160, 2000.

[108] M. Bagnat, S. Keranen, A. Shevchenko, A. Shevchenko, and K. Simons. Lipid rafts function in biosynthetic delivery of proteins to the cell surface in yeast. *Proceedings of the National Academy of Sciences*, 97(7):3254–3259, 2000.

[109] Michel Bagnat, Amy Chang, and Kai Simons. Plasma Membrane Proton ATPase Pma1p Requires Raft Association for Surface Delivery in Yeast. *Molecular Biology of the Cell*, 12(12):4129–4138, 2001.

[110] Guido Grossmann, Miroslava Opekarová, Jan Malinsky, Ina Weig-Meckl, and Widmar Tanner. Membrane potential governs lateral segregation of plasma membrane proteins and lipids in yeast. *EMBO Journal*, 26(1):1–8, 1 2007.

[111] Francisco Aresta-Branco, André M. Cordeiro, H. Susana Marinho, Luísa Cyrne, Fernando Antunes, and Rodrigo F.M. De Almeida. Gel domains in the plasma membrane of Saccharomyces cerevisiae: Highly ordered, ergosterol-free, and sphingolipid-enriched lipid rafts. *Journal of Biological Chemistry*, 286(7):5043–5054, 2 2011.

[112] Katerina Malinska, Jan Malinsky, Miroslava Opekarová, and Widmar Tanner. Visualization of Protein Compartmentation within the Plasma Membrane of Living Yeast Cells. *Molecular Biology of the Cell*, 14:4427–4436, 2003.

[113] Katerina Malinska, Jan Malinsky, Miroslava Opekarova, and Widmar Tanner. Distribution of Can1p into stable domains reflects lateral protein segregation within the plasma membrane of living S. cerevisiae cells. *Journal of Cell Science*, 117(25):6031–6041, 12 2004.

[114] Doris Berchtold and Tobias C. Walther. TORC2 Plasma Membrane Localization Is Essential for Cell Viability and Restricted to a Distinct Domain. *Molecular biology of the cell*, 20:1565–1575, 2009.

[115] Joury S. van 't Klooster, Tan Yun Cheng, Hendrik R. Sikkema, Aike Jeucken, Branch Moody, and Bert Poolman. Periprotein lipidomes of saccharomyces cerevisiae provide a flexible environment for conformational changes of membrane proteins. *eLife*, 9, 4 2020.

[116] R H Davis. Neurospora: Contributions of a Model Organism. *Oxford University press*, 2000.

[117] R. H. Davis and D. D. Perkins. Neurospora: A model of model microbes. *Nature Rev. Genet.*, (3):7–13, 2002.

[118] D. D. Perkins and R. H. Davis. Neurospora at the millennium. *Fungal Genet. Biol.*, (31):153–167, 2000.

[119] D. D. Perkins and R. H. Davis. Neurospora chronology – 1843-2002. *Fungal Genet. Newslett.*, (49):4–8, 2002.

[120] Gene A Scarborough. Isolation and characterization of Neurospora crassa plasma membranes. *Journal of Biological Chemistry*, 250(3):1106–1111, 1975.

[121] Gene A. Scarborough. A variant of the cell wall-less fz;sg;os-1 strain of Neurospora crassa with altered morphology and improved growth. *Experimental Mycology*, 9(3):5–78, 1985.

[122] Gene A Scarborough. Large-Scale Purification of Plasma Membrane H+-ATPase from a Cell Wall-Less Mutant of Neurospora crassa. *Methods in Enzymology*, 157(C):574–579, 1988.

[123] C. H. Bigger, M. R. White, and H. D. Braymer. Ultrastructure and Invertase Secretion of the Slime Mutant of Neurospora crassa. *Journal of General Microbiology*, 71(1):159–166, 1972.

[124] M. Buzzi, M. S. S. Felipe, M. de Oliveira Azevedo, and R. de Araujo Caldas. Membrane lipid composition and invertase secretion of Neurospova crassa and its wall-less mutant slime: effects of temperature and the surfactant Tween 80. *Journal of General Microbiology*, 139(8):1885–1889, 1993.

[125] Sterling Emerson. Slime a plasmodioid variant of Neurospora crassa. *Genetica*, 34(1):162–182, 1964.

[126] Lina Lindberg, Aline X.S. Santos, Howard Riezman, Lisbeth Olsson, and Maurizio Bettiga. Lipidomic Profiling of Saccharomyces cerevisiae and Zygosaccharomyces bailii Reveals Critical Changes in Lipid Composition in Response to Acetic Acid Stress. *PLoS ONE*, 8(9):1–12, 2013.

[127] Filipa C. Santos, Andreia S. Fernandes, Catarina A.C. Antunes, Filipe P. Moreira, Arnaldo Videira, H. Susana Marinho, and Rodrigo F.M. de Almeida. Reorganization of plasma membrane lipid domains during conidial germination. *Biochimica et Biophysica Acta - Molecular and Cell Biology of Lipids*, 1862(2):156–166, 2017.

[128] R. Addison and G. A. Scarborough. Solubilization and purification of the Neurospora plasma membrane H+-ATPase. *Journal of Biological Chemistry*, 256(24):13165–13171, 1981.

[129] Dieter Oesterhelt and Walter Stockenius. Rhodopsin-like Protein from the Purple Membrane of Halobacterium halobium. *Nature New Biology*, 233:149, 1971.

[130] Michael T. Marty, Kin Kuan Hoi, and Carol V. Robinson. Interfacing Membrane Mimetics with Mass Spectrometry. *Accounts of Chemical Research*, 49(11):2459–2467, 2016.

[131] David Hardy, Elodie Desuzinges Mandon, Alice J. Rothnie, and Anass Jawhari. The yin and yang of solubilization and stabilization for wild-type and full-length membrane protein. *Methods*, 147(2018):118–125, 9 2018.

[132] Annela M. Seddon, Paul Curnow, and Paula J. Booth. Membrane proteins, lipids and detergents: Not just a soap opera, 11 2004.

[133] Marcella Orwick-Rydmark, Thomas Arnold, and Dirk Linke. The use of detergents to purify membrane proteins. *Current Protocols in Protein Science*, 2016(April):1–4, 2016.

[134] Daniel A.P. Gutmann, Eiichi Mizohata, Simon Newstead, Sebastian Ferrandon, Vincent Postis, Xiaobing Xia, Peter J.F. Henderson, Hendrik W. Van Veen, and Bernadette Byrne. A high-throughput method for membrane protein solubility screening: The ultracentrifugation dispersity sedimentation assay. *Protein Science*, 16(12):2775, 2007.

[135] Oliver Adams, Justin C. Deme, Joanne L. Parker, Philip W. Fowler, Susan M. Lea, and Simon Newstead. Cryo-EM structure and resistance landscape of M. tuberculosis MmpL3: An emergent therapeutic target. *Structure*, 29(10):1182–1191, 2021.

[136] Robert S. Cantor. Lipid composition and the lateral pressure profile in bilayers. *Biophysical Journal*, 76(5):2625–2639, 1999.

[137] Mary A. Schuler, Ilia G. Denisov, and Stephen G. Sligar. Nanodiscs as a new tool to examine lipid-protein interactions. *Methods in Molecular Biology*, 974:415–433, 2013.

[138] Jens Frauenfeld, Robin Löving, Jean Paul Armache, Andreas F.P. Sonnen, Fatma Guettou, Per Moberg, Lin Zhu, Caroline Jegerschöld, Ali Flayhan, John A.G. Briggs, Henrik Garoff, Christian Löw, Yifan Cheng, and Pär Nordlund. A saposin-lipoprotein nanoparticle system for membrane proteins. *Nature Methods*, 13(4):345–351, 2016.

[139] Jens Frauenfeld, James Gumbart, Eli O.Van Der Sluis, Soledad Funes, Marco Gartmann, Birgitta Beatrix, Thorsten Mielke, Otto Berninghausen, Thomas Becker, Klaus Schulten, and Roland Beckmann. Cryo-EM structure of the ribosome-SecYE complex in the membrane environment. *Nature Structural and Molecular Biology*, 18(5):614–621, 5 2011.

[140] Marcella C. Orwick, Peter J. Judge, Jan Procek, Ljubica Lindholm, Andrea Graziadei, Andreas Engel, Gerhard Gröbner, and Anthony Watts. Detergent-free formation and physicochemical characterization of nanosized lipid-polymer complexes: Lipodisq. *Angewandte Chemie - International Edition*, 51(19):4653–4657, 5 2012.

[141] Timothy J. Knowles, Rachael Finka, Michael Overduin, Corinne Smith, Tim Dafforn, Yu-Pin Lin, and Timothy J. Knowles. Membrane Proteins Solubilized Intact in Lipid Containing Nanoparticles Bounded by Styrene Maleic Acid Copolymer. *Journal of the American Chemical Society*, 131(22):7484–7485, 2009.

[142] Sarah C. Lee and Naomi L. Pollock. Membrane proteins: is the future disc shaped? *Biochemical Society Transactions*, 44(4):1011–1018, 8 2016.

[143] Sarah C. Lee, Tim J. Knowles, Vincent L.G. Postis, Mohammed Jamshad, Rosemary A. Parslow, Yu Pin Lin, Adrian Goldman, Pooja Sridhar, Michael Overduin, Stephen P. Muench, and Timothy R. Dafforn. A method for detergent-free isolation of membrane proteins in their local lipid environment. *Nature Protocols*, 11(7):1149–1162, 2016.

[144] Marcella Orwick-Rydmark, Janet E. Lovett, Andrea Graziadei, Ljubica Lindholm, Matthew R. Hicks, and Anthony Watts. Detergent-free incorporation of a seven-transmembrane receptor protein into nanosized bilayer lipodisq particles for functional and biophysical studies. *Nano Letters*, 12(9):4687–4692, 2012.

[145] Naomi L. Pollock, Sarah C. Lee, Jaimin H. Patel, Aiman A. Gulamhussein, and Alice J. Rothnie. Structure and function of membrane proteins encapsulated in a polymer-bound lipid bilayer. *Biochimica et Biophysica Acta - Biomembranes*, 1860(4):809–817, 2018.

[146] Naomi L. Pollock, Megha Rai, Kailene S. Simon, Sophie J. Hesketh, Alvin C.K. Teo, Mayuriben Parmar, Pooja Sridhar, Richard Collins, Sarah C. Lee, Zoe N. Stroud, Saskia E. Bakker, Stephen P. Muench, C. Howard Barton, Gregory Hurlbut, David I. Roper, Corinne J.I. Smith, Timothy J. Knowles, Corinne M. Spickett, J. Malcolm East, Vincent L.G. Postis, and Tim R. Dafforn. SMA-PAGE: A new method to examine complexes of membrane proteins using SMALP nanoencapsulation and native gel electrophoresis. *Biochimica et Biophysica Acta - Biomembranes*, 1861(8):1437–1445, 8 2019.

[147] Michael Overduin, Holger Wille, and David Westaway. Multisite interactions of prions with membranes and native nanodiscs. *Chemistry and Physics of Lipids*, 236, 5 2021.

[148] Sonali Gulati, Mohammed Jamshad, Timothy J. Knowles, Kerrie A. Morrison, Rebecca Downing, Natasha Cant, Richard Collins, Jan B. Koenderink, Robert C. Ford, Michael Overduin, Ian D. Kerr, Timothy R. Dafforn, and Alice J. Rothnie. Detergent-free purification of ABC (ATP-binding-cassette) transporters. *Biochemical Journal*, 461(2):269–278, 2014.

[149] Christel Logez, Marjorie Damian, Céline Legros, Clémence Dupré, Mélody Guéry, Sophie Mary, Renaud Wagner, Céline M'Kadmi, Olivier Nosjean, Benjamin Fould, Jacky Marie, Jean Alain Fehrentz, Jean Martinez, Gilles Ferry, Jean A. Boutin, and Jean Louis Baneìres. Detergent-free Isolation of Functional G Protein-Coupled Receptors into Nanometric Lipid Particles. *Biochemistry*, 55(1):38–48, 2016.

[150] Steven Lavington and Anthony Watts. Lipid nanoparticle technologies for the study of G protein-coupled receptors in lipid environments. *Biophysical Reviews*, 12(6):1287–1302, 2020.

[151] M. G. Karlova, N. Voskoboynikova, G. S. Gluhov, D. Abramochkin, O. A. Malak, A. Mulkidzhanyan, G. Loussouarn, H. J. Steinhoff, K. V. Shaitan, and O. S. Sokolova. Detergent-free solubilization of human Kv channels expressed in mammalian cells. *Chemistry and Physics of Lipids*, 219(January):50–57, 3 2019.

[152] Nate Yoder and Eric Gouaux. The his-gly motif of acid-sensing ion channels resides in a reentrant 'loop' implicated in gating and ion selectivity. *eLife*, 9:1–18, 6 2020.

[153] Abraham Olusegun Oluwole, Bartholomäus Danielczak, Annette Meister, Jonathan Oyebamiji Babalola, Carolyn Vargas, and Sandro Keller. Solubilization of Membrane Proteins into Functional Lipid-Bilayer Nanodiscs Using a Diisobutylene/Maleic Acid Copolymer. *Angewandte Chemie - International Edition*, 56(7):1919–1924, 2017.

[154] Kazuma Yasuhara, Jin Arakida, Thirupathi Ravula, Sudheer Kumar Ramadugu, Bikash Sahoo, Jun Ichi Kikuchi, and Ayyalusamy Ramamoorthy. Spontaneous Lipid Nanodisc Fomation by Amphiphilic Polymethacrylate Copolymers. *Journal of the American Chemical Society*, 139(51):18657–18663, 2017.

[155] Thirupathi Ravula, Nathaniel Z. Hardin, Sudheer Kumar Ramadugu, and Ayyalusamy Ramamoorthy. PH Tunable and Divalent Metal Ion Tolerant Polymer Lipid Nanodiscs. *Langmuir*, 33(40):10655–10662, 2017.

[156] Simon Lindhoud, Vanessa Carvalho, Joachim W. Pronk, and Marie Eve Aubin-Tam. SMA-SH: Modified Styrene-Maleic Acid Copolymer for Functionalization of Lipid Nanodiscs. *Biomacromolecules*, 17(4):1516–1522, 2016.

[157] Thirupathi Ravula, Nathaniel Z. Hardin, Giacomo M. Di Mauro, and Ayyalusamy Ramamoorthy. Styrene maleic acid derivates to enhance the applications of bio-inspired polymer based lipid-nanodiscs. *European Polymer Journal*, 108(September):597–602, 11 2018.

[158] Nathaniel Z. Hardin, Thirupathi Ravula, Giacomo Di Mauro, and Ayyalusamy Ramamoorthy. Hydrophobic Functionalization of Polyacrylic Acid as a Versatile Platform for the Development of Polymer Lipid Nanodisks. *Small*, 15(9), 3 2019.

[159] Stephen C.L. Hall, Cecilia Tognoloni, Jack Charlton, Éilís C. Bragginton, Alice J. Rothnie, Pooja Sridhar, Mark Wheatley, Timothy J. Knowles, Thomas Arnold, Karen J. Edler, and Tim R. Dafforn. An acid-compatible co-polymer for the solubilization of membranes and proteins into lipid bilayer-containing nanoparticles. *Nanoscale*, 10(22):10609–10619, 6 2018.

[160] Thirupathi Ravula, Nathaniel Z. Hardin, Sudheer Kumar Ramadugu, Sarah J. Cox, and Ayyalusamy Ramamoorthy. Formation of pH-Resistant Monodispersed Polymer–Lipid Nanodiscs. *Angewandte Chemie - International Edition*, 57(5):1342–1345, 1 2018.

[161] Anton A.A. Smith, Henriette E. Autzen, Bryan Faust, Joseph L. Mann, Benjamin W. Muir, Shaun Howard, Almar Postma, Andrew J. Spakowitz, Yifan Cheng, and Eric A. Appel. Lipid Nanodiscs via Ordered Copolymers. *Chem*, 6(10):2782–2795, 2020.

[162] Philipp S. Orekhov, Marine E. Bozdaganyan, Natalia Voskoboynikova, Armen Y. Mulkidjanian, Maria G. Karlova, Anna Yudenko, Alina Remeeva, Yury L. Ryzhykau, Ivan Gushchin, Valentin I. Gordeliy, Olga S. Sokolova, Heinz Jürgen Steinhoff, Mikhail P. Kirpichnikov, and Konstantin V. Shaitan. Mechanisms of Formation, Structure, and Dynamics of Lipoprotein Discs Stabilized by Amphiphilic Copolymers: A Comprehensive Review. *Nanomaterials*, 12(3), 2022.

[163] Giedre Ratkeviciute, Benjamin F. Cooper, and Timothy J. Knowles. Methods for the solubilisation of membrane proteins: The micelle-aneous world of membrane protein solubilisation. *Biochemical Society Transactions*, 49(4):1763–1777, 8 2021.

[164] Juan Francisco Bada Juarez, Andrew J. Harper, Peter J. Judge, Stephen R. Tonge, and Anthony Watts. From polymer chemistry to structural biology: The development of SMA and related amphipathic polymers for membrane protein extraction and solubilisation. *Chemistry and Physics of Lipids*, 221(October 2018):167–175, 7 2019.

[165] Mansoore Esmaili and Michael Overduin. Membrane biology visualized in nanometer-sized discs formed by styrene maleic acid polymers. *Biochimica et Biophysica Acta - Biomembranes*, 1860(2):257–263, 2018.

[166] Jonas M. Dörr, Stefan Scheidelaar, Martijn C. Koorengevel, Juan J. Dominguez, Marre Schäfer, Cornelis A. van Walree, and J. Antoinette Killian. The styrene–maleic acid copolymer: a versatile tool in membrane research. *European Biophysics Journal*, 45(1):3–21, 2016.

[167] Jana Broecker, Bryan T. Eger, and Oliver P. Ernst. Crystallogenesis of Membrane Proteins Mediated by Polymer-Bounded Lipid Nanodiscs. *Structure*, 25(2):384–392, 2017.

[168] Aiman A. Gulamhussein, Romez Uddin, Brian J. Tighe, David R. Poyner, and Alice J. Rothnie. A comparison of SMA (styrene maleic acid) and DIBMA (di-isobutylene maleic acid) for membrane protein purification. *Biochimica et Biophysica Acta - Biomembranes*, 1862(7):183281, 7 2020.

[169] Steven Lavington and Anthony Watts. Detergent-free solubilisation & purification of a G protein coupled receptor using a polymethacrylate polymer. *Biochimica et Biophysica Acta - Biomembranes*, 1863(1):183441, 2021.

[170] Max Bernhard and Bodo Laube. Thermophoretic analysis of ligand-specific conformational states of the inhibitory glycine receptor embedded in copolymer nanodiscs. *Scientific Reports*, 10(1), 12 2020.

[171] Juan Francisco Bada Juarez, Juan C. Muñoz-García, Rosana Inácio dos Reis, Alistair Henry, David McMillan, Marco Kriek, Martyn Wood, Catherine Vandenplas, Zara Sands, Luis Castro, Richard Taylor, and Anthony Watts. Detergent-free extraction of a functional low-expressing GPCR from a human cell line. *Biochimica et Biophysica Acta - Biomembranes*, 1862(3), 3 2020.

[172] Kin Kuan Hoi, Juan Francisco Bada Juarez, Peter J. Judge, Hsin Yung Yen, Di Wu, Javier Vinals, Garrick F. Taylor, Anthony Watts, and Carol V. Robinson. Detergent-free Lipodisq Nanoparticles Facilitate High-Resolution Mass Spectrometry of Folded Integral Membrane Proteins. *Nano Letters*, 21(7):2824–2831, 2021.

[173] Rachael L. Grime, Joelle Goulding, Romez Uddin, Leigh A. Stoddart, Stephen J. Hill, David R. Poyner, Stephen J. Briddon, and Mark Wheatley. Single molecule binding of a ligand to a G-protein-coupled receptor in real time using fluorescence correlation spectroscopy, rendered possible by nano-encapsulation in styrene maleic acid lipid particles. *Nanoscale*, 12(21):11518–11525, 6 2020.

[174] Wageiha Mosslehy, Natalia Voskoboynikova, Alexandr Colbasevici, Adrian Ricke, Daniel Klose, Johann P. Klare, Armen Y. Mulkidjanian, and Heinz Jürgen Steinhoff. Conformational Dynamics of Sensory Rhodopsin II in Nanolipoprotein and Styrene–Maleic Acid Lipid Particles. *Photochemistry and Photobiology*, 95(5):1195–1204, 9 2019.

[175] Natalia Voskoboynikova, Maria Karlova, Rainer Kurre, Armen Y. Mulkidjanian, Konstantin V. Shaitan, Olga S. Sokolova, Heinz Jürgen Steinhoff, and Jürgen J. Heinisch. A three-dimensional model of the yeast transmembrane sensor Wsc1 obtained by SMA-based detergent-free purification and transmission electron microscopy. *Journal of Fungi*, 7(2):1–17, 2 2021.

[176] Kaushik Sarkar, Lisa Joedicke, Marta Westwood, Rebecca Burnley, Michael Wright, David McMillan, and Bernadette Byrne. Modulation of PTH1R signaling by an ECD binding antibody results in inhibition of β-arrestin 2 coupling. *Scientific Reports*, 9(1), 12 2019.

[177] Nils Hellwig, Oliver Peetz, Zainab Ahdash, Igor Tascón, Paula J. Booth, Vedrana Mikusevic, Marina Diskowski, Argyris Politis, Yvonne Hellmich, Inga Hänelt, Eamonn Reading, and Nina Morgner. Native mass spectrometry goes more native: Investigation of membrane protein complexes directly from SMALPs. *Chemical Communications*, 54(97):13702–13705, 2018.

[178] Ya Nan Deng, Hamdy Kashtoh, Quan Wang, Guang Xiao Zhen, Qi Yu Li, Ling Hui Tang, Hai Long Gao, Chun Rui Zhang, Li Qin, Min Su, Fei Li, Xia He Huang, Ying Chun Wang, Qi Xie, Oliver B. Clarke, Wayne A. Hendrickson, and Yu Hang Chen. Structure and activity of SLAC1 channels for stomatal signaling in leaves. *Proceedings of the National Academy of Sciences of the United States of America*, 118(18):1–8, 2021.

[179] Chang Sun, Samir Benlekbir, Padmaja Venkatakrishnan, Yuhang Wang, Sangjin Hong, Jonathan Hosler, Emad Tajkhorshid, John L. Rubinstein, and Robert B. Gennis. Structure of the alternative complex III in a supercomplex with cytochrome oxidase. *Nature*, 557(7703):123–126, 5 2018.

[180] Hiroshi Maeda. SMANCS and polymer-conjugated macromolecular drugs: Advantages in cancer chemotherapy. *Advanced Drug Delivery Reviews*, 46(1-3):169–185, 2001.

[181] Weihua Qiu, Ziao Fu, Guoyan G. Xu, Robert A. Grassucci, Yan Zhang, Joachim Frank, Wayne A. Hendrickson, and Youzhong Guo. Structure and activity of lipid bilayer within a membrane-protein transporter. *Proceedings of the National Academy of Sciences*, 115(51):12985–12990, 12 2018.

[182] Vanessa Judith Flegler, Akiko Rasmussen, Shanlin Rao, Na Wu, Renato Zenobi, Mark S.P. Sansom, Rainer Hedrich, Tim Rasmussen, and Bettina Böttcher. The MscS-like channel YnaI has a gating mechanism based on flexible pore helices. *Proceedings of the National Academy of Sciences of the United States of America*, 117(46):28754–28762, 2020.

[183] H.J. Vogel. A Convenient Growth Medium for Neurospora crassa. *Microbial Genetics Bulletin*, 13:42–47, 1956.

[184] David Drew, Simon Newstead, Yo Sonoda, Hyun Kim, Gunnar von Heijne, and So Iwata. GFP-based optimization scheme for the overexpression and purification of eukaryotic membrane proteins in Saccharomyces cerevisiae. *Nature Protocols*, 3(5):784–798, 2008.

[185] Henry L D Sawczyc. *Biophysical Characterisation of Self-assembling Nanoparticles, PhD Thesis*. PhD thesis, University of Oxford, UK, 2020.

[186] E. S. Baginski, P. P. Foa, and B. Zak. Determination of phosphate: Study of labile organic phosphate interference. *Clinica Chimica Acta*, 15(1):155–158, 1 1967.

[187] Yongqing Yang, Lei Hu, Xuemei Chen, Eric A. Ottow, Andrea Polle, and Xiangning Jiang. A novel method to quantify H+-ATPase-dependent Na+ transport across plasma membrane vesicles. *Biochimica et Biophysica Acta - Biomembranes*, 1768(9):2078–2088, 2007.

[188] Sean R Gallagher and Robert T Leonard. Effect of vanadate, molybdate, and azide on membrane-associated ATPase and soluble phosphatase activities of corn roots. *Plant Physiology*, 70(5):1335–1340, 1982.

[189] K. Don D. Gunaratne, Grant E. Johnson, Amity Andersen, Dan Du, Weiying Zhang, Venkateshkumar Prabhakaran, Yuehe Lin, and Julia Laskin. Controlling the charge state and redox properties of supported polyoxometalates via soft landing of mass-selected ions. *Journal of Physical Chemistry C*, 118(48):27611–27622, 2014.

[190] E G Bligh and W J Dyer. A Rapid Method of Total Lipid Extraction and Purification. *Canadian Journal of Biochemistry and Physiology*, 37(8):911–917, 1959.

[191] Kasparas Petkevicius, Sam Virtue, Guillaume Bidault, Benjamin Jenkins, Cankut Cubuk, Cecilia Morgantini, Myriam Aouadi, Joaquin Dopazo, Mireille J. Serlie, Albert Koulman, and Antonio Vidal-Puig. Accelerated phosphatidylcholine turnover in macrophages promotes adipose tissue inflammation in obesity. *eLife*, 8:1–29, 2019.

[192] Valerie B. O'Donnell, Edward A. Dennis, Michael J.O. Wakelam, and Shankar Subramaniam. LIPID MAPS: Serving the next generation of lipid researchers with tools, resources, data, and training. *Science Signaling*, 12(563):4–7, 2019.

[193] Stefan Scheidelaar, Martijn C. Koorengevel, Cornelius A. van Walree, Juan J. Dominguez, Jonas M. Dörr, and J. Antoinette Killian. Effect of Polymer Composition and pH on Membrane Solubilization by Styrene-Maleic Acid Copolymers. *Biophysical Journal*, 111(9):1974–1986, 2016.

[194] Adrian H. Kopf, Jonas M. Dörr, Martijn C. Koorengevel, Federico Antoniciello, Helene Jahn, and J. Antoinette Killian. Factors influencing the solubilization of membrane proteins from Escherichia coli membranes by styrene–maleic acid copolymers. *Biochimica et Biophysica Acta - Biomembranes*, 1862(2), 2 2020.

[195] Rong Guo, Jacob Sumner, and Shuo Qian. Diisobutylene Maleic Acid Copolymer (DIBMA) Lipid Particle- A "Stealth" Membrane Mimetic for Neutron Scattering. *ACS Applied Bio Materials*, 4(6):4760–4768, 6 2021.

[196] Dov Lichtenberg, Hasna Ahyayauch, and Félix M. Goñi. The mechanism of detergent solubilization of lipid bilayers. *Biophysical Journal*, 105(2):289–299, 2013.

[197] Stefan Scheidelaar, Martijn C. Koorengevel, Juan Dominguez Pardo, Johannes D. Meeldijk, Eefjan Breukink, and J. Antoinette Killian. Molecular Model for the solubilization of membranes into nanodisks by styrene maleic acid copolymers. *Biophysical Journal*, 108(2):279–290, 2015.

[198] Bartholomäus Danielczak, Annette Meister, and Sandro Keller. Influence of Mg 2+ and Ca 2+ on nanodisc formation by diisobutylene/maleic acid (DIBMA) copolymer. *Chemistry and Physics of Lipids*, 221(March):30–38, 7 2019.

[199] Inge Bos, Kaitlyn M. Bland, Lijin Tian, Roberta Croce, Laurie K. Frankel, Herbert van Amerongen, Terry M. Bricker, and Emilie Wientjes. Multiple LHCII antennae can transfer energy efficiently to a single Photosystem I. *Biochimica et Biophysica Acta - Bioenergetics*, 1858(5):371–378, 2017.

[200] Marta Barniol-Xicota and Steven H.L. Verhelst. Stable and Functional Rhomboid Proteases in Lipid Nanodiscs by Using Diisobutylene/Maleic Acid Copolymers. *Journal of the American Chemical Society*, 140(44):14557–14561, 11 2018.

[201] Marta Barniol-Xicota and Steven H.L. Verhelst. Lipidomic and in-gel analysis of maleic acid co-polymer nanodiscs reveals differences in composition of solubilized membranes. *Communications Biology*, 4(1), 12 2021.

[202] Olivia P. Hawkins, Christine Parisa T. Jahromi, Aiman A. Gulamhussein, Stephanie Nestorow, Taranpreet Bahra, Christian Shelton, Quincy K. Owusu-Mensah, Naadiya Mohiddin, Hannah O'Rourke, Mariam Ajmal, Kara Byrnes, Madiha Khan, Nila N. Nahar, Arcella Lim, Cassandra Harris, Hannah Healy, Syeda W. Hasan, Asma Ahmed, Lora Evans, Afroditi Vaitsopoulou, Aneel Akram, Chris Williams, Johanna Binding, Rumandeep K. Thandi, Aswathy Joby, Ashley Guest, Mohammad Z. Tariq, Farah Rasool, Luke Cavanagh, Simran Kang, Biser Asparuhov, Aleksandr Jestin, Timothy R. Dafforn, John Simms, Roslyn M. Bill, Alan D. Goddard, and Alice J. Rothnie. Membrane protein extraction and purification using partially-esterified SMA polymers. *Biochimica et Biophysica Acta - Biomembranes*, 1863(12), 12 2021.

[203] Gabriel Antonio Sánchez, Daniel Eduardo Di Croce, Ana Clara Casadoumecq, Susana Beatriz Richard, and Delia Takara. Characterization of the sarcoplasmic reticulum Ca-ATPase from rabbit temporalis muscle. *Archives of Oral Biology*, 57(10):1429–1437, 2012.

[204] Arianna Rath, Mira Glibowicka, Vincent G. Nadeau, Gong Chen, and Charles M. Deber. Detergent binding explains anomalous SDS-PAGE migration of membrane proteins. *Proceedings of the National Academy of Sciences of the United States of America*, 106(6):1760–1765, 2 2009.

[205] Dermot Walls and Sinéad T. Loughran, editors. *Protein Chromatography - Methods and Protocols*. Springer, 2017.

[206] Rachael L. Grime, Richard T. Logan, Stephanie A. Nestorow, Pooja Sridhar, Patricia C. Edwards, Christopher G. Tate, Bert Klumperman, Tim R. Dafforn, David R. Poyner, Philip J. Reeves, and Mark Wheatley. Differences in SMA-like polymer architecture dictate the conformational changes exhibited by the membrane protein rhodopsin encapsulated in lipid nano-particles. *Nanoscale*, 13(31):13519–13528, 2021.

[207] Sophie J. Hesketh, David P. Klebl, Anna J. Higgins, Maren Thomsen, Isabelle B. Pickles, Frank Sobott, Asipu Sivaprasadarao, Vincent L.G. Postis, and Stephen P. Muench. Styrene maleic-acid lipid particles (SMALPs) into detergent or amphipols: An exchange protocol for membrane protein characterisation. *Biochimica et Biophysica Acta - Biomembranes*, 1862(5):183192, 2020.

[208] Kyong Hi Rhee, Gene A. Scarborough, and Richard Henderson. Domain movements of plasma membrane H+-ATPase: 3D structures of two states by electron cryo-microscopy. *EMBO Journal*, 21(14):3582–3589, 2002.

[209] Jonas M. Dörr, Martijn C. Koorengevel, Marre Schäfer, Alexander V. Prokofyev, Stefan Scheidelaar, Elwin A. W. van der Cruijsen, Timothy R. Dafforn, Marc Baldus, and J. Antoinette Killian. Detergent-free isolation, characterization, and functional reconstitution of a tetrameric K + channel: The power of native nanodiscs. *Proceedings of the National Academy of Sciences*, 111(52):18607–18612, 2014.

[210] Vincent Postis, Shaun Rawson, Jennifer K. Mitchell, Sarah C. Lee, Rosemary A. Parslow, Tim R. Dafforn, Stephen A. Baldwin, and Stephen P. Muench. The use of SMALPs as a novel membrane protein scaffold for structure study by negative stain electron microscopy. *Biochimica et Biophysica Acta - Biomembranes*, 1848(2):496–501, 2015.

[211] Christoph M. Ernst, Sebastian Kuhn, Christoph J. Slavetinsky, Bernhard Krismer, Simon Heilbronner, Cordula Gekeler, Dirk Kraus, Samuel Wagner, and Andreas Peschel. The lipid-modifying multiple peptide resistance factor is an oligomer consisting of distinct interacting synthase and flippase subunits. *mBio*, 6(1):1–9, 2015.

[212] Steven C. Wang, Pauldeen Davejan, Kevin J. Hendargo, Ida Javadi-Razaz, Amy Chou, Daniel C. Yee, Faezeh Ghazi, Katie Jing Kay Lam, Adam M. Conn, Assael Madrigal, Arturo Medrano-Soto, and Milton H. Saier. Expansion of the Major Facilitator Superfamily (MFS) to include novel transporters as well as transmembrane-acting enzymes. *Biochimica et Biophysica Acta - Biomembranes*, 1862(9):183277, 2020.

[213] Janna Nadine Hauser, Arnaud Kengmo Tchoupa, Susanne Zabel, Kay Nieselt, Christoph M Ernst, Christoph Josef Slavetinsky, and Andreas Peschel. Prokaryotic phospholipid translocation by ubiquitous PplT domain proteins. *bioRxiv*, page 2022.03.11.483950, 2022.

[214] Danfeng Song, Haizhan Jiao, and Zhenfeng Liu. Phospholipid translocation captured in a bifunctional membrane protein MprF. *Nature Communications*, 12(1):1–16, 2021.

[215] Maxwell M.G. Geurts. *Structural and functional characterisation of the fungal plasma membrane proton pump, Pma1, and related P-Type ATPases*. PhD thesis, University of Oxford, 2022.

[216] Angel Cid, Rosario Perona, and Ramón Serrano. Replacement of the promoter of the yeast plasma membrane ATPase gene by a galactose-dependent promoter and its physiological consequences. *Current Genetics*, 12(2):105–110, 1987.

[217] Michael Schlame, Mindong Ren, Yang Xu, Miriam L. Greenberg, and Ivan Haller. Molecular symmetry in mitochondrial cardiolipins. *Chemistry and Physics of Lipids*, 138(1-2):38–49, 2005.

[218] Sebastian Schuck, Masanori Honsho, Kim Ekroos, Andrej Shevchenko, and Kai Simons. Resistance of cell membranes to different detergents. *PNAS*, 100(10):5795–5800, 2003.

[219] Hayley J. Sharpe, Tim J. Stevens, and Sean Munro. A Comprehensive Comparison of Transmembrane Domains Reveals Organelle-Specific Properties. *Cell*, 142(1):158–169, 2010.

[220] Satoshi Uemura, Fumi Shishido, Motohiro Tani, Takahiro Mochizuki, Fumiyoshi Abe, and Jin Ichi Inokuchi. Loss of hydroxyl groups from the ceramide moiety can modify the lateral diffusion of membrane proteins in S. cerevisiae. *Journal of Lipid Research*, 55(7):1343–1356, 2014.

[221] Daniel Lingwood and Kai Simons. Lipid rafts as a membrane-organizing principle. *Science*, 327(5961):46–50, 2010.

[222] Christopher R. Gault, Lina M. Obeid, and Yusuf A. Hannun. An overview of sphingolipid metabolism: From synthesis to breakdown. *Advances in Experimental Medicine and Biology*, 688:1–23, 2010.

[223] Rodrigo Rollin-Pinheiro, Ashutosh Singh, Eliana Barreto-Bergter, and Maurizio Del Poeta. Sphingolipids as targets for treatment of fungal infections, 2016.

[224] Kyle McEvoy, Tyler G Normile, and Maurizio Del Poeta. Antifungal drug development: Targeting the fungal sphingolipid pathway, 2020.

[225] James E Galagan, Sarah E Calvo, Katherine A Borkovich, Eric U Selker, Nick O. Read, David Jaffe, William FitzHugh, Li Jun Ma, Serge Smirnov, Seth Purcell, Bushra Rehman, Timothy Elkins, Reinhard Engels, Shunguang Wang, Cydney B Nielsen, Jonathan Butler, Matthew Endrizzi, Dayong Qui, Peter Ianakiev, Deborah Bell-Pedersen, Mary Anne Nelson, Margaret Werner-Washburne, Claude P Selitrennikoff, John A Kinsey, Edward L Braun, Alex Zelter, Ulrich Schulte, Gregory O. Kothe, Gregory Jedd, Werner Mewes, Chuck Staben, Edward Marcotte, David Greenberg, Alice Roy, Karen Foley, Jerome Naylor, Nicole Stange-Thomann, Robert Barrett, Sante Gnerre, Michael Kamal, Manolis Kamvysselis, Evan Mauceli, Cord Bielke, Stephen Rudd, Dmitrij Frishman, Svetlana Krystofova, Carolyn Rasmussen, Robert L. Metzenberg, David D. Perkins, Scott Kroken, Carlo Cogoni, Giuseppe Macino, David Catcheside, Weixi Li, Robert J. Pratt, Stephen A. Osmani, Colin P.C. DeSouza, Louise Glass, Marc J. Orbach, J. Andrew Berglund, Rodger Voelker, Oded Yarden, Michael Plamann, Stephan Seiler, Jay Dunlap, Alan Radford, Rodolfo Aramayo, Donald O. Natvig, Lisa A. Alex, Gertrud Mannhaupt, Daniel J. Ebbole, Michael Freitag, Ian Paulsen, Matthew S. Sachs, Eric S. Lander, Chad Nusbaum, and Bruce Birren. The genome sequence of the filamentous fungus Neurospora crassa. *Nature*, 422(6934):859–868, 2003.

[226] Miao Xu, Ke Liu, Noel Southall, Juan J Marugan, Alan T. Remaley, and Wei Zheng. A high-throughput sphingomyelinase assay using natural substrate. In *Analytical and Bioanalytical Chemistry*, volume 404, pages 407–414, 2012.

[227] Nora S. Plesofsky, Steven B. Levery, Sherry A. Castle, and Robert Brambl. Stress-induced cell death is mediated by ceramide synthesis in Neurospora crassa. *Eukaryotic Cell*, 7(12):2147–2159, 2008.

[228] Naoya Takakuwa, Mikio Kinoshita, Yuji Oda, and Masao Ohnishi. Existence of cerebroside in Saccharomyces kluyveri and its related species. *FEMS Yeast Research*, 2(4):533–538, 2002.

[229] Jin Hwan Do, Tae Kyu Park, and Dong Kug Choi. A computational approach to the inference of sphingolipid pathways from the genome of Aspergillus fumigatus. *Current Genetics*, 48(2):134–141, 2005.

[230] Chaeho Park, Beau Bennion, Isabelle E.J.A. J. A. François, Kathelijne K.A. A. Ferket, Bruno P.A. A. Cammue, Karin Thevissen, and Steven B. Levery. Neutral glycolipids of the filamentous fungus Neurospora crassa : altered expression in plant defensin-resistant mutants. *Journal of Lipid Research*, 46(4):759–768, 2005.

[231] Karin Thevissen, Patricia De Mello Tavares, Deming Xu, Jill Blankenship, Davy Vandenbosch, Jolanta Idkowiak-Baldys, Gilmer Govaert, Anna Bink, Sonia Rozental, Piet W.J. De Groot, Talya R Davis, Carol A Kumamoto, Gabriele Vargas, Leonardo Nimrichter, Tom Coenye, Aaron Mitchell, Terry Roemer, Yusuf A Hannun, and Bruno P.A. Cammue. The plant defensin RsAFP2 induces cell wall stress, septin mislocalization and accumulation of ceramides in Candida albicans. *Molecular Microbiology*, 84(1):166–180, 2012.

[232] Daniela M. Maciel, Marcio L. Rodrigues, Robin Wait, Maria Helena S. Villas Boas, Cesar A Tischer, and Eliana Barreto-Bergter. Glycosphingolipids from Magnaporthe grisea cells: Expression of a ceramide dihexoside presenting phytosphingosine as the long-chain base. *Archives of Biochemistry and Biophysics*, 405(2):205–213, 2002.

[233] Marcos S. Toledo, Steven B. Levery, Anita H. Straus, Erika Suzuki, Michelle Momany, John Glushka, J. Michael Moulton, and Helio K. Takahashi. Characterization of sphingolipids from mycopathogens: Factors correlating with expression of 2-hydroxy fatty acyl (E)-Δ3-unsaturation in cerebrosides of Paracoccidioides brasiliensis and Aspergillus fumigatus. *Biochemistry*, 38(22):7294–7306, 1999.

[234] Chunmiao Jiang, Jinxin Ge, Bin He, and Bin Zeng. Glycosphingolipids in Filamentous Fungi: Biological Roles and Potential Applications in Cosmetics and Health Foods. *Frontiers in Microbiology*, 12(July):1–17, 2021.

[235] Satoshi Uemura, Akio Kihara, Jin Ichi Inokuchi, and Yasuyuki Igarashi. Csg1p and Newly Identified Csh1p Function in Mannosylinositol Phosphorylceramide Synthesis by Interacting with Csg2p. *Journal of Biological Chemistry*, 278(46):45049–45055, 2003.

[236] Mikiko Otsu, Moeko Toume, Yutaro Yamaguchi, and Motohiro Tani. Proper regulation of inositolphosphorylceramide levels is required for acquirement of low pH resistance in budding yeast. *Scientific Reports*, 10(1):1–20, 2020.

[237] Robert C. Dickson, Elzbieta E. Nagiec, Gerald B. Wells, M. Marek Nagiec, and Robert L. Lester. Synthesis of mannose-(inositol-P)2-ceramide, the major sphingolipid in Saccharomyces cerevisiae, requires the IPT1 (YDR072c) gene. *Journal of Biological Chemistry*, 272(47):29620–29625, 1997.

[238] Martina Leipelt, Dirk Warnecke, Ulrich Zähringer, Claudia Ott, Frank Müller, Bernhard Hube, and Ernst Heinz. Glucosylceramide Synthases, a Gene Family Responsible for the Biosynthesis of Glucosphingolipids in Animals, Plants, and Fungi. *Journal of Biological Chemistry*, 276(36):33621–33629, 2001.

[239] Bankala Krishnarjuna, Thirupathi Ravula, and Ayyalusamy Ramamoorthy. Detergent-free isolation of CYP450-reductase's FMN-binding domain in E. coli lipid-nanodiscs using a charge-free polymer. *Chemical Communications*, 58(31):4913–4916, 3 2022.

[240] Xingxuan He, Fei Chen, Shimon Gatt, and Edward H Schuchman. An enzymatic assay for quantifying sphingomyelin in tissues and plasma from humans and mice with Niemann-Pick disease. *Analytical Biochemistry*, 293(2):204–211, 2001.

[241] Jennifer L. Macdonald and Linda J. Pike. A simplified method for the preparation of detergent-free lipid rafts. *Journal of Lipid Research*, 46(5):1061–1067, 2005.

[242] Djurre H. De Jong, Gurpreet Singh, W. F.Drew Bennett, Clement Arnarez, Tsjerk A. Wassenaar, Lars V. Schäfer, Xavier Periole, D. Peter Tieleman, and Siewert J. Marrink. Improved parameters for the martini coarse-grained protein force field. *Journal of Chemical Theory and Computation*, 9(1):687–697, 2013.

[243] S.C. C. Kushwaha, M. Kates, J. K.G. Kramer, and R. E. Subden. Lipid Composition of Neurospora crassa. *Lipids*, 11(10):778–780, 1976.

[244] S. C. Hubbard and S. Brody. Glycerophospholipid variation in choline and inositol auxotrophs of Neurospora crassa. Internal compensation among zwitterionic and anionic species. *Journal of Biological Chemistry*, 250(18):7173–7181, 1975.

[245] Kenneth J. Friedman. Role of Lipids in the Neurospora crassa Membrane. I. Influence of Fatty Acid Composition on Membrane Lipid Phase Transitions. *The Journal of Membrane Biology*, 32(1):33–47, 1977.

[246] Stuart Brody. Altered Fatty Acid Distribution. *Journal of Bacteriology, American Society for Microbiology*, 104(2):780–786, 1970.

[247] Tsjerk A. Wassenaar, Helgi I. Ingólfsson, Rainer A. Böckmann, D. Peter Tieleman, and Siewert J. Marrink. Computational lipidomics with insane: A versatile tool for generating custom membranes for molecular simulations. *Journal of Chemical Theory and Computation*, 11(5):2144–2155, 2015.

Appendices

Appendix A

Appendix for polymer solubilisation of biological membranes

A.1 Formula deduction for calculation of relative protein solubilisation efficiency (E_{rel})

The formula used to calculate relative protein solubilisation efficieny E_{rel} of various biological membranes in Chapter 3 (Section 3.2 and 3.3) is derived below. As described in Section 2.2.3 the protein concentration of each sample is determined with colourimetric reaction of the BCA assay. The absorption value measured at 562 nm (A_{562nm}, A) depends therfore on the total protein concentration in each sample. The absorption of the supernatant (A_{super}) and the pellet samples (A_{pellet}) are measured. Furthermore, each 96-well plate contains a standard curve with known protein concentrations following the manufacturer's protocol.

1) Protein content of in the supernatant: To infer the solubilisation efficiency from the supernatant directly, the protein standard curve is linearly fitted. It is possible to relate the known protein content to the measured absorption value (A) via a linear fit, following formula A.1.

$$A = a \cdot c_{\mathrm{prot}} + b \tag{A.1}$$

with $prot$= protein content, a = slope of the linear fit and b intercept of the linear fit.

Using the values of the fit allows to calculate the unknown protein content of each sample:

$$c_{\mathrm{prot(super)}} = \frac{A_{\mathrm{super}} - b}{a} \tag{A.2}$$

with a - slope of the standard curve, b - intersection of the standard curve

2) Relative protein content: A relative protein content (rel.prot.conc.) between supernatant and pellet can be calculated, resulting in a relative solubilisation value. This relative protein content could either be calculated relative to an external sample, e.g. a membrane sample (2a) or an internal protein content evaluation (2b).

2a) Relative protein content of the supernatant in relation to an external total protein content (membrane): Firstly, the protein content of the supernatant can be put in relation to the protein content of a non-solubilised membrane sample ($c_{\mathrm{prot(membrane)}}$) as an indicator for the total protein content of the sample before solubilisation.

$$rel.c_{\mathrm{(membrane)}} = \frac{c_{\mathrm{prot(super)}}}{c_{\mathrm{prot(membrane)}}} = \frac{\frac{A_{\mathrm{super}} - b}{a}}{\frac{A_{\mathrm{membrane}} - b}{a}} \tag{A.3}$$

with a - slope of the standard curve, b - intersection of the standard curve

2b) Relative protein content of the supernatant related to an internal total protein content (sum of protein concentration supernatant and pellet):
Secondly, it is assumed that the initial protein concentration in the membrane per vial can be deduced from the sum of protein content ($c_{\mathrm{prot(sum)}}$) in supernatant ($c_{\mathrm{prot(super)}}$) and pellet ($c_{\mathrm{prot(pellet)}}$).

$$c_{\mathrm{prot(sum)}} = c_{\mathrm{prot(super)}} + c_{\mathrm{prot(pellet)}} \text{ with } c_{\mathrm{prot(sum)}} \sim c_{\mathrm{prot(membrane)}} \tag{A.4}$$

On this basis, the relative protein concentration per vial (per solubilised membrane sample) can be determined in relation to the sum of the protein content in the supernatant and the pellet ($c_{\mathrm{prot(super)}} + c_{\mathrm{prot(pellet)}}$).

$$rel.c_{(\text{pervial})} = \frac{c_{\text{prot(super)}}}{c_{\text{prot(sum)}}} = \frac{c_{\text{prot(super)}}}{c_{\text{prot(super)}} + c_{\text{prot(pellet)}}} = \frac{\frac{A_{\text{super}}-b}{a}}{\frac{A_{\text{super}}-b}{a} + \frac{A_{\text{pellet}}-b}{a}} \tag{A.5}$$

with a - slope of the standard curve, b - intersection of the standard curve

3) Relative solubilisation efficiency (E_{rel}) calculated via the Absorption values directly:

Thirdly, since the respective protein concentrations on each 96-well plate are calculated with the same standard curve and a linear fit, giving the slope a, formula A.5 can be reduced by slope a of the standard curve.

Additionally, the intersection of the standard curve (b) can be assumed to result from the background readout of the BCA assay, which can be determined by measuring a buffer-only sample ($A_{\text{buffer}} = b'$).

Combiniation of all these assumptions leads to the final calculation of the relative solubilisation efficiency (E_{rel}) based on the absorption values directly, corrected by the corresponding background readout of the BCA assay per 96-well plate (b').

$$\begin{aligned} E_{rel} &\approx \frac{c_{\text{prot(super)}}}{c_{\text{prot(super)}} + c_{\text{prot(pellet)}}} \\ &\approx \frac{A_{\text{super}} - b'}{A_{\text{super}} - b' + A_{\text{pellet}} - b'} = \frac{A_{\text{super}} - b'}{A_{\text{super}} + A_{\text{pellet}} - 2b'} \\ &= \frac{A_{\text{super}} - A_{\text{buffer}}}{A_{\text{super}} + A_{\text{pellet}} - 2 \cdot A_{\text{buffer}}} \end{aligned} \tag{A.6}$$

with b' the background readout of the BCA assay ($b' = A_{\text{buffer}}$).

The corresponding error σf^2 can be calculated by derivation of formula 6.

$$\begin{aligned} f = E_{rel} &= \frac{x - b'}{x + y - 2 \cdot b'} \\ \sigma_f^2 &= \left(\frac{\delta f}{\delta x}\right)^2 \cdot \sigma x^2 + \left(\frac{\delta f}{\delta y}\right)^2 \cdot \sigma y^2 + \left(\frac{\delta f}{\delta b'}\right)^2 \cdot \sigma b'^2 \\ \sigma_f^2 &= \left(\frac{y - b'}{x + y - 2b'^2}\right)^2 \cdot \sigma x^2 + \left(\frac{b - x'}{x + y - 2b'^2}\right)^2 \cdot \sigma y^2 + \left(\frac{x - y}{x + y - 2b'^2}\right)^2 \cdot \sigma b'^2 \end{aligned} \tag{A.7}$$

with $x = A_{\text{super}}$, $y = A_{\text{pellet}}$, $b' = A_{\text{buffer}}$ and their standard deviations from triplicate measurements $\sigma x = \sigma A_{\text{super}}$, $\sigma y = \sigma A_{\text{pellet}}$, $\sigma b' = \sigma A_{\text{buffer}}$.
The resulting standard deviation of E_{rel} (σE_{rel}) is $\sigma E_{rel} = \sqrt{\sigma_f^2}$.
All relative values are multiplied by 100 and presented in percentages.

A.2 Results estimation of relative protein solubilisation efficiency (E_{rel}) by total protein quantification

The following tables contain the results from small scale membrane solubilisation assay by total protein quantification in Chapter 3, Section 3.2 and 3.3. Table A.1 outlines the calculated E_{rel} values and Table A.2 the total protein concentration in the supernatant.

Furthermore example A_{562nm} values from the executed BCA assay on inital measurements of membrane solubilisation are presented in Fig A.1 for one 96-Well plate with its corresponding protein standard curve (BSA, provided by the manufacture).
As mentioned in Chapter 3 due to the Covid pandemic these experiments could not be executed several times and the lack of repeats should be taken into account when interpreting the presented results. For future experiments it would be advisable to work with membrane diluted enough to contain less than 2 mg/ml total protein to be well in the linear range of the BCA assay.

Table A.1: Relative protein solubilisation efficiency (E_{rel})

Organism		***N. crassa*** 4.6 ± 0.4 mg/ml total protein				***S. cerevisiae*** 1.8 ± 0.2 mg/ml total protein				***E. coli*** pH 7 2.5 ± 0.2 mg/ml total protein pH 8 1.8 ± 0.2 mg/ml total protein			
	PH	7		8		7		8		7		8	
	salt	100	500	100	500	100	500	100	500	100	500	100	500
Agent	Temp												
Buffer	4°C ON	-	-	-	-	4 (±2)	1 (±4)	4 (±2)	1 (±2)	16 (±2)	15 (±4)	20 (±2)	15 (±5)
	RT	-	-	-	-	3 (±2)	-1 (±3)	-5 (±5)	0 (±3)	18 (±2)	17 (±3)	21 (±3)	14 (±3)
	37°C	-	-	4 (±1)	-	3 (±3)	0 (±2)	-5 (±5)	-4 (±7)	5 (±5)	5 (±6)	15 (±2)	14 (±3)
DDM	4°C ON	-	-	-	-	21 (±2)	26 (±1)	22 (±2)	26 (±2)	61 (±4)	67 (±3)	66 (±3)	75 (±4)
	RT	-	-	-	-	17 (±3)	25 (±4)	20 (±2)	26 (±2)	60 (±3)	65 (±2)	71 (±2)	75 (±3)
	37°C	-	-	13 (±2)	-	15 (±2)	20 (±2)	15 (±3)	20 (±4)	55 (±5)	59 (±3)	64 (±3)	64 (±2)
SMA 2:1	4°C ON	-	-	-	-	28 (±3)	18 (±2)	29 (±1)	13 (±4)	48 (±5)	34 (±3)	52 (±4)	34 (±3)
	RT	-	-	-	-	28 (±2)	18 (±4)	27 (±2)	20 (±2)	54 (±3)	40 (±2)	57 (±1)	36 (±2)
	37°C	-	-	10 (±1)	-	37 (±1)	22 (±2)	30 (±2)	18 (±5)	50 (±5)	38 (±3)	59 (±3)	40 (±3)
SMA 3:1	4°C ON	-	-	-	-	23 (±3)	10 (±3)	31 (±2)	20 (±4)	48 (±5)	20 (±3)	52 (±4)	48 (±2)
	RT	-	-	-	-	25 (±1)	10 (±2)	36 (±2)	35 (±6)	49 (±3)	26 (±2)	55 (±3)	48 (±2)
	37°C	-	-	11 (±2)	-	26 (±2)	14 (±2)	37 (±3)	27 (±5)	50 (±4)	20 (±3)	56 (±3)	55 (±4)
DIBMA	4°C ON	-	-	-	-	15 (±3)	13 (±2)	25 (±6)	12 (±2)	27 (±4)	30 (±2)	51 (±2)	36 (±2)
	RT	-	-	-	-	17 (±2)	17 (±2)	26 (±3)	22 (±4)	29 (±3)	42 (±2)	56 (±2)	35 (±1)
	37°C	-	-	9 (±2)	-	24 (±2)	27 (±1)	38 (±1)	18 (±5)	27 (±4)	41 (±2)	59 (±4)	35 (±1)
PMA	4°C ON	-	-	-	-	35 (±1)	25 (±1)	38 (±1)	26 (±1)	29 (±3)	42 (±2)	29 (±4)	43 (±2)
	RT	-	-	-	-	40 (±1)	25 (±2)	39 (±1)	33 (±2)	29 (±3)	41 (±1)	31 (±2)	45 (±2)
	37°C	-	-	16 (±1)	15 (±0)	42 (±2)	25 (±1)	41 (±1)	25 (±3)	22 (±4)	35 (±2)	28 (±2)	42 (±1)
SDS	4°C ON	-	-	-	-	82 (±1)	91 (±1)	83 (±6)	86 (±4)	85 (±1)	83 (±1)	87 (±2)	90 (±2)
	RT	-	-	-	-	83 (±2)	83 (±2)	87 (±5)	88 (±5)	89 (±2)	79 (±2)	90 (±2)	83 (±2)
	37°C	-	-	-	-	82 (±3)	86 (±3)	89 (±5)	89 (±4)	89 (±2)	95 (±3)	91 (±2)	83 (±2)

Table A.2: Total protein concentration in supernatant ($c_{\mathrm{prot(super)}}$)

Organism		***N. crassa*** 4.6 ± 0.4 mg/ml total protein				***S. cerevisiae*** 1.8 ± 0.2 mg/ml total protein				***E. coli*** pH 7 2.5 ± 0.2 mg/ml total protein pH 8 1.8 ± 0.2 mg/ml total protein			
	PH	7		8		7		8		7		8	
	salt	100	500	100	500	100	500	100	500	100	500	100	500
Agent	Temp												
Buffer	4°C ON	-	-	-	-	0.00 (±0.01)	0.01 (±0.00)	-0.03 (±0.00)	0.02 (±0.00)	0.42 (±0.08)	0.31 (±0.10)	0.27 (±0.03)	0.19 (±0.06)
	RT	-	-	-	-	-0.03 (±0.01)	-0.01 (±0.00)	-0.06 (±0.00)	0.00 (±0.00)	0.45 (±0.05)	0.36 (±0.08)	0.34 (±0.02)	0.20 (±0.03)
	37°C	-	-	0.72 (±0.01)	-	-0.06 (±0.01)	0.00 (±0.01)	-0.06 (±0.00)	-0.06 (±0.02)	0.05 (±0.09)	0.07 (±0.08)	0.26 (±0.02)	0.21 (±0.04)
DDM	4°C ON	-	-	-	-	0.39 (±0.04)	0.58 (±0.01)	0.44 (±0.02)	0.59 (±0.02)	1.74 (±0.13)	1.75 (±0.03)	1.22 (±0.05)	1.16 (±0.03)
	RT	-	-	-	-	0.32 (±0.01)	0.61 (±0.01)	0.35 (±0.00)	0.50 (±0.01)	1.71 (±0.14)	1.66 (±0.06)	1.31 (±0.02)	1.30 (±0.06)
	37°C	-	-	1.12 (±0.04)	-	0.26 (±0.02)	0.39 (±0.04)	0.23 (±0.01)	0.38 (±0.07)	1.22 (±0.16)	1.24 (±0.03)	1.23 (±0.04)	1.15 (±0.01)
SMA 2:1	4°C ON	-	-	-	-	0.46 (±0.05)	0.31 (±0.02)	0.49 (±0.01)	0.28 (±0.01)	1.32 (±0.13)	0.74 (±0.08)	0.77 (±0.06)	0.47 (±0.05)
	RT	-	-	-	-	0.43 (±0.00)	0.33 (±0.01)	0.43 (±0.01)	0.29 (±0.02)	1.37 (±0.13)	0.90 (±0.07)	0.91 (±0.03)	0.60 (±0.04)
	37°C	-	-	0.99 (±0.03)	-	0.56 (±0.02)	0.40 (±0.03)	0.48 (±0.01)	0.31 (±0.09)	1.06 (±0.15)	0.72 (±0.05)	1.01 (±0.03)	0.67 (±0.05)
SMA 3:1	4°C ON	-	-	-	-	0.37 (±0.05)	0.14 (±0.01)	0.54 (±0.01)	0.39 (±0.01)	1.16 (±0.14)	0.41 (±0.06)	0.82 (±0.09)	0.72 (±0.04)
	RT	-	-	-	-	0.36 (±0.01)	0.19 (±0.00)	0.55 (±0.04)	0.44 (±0.02)	1.20 (±0.10)	0.55 (±0.04)	0.98 (±0.09)	0.88 (±0.03)
	37°C	-	-	1.01 (±0.06)	-	0.43 (±0.03)	0.24 (±0.04)	0.55 (±0.06)	0.51 (±0.08)	0.97 (±0.11)	0.37 (±0.05)	1.01 (±0.06)	0.98 (±0.04)
DIBMA	4°C ON	-	-	-	-	0.22 (±0.05)	0.24 (±0.02)	0.44 (±0.01)	0.23 (±0.00)	0.59 (±0.11)	0.70 (±0.06)	0.74 (±0.04)	0.42 (±0.02)
	RT	-	-	-	-	0.23 (±0.01)	0.33 (±0.01)	0.44 (±0.02)	0.28 (±0.02)	0.68 (±0.08)	1.05 (±0.02)	0.93 (±0.03)	0.63 (±0.01)
	37°C	-	-	0.88 (±0.08)	-	0.39 (±0.02)	0.50 (±0.02)	0.59 (±0.02)	0.28 (±0.05)	0.53 (±0.10)	0.86 (±0.06)	1.01 (±0.08)	0.70 (±0.04)
PMA	4°C ON	-	-	-	-	0.75 (±0.03)	0.60 (±0.01)	0.84 (±0.01)	0.56 (±0.01)	0.74 (±0.11)	1.14 (±0.04)	0.49 (±0.08)	0.80 (±0.02)
	RT	-	-	-	-	0.99 (±0.01)	0.58 (±0.02)	0.94 (±0.02)	0.56 (±0.01)	0.77 (±0.10)	1.04 (±0.05)	0.57 (±0.05)	0.99 (±0.03)
	37°C	-	-	1.35 (±0.08)	0.86 (±0.09)	1.04 (±0.03)	0.54 (±0.03)	1.00 (±0.02)	0.51 (±0.06)	0.48 (±0.12)	0.79 (±0.08)	0.62 (±0.04)	0.80 (±0.02)
SDS	4°C ON	-	-	-	-	1.90 (±0.05)	2.18 (±0.15)	1.45 (±0.13)	1.66 (±0.10)	2.27 (±0.05)	2.23 (±0.08)	1.43 (±0.15)	1.42 (±0.05)
	RT	-	-	-	-	1.76 (±0.13)	1.81 (±0.06)	1.55 (±0.14)	1.65 (±0.17)	2.05 (±0.10)	1.85 (±0.11)	1.70 (±0.07)	1.52 (±0.03)
	37°C	-	-	-	-	1.74 (±0.13)	1.77 (±0.10)	1.81 (±0.12)	1.74 (±0.14)	1.74 (±0.11)	1.53 (±0.03)	1.40 (±0.15)	1.37 (±0.04)

(a) 96-Well plate readout (A_{562nm}) (Example)

Raw Data (562)

	1	2	3	4	5	6	7	8	9	10	11	12
A	0.291	0.469	0.739	1.009	1.511	1.587	2.26	3.203	0.244	0.413	0.711	0.985
B	0.286	0.443	0.734	0.942	1.408	1.513	2.119	2.922	1.442	1.456	2.241	2.833
C	0.324	0.967	0.731	0.879	0.72	1.091	0.157	0.151	0.15	0.33	0.16	0.172
D	0.317	0.996	0.718	0.904	0.671	1.06	0.153	0.153	0.16	0.161	0.171	0.178
E	0.325	0.98	0.69	0.922	0.688	1.058	0.15	0.149	0.152	0.155	0.168	0.179
F	2.145	2.186	1.834	1.272	1.732	1.742	0.181	0.181	0.189	0.204	0.156	2.587
G	2.203	2.119	2.026	1.743	1.812	1.87	0.153	0.155	0.169	0.182	0.141	2.669
H	2.343	2.313	1.896	1.237	1.376	1.941	0.151	0.155	0.17	0.195	0.144	2.743

Sample Layout

	1	2	3	4	5	6	7	8	9	10	11	12
A	0.00	0.13	0.25	0.50	0.75	1.00	1.50	2.00	0.00	0.13	0.25	0.50
B	0.00	0.13	0.25	0.50	0.75	1.00	1.50	2.00	0.75	1.00	1.50	2.00
C	buffer super	DDM super	Sma 2:1 super	Sma 3:1 super	DIBMA super	PMA super	SDS super	-	Buffer	DDM	SMA 2:1	SMA 3:1
D	buffer super	DDM super	Sma 2:1 super	Sma 3:1 super	DIBMA super	PMA super	SDS super	-	Buffer	DDM	SMA 2:1	SMA 3:1
E	buffer super	DDM super	Sma 2:1 super	Sma 3:1 super	DIBMA super	PMA super	SDS super	-	Buffer	DDM	SMA 2:1	SMA 3:1
F	buffer pellet	DDM pellet	Sma 2:1 pellet	SMA 3:1 pellet	DIBMA pellet	PMA pellet	SDS pellet	-	DIBMA	PMA	SDS	membrane
G	buffer pellet	DDM pellet	Sma 2:1 pellet	SMA 3:1 pellet	DIBMA pellet	PMA pellet	SDS pellet	-	DIBMA	PMA	SDS	membrane
H	buffer pellet	DDM pellet	Sma 2:1 pellet	SMA 3:1 pellet	DIBMA pellet	PMA pellet	SDS pellet	-	DIBMA	PMA	SDS	membrane

(b) Protein standard curve (BSA) from BCA assay (Example)

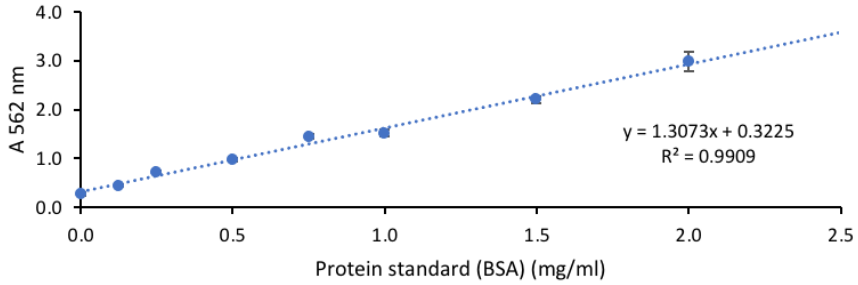

Figure A.1: Example results from 96-Well plate readout for small scale membrane solubilisation assay by total protein quantification, Chapter 3, Section 3.2 and 3.3. Example values for the BCA assay on solublised *S. cerevisiae* membrane at RT for 30 min, in 20 mM HEPES, 500 mM NaCl, pH 8 with various solubilisation agents. A_{562nm} values a) from the executed BCA assay are presented for one 96-Well plate (top: Raw data, bottom: sample layout (Fig 2.3) and b) its corresponding protein standard curve (BSA, provided by the manufacture).

A.3 SMA 3:1 solubilisation of *N. crassa* plasma membrane w/o DOC wash

N. crassa membrane solubilisation with SMA 3:1 was analysed for a modified plasma membrane preparation protocol, where the DOC wash was replaced by a high molar NaCl wash analogously to Section 3.3.

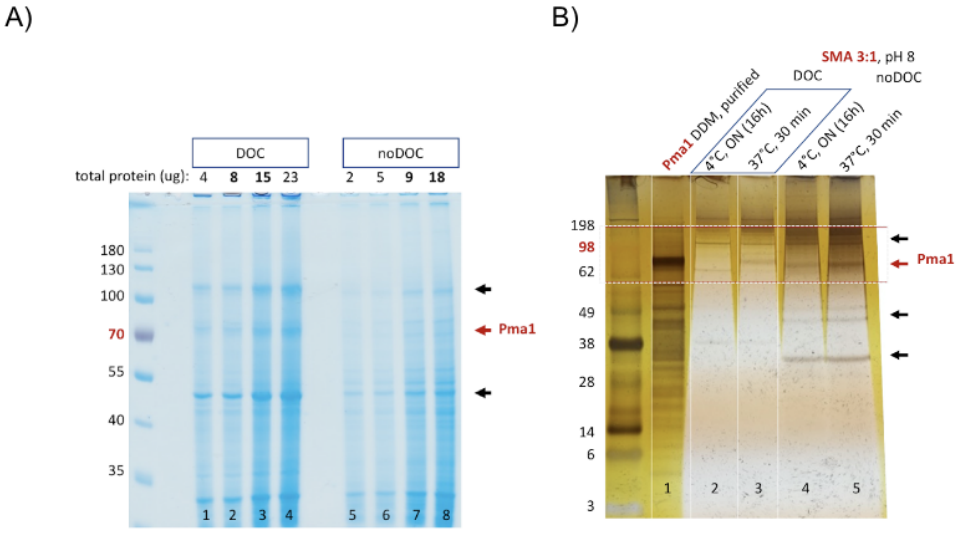

Figure A.2: SMA 3:1 Solubilisation of *N. crassa* plasma membrane samples, with and without a prior DOC washing step
A) SDS PAGE of *N. crassa* plasma membrane samples, coomassie stained. The regular *N. crassa* plasma membrane preparation includes a Deoxycholat (DOC) wash, this membrane was compared with a plasma membrane preparation where the DOC washing step was replaced with high molar NaCl washes (noDOC). B) SDS PAGE of SMA 3:1 solubilised *N. crassa* plasma membrane samples, silver stained. Solubilisation with 2.5 % SMA 3:1 was achieved at 20 mg/ml wet weight membrane (DOC yielding ~3.4 mg/ml total protein and noDOC ~3 mg/ml total protein). Highlighted are the target protein Pma1 (red arrow) and contaminants (black arrows). *N. crassa* membranes were kindly provided by Dr Sabine Heit.

The initial results judged by SDS PAGE (Fig A.2) show more prominent proteins bands and bands at the expected height of Pma1 for the NaCl washed membrane (noDOC), suggesting a higher solubilisation with SMA 3:1 in general when omitted the DOC wash, but also more contaminants seen at the band just below 38 kDa (maybe mitochondrial Complex I) suggesting a higher amount of non plasma membrane residues in the sample. The *N. crassa* membrane samples Fig A.2 A) indicate a higher relative Pma1 content in DOC membrane (red arrow) compared to plasma membrane without prior DOC treatment. The SDS page (Fig A.2 B) shows generally more prominent bands in the noDOC-membrane suggesting that SMA 3:1 solubilises this membrane better. Within this higher protein content, the Pma1 band is more prominent, indicating a higher yield of Pma1. Maybe DOC helps enriching Pma1 during Plasma membrane preparation by providing a cleaner separation of the plasma membrane from other remaining membranes, but might restrict solubilisation efficiency with polymers, due

to a potential depletion of easily soluble lipids.

A.4 Amino acid sequence of *N. crassa* Pma1

Amino acid sequence of *N. crassa* Pma1 (920 AA - 99.887 kDa), UniProt entry P07038, forms a hexamer $\sim$ 600 kDa

```
        10         20         30         40         50         60
MADHSASGAP ALSTNIESGK FDEKAAEAAA YQPKPKVEDD EDEDIDALIE DLESHDGHDA
        70         80         90        100        110        120
EEEEEEATPG GGRVVPEDML QTDTRVGLTS EEVVQRRRKY GLNQMKEEKE NHFLKFLGFF
       130        140        150        160        170        180
VGPIQFVMEG AAVLAAGLED WVDFGVICGL LLLNAVVGFV QEFQAGSIVD ELKKTLALKA
       190        200        210        220        230        240
VVLRDGTLKE IEAPEVVPGD ILQVEEGTII PADGRIVTDD AFLQVDQSAL TGESLAVDKH
       250        260        370        380        390        300
KGDQVFASSA VKRGEAFVVI TATGDNTFVG RAAALVNAAS GGSGHFTEVL NGIGTILLIL
       310        320        330        340        350        360
VIFTLLIVWV SSFYRSNPIV QILEFTLAIT IIGVPVGLPA VVTTTMAVGA AYLAKKKAIV
       370        380        390        400        410        420
QKLSAIESLA GVEILCSDKT GTLTKNKLSL HDPYTVAGVD PEDLMLTACL AASRKKKGID
       430        440        450        460        470        480
AIDKAFLKSL KYYPRAKSVL SKYKVLQFHP FDPVSKKVVA VVESPQGERI TCVKGAPLFV
       490        500        510        520        530        540
LKTVEEDHPI PEEVDQAYKN KVAEFATRGF RSLGVARKRG EGSWEILGIM PCMDPPRHDT
       550        560        570        580        590        600
YKTVCEAKTL GLSIKMLTGD AVGIARETSR QLGLGTNIYN AERLGLGGGG DMPGSEVYDF
       610        620        630        640        650        660
VEAADGFAEV FPQHKYNVVE ILQQRGYLVA MTGDGVNDAP SLKKADTGIA VEGSSDAARS
       670        680        690        700        710        720
AADIVFLAPG LGAIIDALKT SRQIFHRMYA YVVYRIALSI HLEIFLGLWI AILNRSLNIE
       730        740        750        760        770        780
LVVFIAIFAD VATLAIAYDN APYSQTPVKW NLPKLWGMSV LLGVVLAVGT WITVTTMYAQ
       790        800        810        820        830        840
GENGGIVQNF GNMDEVLFLQ ISLTENWLIF ITRANGPFWS SIPSWQLSGA IFLVDILATC
       850        860        870        880        890        900
FTIWGWFEHS DTSIVAVVRI WIFSFGIFCI MGGVYYILQD SVGFDNLMHG KSPKGNQKQR
       910        920
SLEDFVVSLQ RVSTQHEKSQ
```

A.5 Evaluation of methods to enhance visualisation of Pma1 solubilised by SMA 3:1 and other polymers

Due to the in Chapter 4 outlined difficulties to verify the presence of Pma1 in polymer particles, further ideas to optimise/enhance the characterisation of Pma1 particulary for immunostaining with anti-Pma1 AB were explored and and are presented following. Similar ideas could be further explored with other polymers to identify a suitable system for the native solubilisation of Pma1 from *N. crassa*.

Table A.3: Summary optimisation trials of immunostaining of Pma1
methods outlined were used to treat polymer solubilised *N. crassa* membranes and tried to optimise for Pma1 equivalent band in SDS PAGE or for signal of anti-Pma1 in immunoblotting trials.

Method	Fig	Note
Solubilisation with 2–5 % SDS and DTT	Fig A.3	no improvement; polymer remains in sample
PCA (perchloric acid) precipitation of protein	N/A	could be further tried in the future
Optimising immunostaining conditions (similar to Section 4.2.2)		
Immobilon® signal enhancer see Section 2.4.7	Fig A.4	Enhanced the westernblotting signal, but anti-Pma1 AB showed non-specific staining in presence of SMA and DIBMA
L-Arginin to shield polymer charge [146]	Fig A.4	reduced non-specific staining, but no signal of anti-Pma1 AB in the presence of polymers except for PMA
Ways to remove polymers and lipids from the sample		
precipitation of protein with $CH_3OH/CHCl_3/H_2O$ while removing polymers and lipids [153]	Fig A.4	unsuccessful; polymers were removed but loss of protein content; initally too low protein yield from polymer solubilisation
Exchanging protein into detergents and precipitation of SMA with Mg^{2+} [207]	Fig A.5	inital tries but probably require higher protein content in sample
TCA (trichloroacetic acid) precipitation	Fig A.5	inital tries unsucessful, but probably requires higher protein content in sample
Size exclusion chromatography for removal of free polymer	Fig A.5	SEC fractions show sharper signals, but only sin the presence of signal enhancer blotting solution
Westernblot: inital blotting for a few minutes and then changing the blotting paper [146]	N/A	could be potentially used to remove free polymer from the sample

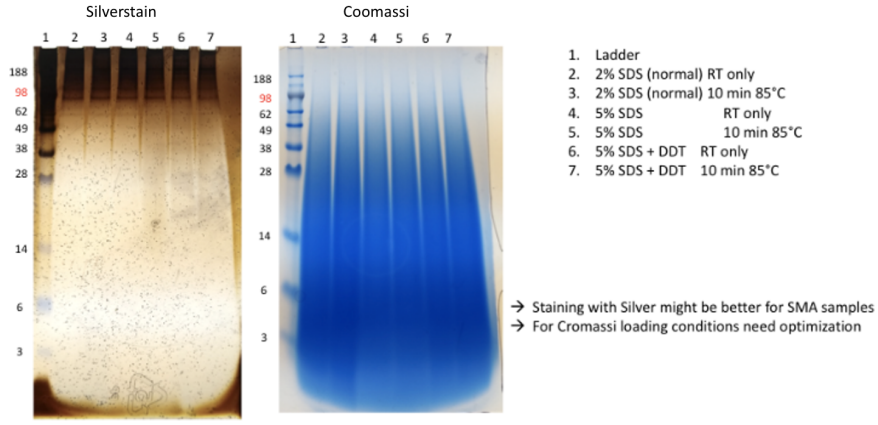

Figure A.3: Optimisation of staining/ Optimisation for loading conditions for SDS PAGE
SMA 3:1 solubilises *N. crassa* membrane samples preparation with SDS and DDT

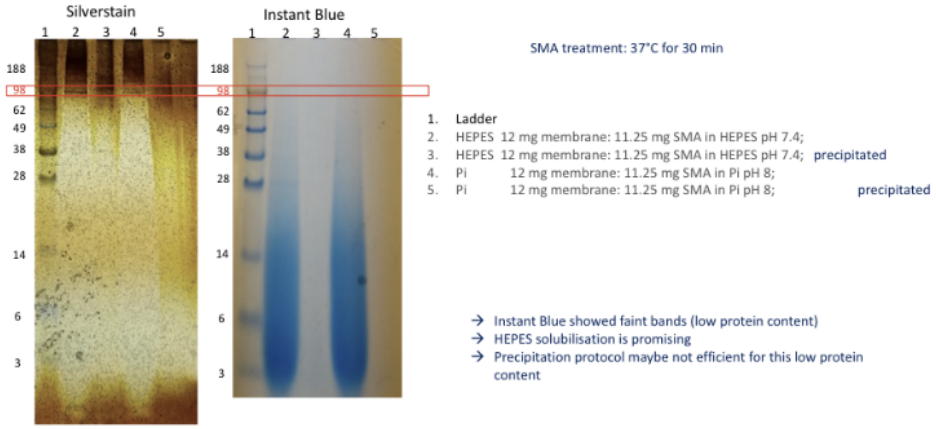

Figure A.4: Precipitation of protein: removal of lipids and polymers
Check the paragraph: Solubilization of native E. Coli membranes (page 6), near the end of the paragraph they explain how to do it. Precipitation of protein from SMA - lipid nanoparticle using $CH_3OH/CHCl_3/H_2O$ precipitated [153]

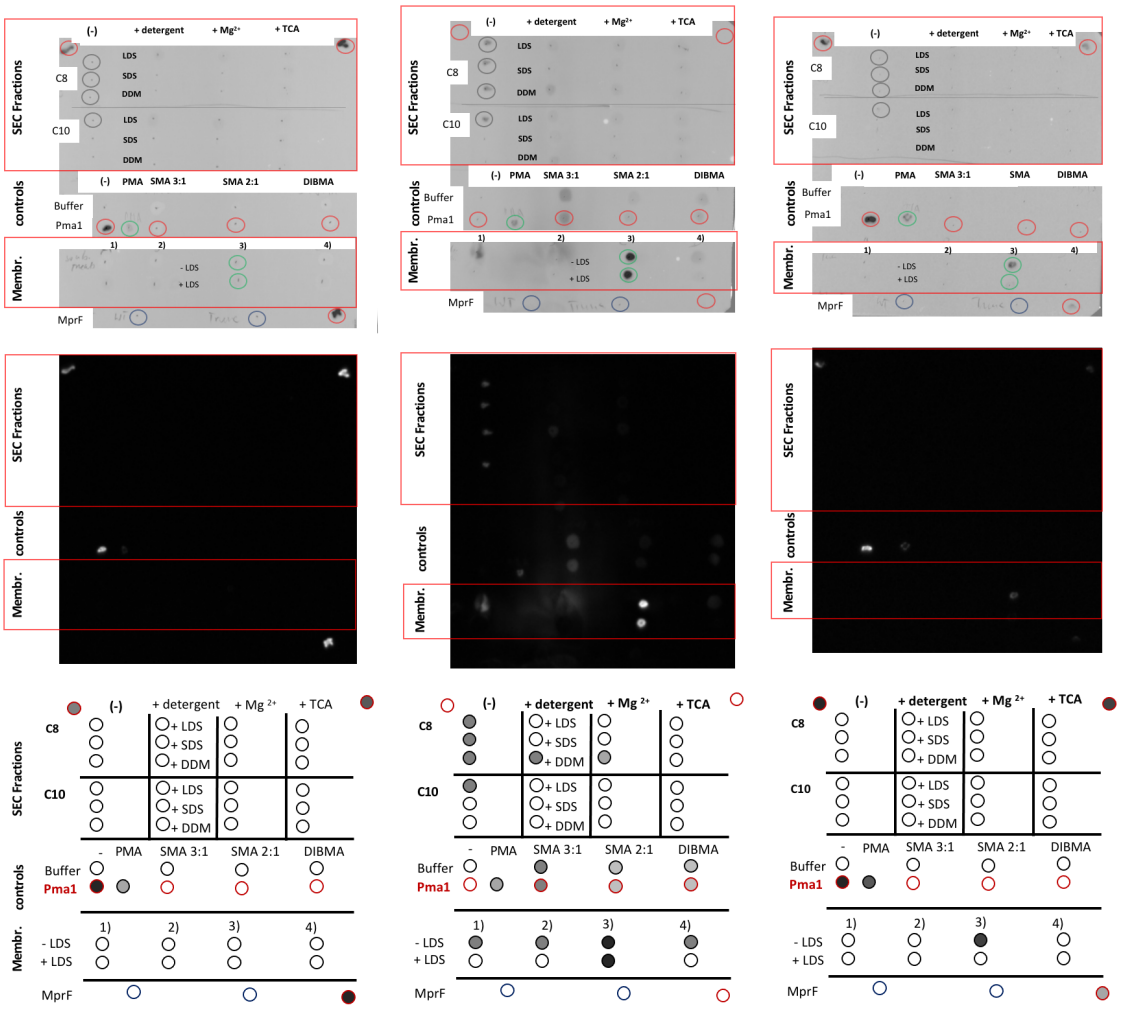

Figure A.5: Dotblots of different immunoblotting conditions analogously to 4.5 blotting conditions are outlined in Section2.4.7. Immunoblotting of Pma1 using an anti Pma1 antibody, developed in A) Immobilon Signal Enhancer (Merck) or B) skim milk powder and L-Arginine (to shield negatively charged polymer), with top: dot blot results, middle: raw image, bottom: schematic sample arrangement.
SEC fractions from Section 4.1 were stepwise treated: no treatment (-), then added detergent (either LDS, SDS or DDM), Mg^{2+} addition, TCA precipitation.
Control samples (DDM purified Pma1 protein (circled in red) and buffer 20 mM Hepes pH 8) were added with or without one of the polymers SMA 3:1, SMA 2:1, DIBMA or PMA.
Membranes (Membr.) samples were solubilised and are as following: 1) PM-NaCl (noDOC), SMA 3:1, 37°C, 2) PM, SMA 3:1 37°C, 3) PM, pH 7.5, 37°C, 4) PM, DIBMA , pH 7.5 37°C.
MprF protein was added as a negative controll.

A.6 Preliminary DLS measurements of SMA 3:1 particles from *N. crassa* membranes

Table A.4: Preliminary DLS measurements of SMA 3:1 particles from *N. crassa* membranes
Preliminary particle analysis of hydrodynamic diameter (DH) from dynamic light scattering (DLS) measurement on samples from SEC of SMA 3:1 solubilised *N. crassa* membrane (Section 4.1). Total concentration of protein and polymer was estimated by Nanodrop™spectrophotometer. Samples were filtered through a 0.22 µm filter before DLS measurement, n=1.

	% Area	*Rn(nm)*	*Sd.Dev*	*Notes*
SEC 3 B5 (1:10) 0.0625 mg/ml	87.0 %	0.11	0.01	Potentially empty SMA discs
	13 %	0.38	0.11	Potentially empty SMA discs
SEC 2 D1 (1:10) 0.125 mg/ml	17.2 %	6.45	1.23	Potentially protein containing SMA particles
	14.6 %	42.05	10.15	potentially lipids aggregates
	62.5 %	169.57	58.82	potentially lipids aggregates

Appendix B

Appendix for lipid analysis of *N. crassa* samples

B.1 Chapter 3 Appendix

Table B.1: Phospholipid lipid distribution *N. crassa* according to [64]
* only Serine measured; values in mol% of total phospholipids and rounded for clarity

		Diacylglycerophospholipids				
Growth	Source	PC	PE	PI/PS	PA	Cardio
WT 25°C WC	[243]	47	25	5*	21	3
WT (22) 34°C WC	[244]	43	23	14	3	7
WT WC	[63]	37	34	6 / 3	4	5
slime 31°C WC	[64]	45	36	11	4	4
slime 31°C PM	[64]	29	28	19	20	4

Table B.2: Lipids composition of *N. crassa* plasma membrane accordingly to [65], values in mol% of total plasma membrane lipids and rounded for clarity.

	37°C	15°C
Phospholipids	51	21
Free sterols	42	41
Glycosphingolipids	6	37

Table B.3: long chain base composition of glycosphingolipids of *N. crassa*

Growth	Phytosphingosine C18 C18 C4 OH	Spingosine C18 C18:1	Dihydrosphingosine C18	Sphinganine C19 C19	Spinganine C20 C20
PM slime 15°C [65]	8.3	19.6	41.6	10.7	19.7
PM slime 37°C [65]	2.8	34.5	43	11.2	8.5

Table B.4: Lipid distribution of *N. crassa* slime(according to [64] and [65]) * only Serine measured; ** refered to as sphingomyelin, (-) not measured (or reported); values in mol% of total plasma membrane lipids and rounded for clarity.

		Diacylglycerophospholipids					
Growth	Source	PC	PE	PI/PS	PA	**CL**	SL
slime 15°C WC	[65]	39	34	15	5	7	-
slime 31°C WC	[64]	45	36	11	4	5	-
slime 37°C WC	[65]	42	40	11	12	4	0**
slime 15°C PM	[65]	28	32	22	11	0	9**
slime 31°C PM	[64]	29	28	19	20	4	-
slime 37°C PM	[65]	25	54	6	8	0	4**

Table B.5: Reported fatty acid composition of phospholipid in *N. crassa* WT and slime, WC and PM, Reference * from [64], Table 1, ** from [64], Fig 1, *** cells were grown at 30°C (24h) and then transferred to 15 °C (another 24h)

Cell type	*N. crassa* slime strain (FGSC)	Reference	14:0	15:0	16:0	16:1	16:2	18:0	18:1	18:2	18:3
WC WT 15°C***	-	[124]	-	0	15.3	1.5	-	1.3	5.8	35.7	36.4
WC WT 22°C	-	[245] *	-	-	14	2.6	1.6	1.5	6.1	58.7	15.5
WC WT 30°C	-	[124]	-	1.6	20.3	2.3	-	1.8	18.8	46.8	7.5
WC WT 34°C	-	[246] *	-	-	24.4	-	-	4.5	11.9	45.4	13.5
WC slime 15°C***	#1118	[124]	-	0	12.9	2.5	-	1.5	6.3	33.2	40.8
WC slime 30°C	#1118	[124]	-	1.3	13.2	3.8	-	1.2	27.6	37.1	13.5
WC slime 31°C		[64] *	0.85	0.6	23.3	3.1	-	1.6	3.8	53.7	13.1
PM slime 15°C	#326	[65]	1.2	-	20	0.8	-	3.2	6.8	52.9	15.1
PM slime 31°C		[64] **	2	1	26	5	-	3	5	55	4
PM slime 37°C	#326	[65]	1	-	19.9	1.4	-	2.1	29.7	43.1	2.8

Table B.6: Calculated relative content of fatty acid composition of phospholipid in *N. crassa* WT and slime, WC and PMReference * from [64], Table 1, ** from [64], Fig 1, *** cells were grown at 30°C (24h) and then transferred to 15 °C (another 24h)

Cell type	*N. crassa* slime strain (FGSC)	Reference	% saturated	% unsaturated	% 16 C	% 18 C
WC WT 15°C***	-	[124]	16.6	79.4	16.8	79.2
WC WT 22°C	-	[245] *	15.5	84.5	18.2	81.8
WC WT 30°C	-	[124]	23.7	75.4	22.6	74.9
WC WT 34°C	-	[246] *	28.9	70.8	24.4	75.3
WC slime 15°C***	#1118	[124]	14.4	82.8	15.4	81.2
WC slime 30°C	#1118	[124]	15.7	82	17	79.4
WC slime 31°C		[64] *	28	76.5	28	74.5
PM slime 15°C	#326	[65]	24.4	75.6	20.8	78
PM slime 31°C		[64] **	32	69	31	67
PM slime 37°C	#326	[65]	23	77	21.3	77.7

Table B.7: Table overview of reported lipid species outlines the frequency and specifics of all reported lipid classes for all samples sent for analysis, see Table B.8.

Lipid class	number individually measured species	range of sum of carbon atoms (lipid chains)	range of double bonds	range hydroxyl groups
Lysophospholipids (LysoPL)				
LPC	20	12 - 22	0 - 6	
LPE	13	14 - 20	0 - 5	
LPS	11	16 - 24	0 - 5	
LPI	9	16 - 21	0 - 4	
Diacyl glycerophospholipids (DGPL)				
PC	36	30 - 40	0 - 6	
PS	19	32 - 40	0 - 6	
PE	17	30 - 38	0 - 6	
PI	16	32 - 40	0 - 5	
PG	16	32 - 42	0 - 7	
PA	15	30 - 40	0 - 5	
Cardiolipin (CardioL)				
CL	41	66 - 74	1 - 11	
Sphingolipids (SL)				
Cer	54	32 - 50	0 - 2	2 - 3
S	32	32 - 48	0 - 2	2 - 3
SM	24	30 - 48	0 - 3	0 - 1
MIP-Cer	14	42 - 50	0 - 0	1 - 3
IP-Cer	12	42 - 50	0 - 0	1 - 5
MDIP-Cer	3	46 - 50	0 - 0	1 - 1
Gang	2	39 - 39	0 - 1	
Glycerides (SF)				
TG	59	6-62	0 - 14	
DG	6	32 - 36	0 - 2	
MG	1	20 - 20	5 - 5	
Sterols				
Sterols,e.g. Ergosterol, have not been reported in this measurement				

Table B.8: LC/MS-Sample codes outlined in Section 2.5.1

'WC30'	*N. crassa* whole cell (WC) grown at 30°C
'WC35'	*N. crassa* WC grown at 35°C
'PM30'	*N. crassa* plasma membrane (PM) grown at 30°C (incl DOC A and B)
'PM-DOCA'	*N. crassa* PM, 30°C, DOC A
'PM30-DOCB'	*N. crassa* PM, 30°C, DOC B
'PM-NaCl'	*N. crassa* PM, 30°C w/o DOC, but high molar NaCl wash
'PM35'	*N. crassa* PM, 35°C
'PM-DDM'	Solubilised fraction of DOC A solubilised with 0.5 % DDM
'Pma130hex'	*N. crassa* Pma1 hexamer, grown at 30°C, glycerol gradient
'Pma130hex-suc'	*N. crassa* Pma1 hexamer, grown at 30°C, sucrose gradient
'Pma135hex'	*N. crassa* Pma1 hexamer, grown at 35°C, glycerol gradient, AEX
'Pma135lower'	*N. crassa* Pma1 lower oligomer, grown at 35°C, glycerol gradient, AEX
'ScWC30'	*S. cerevisiae* whole cell (WC) 30°C
'ScMembr30'	*S. cerevisiae* membrane preparation 30°C

Table B.9: All lipids - Distribution of lipid categories, sample codes outlined in Table B.8

	N. crassa												*S. cerevisiae*	
	WC		PM					DDM	Pma1				WC	membrane
	WC30 n=6	WC35 n=2	PM30 n=3	PM-DOCA n=2	PM-DOCB n=1	PM-NaCl n=1	PM35 n=2	PM-DDM n=1	Pma130hex n=1	Pma130hex-suc n=1	Pma135hex n=1	Pma135lower n=1	ScWC30 n=1	ScMembr30 n=1
	mean (std)	mean (std)	mean (std)	mean (std)	mean (std)	mean (std)	mean (std)	mean (std)	mean (std)	mean (std)	mean (std)	mean (std)	mean (std)	mean (std)
CardioL	26.39 (±3.03)	21.69 (±1.91)	20.32 (± 11.58)	23.84 (±13.92)	13.28 (-)	15.45 (-)	6.19 (±1.48)	26.77 (-)	13.63 (-)	2.22 (-)	24.53 (-)	34.33 (-)	10.56 (-)	6.0 (-)
DGPL	56.96 (±3.2)	58.03 (±2.74)	21.74 (±5.79)	22.59 (±7.93)	20.04 (-)	58.9 (-)	3.71 (±0.39)	26.63 (-)	41.01 (-)	0.77 (-)	25.02 (-)	36.07 (-)	31.56 (-)	49.9 (-)
LysoPL	1.18 (±0.15)	0.42 (±0.035)	0.14 (±0.065)	0.18 (±0.022)	0.07 (-)	0.72 (-)	0.035 (±0.004)	1.16 (-)	1.06 (-)	0.017 (-)	1.89 (-)	1.33 (-)	0.22 (-)	0.6 (-)
SF	14.15 (±1.2)	18.08 (±1.19)	52.93 (±8.29)	48.27 (±2.69)	62.25 (-)	23.36 (-)	89.45 (±1.99)	40.07 (-)	37.09 (-)	96.85 (-)	39.12 (-)	23.71 (-)	57.51 (-)	43.5 (-)
SL	1.32 (±0.21)	1.79 (±0.32)	4.87 (±2.37)	5.12 (±3.29)	4.37 (-)	1.57 (-)	0.61 (±0.11)	5.36 (-)	7.21 (-)	0.13 (-)	9.44 (-)	4.56 (-)	0.15 (-)	0.0 (-)

Table B.10: Membrane forming lipids - Distribution of lipid categories, sample codes outlined in Table B.8

	N. crassa												*S. cerevisiae*	
	WC		PM					DDM	Pma1				WC	membrane
	WC30 n=6	WC35 n=2	PM30 n=3	PM-DOCA n=2	PM-DOCB n=1	PM-NaCl n=1	PM35 n=2	PM-DDM n=1	Pma130hex n=1	Pma130hex-suc n=1	Pma135hex n=1	Pma135lower n=1	ScWC30 n=1	ScMembr30 n=1
	mean (std)	mean (std)	mean (std)	mean (std)	mean (std)	mean (std)	mean (std)	mean (std)	mean (std)	mean (std)	mean (std)	mean (std)	mean (std)	mean (std)
CardioL	30.74 (±3.52)	26.49 (±2.71)	42.03 (±18.35)	45.45 (±24.55)	35.18 (-)	20.16 (-)	58.38 (±3.06)	44.67 (-)	21.67 (-)	70.72 (-)	40.29 (-)	45.0 (-)	24.86 (-)	10.64 (-)
DGPL	66.34 (±3.53)	70.82 (±2.32)	47.11 (±13.49)	44.12 (±17.61)	53.08 (-)	76.85 (-)	35.49 (±3.01)	44.67 (-)	65.18 (-)	24.55 (-)	41.1 (-)	47.28 (-)	74.28 (-)	88.18 (-)
LysoPL	1.38 (±0.18)	0.51 (±0.035)	0.29 (±0.1)	0.34 (±0.061)	0.18 (-)	0.94 (-)	0.33 (±0.023)	1.94 (-)	1.69 (-)	0.54 (-)	3.1 (-)	1.74 (-)	0.51 (-)	1.13 (-)
SL	1.54 (±0.24)	2.18 (±0.36)	10.58 (±4.94)	10.08 (±6.88)	11.56 (-)	2.05 (-)	5.8 (±0.036)	8.94 (-)	11.45 (-)	4.19 (-)	15.51 (-)	5.98 (-)	0.34 (-)	0.04 (-)

Table B.11: Plasma membrane forming lipids - Distribution of lipid categories, sample codes outlined in Table B.8

	N. crassa												*S. cerevisiae*	
	WC		PM					DDM	Pma1				WC	membrane
	WC30 n=6	WC35 n=2	PM30 n=3	PM-DOCA n=2	PM-DOCB n=1	PM-NaCl n=1	PM35 n=2	PM-DDM n=1	Pma130hex n=1	Pma130hex-suc n=1	Pma135hex n=1	Pma135lower n=1	ScWC30 n=1	ScMembr30 n=1
	mean (std)	mean (std)	mean (std)	mean (std)	mean (std)	mean (std)	mean (std)	mean (std)	mean (std)	mean (std)	mean (std)	mean (std)	mean (std)	mean (std)
DGPL	95.78 (±0.42)	96.35 (±0.4)	81.91 (±3.24)	81.92 (±4.58)	81.89 (-)	96.26 (-)	85.24 (±0.95)	80.32 (-)	83.22 (-)	83.85 (-)	68.84 (-)	85.96 (-)	98.86 (-)	98.68 (-)
LysoPL	2 (±0.28)	0.69 (±0.022)	0.54 (±0.26)	0.67 (±0.19)	0.27 (-)	1.17 (-)	0.8 (±0.0037)	3.51 (-)	2.15 (-)	1.83 (-)	5.19 (-)	3.17 (-)	0.68 (-)	1.27 (-)
SL	2.22 (±0.36)	2.96 (±0.38)	17.55 (±3.38)	17.41 (±4.77)	17.84 (-)	2.57 (-)	13.96 (±0.94)	16.17 (-)	14.62 (-)	14.32 (-)	25.97 (-)	10.87 (-)	0.46 (-)	0.05 (-)

Table B.12: Diacylglycerophospholipids -Distribution of lipid classes, sample codes outlined in Table B.8

	N. crassa												*S. cerevisiae*	
	WC		PM					DDM	Pma1				WC	membrane
	WC30 n=6	WC35 n=2	PM30 n=3	PM-DOCA n=2	PM-DOCB n=1	PM-NaCl n=1	PM35 n=2	PM-DDM n=1	Pma130hex n=1	Pma130hex-suc n=1	Pma135hex n=1	Pma135lower n=1	ScWC30 n=1	ScMembr30 n=1
	mean (std)	mean (std)	mean (std)	mean (std)	mean (std)	mean (std)	mean (std)	mean (std)	mean (std)	mean (std)	mean (std)	mean (std)	mean (std)	mean (std)
total DGPL	56.96 (±3.2)	58.03 (±2.74)	21.74 (±5.79)	22.59 (±7.93)	20.04 (-)	58.9 (-)	3.71 (±0.39)	26.63 (-)	41.01 (-)	0.77 (-)	25.02 (-)	36.07 (-)	31.56 (-)	49.9 (-)
headgroup	mean (std)	mean (std)	mean (std)	mean (std)	mean (std)	mean (std)	mean (std)	mean (std)	mean (std)	mean (std)	mean (std)	mean (std)	mean (std)	mean (std)
PA	24.62 (±5.84)	36.1 (±8.17)	25.25 (±6.21)	28.03 (±5.54)	19.69 (-)	52.7 (-)	38.86 (±0.63)	21.93 (-)	11.18 (-)	10.57 (-)	22.51 (-)	27.68 (-)	20.29 (-)	12.73 (-)
PC	32.67 (±5.31)	25.51 (±5.04)	29.45 (±8.36)	34.03 (±3.78)	20.31 (-)	21.8 (-)	23.28 (±2.28)	36.60 (-)	35.69 (-)	71.69 (-)	44.68 (-)	44.77 (-)	44.33 (-)	42.02 (-)
PE	24.44 (±2.6)	16.48 (±1.04)	19.08 (±2.53)	20.54 (±0.003)	16.15 (-)	12.73 (-)	17.02 (±0.2)	23.81 (-)	29.71 (-)	6.98 (-)	15.97 (-)	16.69 (-)	15.55 (-)	19.01 (-)
PG	0.39 (±0.13)	0.18 (±0.027)	0.46 (±0.1)	0.51 (±0.074)	0.36 (-)	0.14 (-)	3.67 (±0.03)	0.61 (-)	6.08 (-)	0.13 (-)	0.92 (-)	1.24 (-)	0.2 (-)	0.11 (-)
PI	12.67 (±1.61)	14.97 (±1.51)	8.84 (±0.92)	9.13 (±1.1)	8.27 (-)	7.99 (-)	8.45 (±1.71)	10.05 (-)	12.25 (-)	8.25 (-)	11.57 (-)	5.48 (-)	9.52 (-)	22.38 (-)
PS	5.21 (±0.69)	6.76 (±0.55)	16.92 (±15.86)	7.77 (±0.58)	35.23 (-)	4.64 (-)	8.72 (±1.44)	7.01 (-)	5.09 (-)	2.38 (-)	4.34 (-)	4.14 (-)	10.11 (-)	3.75 (-)

Table B.13: Diacylglycerophospholipids - Distribution of chain length, sample codes outlined in Table B.8

	N. crassa												*S. cerevisiae*	
	WC		PM					DDM	Pma1				WC	membrane
	WC30 n=6	WC35 n=2	PM30 n=3	PM-DOCA n=2	PM-DOCB n=1	PM-NaCl n=1	PM35 n=2	PM-DDM n=1	Pma130hex n=1	Pma130hex-suc n=1	Pma135hex n=1	Pma135lower n=1	ScWC30 n=1	ScMembr30 n=1
number carbon atoms	mean (std)	mean (std)	mean (std)	mean (std)	mean (std)	mean (std)	mean (std)	mean (std)	mean (std)	mean (std)	mean (std)	mean (std)	mean (std)	mean (std)
30	0.04 (±0.005)	0.03 (±0.004)	0.15 (±0.02)	0.14 (±0.02)	0.16 (-)	0.04 (-)	0.11 (±0.02)	0.36 (-)	0.96 (-)	0.22 (-)	0.48 (-)	*0.21 (-)*	*1.32 (-)*	*1.00 (-)*
31	0.04 (±0.01)	0.05 (±0.01)	0.03 (±0.02)	0.02 (±0.0008)	0.05 (-)	0.01 (-)	0.16 (±0.007)	0.02 (-)	0 (-)	0 (-)	0.16 (-)	0.16 (-)	0 (-)	0.00 (-)
32	3.82 (±0.37)	4.05 (±0.12)	3.23 (±0.37)	3.03 (±0.15)	3.64 (-)	4.24 (-)	3.8 (±0.26)	5.09 (-)	16.6 (-)	7.25 (-)	8.85 (-)	4.76 (-)	26.92 (-)	20.22 (-)
33	2.74 (±0.35)	2.57 (±0.58)	1.52 (±0.53)	1.82 (±0.14)	0.92 (-)	1.88 (-)	1.44 (±0.15)	1.38 (-)	1.42 (-)	0.63 (-)	1.77 (-)	2.64 (-)	0.6 (-)	0.51 (-)
34	55.99 (±1.08)	55.01 (±0.9)	49.51 (±3.2)	51.31 (±0.94)	45.9 (-)	54.88 (-)	42.82 (±0.97)	56.01 (-)	57.26 (-)	44.5 (-)	59.76 (-)	52.79 (-)	61.69 (-)	62.26 (-)
35	2.21 (±0.16)	2.79 (±0.09)	2.26 (±1)	2.84 (±0.09)	1.1 (-)	2.03 (-)	1.34 (±0.03)	1.77 (-)	1.62 (-)	0.56 (-)	0.96 (-)	1.37 (-)	0.17 (-)	0.23 (-)
36	33.99 (±1.24)	34.47 (±0.04)	42.06 (±4.18)	39.66 (±0.58)	46.86 (-)	36.16 (-)	49.48 (±0.63)	34.68 (-)	21.78 (-)	46.02 (-)	27.47 (-)	37.36 (-)	9.08 (-)	15.60 (-)
37	0.059 (±0.008)	0.11 (±0.02)	0.11 (±0.09)	0.16 (±0.01)	0.01 (-)	0.05 (-)	0.03 (±0.001)	0.07 (-)	0.003 (-)	0.01 (-)	0.006 (-)	0.02 (-)	0.001 (-)	0.00 (-)
38	0.7 (±0.08)	0.79 (±0.1)	0.96 (±0.17)	0.88 (±0.13)	1.13 (-)	0.65 (-)	0.65 (±0.04)	0.57 (-)	0.34 (-)	0.75 (-)	0.38 (-)	0.59 (-)	0.17 (-)	0.18 (-)
40	0.096 (±0.02)	0.08 (±0.0003)	0.1 (±0.08)	0.06 (±0.001)	0.2 (-)	0.07 (-)	0.17 (±0.008)	0.01 (-)	0.006 (-)	0.02 (-)	0.12 (-)	0.08 (-)	0.04 (-)	0.01 (-)
42	0.31 (±0.11	0.05 (±0.02	0.06 (±0.04	0.08 (±0.02	0.02 (-)	0.001 (-)	0.007 (±0.001	0.04 (-)	0.02 (-)	0.02 (-)	0.04 (-)	0.01 (-)	0.0005 (-)	0.00 (-)

Table B.14: Diacylglycerophospholipids - Distribution of double bonds, sample codes outlined in Table B.8

	N. crassa												*S. cerevisiae*	
	WC		PM					DDM	Pma1				WC	membrane
	WC30 n=6	WC35 n=2	PM30 n=3	PM-DOCA n=2	PM-DOCB n=1	PM-NaCl n=1	PM35 n=2	PM-DDM n=1	Pma130hex n=1	Pma130hex-suc n=1	Pma135hex n=1	Pma135lower n=1	ScWC30 n=1	ScMembr30 n=1
number double bonds	mean (std)	mean (std)	mean (std)	mean (std)	mean (std)	mean (std)	mean (std)	mean (std)	mean (std)	mean (std)	mean (std)	mean (std)	mean (std)	mean (std)
0	3.3 (±0.35)	2.1 (±0.2)	13.7 (±16.11)	4.4 (±0.12)	32.3 (-)	3.82 (-)	7.3 (±0.32)	3.65 (-)	5.77 (-)	1.53 (-)	5.37 (-)	2.9 (-)	0.32 (-)	0.14 (-)
1	4.69 (±0.24)	5.01 (±0.41)	6.78 (±0.65)	7.12 (±0.41)	6.1 (-)	6.62 (-)	8.04 (±0.54)	14.48 (-)	41.03 (-)	19.5 (-)	30.01 (-)	30.94 (-)	57.95 (-)	44.11 (-)
2	55.29 (±0.49)	55.9 (±0.22)	48.45 (±6.25)	52.04 (±0.83)	41.3 (-)	50.41 (-)	54.35 (±0.54)	52.23 (-)	42.81 (-)	40.65 (-)	48.87 (-)	38.59 (-)	41.47 (-)	55.46 (-)
3	11.65 (±0.62)	9.78 (±0.09)	8.17 (±1.09)	8.79 (±0.2)	6.9 (-)	14.41 (-)	7.54 (±0.25)	6.23 (-)	1.98 (-)	9.39 (-)	4.63 (-)	10.14 (-)	0.1 (-)	0.24 (-)
4	24.66 (±0.69)	27.11 (±0.51)	22.63 (±8.13)	27.32 (±0.45)	13.2 (-)	24.71 (-)	22.59 (±0.06)	23.08 (-)	8.33 (-)	28.43 (-)	10.86 (-)	17.15 (-)	0.15 (-)	0.06 (-)
5	0.05 (±0.02)	0.033 (±0.007)	0.05 (±0.02)	0.06 (±0.02)	0.0 (-)	0.02 (-)	0.07 (±0.01)	0.08 (-)	0.06 (-)	0.08 (-)	0.13 (-)	0.09 (-)	0.02 (-)	0.00 (-)
6	0.06 (±0.02)	0.02 (±0.001)	0.16 (±0.051)	0.19 (±0.01)	0.1 (-)	0.014 (-)	0.1 (±0.005)	0.20 (-)	0.005 (-)	0.4 (-)	0.09 (-)	0.17 (-)	0.0005 (-)	0.00 (-)
7	0.3 (±0.11)	0.05 (±0.02)	0.06 (±0.04)	0.08 (±0.02)	0.0 (-)	0.001 (-)	0.007 (±0.001)	0.04 (-)	0.01 (-)	0.02 (-)	0.04 (-)	0.01 (-)	0 (-)	0.00 (-)

Table B.15: Diacylglycerophospholipids - Distribution of individual lipid species, sample codes outlined in Table B.8

	N. crassa												*S. cerevisiae*	
	WC		PM					DDM	Pma1				WC	membrane
	WC30 n=6	WC35 n=2	PM30 n=3	PM-DOCA n=2	PM-DOCB n=1	PM-NaCl n=1	PM35 n=2	PM-DDM n=1	Pma130hex n=1	Pma130hex-suc n=1	Pma135hex n=1	Pma135lower n=1	ScWC30 n=1	ScMembr30 n=1
number carbon atoms	mean (std)	mean (std)	mean (std)	mean (std)	mean (std)	mean (std)	mean (std)	mean (std)	mean (std)	mean (std)	mean (std)	mean (std)	mean (std)	mean (std)
PA 30:0	<0.01 (<0.001)	<0.01 (±0.00)	0 (±0)	0 (±0)	0 (-)	<0.01 (-)	0.02 (±0.006)	0 (-)	0 (-)	0 (-)	0.02 (-)	0.05 (-)	0 (-)	0 (-)
PA 32:0	0.02 (±0.01)	0.04 (±0.02)	0.06 (±0.03)	0.07 (±0.03)	0.04 (-)	0.04 (-)	0.41 (±0.12)	0 (-)	0 (-)	0 (-)	0.33 (-)	0.21 (-)	0 (-)	0 (-)
PA 32:1	0.18 (±0.05)	0.33 (±0.09)	0.16 (±0.07)	0.20 (±0.04)	0.08 (-)	0.49 (-)	0.21 (±0.02)	0.24 (-)	0.24 (-)	0.23 (-)	0.56 (-)	0.73 (-)	2.64 (-)	1.23 (-)
PA 32:2	0.90 (±0.31)	1.28 (±0.27)	0.41 (±0.03)	0.40 (±0.03)	0.44 (-)	2.07 (-)	0.50 (<0.001)	0.28 (-)	0.09 (-)	0.22 (-)	0.20 (-)	0.28 (-)	2.96 (-)	1.89 (-)
PA 33:1	0.05 (±0.03)	0.15 (±0.10)	0.11 (±0.10)	0.16 (±0.04)	0 (-)	0.32 (-)	0.19 (±0.002)	0.04 (-)	0.84 (-)	0 (-)	0.86 (-)	1.47 (-)	0 (-)	0 (-)
PA 34:1	0.48 (±0.07)	0.61 (±0.11)	0.95 (±0.25)	1.06 (±0.20)	0.71 (-)	1.67 (-)	0.86 (±0.06)	0.98 (-)	0.91 (-)	1.68 (-)	5.66 (-)	7.82 (-)	9.68 (-)	3.93 (-)
PA 34:2	11.25 (±2.31)	15.09 (±4.43)	11.87 (±2.86)	13.22 (±2.34)	9.18 (-)	22.95 (-)	15.29 (±0.59)	11.55 (-)	5.65 (-)	3.85 (-)	8.79 (-)	8.18 (-)	4.65 (-)	5.17 (-)
PA 34:3	3.47 (±1.10)	2.95 (±0.36)	2.06 (±0.66)	1.70 (±0.31)	2.77 (-)	6.48 (-)	2.41 (±0.01)	1.18 (-)	0.44 (-)	0.20 (-)	0.64 (-)	0.61 (-)	0 (-)	0 (-)
PA 35:1	0.03 (±0.01)	0.06 (±0.02)	0.06 (±0.06)	0.10 (±0.03)	0 (-)	0.08 (-)	0.02 (±0.002)	0.01 (-)	0.02 (-)	<0.01 (-)	0.18 (-)	0.33 (-)	0.03 (-)	0.02 (-)
PA 35:2	0.50 (±0.09)	0.75 (±0.17)	0.60 (±0.47)	0.86 (±0.15)	0.07 (-)	0.96 (-)	0.45 (±0.005)	0.40 (-)	0.14 (-)	0.19 (-)	0.20 (-)	0.40 (-)	0 (-)	0 (-)
PA 36:2	0.38 (±0.03)	0.31 (±0.07)	0.50 (±0.46)	0.75 (±0.23)	0 (-)	0.96 (-)	1.65 (±0.004)	0.46 (-)	0.40 (-)	0.57 (-)	1.05 (-)	1.66 (-)	0.32 (-)	0.36 (-)
PA 36:3	0.51 (±0.10)	1.13 (±0.33)	1.04 (±0.66)	1.40 (±0.29)	0.32 (-)	2.21 (-)	1.24 (±0.1)	0.69 (-)	0.13 (-)	0.50 (-)	1.12 (-)	2.30 (-)	0.02 (-)	0.14 (-)
PA 36:4	6.84 (±1.76)	13.39 (±2.21)	7.42 (±1.77)	8.09 (±1.87)	6.07 (-)	14.46 (-)	15.59 (±0.25)	6.10 (-)	2.22 (-)	3.12 (-)	2.89 (-)	3.63 (-)	0 (-)	0 (-)
PA 38:4	<0.01 (±0.00)	0.01 (<0.001)	0.01 (±0.01)	0.02 (±0.00)	0 (-)	0.02 (-)	<0.01 (±0.004)	0 (-)	0.10 (-)	0 (-)	0 (-)	0 (-)	0 (-)	0 (-)
PA 40:5	<0.01 (-)	0 (-)	0 (-)	0 (-)	0 (-)	<0.01 (-)	0 (-)	0 (-)	0 (-)	0 (-)	0 (-)	0 (-)	0 (-)	0 (-)
PC 30:0	0.01 (-)	<0.01 (-)	0.02 (±0.01)	0.02 (±0.01)	0.02 (-)	<0.01 (-)	0.02 (±0.004)	0.03 (-)	0.02 (-)	0 (-)	0.04 (-)	0.04 (-)	0.08 (-)	0.02 (-)

Continued on next page

Table B.15 – continued from previous page

	N. crassa												*S. cerevisiae*	
	WC		PM					DDM	Pma1				WC	membrane
	WC30 n=6	WC35 n=2	PM30A n=3	PM301 n=2	PM30DOC n=1	PM30NaCl n=1	PM35 n=2	PM30DDM n=1	Pma130glyc n=1	Pma130suc n=1	Pma135Pool1 n=1	Pma135Pool3 n=1	ScWC30 n=1	ScMembr30 n=1
number carbon atoms	mean (std)	mean (std)	mean (std)	mean (std)	mean (std)	mean (std)	mean (std)	mean (std)	mean (std)	mean (std)	mean (std)	mean (std)	mean (std)	mean (std)
PC 30:1	0.02 (±0.00)	0.02 (±0.01)	0.11 (±0.01)	0.11 (±0.02)	0.11 (-)	0.02 (-)	0.06 (±0.01)	0.34 (-)	0.43 (-)	0.22 (-)	0.42 (-)	0.12 (-)	1.25 (-)	0.98 (-)
PC 31:0	0.04 (±0.01)	0.04 (±0.01)	0.03 (±0.02)	0.02 (<0.001)	0.06 (-)	0.01 (-)	0.16 (±0.01)	0.02 (-)	0 (-)	0 (-)	0.16 (-)	0.16 (-)	0 (-)	0 (-)
PC 32:0	0.17 (±0.02)	0.22 (±0.04)	0.25 (±0.12)	0.18 (±0.02)	0.39 (-)	0.07 (-)	0.97 (±0.01)	0.20 (-)	0.17 (-)	0.87 (-)	1.10 (-)	0.55 (-)	0.08 (-)	0.02 (-)
PC 32:1	0.66 (±0.04)	0.64 (±0.16)	0.35 (±0.04)	0.35 (±0.06)	0.36 (-)	0.54 (-)	0.24 (±0.03)	1.25 (-)	2.99 (-)	2.20 (-)	1.61 (-)	0.58 (-)	8.91 (-)	3.97 (-)
PC 32:2	1.48 (±0.07)	1.15 (±0.23)	1.13 (±0.13)	1.08 (±0.14)	1.22 (-)	0.80 (-)	0.69 (±0.08)	2.00 (-)	4.41 (-)	3.01 (-)	3.54 (-)	1.15 (-)	7.84 (-)	10.88 (-)
PC 33:0	0.02 (±0.00)	0.04 (±0.01)	0.04 (±0.02)	0.02 (±0.00)	0.06 (-)	<0.01 (-)	0.18 (±0.02)	0.02 (-)	0 (-)	0.02 (-)	0.15 (-)	0.08 (-)	<0.01 (-)	<0.01 (-)
PC 33:1	0.22 (±0.02)	0.26 (±0.03)	0.26 (±0.10)	0.31 (±0.02)	0.14 (-)	0.28 (-)	0.14 (±0.02)	0.20 (-)	0.05 (-)	0.03 (-)	0.12 (-)	0.35 (-)	0.24 (-)	0.15 (-)
PC 33:2	2.45 (±0.33)	2.07 (±0.64)	1.11 (±0.37)	1.32 (±0.15)	0.71 (-)	1.27 (-)	0.87 (±0.11)	1.12 (-)	0.49 (-)	0.57 (-)	0.60 (-)	0.34 (-)	0.15 (-)	0.27 (-)
PC 34:0	0.03 (±0.00)	0.04 (±0.01)	0.05 (±0.02)	0.04 (±0.01)	0.07 (-)	0.01 (-)	0.23 (±0.03)	0.03 (-)	0.04 (-)	0.17 (-)	0.49 (-)	0.24 (-)	0.03 (-)	<0.01 (-)
PC 34:1	0.83 (±0.10)	0.79 (±0.22)	0.99 (±0.06)	1.00 (±0.08)	0.97 (-)	1.10 (-)	1.04 (±0.13)	3.47 (-)	7.45 (-)	6.04 (-)	5.81 (-)	3.96 (-)	8.99 (-)	5.67 (-)
PC 34:2	9.33 (±1.79)	6.59 (±1.15)	8.33 (±1.04)	8.84 (±0.78)	7.32 (-)	5.59 (-)	4.86 (±0.43)	9.72 (-)	9.20 (-)	17.32 (-)	13.84 (-)	11.40 (-)	11.09 (-)	14.04 (-)
PC 34:3	4.07 (±0.49)	2.53 (±0.36)	1.88 (±0.25)	1.79 (±0.28)	2.06 (-)	2.53 (-)	0.92 (±0.10)	1.57 (-)	0.62 (-)	1.69 (-)	1.03 (-)	1.03 (-)	0.06 (-)	0.07 (-)
PC 35:1	0.06 (±0.01)	0.08 (±0.00)	0.08 (±0.04)	0.11 (±0.03)	0.04 (-)	0.08 (-)	0.05 (<0.001)	0.10 (-)	0 (-)	0.01 (-)	0.09 (-)	0.12 (-)	0.06 (-)	0.03 (-)
PC 35:2	1.10 (±0.08)	1.26 (±0.21)	0.77 (±0.30)	0.94 (±0.05)	0.42 (-)	0.64 (-)	0.53 (±0.02)	0.76 (-)	0.31 (-)	0.32 (-)	0.37 (-)	0.24 (-)	0.04 (-)	0.08 (-)
PC 36:0	<0.01 (<0.001)	<0.01 (<0.001)	<0.01 (-)	<0.01 (-)	0 (-)	<0.01 (-)	0.02 (±0.00)	0 (-)	0 (-)	<0.01 (-)	0.41 (-)	0.05 (-)	<0.01 (-)	0 (-)
PC 36:1	0.07 (±0.01)	0.06 (±0.01)	0.14 (±0.02)	0.15 (±0.02)	0.13 (-)	0.12 (-)	0.89 (±0.16)	0.53 (-)	1.28 (-)	1.52 (-)	1.06 (-)	0.89 (-)	3.31 (-)	2.02 (-)
PC 36:2	1.75 (±0.37)	1.24 (±0.37)	1.31 (±0.43)	1.54 (±0.22)	0.86 (-)	1.38 (-)	4.84 (±0.71)	2.01 (-)	3.31 (-)	5.97 (-)	5.78 (-)	4.52 (-)	1.95 (-)	3.70 (-)
PC 36:3	1.88 (±0.28)	1.64 (±0.28)	1.75 (±0.88)	2.25 (±0.19)	0.74 (-)	1.94 (-)	1.29 (±0.11)	1.48 (-)	0.52 (-)	6.71 (-)	1.38 (-)	5.44 (-)	0.01 (-)	0.02 (-)
PC 36:4	8.20 (±2.12)	6.53 (±1.26)	10.52 (±5.38)	13.54 (±1.79)	4.49 (-)	5.21 (-)	5.07 (±0.28)	11.46 (-)	4.30 (-)	24.42 (-)	6.43 (-)	13.10 (-)	0.04 (-)	0.02 (-)
PC 37:0	0 (±0)	0 (±0)	0 (±0)	0 (±0)	0 (-)	0 (-)	<0.01 (<0.001)	0 (-)	0 (-)	0 (-)	0 (-)	0 (-)	0 (-)	0 (-)
PC 37:2	0.02 (±0.00)	0.03 (±0.01)	0.06 (±0.05)	0.08 (±0.02)	<0.01 (-)	0.01 (-)	<0.01 (<0.001)	0.02 (-)	0 (-)	0 (-)	0 (-)	<0.01 (-)	<0.01 (-)	<0.01 (-)
PC 37:3	0.04 (±0.00)	0.08 (±0.01)	0.05 (±0.04)	0.08 (±0.00)	<0.01 (-)	0.03 (-)	0.02 (<0.001)	0.05 (-)	<0.01 (-)	0.01 (-)	<0.01 (-)	0.02 (-)	0 (-)	0 (-)
PC 37:4	<0.01 (<0.001)	<0.01 (<0.001)	<0.01 (<0.001)	<0.01 (<0.001)	0 (-)	0 (-)	0 (±0)	0 (-)	0 (-)	0 (-)	0 (-)	0 (-)	<0.01 (-)	0 (-)
PC 38:0	<0.01 (<0.001)	<0.01 (<0.001)	0 (±0)	0 (±0)	0 (-)	<0.01 (-)	<0.01 (<0.001)	0 (-)	0 (-)	0 (-)	0 (-)	0 (-)	<0.01 (-)	<0.01 (-)
PC 38:1	<0.01 (<0.001)	<0.01 (<0.001)	0 (±0)	0 (±0)	0 (-)	<0.01 (-)	0 (±0)	0 (-)	0 (-)	0 (-)	0 (-)	0 (-)	0.04 (-)	0.01 (-)
PC 38:2	0.04 (±0.01)	0.03 (±0.00)	0.04 (±0.02)	0.05 (±0.01)	0.01 (-)	0.02 (-)	0.02 (±0.00)	0.03 (-)	0.03 (-)	0 (-)	0.03 (-)	0.06 (-)	0.03 (-)	0.06 (-)
PC 38:3	0.07 (±0.01)	0.10 (±0.03)	0.04 (±0.03)	0.06 (±0.00)	0.01 (-)	0.07 (-)	0.03 (<0.001)	0.04 (-)	<0.01 (-)	0.09 (-)	0.03 (-)	0.08 (-)	<0.01 (-)	0 (-)
PC 38:4	<0.01 (<0.001)	<0.01 (<0.001)	0 (±0)	0 (±0)	0 (-)	<0.01 (-)	0 (±0)	0 (-)	0 (-)	0 (-)	0 (-)	0 (-)	0.06 (-)	0.03 (-)
PC 38:5	0.01 (±0.01)	<0.01 (±0.00)	0.02 (±0.01)	0.03 (±0.01)	0.02 (-)	<0.01 (-)	0.07 (±0.01)	0.05 (-)	0.06 (-)	0.07 (-)	0.12 (-)	0.07 (-)	<0.01 (-)	<0.01 (-)

Continued on next page

Table B.15 – continued from previous page

	N. crassa												*S. cerevisiae*	
	WC		PM					DDM	Pma1				WC	membrane
	WC30 n=6	WC35 n=2	PM30A n=3	PM301 n=2	PM30DOC n=1	PM30NaCl n=1	PM35 n=2	PM30DDM n=1	Pma130glyc n=1	Pma130suc n=1	Pma135Pool1 n=1	Pma135Pool3 n=1	ScWC30 n=1	ScMembr30 n=1
number carbon atoms	mean (std)	mean (std)	mean (std)	mean (std)	mean (std)	mean (std)	mean (std)	mean (std)	mean (std)	mean (std)	mean (std)	mean (std)	mean (std)	mean (std)
PC 38:6	0.03 (±0.01)	<0.01 (±0.00)	0.08 (±0.03)	0.10 (±0.01)	0.05 (-)	0.01 (-)	0.05 (±0.00)	0.11 (-)	0 (-)	0.40 (-)	0.08 (-)	0.16 (-)	0 (-)	<0.01 (-)
PC 40:2	0.02 (±0.00)	0.02 (<0.001)	<0.01 (±0.00)	<0.01 (±0.00)	<0.01 (-)	0.02 (-)	<0.01 (<0.001)	<0.01 (-)	0 (-)	<0.01 (-)	0 (-)	0.02 (-)	<0.01 (-)	<0.01 (-)
PC 40:3	<0.01 (<0.001)	<0.01 (<0.001)	<0.01 (<0.001)	0 (±0)	<0.01 (-)	<0.01 (-)	<0.01 (<0.001)	0 (-)	0 (-)	0 (-)	0 (-)	<0.01 (-)	0 (-)	0 (-)
PC 40:4	<0.01 (<0.001)	<0.01 (<0.001)	0 (±0)	0 (±0)	0 (-)	0 (-)	0 (±0)	0 (-)	0 (-)	0 (-)	0 (-)	0 (-)	0.02 (-)	<0.01 (-)
PC 40:5	0.01 (±0.01)	0.02 (±0.00)	<0.01 (±0.00)	<0.01 (±0.00)	0.01 (-)	<0.01 (-)	<0.01 (<0.001)	<0.01 (-)	0 (-)	<0.01 (-)	0 (-)	0 (-)	0.02 (-)	<0.01 (-)
PC 40:6	0.03 (±0.01)	<0.01 (±0.00)	<0.01 (±0.01)	<0.01 (<0.001)	0.01 (-)	<0.01 (-)	<0.01 (<0.001)	<0.01 (-)	0 (-)	0 (-)	0 (-)	0 (-)	0 (-)	<0.01 (-)
PE 30:0	<0.01 (±0.00)	<0.01 (<0.001)	0.02 (±0.01)	0.01 (±0.01)	0.03 (-)	<0.01 (-)	0 (±0)	0 (-)	0.50 (-)	0 (-)	0 (-)	0 (-)	0 (-)	0 (-)
PE 32:0	0.09 (±0.01)	0.06 (±0.01)	0.38 (±0.20)	0.26 (±0.01)	0.61 (-)	0.05 (-)	0.26 (±0.01)	0.26 (-)	1.33 (-)	0.04 (-)	0.44 (-)	0.16 (-)	<0.01 (-)	0 (-)
PE 32:1	0.24 (±0.03)	0.20 (±0.03)	0.35 (±0.05)	0.38 (±0.01)	0.29 (-)	0.14 (-)	0.15 (±0.00)	0.61 (-)	5.29 (-)	0.46 (-)	0.54 (-)	0.62 (-)	2.53 (-)	1.82 (-)
PE 34:0	0.01 (±0.00)	<0.01 (±0.00)	0.04 (±0.02)	0.03 (±0.00)	0.07 (-)	<0.01 (-)	0.05 (±0.00)	0 (-)	0.02 (-)	0.01 (-)	0.20 (-)	0.07 (-)	<0.01 (-)	<0.01 (-)
PE 34:1	1.02 (±0.11)	0.79 (±0.17)	1.32 (±0.15)	1.27 (±0.17)	1.43 (-)	0.81 (-)	1.10 (±0.05)	2.42 (-)	7.63 (-)	0.82 (-)	4.45 (-)	7.24 (-)	4.75 (-)	5.13 (-)
PE 34:2	12.66 (±1.43)	7.77 (±0.38)	11.31 (±1.06)	11.87 (±0.56)	10.18 (-)	6.26 (-)	4.51 (±0.25)	13.57 (-)	10.53 (-)	4.50 (-)	7.53 (-)	5.23 (-)	7.08 (-)	9.40 (-)
PE 35:1	0.01 (±0.00)	0.02 (±0.00)	0.02 (±0.01)	0.02 (±0.00)	0.01 (-)	<0.01 (-)	0.01 (<0.001)	0.01 (-)	0.21 (-)	0 (-)	<0.01 (-)	0.04 (-)	0 (-)	0 (-)
PE 36:0	0 (±0)	0 (±0)	0 (±0)	0 (±0)	0 (-)	0 (-)	<0.01 (±0.00)	0 (-)	0 (-)	0 (-)	0.03 (-)	0 (-)	0 (-)	0 (-)
PE 36:1	0.04 (±0.01)	0.07 (±0.02)	0.05 (±0.03)	0.07 (±0.01)	0.02 (-)	0.03 (-)	1.56 (±0.20)	0.04 (-)	0.04 (-)	0.02 (-)	0.44 (-)	1.14 (-)	0.34 (-)	0.31 (-)
PE 36:2	0.82 (±0.17)	0.58 (±0.02)	0.77 (±0.13)	0.83 (±0.12)	0.66 (-)	0.46 (-)	6.64 (±0.24)	1.14 (-)	2.35 (-)	0.12 (-)	0.78 (-)	1.44 (-)	0.82 (-)	2.33 (-)
PE 36:3	0.97 (±0.10)	0.75 (±0.07)	0.80 (±0.25)	0.93 (±0.12)	0.53 (-)	0.83 (-)	1.02 (±0.02)	0.91 (-)	0.20 (-)	0.15 (-)	0.25 (-)	0.49 (-)	<0.01 (-)	0.02 (-)
PE 36:4	8.46 (±0.95)	6.12 (±0.36)	3.85 (±1.44)	4.67 (±0.39)	2.22 (-)	4.07 (-)	1.56 (±0.05)	4.77 (-)	1.61 (-)	0.81 (-)	1.30 (-)	0.13 (-)	<0.01 (-)	<0.01 (-)
PE 38:2	0.02 (±0.01)	0.02 (±0.00)	<0.01 (±0.00)	<0.01 (±0.00)	0 (-)	<0.01 (-)	0.01 (±0.01)	0 (-)	0 (-)	0.05 (-)	0 (-)	0.01 (-)	0 (-)	0 (-)
PE 38:3	0.08 (±0.02)	0.08 (±0.00)	0.09 (±0.03)	0.11 (±0.01)	0.06 (-)	0.07 (-)	0.03 (±0.01)	0 (-)	0 (-)	0 (-)	0 (-)	0.02 (-)	0 (-)	0 (-)
PE 38:4	<0.01 (±0.00)	<0.01 (<0.001)	0 (±0)	0 (±0)	0 (-)	<0.01 (-)	0.06 (±0.01)	0 (-)	0 (-)	0 (-)	0 (-)	0.08 (-)	0.01 (-)	0.01 (-)
PE 38:5	<0.01 (±0.00)	<0.01 (±0.00)	0 (±0)	0 (±0)	0 (-)	<0.01 (-)	0 (±0)	<0.01 (-)	0 (-)	0 (-)	<0.01 (-)	0.02 (-)	0 (-)	<0.01 (-)
PE 38:6	<0.01 (±0.00)	0 (±0)	0.07 (±0.03)	0.09 (±0.00)	0.04 (-)	<0.01 (-)	0.05 (±0.01)	0.09 (-)	<0.01 (-)	0 (-)	<0.01 (-)	<0.01 (-)	0 (-)	0 (-)
PG 32:0	<0.01 (<0.001)	0 (±0)	0.01 (±0.00)	0.01 (<0.001)	<0.01 (-)	<0.01 (-)	<0.01 (<0.001)	0.02 (-)	1.74 (-)	0 (-)	0.01 (-)	<0.01 (-)	0 (-)	0 (-)
PG 33:0	0 (±0)	0 (±0)	<0.01 (<0.001)	<0.01 (<0.001)	0 (-)	0 (-)	<0.01 (<0.001)	0 (-)	0.03 (-)	0 (-)	0 (-)	<0.01 (-)	0 (-)	0 (-)
PG 34:0	<0.01 (<0.001)	0 (±0)	0 (±0)	0 (±0)	0 (-)	0 (-)	<0.01 (<0.001)	0 (-)	0.08 (-)	<0.01 (-)	<0.01 (-)	<0.01 (-)	<0.01 (-)	0 (-)
PG 34:1	0.02 (±0.00)	<0.01 (<0.001)	0.08 (±0.03)	0.10 (±0.01)	0.05 (-)	0.01 (-)	0.14 (±0.01)	0.11 (-)	2.82 (-)	0.10 (-)	0.34 (-)	0.15 (-)	0.20 (-)	0.09 (-)
PG 35:1	0 (±0)	0 (±0)	<0.01 (<0.001)	<0.01 (<0.001)	0 (-)	0 (-)	<0.01 (<0.001)	0 (-)	0.70 (-)	0 (-)	0 (-)	<0.01 (-)	0 (-)	0 (-)
PG 36:1	<0.01 (<0.001)	0.02 (<0.001)	<0.01 (<0.001)	<0.01 (<0.001)	<0.01 (-)	<0.01 (-)	0.63 (±0.01)	<0.01 (-)	0.08 (-)	0 (-)	0.13 (-)	0.31 (-)	<0.01 (-)	<0.01 (-)

Continued on next page

Table B.15 – continued from previous page

	N. crassa												*S. cerevisiae*	
	WC		PM					DDM	Pma1				WC	membrane
	WC30 n=6	WC35 n=2	PM30A n=3	PM301 n=2	PM30DOC n=1	PM30NaCl n=1	PM35 n=2	PM30DDM n=1	Pma130glyc n=1	Pma130suc n=1	Pma135Pool1 n=1	Pma135Pool3 n=1	ScWC30 n=1	ScMembr30 n=1
number carbon atoms	mean (std)	mean (std)	mean (std)	mean (std)	mean (std)	mean (std)	mean (std)	mean (std)	mean (std)	mean (std)	mean (std)	mean (std)	mean (std)	mean (std)
PG 36:2	0.01 (±0.00)	0.08 (<0.001)	0.02 (±0.01)	0.02 (±0.00)	<0.01 (-)	<0.01 (-)	2.42 (±0.01)	0.02 (-)	0.60 (-)	0 (-)	0.29 (-)	0.51 (-)	0 (-)	0.01 (-)
PG 36:3	<0.01 (±0.00)	0.01 (±0.00)	0.04 (±0.01)	0.04 (±0.00)	0.03 (-)	0.02 (-)	0.40 (±0.01)	0.06 (-)	0 (-)	0 (-)	0.05 (-)	0.11 (-)	0 (-)	0 (-)
PG 36:4	0.04 (±0.01)	0.01 (<0.001)	0.25 (±0.03)	0.25 (±0.04)	0.24 (-)	0.11 (-)	0.06 (±0.01)	0.35 (-)	0.01 (-)	<0.01 (-)	0.04 (-)	0.13 (-)	<0.01 (-)	<0.01 (-)
PG 38:0	<0.01 (<0.001)	<0.01 (<0.001)	<0.01 (<0.001)	<0.01 (<0.001)	<0.01 (-)	<0.01 (-)	0 (±0)	<0.01 (-)	0 (-)	<0.01 (-)	0 (-)	<0.01 (-)	0 (-)	0 (-)
PG 38:2	0 (±0)	0 (±0)	0 (±0)	0 (±0)	0 (-)	0 (-)	<0.01 (<0.001)	0 (-)	0 (-)	0 (-)	0 (-)	<0.01 (-)	0 (-)	0 (-)
PG 38:5	<0.01 (<0.001)	0 (±0)	0 (±0)	0 (±0)	0 (-)	0 (-)	0 (±0)	0 (-)	0 (-)	0 (-)	0 (-)	<0.01 (-)	0 (-)	0 (-)
PG 40:2	<0.01 (<0.001)	<0.01 (<0.001)	0 (±0)	0 (±0)	0 (-)	0 (-)	<0.01 (<0.001)	<0.01 (-)	<0.01 (-)	<0.01 (-)	<0.01 (-)	<0.01 (-)	0 (-)	0 (-)
PG 40:5	<0.01 (<0.001)	<0.01 (<0.001)	<0.01 (<0.001)	<0.01 (<0.001)	0 (-)	<0.01 (-)	<0.01 (<0.001)	0 (-)	0 (-)	0 (-)	<0.01 (-)	<0.01 (-)	0 (-)	0 (-)
PG 42:6	<0.01 (±0.00)	<0.01 (<0.001)	<0.01 (±0.00)	<0.01 (<0.001)	<0.01 (-)	<0.01 (-)	<0.01 (<0.001)	<0.01 (-)	0 (-)	<0.01 (-)	0 (-)	<0.01 (-)	<0.01 (-)	<0.01 (-)
PG 42:7	0.30 (±0.11)	0.05 (±0.02)	0.06 (±0.04)	0.08 (±0.02)	0.02 (-)	<0.01 (-)	<0.01 (±0.00)	0.04 (-)	0.02 (-)	0.02 (-)	0.04 (-)	0.01 (-)	0 (-)	0 (-)
PI 32:0	0.06 (±0.00)	0.07 (±0.00)	0.10 (±0.07)	0.06 (<0.001)	0.18 (-)	0.04 (-)	0.28 (±0.01)	0.07 (-)	0.04 (-)	0.05 (-)	0.33 (-)	0.31 (-)	0.04 (-)	0.02 (-)
PI 33:0	<0.01 (±0.00)	0.01 (±0.00)	<0.01 (±0.00)	<0.01 (<0.001)	<0.01 (-)	0 (-)	0.04 (±0.00)	<0.01 (-)	0 (-)	<0.01 (-)	0.03 (-)	0.04 (-)	<0.01 (-)	<0.01 (-)
PI 34:0	<0.01 (±0.00)	<0.01 (±0.00)	0.01 (±0.01)	0.01 (<0.001)	0.02 (-)	<0.01 (-)	0.05 (<0.001)	0.01 (-)	0.02 (-)	0.01 (-)	0.06 (-)	0.03 (-)	<0.01 (-)	0 (-)
PI 34:1	0.41 (±0.05)	0.32 (±0.02)	0.71 (±0.14)	0.78 (±0.13)	0.59 (-)	0.60 (-)	0.32 (±0.01)	2.11 (-)	5.66 (-)	3.64 (-)	4.81 (-)	2.49 (-)	5.81 (-)	11.35 (-)
PI 34:2	10.37 (±1.23)	12.93 (±1.36)	6.58 (±0.62)	6.36 (±0.69)	7.01 (-)	6.09 (-)	7.43 (±1.71)	5.95 (-)	3.46 (-)	2.73 (-)	3.88 (-)	1.91 (-)	1.52 (-)	4.46 (-)
PI 35:0	<0.01 (<0.001)	<0.01 (<0.001)	0 (±0)	0 (±0)	0 (-)	0 (-)	<0.01 (<0.001)	0 (-)	0 (-)	0 (-)	0 (-)	0 (-)	0 (-)	0 (-)
PI 35:1	0.02 (±0.00)	0.02 (±0.00)	0.04 (±0.03)	0.06 (±0.01)	<0.01 (-)	0.01 (-)	<0.01 (±0.00)	0.04 (-)	0.01 (-)	0.01 (-)	0.03 (-)	0.05 (-)	0.02 (-)	0.05 (-)
PI 35:2	0.42 (±0.04)	0.47 (±0.04)	0.32 (±0.21)	0.43 (±0.05)	0.08 (-)	0.19 (-)	0.09 (±0.01)	0.25 (-)	0.07 (-)	0.03 (-)	0.06 (-)	0.03 (-)	<0.01 (-)	0.01 (-)
PI 36:0	<0.01 (<0.001)	<0.01 (<0.001)	<0.01 (<0.001)	<0.01 (<0.001)	<0.01 (-)	<0.01 (-)	<0.01 (<0.001)	<0.01 (-)	<0.01 (-)	0.04 (-)	<0.01 (-)	<0.01 (-)	<0.01 (-)	<0.01 (-)
PI 36:1	0.02 (±0.01)	<0.01 (<0.001)	0.20 (±0.06)	0.22 (±0.05)	0.15 (-)	0.01 (-)	0.08 (±0.01)	0.90 (-)	2.50 (-)	1.38 (-)	1.85 (-)	0.51 (-)	1.91 (-)	5.48 (-)
PI 36:2	0.17 (±0.04)	0.07 (±0.00)	0.23 (±0.15)	0.31 (±0.04)	0.06 (-)	0.12 (-)	0.03 (<0.001)	0.24 (-)	0.40 (-)	0.27 (-)	0.38 (-)	0.07 (-)	0.20 (-)	1.02 (-)
PI 36:3	0.08 (±0.02)	0.03 (±0.00)	0.11 (±0.09)	0.17 (±0.02)	0.01 (-)	0.08 (-)	<0.01 (<0.001)	0.06 (-)	0.02 (-)	0 (-)	0.03 (-)	0.01 (-)	0 (-)	0 (-)
PI 36:4	1.10 (±0.27)	1.03 (±0.09)	0.54 (±0.33)	0.72 (±0.10)	0.16 (-)	0.83 (-)	0.12 (±0.02)	0.41 (-)	0.08 (-)	0.08 (-)	0.11 (-)	0.03 (-)	<0.01 (-)	0 (-)
PI 38:4	<0.01 (±0.00)	<0.01 (<0.001)	0 (±0)	0 (±0)	0 (-)	<0.01 (-)	0 (±0)	0 (-)	0 (-)	0 (-)	0 (-)	0 (-)	0 (-)	0 (-)
PI 38:5	<0.01 (±0.00)	<0.01 (<0.001)	<0.01 (±0.00)	<0.01 (<0.001)	0 (-)	<0.01 (-)	0 (±0)	<0.01 (-)	0 (-)	0 (-)	0 (-)	0 (-)	0 (-)	0 (-)
PI 40:4	0 (±0)	0 (±0)	0 (±0)	0 (±0)	0 (-)	0 (-)	0 (±0)	<0.01 (-)	<0.01 (-)	0 (-)	<0.01 (-)	0 (-)	0 (-)	0 (-)
PS 32:0	<0.01 (<0.001)	<0.01 (<0.001)	<0.01 (±0.00)	0.01 (<0.001)	<0.01 (-)	0 (-)	0.08 (±0.00)	<0.01 (-)	0.03 (-)	<0.01 (-)	0.05 (-)	0.06 (-)	0 (-)	0 (-)
PS 32:1	<0.01 (±0.00)	0.04 (±0.01)	0.03 (±0.01)	0.04 (±0.01)	0.02 (-)	<0.01 (-)	0.02 (±0.00)	0.18 (-)	0.28 (-)	0.16 (-)	0.13 (-)	0.10 (-)	1.91 (-)	0.40 (-)
PS 33:1	<0.01 (±0.00)	0.04 (±0.00)	<0.01 (<0.001)	<0.01 (<0.001)	0 (-)	<0.01 (-)	<0.01 (<0.001)	0 (-)	0 (-)	0 (-)	<0.01 (-)	0.37 (-)	0.20 (-)	0.09 (-)

Continued on next page

Table B.15 – continued from previous page

	N. crassa												*S. cerevisiae*	
	WC		PM					DDM	Pma1				WC	membrane
	WC30 n=6	WC35 n=2	PM30A n=3	PM301 n=2	PM30DOC n=1	PM30NaCl n=1	PM35 n=2	PM30DDM n=1	Pma130glyc n=1	Pma130suc n=1	Pma135Pool1 n=1	Pma135Pool3 n=1	ScWC30 n=1	ScMembr30 n=1
number carbon atoms	mean (std)	mean (std)	mean (std)	mean (std)	mean (std)	mean (std)	mean (std)	mean (std)	mean (std)	mean (std)	mean (std)	mean (std)	mean (std)	mean (std)
PS 34:1	0.04 (±0.01)	0.09 (±0.01)	0.21 (±0.05)	0.18 (±0.01)	0.27 (-)	0.06 (-)	0.10 (±0.01)	0.62 (-)	1.33 (-)	0.82 (-)	0.83 (-)	1.38 (-)	5.11 (-)	1.36 (-)
PS 34:2	1.52 (±0.29)	4.02 (±0.29)	2.84 (±0.21)	2.84 (±0.30)	2.84 (-)	0.58 (-)	3.34 (±0.77)	2.55 (-)	1.37 (-)	0.89 (-)	1.36 (-)	1.03 (-)	2.70 (-)	1.62 (-)
PS 34:3	0.48 (±0.09)	0.47 (±0.03)	0.26 (±0.08)	0.22 (±0.03)	0.36 (-)	0.14 (-)	0.17 (±0.03)	0.16 (-)	0.04 (-)	0.02 (-)	0.05 (-)	0.03 (-)	<0.01 (-)	<0.01 (-)
PS 35:1	<0.01 (±0.00)	0.01 (<0.001)	0.18 (±0.09)	0.13 (±0.02)	0.28 (-)	0.03 (-)	0.03 (±0.03)	0.09 (-)	0.16 (-)	0 (-)	0 (-)	0.13 (-)	0 (-)	0 (-)
PS 35:2	0.06 (±0.01)	0.12 (±0.01)	0.19 (±0.02)	0.18 (±0.02)	0.19 (-)	0.03 (-)	0.14 (±0.02)	0.11 (-)	<0.01 (-)	0 (-)	0.03 (-)	0.03 (-)	0.02 (-)	0.04 (-)
PS 36:0	2.61 (±0.36)	1.35 (±0.12)	12.42 (±15.34)	3.56 (±0.07)	30.14 (-)	3.31 (-)	4.35 (±0.50)	2.97 (-)	1.75 (-)	0.29 (-)	1.47 (-)	0.78 (-)	0.05 (-)	0.05 (-)
PS 36:2	0.03 (±0.01)	0.02 (±0.00)	0.06 (±0.05)	0.09 (±0.01)	0 (-)	<0.01 (-)	<0.01 (<0.001)	0.07 (-)	0 (-)	0.03 (-)	0.16 (-)	0.09 (-)	0.08 (-)	0.14 (-)
PS 36:3	<0.01 (<0.001)	<0.01 (<0.001)	0.03 (±0.01)	0.04 (±0.00)	0.02 (-)	<0.01 (-)	0 (±0)	0.01 (-)	<0.01 (-)	<0.01 (-)	0.03 (-)	<0.01 (-)	0 (-)	0 (-)
PS 38:0	0.17 (±0.04)	0.17 (±0.01)	0.22 (±0.26)	0.07 (±0.05)	0.51 (-)	0.22 (-)	0.13 (±0.04)	0.02 (-)	0.01 (-)	<0.01 (-)	0.02 (-)	0.03 (-)	0.02 (-)	0.02 (-)
PS 38:1	0.25 (±0.04)	0.35 (±0.06)	0.36 (±0.07)	0.33 (±0.05)	0.43 (-)	0.21 (-)	0.18 (±0.03)	0.21 (-)	0.12 (-)	0.15 (-)	0.09 (-)	0.04 (-)	0.01 (-)	0.04 (-)
PS 38:3	<0.01 (<0.001)	0 (±0)	<0.01 (<0.001)	<0.01 (<0.001)	0 (-)	<0.01 (-)	0 (±0)	<0.01 (-)	0 (-)	0 (-)	0 (-)	0 (-)	0 (-)	0 (-)
PS 38:5	<0.01 (±0.00)	<0.01 (<0.001)	0.02 (±0.02)	0.03 (±0.00)	0 (-)	0 (-)	<0.01 (<0.001)	0.02 (-)	0 (-)	0 (-)	0 (-)	0 (-)	0 (-)	0 (-)
PS 38:6	<0.01 (±0.00)	0 (±0)	0 (±0)	0 (±0)	0 (-)	0 (-)	0 (±0)	0 (-)	0 (-)	0 (-)	0 (-)	0 (-)	0 (-)	0 (-)
PS 40:0	0.03 (±0.01)	0.03 (<0.001)	0.04 (±0.05)	0.01 (<0.001)	0.10 (-)	0.03 (-)	0.03 (±0.00)	<0.01 (-)	0 (-)	0 (-)	0.02 (-)	0.02 (-)	0 (-)	0 (-)
PS 40:4	<0.01 (±0.00)	<0.01 (<0.001)	0.04 (±0.02)	0.03 (<0.001)	0.06 (-)	<0.01 (-)	0.13 (±0.00)	0 (-)	0 (-)	0 (-)	0.09 (-)	0.05 (-)	<0.01 (-)	<0.01 (-)
PS 40:5	<0.01 (<0.001)	<0.01 (<0.001)	<0.01 (±0.00)	<0.01 (<0.001)	<0.01 (-)	<0.01 (-)	0 (±0)	<0.01 (-)	0 (-)	0 (-)	0 (-)	0 (-)	0 (-)	0 (-)

Table B.16: Diacylglycerophospholipids - selected species with focus on Pma1, sample codes outlined in Table B.8

sample DGPL species	Pma130hex mean	(std)	Pma130hex-suc mean	(std)	Pma135hex mean	(std)	Pma135lower mean	(std)	Notes
total **PA** in DGPL	11.18	-	10.57	-	22.51	-	27.68	-	-
PA 34:1	0.91	-	1.68	-	5.66	-	7.82	-	PA 34:1 more in 35°C than 30°C
PA 34:2	5.65	-	3.85	-	8.79	-	8.18	-	PA 34:2 more than PA 34:1
PA 36:2	0.4	-	0.57	-	1.05	-	1.66	-	PA 36 more unsaturation in 35°C
PA 36:3	0.13	-	0.5	-	1.12	-	2.3	-	
PA 36:4	2.22	-	3.12	-	2.89	-	3.63	-	
sum PA species	9.31		9.72		19.51		23.59		
total **PC** in DGPL	35.69	-	71.69	-	44.68	-	44.77	-	-
PC 32:0	0.17	-	0.87	-	1.1	-	0.55	-	PC 32 more in hexamer than lower, PC 32: 1 and 2 more in hexamer than lower
PC 32:1	2.99	-	2.2	-	1.61	-	0.58	-	
PC 32:2	4.41	-	3.01	-	3.54	-	1.15	-	
PC 34:1	7.45	-	6.04	-	5.81	-	3.96	-	
PC 34:2	9.2	-	17.32	-	13.84	-	11.4	-	PC 34:2 main component (>10% of all DGPL species),
PC 34:3	0.62	-	1.69	-	1.03	-	1.03	-	
PC 36:1	1.28	-	1.52	-	1.06	-	0.89	-	high PC succrose level PC 34:2 and 36:4 (17.32 and 24.42% of all DGPL species)
PC 36:2	3.31	-	5.97	-	5.78	-	4.52	-	PC 36:4 also high in lower oligomer (13%, and Pma1 30 4.3%, Pma1 35 6.4%)
PC 36:3	0.52	-	6.71	-	1.38	-	5.44	-	
PC 36:4	4.3	-	24.42	-	6.43	-	13.1	-	
sum PC species	34.25		69.75		41.58		42.62		
total **PE** in DGPL	29.71	-	6.98	-	15.97	-	16.69	-	-
PE 32:0	1.33	-	0.04	-	0.44	-	0.16	-	
PE 32:1	5.29	-	0.46	-	0.54	-	0.62	-	higher 32 in Pma130, PE 32:1 (5.29%)
PE 34:1	7.63	-	0.82	-	4.45	-	7.24	-	PE 34:1 and PE 34:2
PE 34:2	10.53	-	4.5	-	7.53	-	5.23	-	
PE 36:1	0.04	-	0.02	-	0.44	-	1.14	-	
PE 36:2	2.35	-	0.12	-	0.78	-	1.44	-	
PE 36:4	1.61	-	0.81	-	1.3	-	0.13	-	
sum PE species	28.78		6.77		15.48		15.96		
total **PG** in DGPL	6.08	-	0.13	-	0.92	-	1.24	-	-
PG 32:0	1.74	-	0	-	0.01	-	<0.01	-	Pma1 glyc high levels PG 32:0 and 34:1
PG 34:1	2.82	-	0.1	-	0.34	-	0.15	-	
sum PG species	4.56		0.1		0.35		0.15		
total **PI** in DGPL	12.25	-	8.25	-	11.57	-	5.48	-	-
PI 34:1	5.66	-	3.64	-	4.81	-	2.49	-	PI 34:1, PI 34:2 and PI 36:1 might be the main PI components of Pma1 hexamer
PI 34:2	3.46	-	2.73	-	3.88	-	1.91	-	
PI 36:1	2.5	-	1.38	-	1.85	-	0.51	-	
sum PI species	11.62		7.75		10.54		4.91		
total **PS** in DGPL	5.09	-	2.38	-	4.34	-	4.14	-	-
PS 34:1	1.33	-	0.82	-	0.83	-	1.38	-	PS mainly 34:1, 34:2 and 36:0
PS 34:2	1.37	-	0.89	-	1.36	-	1.03	-	
PS 36:0	1.75	-	0.29	-	1.47	-	0.78	-	
sum PS species	4.45		2		3.66		3.19		

Table B.17: Sphingolipids - Distribution of lipid classes, sample codes outlined in Table B.8

	N. crassa												*S. cerevisiae*	
	WC		PM					DDM	Pma1				WC	membrane
	WC30 n=6	WC35 n=2	PM30 n=3	PM-DOCA n=2	PM-DOCB n=1	PM-NaCl n=1	PM35 n=2	PM-DDM n=1	Pma130hex n=1	Pma130hex-suc n=1	Pma135hex n=1	Pma135lower n=1	ScWC30 n=1	ScMembr30 n=1
total SL	1.32 (±0.21)	1.79 (±0.32)	4.87 (±2.37)	5.12 (±3.29)	4.37 (-)	1.57 (-)	0.61 (±0.11)	5.36 (-)	7.21 (-)	0.13 (-)	9.44 (-)	4.56 (-)	0.15 (-)	0.0 (-)
	mean (std)	mean (std)	mean (std)	mean (std)	mean (std)	mean (std)	mean (std)	mean (std)	mean (std)	mean (std)	mean (std)	mean (std)	mean (std)	mean (std)
	mean (std)	mean (std)	mean (std)	mean (std)	mean (std)	mean (std)	mean (std)	mean (std)	mean (std)	mean (std)	mean (std)	mean (std)	mean (std)	mean (std)
Cer	34.66 (±7.23)	12.11 (±1.76)	59.2 (±5.4)	58.91 (±7.6)	59.79 (-)	28.57 (-)	33.2 (±0.43)	41.55 (-)	21.62 (-)	12.29 (-)	42.36 (-)	52.57 (-)	4.33 (-)	70.95 (-)
IP-Cer	10.16 (±5.69)	4.49 (±0.68)	20.01 (±14.71)	28.33 (±4.19)	3.37 (-)	2.87 (-)	13.99 (±0.18)	47.72 (-)	33.35 (-)	32.7 (-)	41.51 (-)	46.19 (-)	56.59 (-)	19.66 (-)
MIP-Cer	0.02 (±0.01)	0.004 (±0.001)	0.06 (±0.04)	0.09 (±0.02)	0.02 (-)	0.003 (-)	0.01 (±0.001)	0.89 (-)	1.3 (-)	1.16 (-)	0.45 (-)	0.21 (-)	38.78 (-)	8.27 (-)
MDIP-Cer	0.021 (±0.01)	0.004 (±0.001)	0.09 (±0.04)	0.11 (±0.02)	0.06 (-)	0.001 (-)	0.02 (±0.002)	0.13 (-)	0.075 (-)	0.001 (-)	0.17 (-)	0.11 (-)	0 (-)	0 (-)
SM	55.03 (±9.66)	83.36 (±1.08)	20.57 (±14.19)	12.49 (±3.4)	36.72 (-)	68.42 (-)	52.73 (±0.24)	9.62 (-)	43.43 (-)	53.66 (-)	15.49 (-)	0.86 (-)	0.21 (-)	0.40 (-)
S	0.11 (±0.04)	0.03 (±0.01)	0.06 (±0.03)	0.07 (±0.03)	0.04 (-)	0.14 (-)	0.04 (±0.01)	0.1 (-)	0.23 (-)	0.19 (-)	0.02 (-)	0.07 (-)	0.09 (-)	0.7 (-)
Gang	0 (±0)	0 (±0)	0.001 (±0.002)	0 (±0)	0.004 (-)	0 (-)	0.001 (±0.002)	0 (-)	0 (-)	0 (-)	0 (-)	0 (-)	0 (-)	0 (-)

Table B.18: Sphingolipids - Distribution of chain length, sample codes outlined in Table B.8

	N. crassa												*S. cerevisiae*	
	WC		PM					DDM	Pma1				WC	membrane
	WC30 n=6	WC35 n=2	PM30 n=3	PM-DOCA n=2	PM-DOCB n=1	PM-NaCl n=1	PM35 n=2	PM-DDM n=1	Pma130hex n=1	Pma130hex-suc n=1	Pma135hex n=1	Pma135lower n=1	ScWC30 n=1	ScMembr30 n=1
number carbon atoms	mean (std)	mean (std)	mean (std)	mean (std)	mean (std)	mean (std)	mean (std)	mean (std)	mean (std)	mean (std)	mean (std)	mean (std)	mean (std)	mean (std)
30	0.07 (±0.04)	0.07 (±0.01)	0.0005 (±0.0005)	0.0002 (±0.0003)	0.001 (-)	0.06 (-)	0 (±0)	0 (-)	0 (-)	0 (-)	0 (-)	0 (-)	0 (-)	0 (-)
32	5.7 (±0.58)	4.26 (±0.17)	0.73 (±0.26)	0.6 (±0.2)	0.97 (-)	1.64 (-)	0.43 (±0.09)	0.43 (-)	0.21 (-)	0.0013 (-)	0.19 (-)	0.18 (-)	0.02 (-)	0.1 (-)
33	5.46 (±3.59)	9.3 (±1.54)	0.85 (±0.31)	0.87 (±0.44)	0.80 (-)	2.54 (-)	0.28 (±0.09)	1.17 (-)	0.4 (-)	0.02 (-)	0.88 (-)	1.46 (-)	0 (-)	0 (-)
34	33.53 (±9.33)	56.93 (±2.53)	8.78 (±3.44)	7.1 (±2.62)	12.13 (-)	57.05 (-)	6.32 (±0.55)	4.92 (-)	1.1 (-)	0.55 (-)	7.46 (-)	11.22 (-)	0.07 (-)	0.13 (-)
35	1.56 (±0.49)	1.22 (±0.0009)	2.92 (±0.91)	3.18 (±1.12)	2.40 (-)	1.99 (-)	1.66 (±0.054)	2.95 (-)	0.86 (-)	0.31 (-)	4.75 (-)	5.82 (-)	0 (-)	0 (-)
36	10.38 (±2.22)	4.26 (±0.41)	16.51 (±5.04)	17.05 (±7)	15.43 (-)	13.67 (-)	8.57 (±0.024)	16.32 (-)	5.2 (-)	7.47 (-)	13.42 (-)	14.72 (-)	3.36 (-)	21.03 (-)
37	0.12 (±0.06)	0.03 (±0.01)	0.22 (±0.06)	0.22 (±0.08)	0.20 (-)	0.42 (-)	0.16 (±0.006)	0.20 (-)	0.02 (-)	0.009 (-)	0.22 (-)	0.3 (-)	0.003 (-)	0.20 (-)
38	0.42 (±0.07)	0.14 (±0.03)	0.28 (±0.08)	0.3 (±0.08)	0.22 (-)	0.22 (-)	0.26 (±0.009)	0.38 (-)	0.89 (-)	0.97 (-)	0.23 (-)	0.11 (-)	0.02 (-)	0.08 (-)
39	0.09 (±0.05)	0.05 (±0.02)	0.07 (±0.02)	0.06 (±0.02)	0.09 (-)	0.053 (-)	0.13 (±0.02)	0.004 (-)	0.004 (-)	0.009 (-)	0.002 (-)	0.05 (-)	0 (-)	0 (-)
40	3.19 (±0.83)	1.13 (±0.17)	1.33 (±0.07)	1.36 (±0.05)	1.26 (-)	0.75 (-)	1.39 (±0.27)	2.25 (-)	3.39 (-)	13.39 (-)	2.58 (-)	0.88 (-)	0.002 (-)	0 (-)
41	1.47 (±0.52)	0.92 (±0.18)	2.2 (±0.32)	2.14 (±0.42)	2.33 (-)	0.68 (-)	2.77 (±0.11)	0.84 (-)	0.44 (-)	0.01 (-)	1.36 (-)	1.73 (-)	0.004 (-)	0 (-)
42	23.14 (±7.32)	7.96 (±0.03)	39.92 (±8.64)	44.67 (±3.71)	30.42 (-)	8.79 (-)	22.31 (±0.015)	50.95 (-)	36.86 (-)	57.2 (-)	44.58 (-)	51.93 (-)	0.77 (-)	0.32 (-)
43	2.4 (±0.67)	1.11 (±0.13)	3.67 (±0.82)	3.76 (±1.14)	3.49 (-)	1.24 (-)	2.59 (±0.29)	2.28 (-)	1.78 (-)	0.12 (-)	1.97 (-)	2.69 (-)	0 (-)	2.84 (-)
44	2.9 (±1.19)	1.11 (±0.05)	6.08 (±3.27)	7.71 (±2.3)	2.80 (-)	1.59 (-)	3.94 (±0.36)	11.32 (-)	9.72 (-)	8.09 (-)	9.26 (-)	8.12 (-)	61.76 (-)	69.56 (-)
46	7.06 (±1.08)	10.06 (±0.25)	14.71 (±8.48)	10.07 (±3.78)	24.00 (-)	8 (-)	45.92 (±0.43)	5.76 (-)	13.84 (-)	0.96 (-)	1.08 (-)	0.58 (-)	33.98 (-)	5.44 (-)
47	0.0005 (±0.001)	0 (±0)	0 (±0)	0 (±0)	0 (-)	0 (-)	0 (±0)	0 (-)	0 (-)	0 (-)	0 (-)	0 (-)	0 (-)	0.06 (-)
48	2.52 (±0.34)	1.45 (±0.34)	1.74 (±1.48)	0.89 (±0.24)	3.45 (-)	1.31 (-)	3.26 (±0.69)	0.18 (-)	25.13 (-)	10.9 (-)	11.99 (-)	0.21 (-)	0 (-)	0.19 (-)
50	0.002 (±0.0008)	0.0002 (±0.0001)	0.005 (±0.004)	0.007 (±0.003)	0.0004 (-)	0.002 (-)	0 (±0)	0.03 (-)	0.17 (-)	0 (-)	0.031 (-)	0.01 (-)	0.003 (-)	0.05 (-)

Table B.19: Sphingolipids - Distribution of double bonds, sample codes outlined in Table B.8

	N. crassa												*S. cerevisiae*	
	WC		PM					DDM	Pma1				WC	membrane
	WC30 n=6	WC35 n=2	PM30 n=3	PM-DOCA n=2	PM-DOCB n=1	PM-NaCl n=1	PM35 n=2	PM-DDM n=1	Pma130hex n=1	Pma130hex-suc n=1	Pma135hex n=1	Pma135lower n=1	ScWC30 n=1	ScMembr30 n=1
number double bonds	mean (std)	mean (std)	mean (std)	mean (std)	mean (std)	mean (std)	mean (std)	mean (std)	mean (std)	mean (std)	mean (std)	mean (std)	mean (std)	mean (std)
0	40.17 (±8.4)	22.31 (±0.52)	77.76 (±7.35)	81.96 (±1.43)	69.35 (-)	29.63 (-)	81.46 (±0.39)	85.85 (-)	76.22 (-)	45.17 (-)	80.98 (-)	89.23 (-)	95.55 (-)	59.92 (-)
1	37.48 (±9.9)	60.47 (±0.36)	17.36 (±2.19)	16.25 (±1.46)	19.59 (-)	50.09 (-)	15.51 (±0.73)	12.15 (-)	7.94 (-)	25.28 (-)	6.4 (-)	10.25 (-)	1.34 (-)	19.77 (-)
2	22.32 (±11.72)	17.2 (±0.15)	4.88 (±5.35)	1.79 (±0.03)	11.06 (-)	20.27 (-)	3.04 (±0.34)	2.00 (-)	15.83 (-)	29.55 (-)	12.61 (-)	0.52 (-)	3.11 (-)	20.31 (-)
3	0.02 (±0.03	0.02 (±0.009)	0 (±0)	0 (±0)	0 (-)	0.009 (-)	0 (±0)	0 (-)	0 (-)	0 (-)	0 (-)	0 (-)	0 (-)	0 (-)

Table B.20: Sphingolipids - Distribution of hydroxgroups, sample codes outlined in Table B.8

	N. crassa												*S. cerevisiae*	
	WC		PM					DDM	Pma1				WC	membrane
	WC30 n=6	WC35 n=2	PM30 n=3	PM-DOCA n=2	PM-DOCB n=1	PM-NaCl n=1	PM35 n=2	PM-DDM n=1	Pma130hex n=1	Pma130hex-suc n=1	Pma135hex n=1	Pma135lower n=1	ScWC30 n=1	ScMembr30 n=1
	mean (std)	mean (std)	mean (std)	mean (std)	mean (std)	mean (std)	mean (std)	mean (std)	mean (std)	mean (std)	mean (std)	mean (std)	mean (std)	mean (std)
0	54.77 (±9.7)	83.27 (±1.09)	20.47 (±14.25)	12.36 (±3.49)	36.68 (-)	68.32 (-)	52.74 (±0.23)	9.02 (-)	42.42 (-)	53.41 (-)	15.14 (-)	0.78 (-)	0.21 (-)	0.40 (-)
1	0.29 (±0.1)	0.1 (±0.008)	0.2 (±0.1)	0.24 (±0.08)	0.10 (-)	0.1 (-)	0.02 (±0.002)	0.73 (-)	1.08 (-)	0.25 (-)	0.53 (-)	0.2 (-)	0.37 (-)	0.04 (-)
2	9.08 (±1.82)	2.98 (±0.35)	18.52 (±4.42)	20.04 (±5.03)	15.45 (-)	9.64 (-)	9.82 (±0.011)	15.46 (-)	5.15 (-)	6.27 (-)	28.39 (-)	37.42 (-)	5.33 (-)	8.52 (-)
3	35.85 (±9.05)	13.6 (±0.75)	60.7 (±11.29)	67.18 (±1.56)	47.72 (-)	21.91 (-)	37.05 (±0.23)	74.35 (-)	50.73 (-)	39.57 (-)	55.29 (-)	61.35 (-)	92.07 (-)	81.85 (-)
4	0.02 (±0.02)	0.05 (±0.01)	0.12 (±0.11)	0.18 (±0.06)	0.008 (-)	0.03 (-)	0.37 (±0.002)	0.45 (-)	0.62 (-)	0.5 (-)	0.65 (-)	0.25 (-)	2.02 (-)	9.18 (-)
5	0.0002 (±0.0002)	0.00009 (±0.0001)	0 (±0)	0 (±0)	0 (-)	0 (-)	0 (±0)	0 (-)	0 (-)	0 (-)	0 (-)	0 (-)	0 (-)	0 (-)

Table B.21: Sphingolipids - Distribution of selected spingolipid species, sample codes outlined in Table B.8, values rounded for clarity.

	WC 30	PM 30	Pma130hex	Pma135hex	Pma135lower
Cer 34:0;3	1	3	1	3	5
Cer 34:0;2	1	2	0	4	5
Cer 36:0;3	3	7	2	5	5
Cer 36:0;2	3	5	2	7	7
Cer 42:0;3	9	15	8	9	9
IP Cer 42:0;3	9	15	25	23	26
IP Cer 42:0;2	0	1	1	10	13
IP Cer 44:0,3	1	4	7	6	5
SM 48:2	2	1	15	12	0
SM 46:0	7	15	13	1	0
SM 48:0	0	1	10	0	0
% of total Sphingolipids	36	69	84	80	75

Table B.22: Sphingolipids - Distribution of individual lipid species (omitting hydroxy-groups), sample codes outlined in Table B.8

	N. crassa												*S. cerevisiae*	
	WC		PM					DDM	Pma1				WC	membra
	WC30 n=6	WC35 n=2	PM30 n=3	DOCA n=2	DOCB n=1	PMNaCl n=1	PM35 n=2	PMDDM n=1	Pma130hex n=1	Pma130hexsuc n=1	Pma135hex n=1	Pma135lower n=1	ScWC30 n=1	ScMemb n=1
	mean (std)	mean (std)	mean (std)	mean (std)	mean (std)	mean (std)	mean (std)	mean (std)	mean (std)	mean (std)	mean (std)	mean (std)	mean (std)	mean (std)
Cer 32:0	0 (±0)	0 (±0)	0.01 (±0.002)	0.01 (±0.002)	0.01 (-)	0 (-)	0.003 (±0.0002)	0 (-)	0 (-)	0 (-)	0.08 (-)	0.1 (-)	0 (-)	0 (-)
Cer 32:1	0 (±0)	0 (±0)	0.03 (±0.005)	0 (±0)	0.009 (-)	0 (-)	0 (±0)	0 (-)	0 (-)	0 (-)	0 (-)	0 (-)	0 (-)	0 (-)
Cer 33:0	0.01 (±0.01)	0.001 (±0.002)	0.21 (±0.07)	0.2 (±0.09)	0.17 (-)	0.08 (-)	0.04 (±0.008)	0.17 (-)	0 (-)	0 (-)	0.68 (-)	0.95 (-)	0 (-)	0 (-)
Cer 33:1	0.05 (±0.01)	0.02 (±0.008)	0.1 (±0.04)	0.11 (±0.05)	0.08 (-)	0.1 (-)	0.08 (±0.03)	0.04 (-)	0.04 (-)	0 (-)	0.04 (-)	0.31 (-)	0 (-)	0 (-)
Cer 34:0	1.78 (±0.47)	0.69 (±0.07)	5.22 (±1.95)	5.83 (±2.33)	4.01 (-)	2.45 (-)	3.04 (±0.13)	3.71 (-)	0.54 (-)	0.28 (-)	7.18 (-)	9.84 (-)	0.05 (-)	0 (-)
Cer 34:1	0.23 (±0.21)	0.13 (±0.00008)	0.98 (±0.26)	1.03 (±0.35)	0.88 (-)	0.62 (-)	0.59 (±0.04)	0 (-)	0 (-)	0 (-)	0 (-)	1.36 (-)	0 (-)	0 (-)
Cer 35:0	0.48 (±0.2)	0.23 (±0.02)	2.13 (±0.72)	2.38 (±0.81)	1.63 (-)	1.15 (-)	0.87 (±0.01)	2.17 (-)	0.72 (-)	0.31 (-)	3.99 (-)	4.83 (-)	0 (-)	0 (-)
Cer 35:1	0.57 (±0.19)	0.34 (±0.03)	0.78 (±0.21)	0.79 (±0.3)	0.77 (-)	0.66 (-)	0.77 (±0.03)	0.77 (-)	0.13 (-)	0 (-)	0.72 (-)	0.99 (-)	0 (-)	0 (-)
Cer 36:0	5.79 (±1.35)	1.78 (±0.25)	12.28 (±3.97)	12.96 (±5.37)	10.93 (-)	8.36 (-)	5.81 (±0.08)	12.34 (-)	4.04 (-)	5.92 (-)	11.74 (-)	12.27 (-)	0.07 (-)	0.37 (-)
Cer 36:1	2.64 (±0.78)	1 (±0.15)	3.68 (±1.05)	3.65 (±1.49)	3.74 (-)	3.06 (-)	2.34 (±0.02)	3.5 (-)	1.09 (-)	1.11 (-)	1.64 (-)	2.18 (-)	0 (-)	0 (-)
Cer 36:2	0.99 (±0.14)	0.38 (±0.02)	0.4 (±0.2)	0.3 (±0.13)	0.61 (-)	1.69 (-)	0.34 (±0.02)	0.28 (-)	0.07 (-)	0.03 (-)	0.03 (-)	0.25 (-)	3.06 (-)	19.9 (-)
Cer 37:0	0.038 (±0.02)	0.02 (±0.007)	0.14 (±0.04)	0.15 (±0.05)	0.13 (-)	0.09 (-)	0.09 (±0.01)	0.16 (-)	0.02 (-)	0.009 (-)	0.22 (-)	0.18 (-)	0.003 (-)	0.2 (-)
Cer 37:1	0.07 (±0.04)	0.02 (±0.004)	0.07 (±0.02)	0.07 (±0.03)	0.07 (-)	0.32 (-)	0.07 (±0.006)	0.04 (-)	0 (-)	0 (-)	0 (-)	0.12 (-)	0 (-)	0 (-)
Cer 38:0	0.26 (±0.07)	0.08 (±0.01)	0.22 (±0.08)	0.26 (±0.08)	0.16 (-)	0.16 (-)	0.26 (±0.007)	0.2 (-)	0 (-)	0.16 (-)	0 (-)	0.064 (-)	0 (-)	0 (-)
Cer 38:1	0.02 (±0.007)	0.006 (±0.002)	0.009 (±0.004)	0.007 (±0.003)	0.01 (-)	0.02 (-)	0.002 (±0.01)	0.01 (-)	0 (-)	0.05 (-)	0.008 (-)	0.002 (-)	0.02 (-)	0.08 (-)
Cer 39:0	0.06 (±0.03)	0.05 (±0.01)	0.051 (±0.009)	0.05 (±0.01)	0.05 (-)	0.03 (-)	0.09 (±0.01)	0 (-)	0 (-)	0 (-)	0 (-)	0.043 (-)	0 (-)	0 (-)
Cer 39:1	0.02 (±0.02)	0.006 (±0.009)	0.01 (±0.02)	0 (±0)	0.03 (-)	0.01 (-)	0.03 (±0.003)	0 (-)	0 (-)	0 (-)	0 (-)	0 (-)	0 (-)	0 (-)
Cer 40:0	1.08 (±0.39)	0.5 (±0.08)	0.86 (±0.04)	0.88 (±0.01)	0.82 (-)	0.38 (-)	0.78 (±0.001)	0.69 (-)	0 (-)	0.34 (-)	0.69 (-)	0.66 (-)	0 (-)	0 (-)
Cer 40:1	1.25 (±0.32)	0.38 (±0.1)	0.31 (±0.03)	0.31 (±0.05)	0.31 (-)	0.15 (-)	0.45 (±0.23)	0.2 (-)	0.23 (-)	0 (-)	0.15 (-)	0.12 (-)	0 (-)	0 (-)
Cer 40:2	0.19 (±0.05)	0.05 (±0.01)	0.09 (±0.03)	0.07 (±0.01)	0.13 (-)	0.08 (-)	0.16 (±0.04)	0.07 (-)	0.06 (-)	0.08 (-)	0.01 (-)	0.02 (-)	0.002 (-)	0 (-)
Cer 41:0	0.81 (±0.29)	0.47 (±0.11)	1.32 (±0.2)	1.35 (±0.28)	1.26 (-)	0.29 (-)	1.18 (±0.01)	0.78 (-)	0.41 (-)	0 (-)	1.31 (-)	1.33 (-)	0 (-)	0 (-)
Cer 41:1	0.56 (±0.24)	0.39 (±0.07)	0.79 (±0.17)	0.71 (±0.13)	0.96 (-)	0.34 (-)	1.38 (±0.08)	0 (-)	0 (-)	0 (-)	0 (-)	0.35 (-)	0 (-)	0 (-)
Cer 41:2	0.08 (±0.02)	0.05 (±0.008)	0.09 (±0.02)	0.08 (±0.01)	0.11 (-)	0.05 (-)	0.21 (±0.01)	0.07 (-)	0.03 (-)	0.01 (-)	0.05 (-)	0.05 (-)	0.004 (-)	0 (-)
Cer 42:0	9.14 (±2.25)	2.3 (±0.42)	15.52 (±1.83)	14.5 (±0.64)	17.56 (-)	3.61 (-)	4.74 (±0.13)	8.98 (-)	7.5 (-)	2.3 (-)	8.64 (-)	9.38 (-)	0.05 (-)	0.31 (-)
Cer 42:1	4.25 (±1.04)	1.45 (±0.17)	7.24 (±1.37)	6.52 (±0.76)	8.7 (-)	2.35 (-)	5.41 (±0.14)	4.33 (-)	3.15 (-)	0.93 (-)	2.69 (-)	3.46 (-)	0 (-)	0 (-)
Cer 42:2	0.58 (±0.15)	0.21 (±0.02)	0.95 (±0.18)	0.85 (±0.09)	1.15 (-)	0.36 (-)	0.89 (±0.04)	0 (-)	0 (-)	0 (-)	0 (-)	0 (-)	0 (-)	0 (-)
Cer 43:0	1.61 (±0.46)	0.72 (±0.07)	2.48 (±0.7)	2.63 (±0.92)	2.18 (-)	0.78 (-)	1.01 (±0.16)	1.46 (-)	1.33 (-)	0 (-)	1.75 (-)	1.84 (-)	0 (-)	2.68 (-)

Continued on next page

Table B.22 – continued from previous page

	N. crassa												*S. cerevisiae*	
	WC		PM					DDM	Pma1				WC	membra
	WC30 n=6	WC35 n=2	PM30A n=3	PM301 n=2	PM30DOC n=1	PM30NaCl n=1	PM35 n=2	PM30DDM n=1	Pma130glyc n=1	Pma130suc n=1	Pma135Pool1 n=1	Pma135Pool3 n=1	ScWC30 n=1	ScMemb n=1
	mean (std)	mean (std)	mean (std)	mean (std)	mean (std)	mean (std)	mean (std)	mean (std)	mean (std)	mean (std)	mean (std)	mean (std)	mean (std)	mean (std)
Cer 43:1	0.69 (±0.19)	0.34 (±0.06)	1.06 (±0.17)	1.01 (±0.21)	1.15 (-)	0.39 (-)	1.33 (±0.1)	0.83 (-)	0.46 (-)	0.12 (-)	0.22 (-)	0.75 (-)	0 (-)	0.15 (-)
Cer 43:2	0.1 (±0.03)	0.051 (±0.008)	0.13 (±0.03)	0.12 (±0.02)	0.16 (-)	0.06 (-)	0.25 (±0.02)	0 (-)	0 (-)	0 (-)	0 (-)	0.094 (-)	0 (-)	0 (-)
Cer 44:0	0.76 (±0.23)	0.24 (±0.05)	1.27 (±0.19)	1.31 (±0.24)	1.18 (-)	0.52 (-)	0.37 (±0.03)	0 (-)	0 (-)	0 (-)	0 (-)	0.68 (-)	0 (-)	28.3 (-)
Cer 44:1	0.55 (±0.17)	0.21 (±0.02)	0.77 (±0.13)	0.73 (±0.15)	0.85 (-)	0.41 (-)	0.63 (±0.14)	0.72 (-)	1.6 (-)	0.62 (-)	0.49 (-)	0.32 (-)	1.08 (-)	18.7 (-)
Cer 44:2	0.0007 (±0.0004)	0.0002 (±0.00008)	0.004 (±0.0004)	0.003 (±0.0005)	0.004 (-)	0.0008 (-)	0.001 (±0.0004)	0.007 (-)	0.03 (-)	0.031 (-)	0.007 (-)	0.004 (-)	0.0003 (-)	0.09 (-)
Cer 50:0	0.0004 (±0.0005)	0.00008 (±0.0001)	0.0008 (±0.0009)	0.001 (±0.0009)	0 (-)	0.0003 (-)	0 (±0)	0.02 (-)	0.1 (-)	0 (-)	0.007 (-)	0 (-)	0 (-)	0 (-)
Cer 50:1	0.00009 (±0.0002)	0 (±0)	0 (±0)	0 (±0)	0 (-)	0 (-)	0 (±0)	0.01 (-)	0.07 (-)	0 (-)	0.003 (-)	0 (-)	0 (-)	0 (-)
IP-Cer 42:0	9.03 (±4.77)	3.9 (±0.57)	16.1 (±11.52)	22.69 (±2.26)	2.93 (-)	2.43 (-)	11.27 (±0.33)	37.18 (-)	25.38 (-)	25.35 (-)	32.65 (-)	39 (-)	0.68 (-)	0 (-)
IP-Cer 44:0	1.12 (±0.92)	0.58 (±0.11)	3.87 (±3.27)	5.59 (±1.91)	0.44 (-)	0.44 (-)	2.71 (±0.15)	10.13 (-)	7.45 (-)	6.93 (-)	8.58 (-)	7.06 (-)	39.84 (-)	17.1 (-)
IP-Cer 46:0	0.008 (±0.008)	0.003 (±0.0002)	0.03 (±0.03)	0.05 (±0.02)	0 (-)	0.002 (-)	0.006 (±0.0008)	0.42 (-)	0.52 (-)	0.41 (-)	0.28 (-)	0.12 (-)	16.07 (-)	2.47 (-)
IP-Cer 50:0	0.00096 (±0.00042)	0.0002 (±0.00001)	0 (±0)	0 (±0)	0 (-)	0.001 (-)	0 (±0)	0 (-)	0 (-)	0 (-)	0 (-)	0 (-)	0.003 (-)	0.04 (-)
MDIP-Cer 46:0	0.007 (±0.004)	0.001 (±0.0001)	0.01 (±0.003)	0.01 (±0.003)	0.01 (-)	0 (-)	0.004 (±0.002)	0 (-)	0.008 (-)	0 (-)	0.02 (-)	0.02 (-)	0 (-)	0 (-)
MDIP-Cer 48:0	0.01 (±0.007)	0.003 (±0.001)	0.08 (±0.03)	0.1 (±0.02)	0.04 (-)	0.001 (-)	0.02 (±0.0004)	0.13 (-)	0.07 (-)	0.001 (-)	0.15 (-)	0.09 (-)	0 (-)	0 (-)
MDIP-Cer 50:0	0 (±0)	0 (±0)	0 (±0)	0 (±0)	0 (-)	0 (-)	0 (±0)	0 (-)	0 (-)	0 (-)	0.002 (-)	0 (-)	0 (-)	0 (-)
MIP-Cer 42:0	0.0006 (±0.0006)	0.00007 (±0.00009)	0.009 (±0.008)	0.01 (±0.002)	0 (-)	0 (-)	0 (±0)	0.01 (-)	0.002 (-)	0.001 (-)	0 (-)	0 (-)	0.037 (-)	0.01 (-)
MIP-Cer 44:0	0.003 (±0.003)	0.001 (±0.0003)	0.005 (±0.005)	0.008 (±0.003)	0.0003 (-)	0.002 (-)	0.001 (±0.00007)	0.35 (-)	0.62 (-)	0.5 (-)	0.12 (-)	0.04 (-)	20.83 (-)	5.17 (-)
MIP-Cer 46:0	0.002 (±0.003)	0 (±0)	0.007 (±0.006)	0.01 (±0.00008)	0.0004 (-)	0 (-)	0 (±0)	0.46 (-)	0.65 (-)	0.55 (-)	0.18 (-)	0.04 (-)	17.91 (-)	2.97 (-)
MIP-Cer 48:0	0.01 (±0.005)	0.003 (±0.0009)	0.04 (±0.02)	0.05 (±0.02)	0.02 (-)	0.0008 (-)	0.01 (±0.001)	0.05 (-)	0.03 (-)	0.11 (-)	0.13 (-)	0.12 (-)	0 (-)	0.12 (-)
MIP-Cer 50:0	0.00004 (±0.0001)	0 (±0)	0.004 (±0.003)	0.006 (±0.002)	0.0004 (-)	0 (-)	0 (±0)	0.006 (-)	0 (-)	0 (-)	0.02 (-)	0.01 (-)	0 (-)	0.00 (-)
SM 30:0	0.07 (±0.04)	0.07 (±0.011)	0.0005 (±0.0005)	0.0002 (±0.0003)	0.001 (-)	0.06 (-)	0 (±0)	0 (-)	0 (-)	0 (-)	0 (-)	0 (-)	0 (-)	0 (-)
SM 32:1	5.69 (±0.58)	4.25 (±0.17)	0.7 (±0.24)	0.58 (±0.19)	0.93 (-)	1.58 (-)	0.43 (±0.09)	0.43 (-)	0 (-)	0 (-)	0.11 (-)	0.054 (-)	0 (-)	0 (-)
SM 33:1	5.4 (±3.59)	9.28 (±1.53)	0.54 (±0.21)	0.53 (±0.3)	0.56 (-)	2.37 (-)	0.16 (±0.06)	0.96 (-)	0.36 (-)	0.022 (-)	0.16 (-)	0.19 (-)	0 (-)	0 (-)
SM 34:0	0.12 (±0.1)	0.01 (±0.01)	0 (±0)	0 (±0)	0 (-)	0.03 (-)	0 (±0)	0 (-)	0 (-)	0.087 (-)	0 (-)	0 (-)	0 (-)	0 (-)
SM 34:1	13.21 (±8.96)	40.81 (±2.66)	0 (±0)	0 (±0)	0 (-)	36.8 (-)	1.58 (±0.68)	0 (-)	0 (-)	0 (-)	0 (-)	0 (-)	0 (-)	0 (-)
SM 34:2	18.19 (±12.2)	15.28 (±0.039)	2.57 (±4.05)	0.23 (±0.07)	7.24 (-)	17.16 (-)	1.11 (±0.3)	1.20 (-)	0.56 (-)	0.18 (-)	0.27 (-)	0.003 (-)	0 (-)	0 (-)
SM 35:1	0.49 (±0.15)	0.65 (±0.05)	0.003 (±0.005)	0.004 (±0.006)	0 (-)	0.17 (-)	0.006 (±0.002)	0 (-)	0 (-)	0 (-)	0.03 (-)	0 (-)	0 (-)	0 (-)
SM 36:1	0.94 (±0.12)	1.1 (±0.01)	0.13 (±0.02)	0.12 (±0.01)	0.16 (-)	0.53 (-)	0.08 (±0.017)	0.15 (-)	0 (-)	0.23 (-)	0 (-)	0 (-)	0.19 (-)	0.32 (-)
SM 38:0	0.07 (±0.02)	0.02 (±0.002)	0.02 (±0.011)	0.02 (±0.01)	0.01 (-)	0.02 (-)	0.002 (±0.002)	0.08 (-)	0.33 (-)	0.03 (-)	0.08 (-)	0.03 (-)	0 (-)	0 (-)
SM 38:1	0.03 (±0.02)	0.02 (±0.02)	0.02 (±0.02)	0.01 (±0.02)	0.04 (-)	0 (-)	0 (±0)	0.09 (-)	0.56 (-)	0.74 (-)	0.14 (-)	0 (-)	0 (-)	0 (-)

Continued on next page

Table B.22 – continued from previous page

	N. crassa												*S. cerevisiae*	
	WC		PM					DDM	Pma1				WC	membra
	WC30 n=6	WC35 n=2	PM30A n=3	PM301 n=2	PM30DOC n=1	PM30NaCl n=1	PM35 n=2	PM30DDM n=1	Pma130glyc n=1	Pma130suc n=1	Pma135Pool1 n=1	Pma135Pool3 n=1	ScWC30 n=1	ScMemb n=1
	mean (std)	mean (std)	mean (std)	mean (std)	mean (std)	mean (std)	mean (std)	mean (std)	mean (std)	mean (std)	mean (std)	mean (std)	mean (std)	mean (std)
SM 38:3	0.02 (±0.03)	0.02 (±0.009)	0 (±0)	0 (±0)	0 (-)	0.009 (-)	0 (±0)	0 (-)	0 (-)	0 (-)	0 (-)	0 (-)	0 (-)	0 (-)
SM 39:0	0.002 (±0.004)	0 (±0)	0 (±0)	0 (±0)	0 (-)	0 (-)	0.004 (±0.002)	0 (-)	0 (-)	0 (-)	0 (-)	0 (-)	0 (-)	0 (-)
SM 40:0	0.31 (±0.18)	0.19 (±0.02)	0.06 (±0.07)	0.09 (±0.07)	0 (-)	0.14 (-)	0 (±0)	1.28 (-)	3.1 (-)	0 (-)	1.73 (-)	0.08 (-)	0 (-)	0 (-)
SM 40:1	0.37 (±0.43)	0 (±0)	0 (±0)	0 (±0)	0 (-)	0 (-)	0 (±0)	0 (-)	0 (-)	12.97 (-)	0 (-)	0 (-)	0 (-)	0 (-)
SM 42:0	0.06 (±0.01)	0.04 (±0.009)	0.04 (±0.02)	0.04 (±0.03)	0.05 (-)	0.02 (-)	0 (±0)	0.19 (-)	0.25 (-)	0.16 (-)	0.13 (-)	0 (-)	0 (-)	0 (-)
SM 42:1	0 (±0)	0 (±0)	0 (±0)	0 (±0)	0 (-)	0 (-)	0 (±0)	0 (-)	0 (-)	8.46 (-)	0 (-)	0 (-)	0 (-)	0 (-)
SM 42:2	0.06 (±0.03)	0.04 (±0.007)	0.05 (±0.02)	0.06 (±0.03)	0.03 (-)	0.02 (-)	0 (±0)	0.26 (-)	0.57 (-)	19.99 (-)	0.46 (-)	0.08 (-)	0.006 (-)	0 (-)
SM 44:1	0.42 (±0.13)	0.05 (±0.004)	0.11 (±0.17)	0.01 (±0.008)	0.31 (-)	0.14 (-)	0.16 (±0.01)	0.02 (-)	0.01 (-)	0 (-)	0 (-)	0 (-)	0 (-)	0 (-)
SM 44:2	0.05 (±0.04)	0.03 (±0.01)	0.04 (±0.02)	0.05 (±0.01)	0.02 (-)	0.09 (-)	0.07 (±0.03)	0.09 (-)	0 (-)	0 (-)	0.06 (-)	0.03 (-)	0.01 (-)	0.08 (-)
SM 46:0	7.04 (±1.07)	10.06 (±0.25)	14.66 (±8.51)	9.99 (±3.76)	23.99 (-)	7.99 (-)	45.91 (±0.43)	4.88 (-)	12.66 (-)	0 (-)	0.61 (-)	0.4 (-)	0 (-)	0 (-)
SM 48:0	0.48 (±0.15)	0.35 (±0.12)	1.09 (±0.61)	0.74 (±0.2)	1.77 (-)	0.57 (-)	3.23 (±0.69)	0 (-)	10.5 (-)	1.57 (-)	0 (-)	0 (-)	0 (-)	0 (-)
SM 48:2	2.01 (±0.33)	1.09 (±0.22)	0.54 (±0.93)	0 (±0)	1.61 (-)	0.73 (-)	0 (±0)	0 (-)	14.53 (-)	9.22 (-)	11.71 (-)	0 (-)	0 (-)	0 (-)

B.2 Lipid extraction and thin layer chromatography (TLC) *N. crassa*

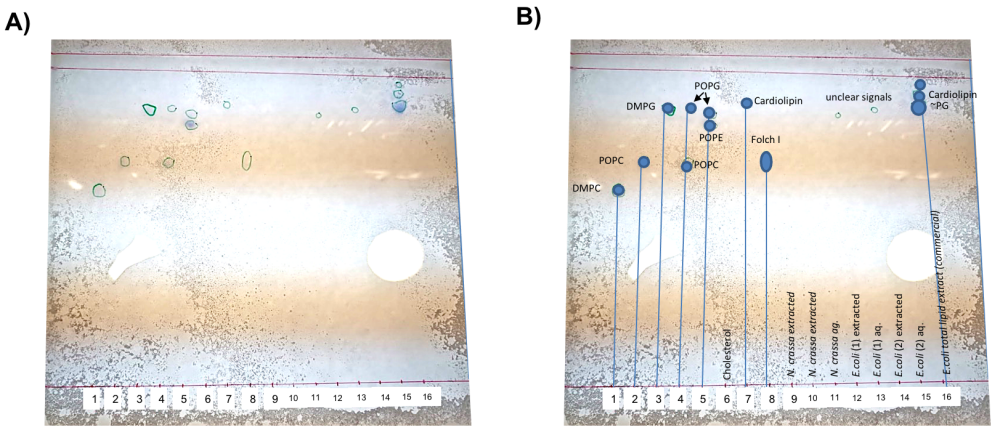

Figure B.1: Lipid extraction [190] from *N. crassa* and thin layer chormatography (TLC) [45] and phosphorus determination of phospholipids [46]. Lack of signal in the samples most likely due to small scale lipid extraction and therefore lack of material. Lipid standards are shown and show signal.

B.3 Proposals for MD simulation of Pma1 lipid environment

Table B.23 outlines a updated *N. crassa* lipid distribution for MD simulation of Pma1 enrionment, similar to [104] based on the presented lipid analysis in Chapter 5.

Table B.23: Proposal of *N. crassa* lipid distribution in plasma membrane for MD simulation; db - double bond MD1: published MD simulation MD2: proposal for new MD simulation.
Note: *The IP Ceramides could be exchanged with PI lipids of the same chain lengths to see if there would be a measurable difference because of the chain lengths (C26) or just between the Headgroup and not the backbone and fatty acids, if MD simulation allows this.

Lipid Name	Headgroup	Tail	sn1: Name			sn2: Name			total C atoms	saturation	net charge	MD1: inner leaf (%)	MD1: outer leaf (%)	MD: type distribution	MD2: inner leaf (%)	MD2: outer leaf (%)
Diacyl Glycerophospholipid																
PIPC	PC	PI	P	16/18	0	I	16/18	2	32-34-36	2	0	11	28	2	11	26
DIPC	PC	DI	I	16/18	2	I	16/18	2	32-34-36	4	0	5	14	1	6	13
PIPE	PE	PI	P	16/18	0	I	16/18	2	32-34-36	2	0	8	13	2	9	13
DIPE	PE	DI	I	16/18	2	I	16/18	2	32-34-36	4	0	4	7	1	4	6
PIPA	PA	PI	P	16/18	0	I	16/18	2	32-34-36	2	-2	11	11	2	13	13
DIPA	PA	DI	I	16/18	2	I	16/18	2	32-34-36	4	-2	5	5	1	7	7
PIPS	PS	PI	P	16/18	0	I	16/18	2	32-34-36	2	-1	17	0	2	10	1
DIPS	PS	DI	I	16/18	2	I	16/18	2	32-34-36	4	-1	9	0	1	5	0
PIPI	PI	PI	I	16/18	2	I	16/18	2	32-34-36	2	-1	8	0		15	1
Sphingomyeline																
XNSM	SM	XN	X	24/26	0	N	24/26	1	48-50-52	1	0	2	2	1	2	2
PVSM	SM	PV	P	16/18	0	V	16/18	1	32-34-36	1	0	4	4	2	3	3
DPCE	Cer	DP	P	16/18	0	P	16/18	0	32-34-36	0	0	3	3	27	1	1
PNCE	Cer	PN	P	16/18	0	N	24/26	1	40-42-44	1	0	8	8	73	4	4
PX IP-Cer*	IP Cer	PX	P	16/18	0	X	24/26	0	40-42-44	0	-1		*	70	4	4
BX IP-Cer*	IP Cer	BX	B	20/22	0	X	24/26	0	44-46-48	0	-1		*	30	2	2
Ergosterol																
ERGO	Erg	–									0	5	5		5	5

A proposal for the building of phosphoinositol containing lipids in insane martini framework based on [247] is given in Table B.24 and in the following code.

Table B.24: A proposal for the building of phosphoinositol containing lipids in insane martini framework based on [247]

Lipid Name	Headgroup	Tail	sn1 Individual Tail			sn2 individual tail			cAtoms total
			Name	C atoms	double bonds	Name	C atoms	double bonds	
PXPI	PI	PX	P	16/18	0	X	24/26	0	40-42-44
BXPI	PI	BX	B	20/22	0	X	24/26	0	44-46-48
PX IP-Cer	IP Cer	PX	P	16/18	0	X	24/26	0	40-42-44
BX IP-Cer	IP Cer	BX	B	20/22	0	X	24/26	0	44-46-48

Code for PI template

```
# HII fix for PI templates and new templates PI(s) with different
    tails, PO-PIP1(3) and POPIP2(4,5)
```

```
#Prototopology for phosphatidylinositol type lipids 5,6,7 are potential phosphates (PIP1,PIP2 and PIP3)
# 1,2,3 - is the inositol and 4 is the phosphate that links to the tail part.
#  5
#   \
#  6-2-1-4-8--10-11-12-13-14-15
#    |/    |
#  7-3     9--16-17-18-19-20-21
moltype = "INOSITOLLIPIDS"
lipidsx[moltype] = (.5, .5,
   0,0,1,.5,0,0,.5,0,0,0,0,0,0,1,1,1,1,1,1)
lipidsy[moltype] = ( 0, 0, 0, 0, 0, 0, 0, 0, 0, 0, 0, 0, 0, 0, 0,
   0, 0, 0, 0, 0, 0)
lipidsz[moltype] = ( 8, 9, 9, 7, 10, 10, 10, 6, 6, 5, 4, 3, 2, 1,
   0, 5, 4, 3, 2, 1, 0)
lipidsa.update({ # 1 2 3 4 5 6 7 8 9 10 11 12 13 14 15 16 17 18 19 20 })

# inositol phospho glyceride:
 "PXPI": (moltype, " C1 C2 C3 CP - - - GL1 GL2 C1A C2A C3A C4A - - C1B C2B C3B C4B C5B C6B "),
 "BXPI": (moltype, " C1 C2 C3 CP - - - GL1 GL2 C1A C2A C3A C4A C5A - C1B C2B C3B C4B C5B C6B "),

# inositol ceramide:
 "PX IP-Cer": (moltype, " C1 C2 C3 CP - - - AM1 AM2 T1A C2A C3A C4A - - C1B C2B C3B C4B C5B C6B "),
 "BX IP-Cer": (moltype, " C1 C2 C3 CP - - - AM1 AM2 T1A C2A C3A C4A C5A - C1B C2B C3B C4B C5B C6B "),
```